THE UNIVERSITY
of EDINBURGH

Applications of the blow-up technique in singularly perturbed chemical kinetics

Zhouqian Miao

Doctor of Philosophy
University of Edinburgh
2019

Declaration

I declare that this thesis was composed by myself and that the work contained therein is my own, except where explicitly stated otherwise in the text.

(*Zhouqian Miao*)

To my parents

Acknowledgements

First and foremost, I would like to express my gratitude to my first supervisor, Dr. Nikola Popović for his guidance through my research and during the writing of my thesis. His patience, support, encouragement and mathematical knowledge have led me to this point. I cannot have a better mentor for my PhD research study.

I would also thank my second supervisor, Dr. Ben Goddard for discussion on topics related to my research, especially for numerical computation. I am very appreciative for the discussion with Prof. Peter Szmolyan on my project in Vienna, his suggestions helped me construct the basic structure of the topic; I also thank Ilona Kosiuk for short discussion. I really enjoyed the winter time in Vienna, especially the Christmas Markets and the food there.

Besides, I have also greatly benefited from the group meetings with Frits Veerman and Annalisa Iuorio. I thank all the friends I have had met during my PhD study.

Finally, I would like to thank my parents for their support throughout my study and my life over the years. I am grateful for the financial support from the School of Mathematics and China Scholarship Council.

Lay Summary

In mathematics, a singular perturbation problem, such as a differential equation, usually contains a small parameter, where the singular limit of the problem as this small parameter to zero will perform a different type or structure with respect to the general solution of the problem. Such feature, is contrasted with that of a regular perturbation problem, as in that we may find a general solution converging to the solution of the limiting problem. This solution usually consist of a power series in terms of the small parameter, which is called a uniform approximation to the problem. However, for a singularly perturbed system, when we set the small parameter to zero, the nature of the problem will change depending on the disparate length-scales or time-scales. To understand the solution of the problem, we can divided the full problem into different subsystems, we can combine the solutions of the subsystems into a full solution by matching certain conditions to make the solution smoothly. To that end, we apply some mathematical techniques, such as the method of matched asymptotic expansions and the method of multiple scales. More recently, the geometric approach under certain regularity assumptions has been developed completely, and based on dynamical system theory. However, when that regularity is lost, we may consider the blow-up technique, which is also known as geometric desingularisation, by appending the small parameter as a new variable that allows us to study the singular problem in an equivalent system, higher dimension, but more regular to explore the whole problem.

In this thesis, we consider two examples: the cut-off problem and the cAMP signaling system, which are both singularly perturbed. So-called cut-off functions have been in introduced into various mathematical models to improve the approximation of discrete phenomena. For instance, in microscopic physics, the underlying numbers of particles are integer-valued; hence, the discrete nature of the underlying models needs to be considered when performing a continuum approximation via reaction-diffusion systems. In particular, the notion of a concentration of particles will be invalid in regimes where no particles exist. Such regimes can be modeled by a cut-off function, like a step function—taking some threshold as the concentration when only one particle is present to react. Hence, there is a necessity to describe the effect of the cut-off on the continuous model.

Secondly, the cAMP signaling system models the propagation of signals that control aggregation of the amoeboid microorganism *Dictyostelium discoideum*. Two main types of dynamic behaviour are observed: autonomous oscillation [23, 24, 26] and relay of super-threshold pulses [59, 63]. In particular, relay behaviour has been linked with autonomous oscillation, representing the excitability of the system, which is naturally motivated by a singularly perturbed model. We discuss the system by several subsystems, and combine the results in an appropriate form by using some mathematical techniques. In particular, we will apply the blow-up technique to explore the dynamics in different subsystems, allowing us to make a geometric display of the structure of the full solution.

Abstract

This thesis addresses the geometric analysis of traveling front propagation in singularly perturbed dynamical systems. The study of front propagation in reaction-diffusion systems has received a significant amount of attention in the past few decades. Frequently, of principal interest is the propagation speed of front solutions that connect various equilibrium states in these systems. Meanwhile, the geometric approach for normally hyperbolic problem is developed completely, and based on dynamical system theory. However, in the degenerate case, where the hyperbolicity is lost, we may consider the blow-up technique, which is also known as geometric desingularisation, to resolve the nonhyperbolic parts.

We start with a two-component reaction-diffusion model with a small cut-off, which is a sigmoidal type of the FitzHugh-Nagumo system with Tonnelier-Gerstner kinetics. We first discuss the basic properties of the model without a cut-off, and we find two feasible cut-off systems for two components. We aim to construct a heteroclinic orbit connecting the nonzero equilibrium to the equilibrium at the origin for the cut-off system. However, the origin becomes degenerate due to the cut-off term. Hence, we apply the blow-up technique, which can resolve the degeneracy at the origin and regularize the dynamics in its neighborhood, where we can use standard dynamical system theory. We perform a formal linearisation and derive a second-order normal form in the blown-up dynamics to obtain the corresponding speed relation, which implies the existence of the heteroclinic orbit. We present the two blow-up patching approaches, numerical simulations and numerical comparison of the obtained results. We also discuss how the cut-off threshold is involved in the global geometry and the effect on the related propagating front speed and discontinuity position.

The second main topic of the thesis is a geometric analysis of a reformulated singularly perturbed problem, based on the Martiel-Goldbeter model of a cyclic AMP (cAMP) signaling system, which models the propagation of cAMP signals during the aggregation of the amoeboid microorganism *Dictyostelium discoideum*. The mechanism is based on desensitisation of the cAMP receptor to extracellular cAMP. We explore the oscillatory dynamics of the reduced two-variable system without diffusion, which can be considered as the core mechanism in the cAMP signaling system, allowing for a phase plane analysis of oscillations due to the simplicity of the governing equations. There are two small parameters, which manifest very differently: while one parameter is a "conventional" singular perturbation parameter which reflects the separation of scales between the slow variable and the fast variable, the other parameter induces a different type of singular perturbation which is reflected by the non-uniformity of the limit. Our resolution, which introduces the blow-up technique to construct a family of periodic (relaxation-type) orbits for the singularly perturbed problem, uncovers a novel singular structure and improves our understanding of the corresponding oscillatory dynamics.

Contents

Chapter 1

Introduction

The study of dynamical systems, which was firstly introduced in celestial mechanics by Henri Poincaré [52], has been popular. In mathematics, a dynamical system consists of a function or functions describing the position of the state points depending on some parameter, which are usually referred to as "time", such as ordinary differential equation(ODE) and difference equation(DE), also known as a vector field and a map in geometry, respectively. The basic forms can be written as

$$\frac{d\mathbf{x}}{dt} = f(\mathbf{x}, t) \tag{1.1}$$

and

$$\mathbf{x} \mapsto g(\mathbf{x}) \tag{1.2}$$

where $\mathbf{x} \in U \subset \mathbb{R}^n$ and $t \in \mathbb{R}^1$, U is an open set in $\mathbb{R}^n$. Here, we focus on the continuous " time" case (1.1) the solution of the system f has the form $\phi(\mathbf{x}, t)$ with $\phi_t(\mathbf{x}) = \phi(\mathbf{x}, t)$, also termed as a flow $\phi_t : U \to \mathbb{R}^n$, which with given initial condition, satisfies $\phi_0(\mathbf{x}) = \mathbf{x}_0$ and $\phi_{t+s} = \phi_t \circ \phi_s$. Here, we say ϕ defines a solution curve, trajectory or orbit for the corresponding ODE. The local existence and uniqueness theorem has been proved, for proof see Coddington and Levinson [12], Hirsch and Smale [34]. There are several important types of solutions, such as equilibrium solutions and periodic solutions. Equilibrium solutions are also called fixed points or steady states, the stability is usually determined by the method of linearisation. An equilibrium is said to be hyperbolic when the eigenvalues of the corresponding linearised system have no zero real part, and it can be called a saddle, a node (stable or unstable), a sink or a center depending on the sign and imaginary part of the eigenvalues. From the geometrical point of view of dynamical systems, we talk about "manifolds", then the stability of a fixed point is described locally by invariant manifolds, e.g., the stable, unstable and center manifolds. Moreover, for some nonlinear systems, periodic solutions or orbits occur rather than equilibrium solutions, where the well-known method of Poincaré Map is considered in the analysis, see Section 1.6 below. And solutions or flows connecting a set of equilibria are termed as heteroclinic orbits connecting distinct equilibria and homoclinic orbits connecting one point to itself. Simple dynamical systems, can be solved explicitly, while for some complex problems, we may try to simplify them by two rigorous mathematical methods, the center manifold theorem and the method of normal forms. The former is aiming to reduce the dimensionality of the space; more information can be found in Marsden and McCracken [45], Carr [11], Henry [33], while the latter helps simplify the nonlinearity by finding proper coordinate transformations, see Wiggins [72] and Guckenheimer and Holmes [31].

In the analysis of dynamical systems, one can apply the basic dynamical system theory for normally hyperbolic systems, when for simple singularly perturbed, one may concern standard geometric singular perturbation theory. However, in case of a loss of hyperbolicity, one may use some additional technique to support the study, such as geometric desingularisation—"blow-up" technique, to resolve the degenerate part; then one can use the standard theory [19].

1.1 Reaction-diffusion systems

A reaction-diffusion system in mathematical modeling can be represented in the form

$$\frac{\partial \mathbf{u}}{\partial t} = \mathbf{f} + \mathbf{D}\,\nabla^2 \mathbf{u} \tag{1.3}$$

where $\mathbf{u}$ is a vector of $u_i(\mathbf{x}, t)$, $i = 1, ..., n$ with $\mathbf{x}$ and t the continuous space and time variables. In models of interacting species or chemicals, u_i is referred to as density or concentration, and D_i of the diagonal matrix $\mathbf{D}$ is the corresponding diffusion coefficient, and $\mathbf{f}$ is the reaction (source) term. It was introduced by Turing [68] to model the mechanism of the chemical basis of morphogenesis in theoretical biology. Since 1970, reaction-diffusion systems have found widespread use in biology, chemistry, physics and ecology, e.g., animal dispersal, tumor invasion, spread of epidemics.

The well known of a reaction-diffusion system containing one component in one spatial dimension is given by

$$\frac{\partial u}{\partial t} = k\,u\,(1-u) + D\frac{\partial^2 u}{\partial x^2} \tag{1.4}$$

where the parameter k and diffusion coefficient D are positive.

It was proposed by Fisher [22] modeling the spatial spread of a favoured gene, which extended the population model with logistic growth. And a classical study was given by Kolmogorov et al. [1]. Therefore, this equation is also well-known as the Fisher-Kolmogorov-Petrovskii-Piskunov (FKPP) equation. More studies can be found in the books by Fife [21], Britton [7] and Grinrod [30]. It has been widely used to develop the standard techniques in single-species models, especially the analysis of travelling wave solutions.

1.2 Traveling waves

What is a travelling wave? Firstly, it is a wave that travels at a certain speed without changing shape. The analysis of travelling waves in chemistry was popularised by Luther [44] who presented the interesting discussion at a conference, and his results have been organized by Showalter and Tyson [64], which has the same analytical form as Kolmogorov et al. [1] and Fisher [22]; also see [3, 4] in biology.

1.2.1 Single-species models

Considering the FKPP equation here, the travelling wave solution is expressed as

$$u(x,t) = u(\xi), \quad \xi = x - ct \tag{1.5}$$

where c denotes the corresponding speed of propagation and ξ is a new coordinate containing spatial and time variable (x, t).

Such a wave is moving in the positive x-direction with speed $c > 0$, which is not determined yet. (Similarly, if we define the travelling wave by $x + ct$, the wave will move in the negative x-direction.) Now, substituting the change of coordinate $\xi = x - ct$ with $c > 0$, we have

$$\frac{\partial u}{\partial t} = -c\frac{du}{d\xi}, \quad \frac{\partial u}{\partial x} = \frac{du}{d\xi}, \quad \frac{\partial^2 u}{\partial x^2} = \frac{d^2 u}{d\xi^2} \tag{1.6}$$

before rewriting Equation (1.4) in $u(\xi)$, we rescale it into a non-dimensional form via $x^* = x\sqrt{\frac{k}{D}}$ and $t^* = kt$. One then has the simple equation

$$\frac{\partial u}{\partial t} = u\,(1-u) + \frac{\partial^2 u}{\partial x^2} \tag{1.7}$$

here, we drop the * for the sake of simplicity.

Now, Equation (1.7) is transformed from a partial differential equation (PDE) in (x, t) into an ordinary equation (ODE) in the wave variable ξ as follows,

$$u'' + cu' + u(1-u) = 0, \tag{1.8}$$

where the prime denotes differentiation with respect to ξ. The valid range of u is $[0, 1]$ which allows the study of travelling front solutions, and $u = 0$ and $u = 1$ are the spatial homogeneous steady states, while $u < 0$ will be biological unrealistic in these models.

To discuss the dynamics in phase plane, one can find the corresponding the two-dimensional first-order system

$$u' = v \tag{1.9a}$$

$$v' = -cv - u(1-u) \tag{1.9b}$$

The steady-states of Equation (1.9) are $(0, 0)$ and $(1, 0)$ in (u, v)-space. The eigenvalues at the point $(0, 0)$ are $\lambda_\pm = -\frac{c}{2} \pm \frac{1}{2}\sqrt{c^2 - 4}$, which indicates the stability of this point: for $c \geqslant 2$, it is a stable node, while for $c \in (0, 2)$, it is a stable spiral. The eigenvalues at the point $(1, 0)$ are $\lambda_\pm = -\frac{c}{2} \pm \frac{1}{2}\sqrt{c^2 + 4}$, which shows it a saddle point. One can construct such trapping region and show that the heteroclinic orbit from $(1, 0)$ to $(0, 0)$ stays in this region for the travelling front solutions, see Figure 1.1. Here, for $\xi \to -\infty$, $(u, v) \to (1, 0)$, and for $\xi \to \infty$, $(u, v) \to (0, 0)$, the travelling wave (or front) is equivalent to the heteroclinic orbit between the two steady states. The orbit is given by

$$\frac{dv}{du} = \frac{-cv - u(1-u)}{v} \tag{1.10}$$

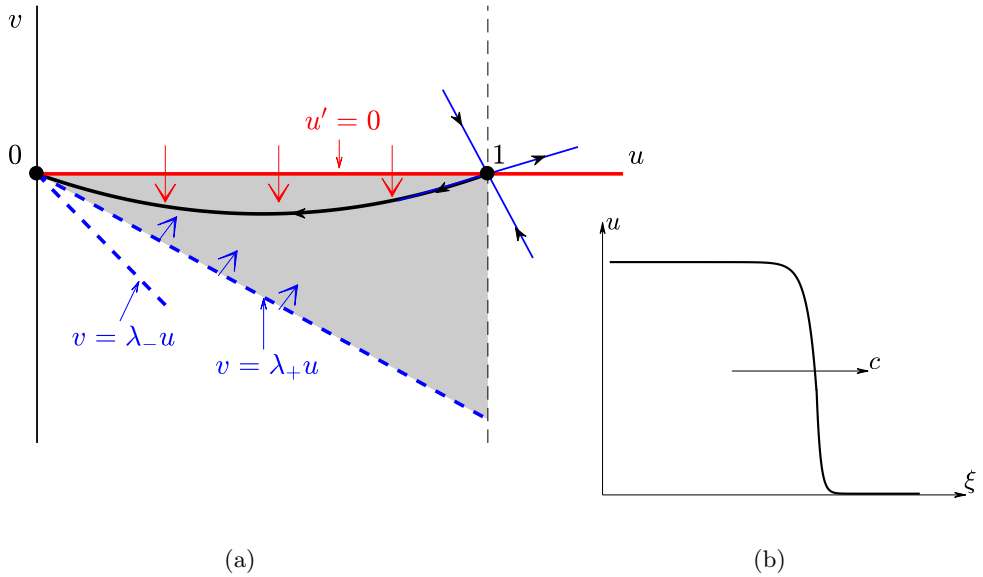

(a) (b)

Figure 1.1: (a) The trapping region of Equation (1.9) and trajectory for $c > 2$. (b) traveling front

There exist travelling wave solutions for all $c \geqslant 2$. Here, $c = 2$ is the critical speed; while for $c < 2$, there will be oscillations around the origin, which is not physically realistic since $u < 0$ for some ξ.

1.2.2 Multi-species models

There are many reaction-diffusion systems with several species, which make the study of solutions more difficult and complex, especially for those with nonlinear reaction kinetics. Princi-

pally, the study of the stability of the travelling wave solutions is an important aspect of the analysis in multi-species models. Due to the number of reactants and the high dimension, there are various possibilities to discuss the dynamics. When there exist several steady states, one can find travelling wave solutions connecting two of them, or there may exist stable periodic limit cycle solutions; one can even find the chaotic oscillations in three or more equation systems. For two-dimensional spatial model with Belousov-Zhabotinsky reaction, target patterns (circular waves) were found experimentally by Zaikin and Zhabotinsky [73], while the analytical approach was studied for the Field-Noyes model by Tyson and Fife [70]. Target pattern behaviour can be found in many biological models. In addition, there are also solutions like spiral waves, which have been discussed by Newell [51], e.g. the dynamic of the slime mould *Dictyostelium discoideum*, however, there still exist travelling wave solutions for certain parameter domains due to the complexity of biological parameters. Relevant research was produced by Keller and Segel [40] and Keller and Odell [39]. Recently, many studies have been done for multi-species models for their variety of wave solutions, however, there is still much more to be discovered. For example, the Fitzhugh-Nagumo equation (FHN) is one important type of system in excitable media of neuroscience, which has the form

$$\frac{\partial u}{\partial t} = u(a-u)(u-1) + D\frac{\partial^2 u}{\partial x^2} \tag{1.11}$$

$$\frac{\partial v}{\partial t} = bu - \gamma v \tag{1.12}$$

with parameters $0 < a < 1$ and $b, \gamma > 0$. The nullclines can be sketched is in Figure 1.2. There are three possibilities of equilibrium state: unique equilibrium, two equilibria and three equilibria.

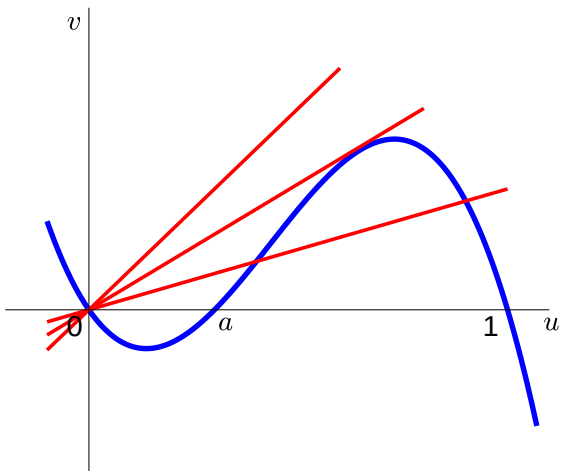

Figure 1.2: Graph for curve $u(a-u)(u-1) = 0$ (thick blue) and line $bu - \gamma v = 0$ (red), the nullclines of Equation (1.11) for various γ

In particular, when $\gamma = 0$, i.e., for a unique equilibrium state, solutions of travelling pulses were obtained by Rinzel and Keller [56]; the three equilibrium state was discussed by Rinzel and Terman [57]. Besides, Mckean studied the piece-wise linear type of FHN system in [47], while Feroe discussed the stability of its travelling pulses in [20]. In addition, more general results have been produced by Keener [38] and Tyson and Keener [71].

For an introduction to mathematical biology and applications, we refer to the book by Murray [49, 50].

1.3 Geometric singular perturbation theory

In mathematics, a perturbation problem usually contains a small parameter, such as ε. For a regularly perturbed problem, one may find a uniformly approximated solution to the limiting problem as $\varepsilon \to 0$, while for a singularly perturbed problem, the solution is not uniformed. Traditionally, there are basic methods of analysis for this kind of problems, such as the method of matched asymptotic expansions and the method of multiple scales. The former provides us to study the full problem by dividing the whole domain into several subdomains, where solutions in those subdomains will be combined together by matching the boundaries to give an approximation of the full problem via an asymptotic series. For the method of multiple scales, one may introduce fast-scale and slow-scale variables for the independent variable, usually refers to the "time"; then we investigate the dynamics with different time scales, and combine the results in an appropriate form. Most recently, the geometric approach has been developed completely under certain regularity and based on dynamical system theorem, for the standard theory, we refer to Fenichel [19].

1.3.1 Two-scale slow-fast system

We consider singular perturbation problems in the following form

$$\varepsilon\dot{\mathbf{x}} = f(\mathbf{x}, \mathbf{y}, \varepsilon) \tag{1.13a}$$

$$\dot{\mathbf{y}} = g(\mathbf{x}, \mathbf{y}, \varepsilon), \tag{1.13b}$$

where the dot denotes differentiation with respect to time scale τ, $(\mathbf{x}, \mathbf{y}) \in \mathbb{R}^m \times \mathbb{R}^n$ with $m, n \geqslant 1$, and $0 < \varepsilon \ll 1$. Here, the functions f and g are assumed to be $\mathcal{C}^k$ with $k \geqslant 3$, and ε is taken as the singular parameter. Introducing a new time scale via $t = \tau/\varepsilon$, the reformulated system of (1.13) becomes

$$\mathbf{x}' = f(\mathbf{x}, \mathbf{y}, \varepsilon) \tag{1.14a}$$

$$\mathbf{y}' = \varepsilon g(\mathbf{x}, \mathbf{y}, \varepsilon) \tag{1.14b}$$

where the prime denotes differentiation with respect to time scale t.

The type of (1.13) belongs to the class of slow-fast systems: we note τ as the slow time scale, while t is the fast time scale. Then Equations (1.13) and (1.14)are referred as the slow and fast system, respectively. When $\varepsilon \neq 0$, both Equation (1.13) and (1.14) are equivalent. When $\varepsilon = 0$ the corresponding limiting problems of systems (1.13) and (1.14) become

$$0 = f(\mathbf{x}, \mathbf{y}, 0), \tag{1.15a}$$

$$\dot{y} = g(\mathbf{x}, \mathbf{y}, 0) \tag{1.15b}$$

and

$$x' = f(\mathbf{x}, \mathbf{y}, 0) \tag{1.16a}$$

$$y' = 0, \tag{1.16b}$$

which are referred to as the reduced problem and the layer problem, respectively. The geometric singular perturbation theory provides the approach for analysing system (1.13) with ε nonzero but small by suitably combining the study of the limiting problems (1.15) and (1.16). The dynamics of the layer problem (1.16) contains a set of equilibria, which is defined as $\mathcal{S} := \left\{(\mathbf{x}, \mathbf{y}) \in \mathbb{R}^{m+n} \,\middle|\, f(\mathbf{x}, \mathbf{y}, 0) = 0\right\}$ and the flow under (1.16) is trivial. In the reduced problem, the flow is defined on the set $\mathcal{S}$, which is nontrivial. Assuming that we have an n-dimensional manifold $\mathcal{S}_0$, which is contained in the set $\mathcal{S}$, possibly with boundary. Under the hypothesis that $\mathcal{S}_0$ is compact and normally hyperbolic (that is, the eigenvalues of the related linearised system (the Jacobian $\frac{\partial f}{\partial \mathbf{x}}\big|_{\mathcal{S}_0}$) are nonzero and uniformly bounded away from the imaginary axis), then the critical manifold $\mathcal{S}_0$ persists as a locally slow manifold $\mathcal{S}_\varepsilon$, which is invariant in the full system (1.13), and lies within $\mathcal{O}(\varepsilon)$ to $\mathcal{S}_0$. The restriction of the flow of (1.13) to $\mathcal{S}_\varepsilon$ is a small and regular perturbation of the flow of the reduced problem (1.15). Moreover,

the corresponding stable and unstable invariant foliations of $\mathcal{S}_0$ of (1.16) persist as those of $\mathcal{S}_\varepsilon$ within $\mathcal{O}(\varepsilon)$, respectively. The fundamental theorems of geometric singular perturbation theory were established by Fenichel [19], and more introduction and applications were given by Jones [35], Hek [32] and Kaper [36].

1.3.2 Nonhyperbolic fold point

The geometric singular perturbation theory was based on normal hyperbolicity, however, it fails when normal hyperbolicity breaks down. One particular case is the fold point on the critical manifold where there exists a zero eigenvalue of the relevant Jacobian matrix. Such phenomena are found in relaxation oscillations problem; for the detailed description see books [29, 48, 53]. The theorem on extended of geometric singular perturbation theory to fold point is proposed by Krupa and Szmolyan [42], where they present a detailed geometric approach for a generic fold in the planar case of system (1.17):

$$\varepsilon\dot{x} = f(x, y, \varepsilon) \tag{1.17a}$$
$$\dot{y} = g(x, y, \varepsilon), \tag{1.17b}$$
$$\dot{\varepsilon} = 0. \tag{1.17c}$$

For the sake of simplicity, one can assume that the non-hyperbolic fold point of the critical manifold $\mathcal{S}$ is at the origin in (x, y, ε)-sphere, i.e., $f(0,0,0) = 0$ and $\frac{\partial f}{\partial x}(0,0,0) = 0$, where $(x, y) \in \mathbb{R}^2$, under the assumption that

$$\frac{\partial^2 f}{\partial x^2}(0,0,0) \neq 0, \quad \frac{\partial f}{\partial y}(0,0,0) \neq 0, \quad g(0,0,0) \neq 0$$

which guarantee the nondegeneracy in the neighbourhood of the origin on $\mathcal{S}$. To facilitate a clear description of the critical manifold and slow manifold, let $\frac{\partial^2 f}{\partial x^2}(0,0,0) > 0$, $\frac{\partial f}{\partial y}(0,0,0) < 0$, the dynamics of the two limiting problem are shown in Figure 1.2(a). The critical manifold consists of the left attracting branch $\mathcal{S}_a$ and the right repelling branch $\mathcal{S}_r$, where $\frac{\partial f}{\partial x}(x, y, 0) < 0$ and $\frac{\partial f}{\partial x}(x, y, 0) > 0$, respectively, i.e., $\mathcal{S} = S_a \cup (0,0) \cup S_r$ in (x, y)-space. Moreover, the origin is degenerate weakly attracting on the left-side and weakly repelling on the right-side. Here, the folded manifold $\mathcal{S}$ is approximated by a parabola with opening to the top, where $g(x, y, 0) < 0$ for all $(x, y) \in S$, which leads the direction of the reduced flow downwards towards the fold point. The only solution of possible orbits approaching the fold point is to leave along the weakly unstable fiber on x-axis in the layer problem.

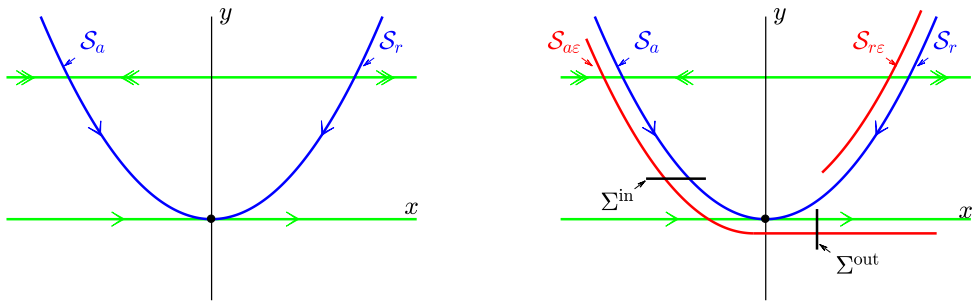

(a) (b)

Figure 1.3: (a)The critical manifold $\mathcal{S}$ (blue), where $\mathcal{S} = \mathcal{S}_a \cup (0,0) \cup \mathcal{S}_r$, and layer problem (green); (b) The smoothly perturbed slow manifold $\mathcal{S}_{a\varepsilon}$, $\mathcal{S}_{r\varepsilon}$(red) and sections.

Without loss of hyperbolicity on $\mathcal{S}_a$ and $\mathcal{S}_r$ away from the fold point, one can imply the persistence of $\mathcal{S}_a$ and $\mathcal{S}_r$ by the standard theory by Fenichel [19] and Jones [35] that there

exist locally smoothly perturbed slow invariant manifolds $\mathcal{S}_{a\varepsilon}$ and $\mathcal{S}_{r\varepsilon}$ for ε nonzero but small, see Figure 1.2(b). Moreover, the stability of $\mathcal{S}_{a\varepsilon}$ remains the same as $\mathcal{S}_a$, which is attracting, while $\mathcal{S}_{r\varepsilon}$ stays repelling, and the slow flow on both is directed towards the origin. For the corresponding layer problem, there are invariant stable foliations on $\mathcal{S}_{a\varepsilon}$ and unstable foliations on $\mathcal{S}_{r\varepsilon}$. The perturbed solutions of possible orbits follow $\mathcal{S}_{a\varepsilon}$ until they enter a section Σ^{in} close to the fold point where there exists a transition connecting $\mathcal{S}_{a\varepsilon}$ to the perturbed fast unstable fiber, which is parallel to the x-axis, in a section is defined as Σ^{out}. The following results have been proven by Krupa and Szmolyan as Theorem 2.1 in [42].

Theorem 1.1. *Under the assumptions made in this section there exists $\varepsilon_0 > 0$ small such that the following assertions hold for $\varepsilon \in (0, \varepsilon_0]$:*

1. *The manifold $\mathcal{S}_{a\varepsilon}$ passes through Σ^{out} at the point $(\rho, \mathcal{O}(\varepsilon^{2/3}))$, where $\rho > 0$ small.*
2. *The transition map $\pi : \Sigma^{\text{in}} \to \Sigma^{\text{out}}$ is a contraction with contraction rate $\mathcal{O}(\mathrm{e}^{-c/\varepsilon})$, where c is a positive constant.*

The proof is based on the analysis of geometric desingularisation— the blow-up technique.

1.4 Geometric desingularisation

To resolve the degenerate origin in Equation (1.17), one can use a blow-up technique, where the desingularisation theorem in a planar case was first introduced by Bendixson in 1901 and rigorously proved by Seidenberg [62]. Later on, the technique as a useful tool in studying nonhyperbolic singularities was extended to $\mathcal{C}^\infty$ vector fields by Dumortier [13]. The blow-up technique is a method of coordinate transformation that allows us to study the singular part in charts where in each chart the dynamics are at least partially hyperbolic and amenable to the standard theory. There are many different types of blowing up a system, such as polar blow-up, related directional blow-up, successive blow-up, quasi-homogeneous blow-up and so on; for more details see Dumortier [14] and the book by Dumortier and Roussarie [17]. There is also a survey on this method in [2], where one can find an overview of different examples of homogeneous and quasi-homogeneous blow-up techniques. For a general introduction of the quasi-homogeneous method, see the book by Bruno [10] and the article by Brunella and Miari [8].

Considering the fold point problem (1.17), where $(x, y) \in \mathbb{R}^2$, one can rewrite the system in a canonical form via a suitably chosen scaling of (x, y, ε) and time t so that the new equation becomes

$$x' = -y + x^2 + \mathcal{O}(\varepsilon, xy, y^2, x^3), \tag{1.18a}$$
$$y' = \varepsilon(-1 + \mathcal{O}(x, y, \varepsilon)), \tag{1.18b}$$
$$\varepsilon' = 0, \tag{1.18c}$$

where the third equation is appended for the blow-up method.

The fold point $(0, 0, 0)$ is the nonhyperbolic equilibrium of (1.18) on the critical manifold $\mathcal{S}$. The blow-up transformation is obtained by quasi-homogeneous blow-up as

$$x = \bar{r}\bar{x}, \quad y = \bar{r}^2\bar{y}, \quad \varepsilon = \bar{r}^3\bar{\varepsilon}, \tag{1.19}$$

with $\bar{r} \in \mathbb{R}$ and $(\bar{x}, \bar{y}, \bar{r} \in \mathbb{S}^2)$, where the dynamics of the degenerate equilibrium of (1.18) are solved in three charts $K_i (i = 1, 2, 3)$, which are determined by $\bar{y} = 1$, $\bar{\varepsilon} = 1$ and $\bar{x} = 1$ in (1.19), respectively. For the rigorous geometric analysis and proof we refer to Krupa and Szmolyan [42].

1.5 Normal forms

Many reaction-diffusion systems are complicated, e.g., containing multiple variables and with nonlinearity; it is time-consuming for solutions for those systems. One may try to simplify the dynamical system by reducing the dimension of a system or transforming into a linear system. Two well-known techniques for simplifying dynamics are centre manifold theory and normal

forms. The former provides an approach of reducing the dimension of phase space, while the normal form method helps simplify the system by changes-of-coordinates. Here, we briefly introduce the method of normal forms for vector fields; for more details see [31, 72].

Considering a system of differential equations

$$\mathbf{x}' = f(\mathbf{x}), \quad \mathbf{x} \in \mathbb{R}^n \tag{1.20}$$

where $f(\mathbf{x})$ is a $\mathcal{C}^r$-function with $r \geqslant 4$. For the sake of simplicity, we assume the equilibrium is the origin, i.e. $f(\mathbf{0}) = \mathbf{0}$. One can rewrite Equation (1.20) by sorting the linear and nonlinear terms as

$$\mathbf{x}' = J\mathbf{x} + F(\mathbf{x}), \quad \mathbf{x} \in \mathbb{R}^n \tag{1.21}$$

where J is the $n \times n$ matrix for the linear part, and $F(\mathbf{x})$ represents the nonlinear part.

To begin with, one can expand the Equation (1.21) into a series, which becomes

$$\mathbf{x}' = J\mathbf{x} + F_2(\mathbf{x}) + F_3(\mathbf{x}) + \cdots + F_{r-1}(\mathbf{x}) + \mathcal{O}(||\mathbf{x}||^r), \tag{1.22}$$

where $F_i(\mathbf{x}), (i \geqslant 2)$ denotes the i-th order term of the Taylor expansion of $F(\mathbf{x})$.

One aims to find a change-of-coordinate form as $\mathbf{x} = h(\mathbf{y})$ so that

$$Dh(\mathbf{y})\mathbf{y}' = f(h(\mathbf{y})); \tag{1.23}$$

here, $Dh(\mathbf{y})$ represents the derivatives of h with respect to $\mathbf{y}$. If (1.23) becomes linear, then the dynamics has been simplified to the simplest one. Otherwise, one can continue to obtain a series of coordinate transformations which eliminate the relevant terms in the expansion of $F(\mathbf{x})$ from low to high order. In a first step, we rewrite the transformation $\mathbf{x} = h(\mathbf{y})$ as

$$\mathbf{x} = \mathbf{y} + h_2(\mathbf{y}), \tag{1.24}$$

where $h_2(\mathbf{y})$ consists of the near-identity transformation of $\mathbf{y}$. After substituting (1.24) into (1.22), we have

$$\begin{aligned}\mathbf{x}' = (I + Dh_2(\mathbf{y}))\mathbf{y}' =& J(\mathbf{y} + h_2(\mathbf{y})) + F_2(\mathbf{y} + h_2(\mathbf{y})) \\ &+ F_3(\mathbf{y} + h_2(\mathbf{y})) + \cdots + F_{r-1}(\mathbf{y} + h_2(\mathbf{y})) + \mathcal{O}(||\mathbf{y}||^r)\end{aligned} \tag{1.25}$$

where I is the $n \times n$ identity matrix, and $F_2(\mathbf{y}+h_2(\mathbf{y})) = F_2(\mathbf{y}) + \mathcal{O}(||\mathbf{y}||^3) + \mathcal{O}(||\mathbf{y}||^4)$; similarly, the i-th order term is given by

$$F_i(\mathbf{y} + h_2(\mathbf{y})) = F_i(\mathbf{y}) + \mathcal{O}(||\mathbf{y}||^{i+1}) + \cdots + \mathcal{O}(||\mathbf{y}||^{2i}), \tag{1.26}$$

which then gives the equation

$$\mathbf{y}' = (I + Dh_2(\mathbf{y}))^{-1}\Big[J\mathbf{y} + Jh_2(\mathbf{y}) + F_2(\mathbf{y}) + G_3(\mathbf{y}) + \cdots + G_{r-1}(\mathbf{y}) + \mathcal{O}(||\mathbf{y}||^r)\Big] \tag{1.27}$$

where $G_j(\mathbf{y})(j \geqslant 3)$ represents the collection of all $\mathcal{O}(||\mathbf{y}||^j)$ terms due to the transformation (1.24).

For $||\mathbf{y}||$ is small enough, that

$$(I + Dh_2(\mathbf{y}))^{-1} = I - Dh_2(\mathbf{y}) + \mathcal{O}(||\mathbf{y}||^2) \tag{1.28}$$

Substituting (1.28) into (1.27), we then have

$$\mathbf{y}' = J\mathbf{y} + Jh_2(\mathbf{y}) - Dh_2(\mathbf{y})J\mathbf{y} + F_2(\mathbf{y}) + \tilde{G}_3(\mathbf{y}) + \cdots + \tilde{G}_{r-1}(\mathbf{y}) + \mathcal{O}(||\mathbf{y}||^r) \tag{1.29}$$

where $\tilde{G}_j$ represents the collection of all $\mathcal{O}(||\mathbf{y}||^j)$ terms due to the transformation (1.28).

To eliminate the second-order term $\mathcal{O}(||\mathbf{y}||^2)$ in (1.29), one requires the equality

$$Jh_2(\mathbf{y}) - Dh_2(\mathbf{y})J\mathbf{y} + F_2(\mathbf{y}) = 0 \tag{1.30}$$

where $h_2(\mathbf{y})$ of the coordinate transformation (1.23) should satisfy the equality (1.30) so that one can simplify (1.29) by removing the term $F_2(\mathbf{y})$. Such a procedure motivates us to proceed to higher order terms. Before moving to next step, we define the space of vector-valued monomials of degree k as H_k, which has the form

$$H_k = \text{span}\Big\{ \prod y_j^{m_j} e_j \Big\}, \quad \sum_{j=1}^{n} m_j = k \tag{1.31}$$

where the set $\{e_j\}, (j = 1, ..., n)$ represents a basis of $\mathbb{R}^n$.

Recall the equality (1.30), which one can view as a linear map L_J of H_2 to H_2 so that

$$L_J(h_2(\mathbf{y})) = Dh_2(\mathbf{y})J\mathbf{y} - Jh_2(\mathbf{y}) \tag{1.32}$$

Now the set H_k can be written as

$$H_2 = L_J(H_2) \oplus L_2 \tag{1.33}$$

where L_2 refers to the complementary space to $L_J(H_2)$. Solution of the Equation (1.30) exists when $F_2(\mathbf{y}) \in L_J(H_2)$, i.e., $L_J(H_2) = H_2$, that all the second-order terms of $\mathcal{O}(||\mathbf{y}||^2)$ can be removed by the coordinate transformation. Therefore, the new equation contains the linear part and nonlinear terms with order from 3 in $\mathbf{y}$,

$$\mathbf{y}' = J\mathbf{y} + \tilde{G}_3(\mathbf{y}) + \cdots + \tilde{G}_{r-1}(\mathbf{y}) + \mathcal{O}(||\mathbf{y}||^r) \tag{1.34}$$

Similarly, for any $h_k(\mathbf{y}) \in H_k$, we have

$$L_J(h_k(\mathbf{y})) = Dh_k(\mathbf{y})J\mathbf{y} - Jh_k(\mathbf{y}) \tag{1.35}$$

and

$$H_k = L_J(H_k) \oplus L_k \tag{1.36}$$

where L_k refers to the complementary space to $L_J(H_k)$. The k-th order terms can be all eliminated iff $L_J(H_k) = H_k$. The normal form theorem [72] is given

Theorem 1.2. *Let $\mathbf{x}' = f(\mathbf{x})$ be a $\mathcal{C}^r$ system of differential equations with $f(\mathbf{0}) = \mathbf{0}$. Then, there exists a sequence of analytical coordinate changes in the neighbourhood of the origin which transforms the system into a normal form*

$$\mathbf{y}' = J\mathbf{y} + F_2^r(\mathbf{y}) + F_3^r(\mathbf{y}) + \cdots + F_{r-1}^r(\mathbf{y}) + \mathcal{O}(||\mathbf{y}||^r), \tag{1.37}$$

where $F_k^r(\mathbf{y}) \in L_k$, $2 \leqslant k \leqslant r-1$, and L_k is the complementary space to $L_J(H_k)$ with $H_k = L_J(H_k) \oplus L_k$.

***Remark* 1.1.** The $F_k^r(\mathbf{y})$ terms are named as resonant terms which cannot be removed by near-identity changes-of coordinates, and the integer r indicates the order of resonance ,which is obtained by $\sum_{j=1}^{n} m_j$, where $\lambda_i = \sum_{j=1}^{n} m_j \lambda_j$ with eigenvalues λ_j $(j = 1, ..., n)$ of the linear operator $L_J(\cdot)$, i.e., $L_J(\cdot)$ is not invertible with zero eigenvalues. For a detailed analysis and applications of normal forms, please refer to the book by Wiggins [72] and Guckenheimer and Holmes [31].

1.6 Poincaré maps

A Poincaré map is a discrete dynamical system which describes the continuous flow of associated ODEs, the basic idea was first addressed by Poincaré [52]. This technique is usually used for dynamical systems with periodic behaviour where one is interested in the periodic solution instead of the entire flow of the system over time. Consider a system with differential equations

$$\mathbf{x}' = f(\mathbf{x}), \quad \mathbf{x} \in \mathbb{R}^n \tag{1.38}$$

where $f : U \mapsto \mathbb{R}^n$ is $\mathcal{C}^r$-function on the open set $U \subset \mathbb{R}^n$. The solution of (1.38) is given by $\phi(t, \cdot)$. Assume that $\phi(t, \cdot)$ is periodic with period time T, i.e., for $\mathbf{x}_0 \in \mathbb{R}^n$ that $\phi(t + T, \mathbf{x}_0) = \phi(t, \mathbf{x}_0)$ is true. One can define a section Σ which is transversal to the vector field of the system at the point $\mathbf{x}_0$ with dimension $n - 1$. Then the Poincaré map P is given as

$$P : \Sigma \mapsto \Sigma, \quad \mathbf{x} \mapsto \phi(t(\mathbf{x}), x) \tag{1.39}$$

where $t(\mathbf{x})$ is the first return time of the point $\mathbf{x}$ returning to Σ. If $\mathbf{x}_0$ is a fixed point of P, i.e., $\mathbf{x}_0 \in \Sigma$, $P(\mathbf{x}_0) = \mathbf{x}_0$, then the trajectory staring at the point will return to it after time T, which refers to the periodic solution of the original system. If there is a point $\mathbf{x}$ belong to the set $S = \{\mathbf{x}_1, \mathbf{x}_2, ..., \mathbf{x}_k\}$ such that $P^k(\mathbf{x}) = \mathbf{x}$ and $P^j(\mathbf{x}) \in S, (j = 1, 2, ..., k - 1)$, which is known as a period k point of P, the corresponding periodic orbit will pass through Σ for k times before closing. One example of a periodic problem is shown geometrically in Figure 1.4. For more examples see Wiggins [72].

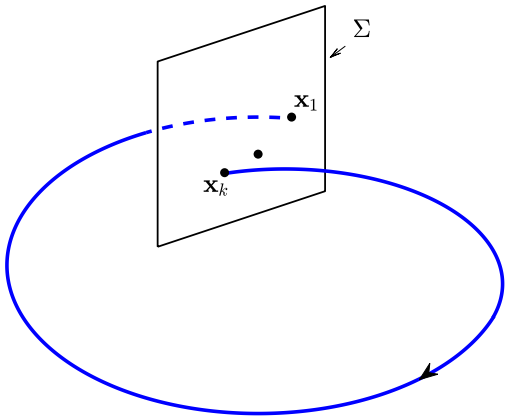

Figure 1.4: The Poincaré map for the analysis of periodic orbits.

Chapter 2

Front propagation in two-component reaction-diffusion systems with a cut-off

2.1 Introduction

The study of front propagation in reaction-diffusion systems has received a significant amount of attention in the past few decades. Frequently, of principal interest is the propagation speed of front solutions that connect various equilibrium states in these systems. In microscopic physics, the underlying numbers of particles are integer-valued; hence, the discrete nature of the underlying models needs to be considered when performing a continuum approximation via reaction-diffusion systems. In particular, the notion of a concentration of particles will be invalid in regimes where no particles exist. Such regimes can be modeled by taking some threshold ε as the concentration when only one particle is present to react. In [9], Brunet and Derrida introduced the basic idea of a cut-off, by including a so-called cut-off function in the reaction kinetics of the Fisher-Kolmogorov-Petrowskii-Piscounov(FKPP) equation [1,22]. They then discussed the effect of such a cut-off on the front propagation speed in FKPP-type systems. They began with one FKPP-type equation in discrete space and time; the numerically simulated results indicated that a logarithmic term was subtracted from the minimal speed obtained by the same equation in the absence of a cut-off. To support this observation, they calculated the leading correction of the traveling wave speed in the modified FKPP equation with a cut-off threshold ε. By applying perturbation techniques and, specifically, matched asymptotics, they found that $v_\varepsilon \sim v_0 - \frac{\pi^2}{(\ln \varepsilon)^2}$; here, the logarithmic term represents the difference to the critical propagation speed v_0 defined in the system without cut-off as simulation had observed.

In 2007, a rigorous asymptotic analysis for proving the shift in the speed of the FKPP equation in the presence of a cut-off was given by Dumortier, Popović, and Kaper [15], via geometric singular perturbation theory [35] and the blow-up technique [14]. They obtained the same expansion of the speed as in [9] for a variety of cut-off functions. Moreover, they addressed the geometric reasons of the structure in the leading order of the speed correction. Meanwhile, Benguria and Depassier [5] obtained similar analytical results with a variational approach in the same year. Most available studies have concluded that the single velocity of front propagation in one-component systems will converge to the critical speed of the corresponding system with no cut-off. However, there has been a lack of research into two-component systems with a cut-off. The analysis of pattern formation arises in two-component non-equilibrium systems [37]. Front solutions in such systems can propagate with various speeds, which leads to more complex dynamics. The general two-component reaction-diffusion model with a cut-off considered in the

present chapter reads

$$\frac{\partial u}{\partial t} = -\gamma_1 u - v + \theta(u-a) + \frac{\partial^2 u}{\partial x^2}, \tag{2.1a}$$

$$\frac{\partial v}{\partial t} = \eta(\gamma_2 u - v) + \alpha\theta(u-a) + D\frac{\partial^2 v}{\partial x^2}. \tag{2.1b}$$

where the parameters $\gamma_1, \gamma_2, \alpha$, the ratio of the time scales η, the ratio of the diffusion coefficients D and the discontinuity position a are constants; here, $\theta(u-a)$ is the standard Heaviside function, with $\theta(u-a) = 1$ for $u \geqslant a$ and $\theta(u-a) = 0$ for $u < a$. Equation (2.1) contains both the so-called Rinzel-Keller kinetics [56] and the Tonnelier-Gerstner kinetics [74] as particular cases:

- For $\alpha > 0$ and $\gamma_2 = 0$, we obtain a sigmoidal system with Tonnelier-Gerstner kinetics. The two-component system with Tonnelier-Gerstner reaction kinetics is one example of the Morris-Lecar model, which is used to illustrate oscillations in the giant muscle fiber of barnacles [67]. Due to its biophysical meaning and the fact that parameters are measurable, it has received increasing attention in the computational neuroscience community [74].

- For $\alpha = 0$, the resulting equations are of classical FitzHugh-Nagumo (FHN) type, with piecewise linear inhibition. While the classical FHN system was modified by Zemskov and Méndez in [75], where they introduced a cut-off function $\theta(u-\varepsilon)$ in the reaction terms with $\gamma_1 = 1$, $\alpha = 0$, and $D = 1$. They derived a relationship for the propagation front speed c with the cut-off threshold ε and the discontinuity position a.

Here, we define the cut-off function by $\theta(\phi - \varepsilon)$, where $\phi = u$ or $\phi = v$, and θ again denotes the Heaviside function. Consider the following two-component system of reaction-diffusion equations with the cut-off,

$$\frac{\partial u(x,t)}{\partial t} = f(u,v)\theta(\phi-\varepsilon) + \frac{\partial^2 u(x,t)}{\partial x^2}, \tag{2.2a}$$

$$\frac{\partial v(x,t)}{\partial t} = g(u,v)\theta(\phi-\varepsilon) + D\frac{\partial^2 v(x,t)}{\partial x^2} \tag{2.2b}$$

with what is known as (piecewise linear) Tonnelier-Gerstner kinetics [74], whereby $f(u,v) = -u - v + \theta(u-a)$ and $g(u,v) = -\eta v + \alpha\theta(u-a)$, as shown in Figure 2.1. Here, ε is assumed to be small and positive.

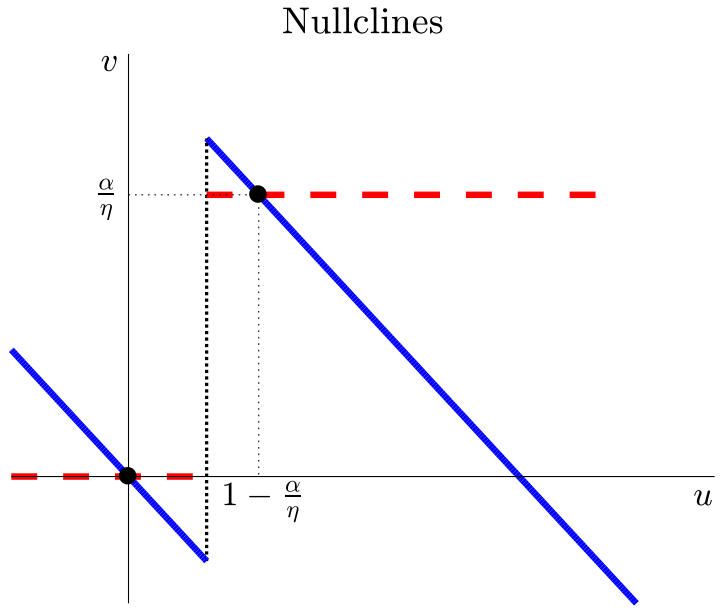

Figure 2.1: Nullclines of $f(u,v) = -u - v + \theta(u-a) = 0$ (solid blue) and $g(u,v) = -\eta v + \alpha\theta(u-a) = 0$ (dashed red).

We study propagating front solutions to Equation (2.2); to that end, we introduce the traveling wave variable $\xi = x - ct$, with $c > 0$ denoting the front propagation speed. Substituting into (2.2), we obtain the pair of second-order ordinary differential equations

$$u'' + cu' + f(u,v)\theta(\phi - \varepsilon) = 0, \tag{2.3a}$$
$$Dv'' + cv' + g(u,v)\theta(\phi - \varepsilon) = 0, \tag{2.3b}$$

where the prime denotes differentiation with respect to ξ. Introducing the new variables $w = u'$ and $z = v'$ in (2.3), we find the four-dimensional first-order system

$$u' = w, \tag{2.4a}$$
$$v' = z, \tag{2.4b}$$
$$w' = -cw - f(u,v)\theta(\phi - \varepsilon), \tag{2.4c}$$
$$z' = -\frac{c}{D}z - \frac{1}{D}g(u,v)\theta(\phi - \varepsilon), \tag{2.4d}$$

which will be the starting point for our analysis. In the absence of a cut-off, Equation (2.4) has the steady states $Q^+ = (0,0,0,0)$ and $Q^- = (1 - \frac{\alpha}{\eta}, \frac{\alpha}{\eta}, 0, 0)$, both with the same eigenvalues $\lambda_{1,2} = \frac{1}{2}(-c \pm \sqrt{c^2+4})$, $\lambda_{3,4} = \frac{1}{2D}(-c \pm \sqrt{c^2 + 4D\eta})$. The front solution connecting $Q^-(\xi \to -\infty)$ to $Q^+(\xi \to \infty)$ will generate the discontinuity position a as a function of the front speed c,

$$a(c) = (1 - \frac{\alpha}{\eta})\frac{\lambda_1}{\lambda_1 - \lambda_2} - \frac{\alpha}{\eta}\frac{1}{(\lambda_1 - \lambda_2)(\lambda_3 - \lambda_4)}\Big[\frac{\lambda_3}{\mu_4}(\lambda_2 - \lambda_4) - \frac{\lambda_4}{\mu_3}(\lambda_1 - \lambda_3)\Big],$$

where $\mu_j = \lambda_j^2 + c\lambda_j - 1$, $(j = 3, 4)$; for details see [74].

The study of Equation (2.4) is naturally performed in three regions I, II, and III, which are defined by

Region I:	$\{a < u < 1,\ \phi > \varepsilon\}$
Region II:	$\{u < a,\ \phi > \varepsilon\}$
Region III:	$\{u < a,\ 0 < \phi < \varepsilon\}$

Our analysis of Equation (2.4) is motivated by the study of the FKPP model in [15]; there, a rigorous geometric analysis was derived for the FKPP equation with a cut-off, where the blow-up technique was applied to obtain a complete desingularisation of the flow around the degenerate fixed point. While Equation (2.4) is also a cut-off problem, it is more complicated: see Equation (2.4), the two-component system has a higher dimension than one one-component after transformation to travelling wave ODEs; here, we have a 2-dimensional stable and unstable manifold, which increases the difficulty in constructing the geometry. Therefore, our results on two-component reaction-diffusion systems with a cut-off improve the understanding of the cut-off effect on multi-species systems. The present chapter is intended to showcase how a classical asymptotic analysis of cut-off reaction-diffusion dynamics can be re-interpreted within the framework of dynamical systems theory; in particular, the structure of the corresponding heteroclinic orbit in the equivalent blown-up space depends significantly on the speed c and diffusion ratio D. Our analysis will rely on the blow-up technique in its formulation due to [14], which was first applied in the study of limit cycles near a cuspidal loop in planar vector fields [18]. The technique has since been applied in a variety of situations; it allows for an extension of the classical geometric singular perturbation theory [35] past non-hyperbolic singularities. Specifically, blow-up has allowed for a resolution of the effects of a cut-off in reaction-diffusion systems; see [15,16,54,55]. We remark that, in that context, blow-up resolves the discontinuities in the corresponding vector fields that may be induced by a cut-off.

The main result of our analysis can be summarised as follows

Principal Result 1. *Let $\varepsilon \in (0, \varepsilon_0)$, with ε_0 positive and sufficiently small, and let $\phi = v$, $\eta = 0.12$ and $\alpha = 0.08$ be fixed. Then,*

i. There exists a family of traveling front solutions of Equation (2.2) propagating between Q^- and Q^+ with corresponding c-a relation $a_\varepsilon(c)$ with maximum speed $c_{max} = (\alpha - \eta\varepsilon)\sqrt{\frac{D}{\alpha\varepsilon}}$ obtained by formal linearisation that region II vanishes, and c_{max} tends to ∞ as $\varepsilon \to 0$.

ii. There also exists a critical value of the speed c_{crit} represents the intersection of curves of $a_\varepsilon(c)$ and $a_0(c)$ such that $a_\varepsilon(c) - a_0(c)|_{c=c_{crit}} = 0$.

iii. In panel (a) of Figure 2.2, there exists a saddle-node bifurcation in the c-a relation curve for $D \in (1, D^*)$, the node point labeled by (a_b, c_b); note, $D^* \approx 5.1287$ is obtained by $da_0(c)/dc = 0$. For $a < a_b$, the traveling fronts with speeds $c > c_b$ are stable, while for $c < c_b$, the corresponding fronts are unstable; two branches merge at $a = a_b$, while for $a > a_b$, no front solutions exist. In particular, the cut-off accelerates the front for $c \in \{(0, c_b) \bigcup (c_{crit}, c_{max})\}$; slows down the front in $c \in (c_b, c_{crit})$.

iv. In panel (b) of Figure 2.2, no bifurcation occurs for $D \in (D^*, 22)$, the cut-off accelerates the front for $c \in (0, c_{crit})$; slows down the front for $c \in (c_{crit}, c_{max})$.

v. For c fixed, cut-off pushes down the discontinuity position a corresponding to the singular front solution for $c \in (0, c_{crit})$, pulls up the position in $c \in (c_{crit}, c_{max})$.

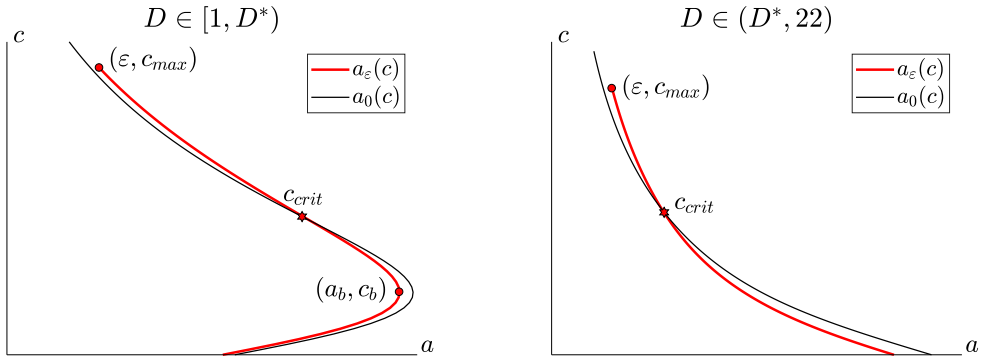

(a) (b)

Figure 2.2: The illustration of c-a relation: the perturbed solution $a_\varepsilon(c)$ (red) and the singular solution (thin black). (a) one bifurcation. (b) no bifurcations.

The proof of Principal Result 1 is organized as follows. In Section 2.2, we reproduce some basic properties of Equation (2.4) in the absence of a cut-off: we restrict the flow to the 2-dimensional unstable manifold in the "outer" region, see Section 2.2.1; similarly, we restrict the flow to the 2-dimensional stable manifold in the "inner" region, see Section 2.2.2; then, we discuss the two feasible types of trapping region around the origin depending on the speed c and the diffusion ratio D, see Section 2.2.2.1, where for considering $D \geqslant 1$ throughout our analysis, the orbit is tangent to the weak-stable eigendirection around Q^+, which lies in the second quadrant in the (u, v)-phase space. In Section 2.2.3, we investigate the cut-off affected region of the u-component and the v-component cut-off systems. Then, we mainly focus on the geometric analysis of the v-component cut-off system, as the related orbit remains in a neighborhood of Q^+, where the blow-up technique is applied with no restrictions. The dynamics in the three regions are illustrated in Section 2.3, where we establish the local and global geometric structure of the singular orbit as well as the perturbed orbits in different ranges of the speeds. For a detailed derivation, we study the transition in chart K_1 via a normal form transformation in Section 2.4: in Section 2.4.2, we start with the formal linearisation in region II in chart K_1, find the general solution by patching the boundaries and obtain the corresponding c-a relation $a_\varepsilon(c)$, which is actually an implicit formulae; we prove the existence of $a_0(c)$ and persistence by the Implicit Function Theorem. In particular, we observe the bifurcation scenarios in the c-a relation and investigate the corresponding geometry in Section 2.4.3. To improve the accuracy of our method, we proceed to a second-order normal form transformation in Section 2.4.4. In Section 2.5, we perform the simulation, comparison and discussion of our results obtained in the previous sections. We also discuss some results of the u-component cut-off system in Section 2.6, which are obtained in a similar fashion as for the v-component problem; the details are attached in Appendix A.3. In Section 2.7, we conclude with a summary of our observations on the effect of a cut-off.

***Remark* 2.1.** As we only consider front solutions in Equation (2.2), we need to restrict the parameters α, η and the discontinuity position a in order to ensure that two steady states exist, which implies the existence of a heteroclinic connection between the two states. We then get a related range for a, with $a \in (0, 1 - \frac{\alpha}{\eta})$; see Figure 2.1. When $a > 1 - \frac{\alpha}{\eta}$, there is only one trivial steady state at the origin, and for $a < 0$, there is a single non-trivial steady state.

2.2 Basic properties

We begin by reproducing some basic properties of Equation (2.4) in the absence of a cut-off, where the governing equations read

$$u' = w, \tag{2.5a}$$
$$v' = z, \tag{2.5b}$$
$$w' = -cw + u + v - \theta(u-a), \tag{2.5c}$$
$$z' = -\frac{c}{D}z + \frac{\eta}{D}v - \frac{\alpha}{D}\theta(u-a). \tag{2.5d}$$

We consider travelling front solutions propagating from $Q^- = (1-\frac{\alpha}{\eta}, \frac{\alpha}{\eta}, 0, 0)$ when $\xi \to -\infty$ to $Q^+ = (0,0,0,0)$ when $\xi \to +\infty$. The general solution to (2.5) can be written in the standard Ansatz of the form $u = Ae^{\lambda\xi}$ and $v = Be^{\lambda\xi}$ in the "outer" region and "inner" region, which are denoted by $\{u > a\}$ and$\{u < a\}$, respectively. Here, λ denotes one of the four possible eigenvalues of the corresponding linearisation of (2.5).

The following result is obtained by a straightforward calculation:

Lemma 2.1. *The steady states $Q^+ = (0,0,0,0)$ and $Q^- = (1-\frac{\alpha}{\eta}, \frac{\alpha}{\eta}, 0, 0)$ of Equation (2.5)are hyperbolic saddle points. Both have eigenvalues $\lambda_i\,(i = 1, ..., 4)$, with $\lambda_1 = \frac{1}{2}(-c+\sqrt{c^2+4})\,(+)$, $\lambda_2 = \frac{1}{2}(-c-\sqrt{c^2+4})\,(-)$, $\lambda_3 = \frac{1}{2D}(-c+\sqrt{c^2+4D\eta})\,(+)$ and $\lambda_4 = \frac{1}{2D}(-c-\sqrt{c^2+4D\eta})\,(-)$, here the eigenvalues λ_1 and λ_3 are positive, while λ_2 and λ_4 are negative. The corresponding eigenvectors $\mathbf{v}_1 = \big(1,0,\lambda_1,0\big)^T$, $\mathbf{v}_2 = \big(1,0,\lambda_2,0\big)^T$, $\mathbf{v}_3 = \big(1,\mu_3,\lambda_3,\mu_3\lambda_3\big)^T$ and $\mathbf{v}_4 = \big(1,\mu_4,\lambda_4,\mu_4\lambda_4\big)^T$, respectively, where $\mu_j = \lambda_j^2 + c\lambda_j - 1$, $(j = 3, 4)$.*

The dynamics in the "outer" region $\{u > a\}$ can be restricted to the 2-dimensional unstable manifold at Q^-, where the general solution is expressed in the positive eigenvalues λ_1 and λ_3, while the dynamics in the "inner" region $\{u < a\}$ can be restricted to the 2-dimensional stable manifold at Q^+ where the general solution is expressed in the negative eigenvalues λ_2 and λ_4. In other words, the orbit leaving at Q^- flows along the unstable eigendirections and passes through the discontinuity point $u = a$, then to be attracted to the point Q^+ via the 2-dimensional stable eigendirections; for details see Appendix A.2 or [74].

2.2.1 Dynamics in the "outer" region

In the "outer" region, where $u > a$, Equation (2.5) reduces to

$$u' = w, \tag{2.6a}$$
$$v' = z, \tag{2.6b}$$
$$w' = -cw + u + v - 1, \tag{2.6c}$$
$$z' = -\frac{c}{D}z + \frac{\eta}{D}v - \frac{\alpha}{D}, \tag{2.6d}$$

as $\theta(u-a) \equiv 1$ in that region.

Our aim in the present section is to describe the flow of Equation (2.6); to that end, we will derive an expression for the unstable manifold $\mathcal{W}^{\mathrm{u}}(Q^-)$, where we recall that $Q^- = (1-\frac{\alpha}{\eta}, \frac{\alpha}{\eta}, 0, 0)$ denotes the unique steady state of (2.6). Then, we will restrict Equation (2.6) to that manifold, as any traveling front solution to the corresponding system of reaction-diffusion equations defined in (2.2) must leave a neighborhood of Q^- along $\mathcal{W}^{\mathrm{u}}(Q^-)$. We have the following result:

Proposition 2.1. *The unstable manifold $\mathcal{W}^{\mathrm{u}}(Q^-)$ can be written as a graph over (u, v), with*

$$w(u,v) = \lambda_1\Big(u - 1 + \frac{\alpha}{\eta}\Big) + \frac{\lambda_3 - \lambda_1}{\mu_3}\Big(v - \frac{\alpha}{\eta}\Big) \quad \textit{and} \tag{2.7a}$$
$$z(u,v) = \lambda_3\Big(v - \frac{\alpha}{\eta}\Big); \tag{2.7b}$$

here, $\lambda_1 = \frac{1}{2}(-c + \sqrt{c^2+4})$ *and* $\lambda_3 = \frac{1}{2D}(-c + \sqrt{c^2 + 4D\eta})$ *denote the positive eigenvalues of Equation* (2.6) *at* Q^-*. The restriction of the flow of* (2.6) *to* $\mathcal{W}^{\mathrm{u}}(Q^-)$ *reads*

$$u(\xi) = A_2 \mathrm{e}^{\lambda_1 \xi} + \frac{A_1}{\mu_3} \mathrm{e}^{\lambda_3 \xi} + 1 - \frac{\alpha}{\eta}, \tag{2.8a}$$

$$v(\xi) = A_1 \mathrm{e}^{\lambda_3 \xi} + \frac{\alpha}{\eta}, \tag{2.8b}$$

with $\mu_3 = \lambda_3^2 + c\lambda_3 - 1$*, where* $A_1 < 0$ *and* A_2 *are coefficients that are as yet undetermined.*

Proof. For the sake of simplicity, we first shift the steady state at Q^- to the origin: introducing the new variables $\hat{u}$ and $\hat{v}$ via $u = 1 - \frac{\alpha}{\eta} + \hat{u}$ and $v = \frac{\alpha}{\eta} + \hat{v}$, respectively, and rewriting (2.6) accordingly, we find

$$\hat{u}' = w, \tag{2.9a}$$

$$\hat{v}' = z, \tag{2.9b}$$

$$w' = -cw + \hat{u} + \hat{v}, \tag{2.9c}$$

$$z' = -\frac{c}{D} z + \frac{\eta}{D} \hat{v}. \tag{2.9d}$$

The eigenvalues and eigenvectors of (the linear system in) Equation (2.9) are given by λ_i and $\mathbf{v}_1$ $(i = 1, ..., 4)$, respectively, in Lemma 2.1.

The unstable manifold $\widehat{\mathcal{W}}^{\mathrm{u}}(\mathbf{0})$ is most easily determined by diagonalising Equation (2.9): defining the change-of-variable matrix $\mathbf{P} = [\mathbf{v}_1|\mathbf{v}_2|\mathbf{v}_3|\mathbf{v}_4]$, we write $\mathbf{u} = \mathbf{P}\mathbf{x}$, where $\mathbf{u} = (\hat{u}, \hat{v}, w, z)^T$ and $\mathbf{x} = (x_1, x_2, x_3, x_4)^T$. One easily sees that, in terms of the new variable $\mathbf{x}$, Equation (2.9) becomes $\mathbf{x}' = \mathrm{diag}(\lambda_1, \lambda_2, \lambda_3, \lambda_4)\mathbf{x}$. Since, clearly, λ_1 and λ_3 are positive, while λ_2 and λ_4 are negative, the manifold $\mathcal{W}^{\mathrm{u}}(\mathbf{0})$ is expressed as $\{x_2 = 0 = x_4\}$ in $\mathbf{x}$-space which, together with $\mathbf{u} = \mathbf{P}\mathbf{x}$, implies

$$\begin{aligned} \hat{u} &= x_1 + x_3, \\ \hat{v} &= \mu_3 x_3, \\ w &= \lambda_1 x_1 + \lambda_3 x_3, \\ z &= \mu_3 \lambda_3 x_3. \end{aligned}$$

Solving the above relations for $w(\hat{u}, \hat{v})$ and $z(\hat{u}, \hat{v})$ and reverting to the original variables u and v, we find Equation (2.7), as claimed.

Next, we substitute Equation (2.7) into (2.6), which allows us to describe the flow on $\mathcal{W}^{\mathrm{u}}(Q^-)$ in terms of (u, v) only:

$$\begin{aligned} u' &= \lambda_1 \Big(u - 1 + \frac{\alpha}{\eta} \Big) + \frac{\lambda_3 - \lambda_1}{\mu_3} \Big(v - \frac{\alpha}{\eta} \Big), \\ v' &= \lambda_3 \Big(v - \frac{\alpha}{\eta} \Big). \end{aligned}$$

Solving, we obtain the general solution for the flow of (2.6) on $\mathcal{W}^{\mathrm{u}}(Q^-)$, as stated in Equation (2.8). □

2.2.2 Dynamics in the "inner" region

In the "inner" region, where $u < a$, Equation (2.5) reduces to

$$u' = w, \tag{2.10a}$$

$$v' = z, \tag{2.10b}$$

$$w' = -cw + u + v, \tag{2.10c}$$

$$z' = -\frac{c}{D} z + \frac{\eta}{D} v, \tag{2.10d}$$

as $\theta(u-a) \equiv 0$ in that region; where we recall that $Q^+ = (0,0,0,0)$ denotes the unique steady state of (2.10). We have the following results:

Proposition 2.2. *The stable manifold $\mathcal{W}^{\mathrm{s}}(Q^+)$ can be written as a graph over (u,v), with*

$$w(u,v) = \lambda_2 u + \frac{\lambda_4 - \lambda_2}{\mu_4} v \quad \textit{and} \tag{2.11a}$$

$$z(u,v) = \lambda_4 v; \tag{2.11b}$$

here, $\lambda_2 = \frac{1}{2}(-c - \sqrt{c^2+4})$ and $\lambda_4 = \frac{1}{2D}(-c - \sqrt{c^2 + 4D\eta})$ denote the negative eigenvalues of Equation (2.6) at Q^+. The restriction of the flow of (2.6) to $\mathcal{W}^{\mathrm{s}}(Q^+)$ reads

$$u(\xi) = B_2 \mathrm{e}^{\lambda_2 \xi} + \frac{B_1}{\mu_4} \mathrm{e}^{\lambda_4 \xi}, \tag{2.12a}$$

$$v(\xi) = B_1 \mathrm{e}^{\lambda_4 \xi}, \tag{2.12b}$$

with $\mu_4 = \lambda_4^2 + c\lambda_4 - 1$, where $B_1 > 0$ and B_2 are coefficients that are as yet undetermined.

Proof. The derivation of Equation (2.11) is analogous to that of Equation (2.7), the details are hence omitted. Substituting Equation (2.11) into (2.10), we obtain the flow on $\mathcal{W}^{\mathrm{s}}(Q^+)$ in terms of (u,v) only:

$$u' = \lambda_2 u + \frac{\lambda_4 - \lambda_2}{\mu_4} v, \tag{2.13a}$$

$$v' = \lambda_4 v. \tag{2.13b}$$

Solving, we find the general solution for the flow of (2.10) on $\mathcal{W}^{\mathrm{s}}(Q^+)$, as stated in Equation (2.12). □

2.2.2.1 Orbits behavior

The existence of orbits connecting Q^- and Q^+ is guaranteed by patching method, cf. Appendix A.2 or [74]. Here, we discuss the qualitative orbits near the origin. To that end, we construct a trapping region of (2.13) in the "inner" region, and show that the completed orbit starting at Q^- along the unstable manifold $\mathcal{W}^{\mathrm{u}}(Q^-)$ must enter it and approach Q^+ inside it. Here, we keep the notation of steady states $Q^{\pm}$ with $Q^+ = (0,0)$ in the (u,v)-phase plane, which is a stable node as defined in Equation (2.13). The boundaries of the trapping region consist of one of the stable eigendirections and one of the nullclines; there exists two structures of trapping region as the corresponding strong/weak eigendirections may switch roles in terms of the speed c and diffusion ratio D. To distinguish the strong/weak eigendirections, we obtain the critical curve in (c,D) with the criteria: $\lambda_2 = \lambda_4$, where the two stable eigendirections merge together into a single direction, which is equivalent to $\mu_4 = 0$, i.e., $c = \frac{D-\eta}{(1-D)(1-\eta)}$; see Figure 2.3. Resonance takes place along the curve; in particular, for $D \geqslant 1$, there is no resonance. Moreover, our construction of the trapping region helps to check if u will become negative.

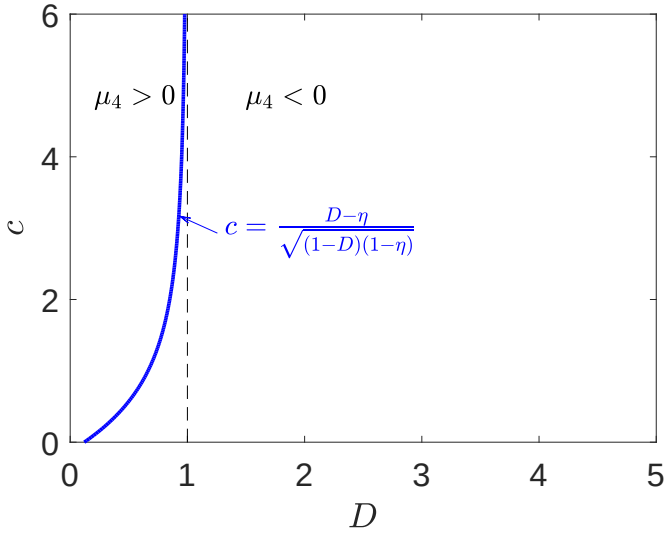

Figure 2.3: The critical curve in (c, D): $\lambda_2 = \lambda_4$ (blue), i.e., $\mu_4 = 0$ $\left(c = \frac{D-\eta}{(1-D)(1-\eta)}\right)$.

We have the following results:

i. Trapping region T_1: $\lambda_2 < \lambda_4$ and $\mu_4 < 0$. The upper boundary is given by the nullcline of $u' = 0$, i.e., the line $\lambda_2 u + \frac{\lambda_4 - \lambda_2}{\mu_4} v = 0$, where $v' < 0$ for $v \in (0, \frac{\alpha}{\eta})$ implies that the vector field points downward into the trapping region. The lower boundary is the line corresponding to the weak-stable eigendirection with eigenvalue λ_4, i.e., the line $\mu_4 u - v = 0$. As the derivative of the line is given by $(\mu_4 u - v)' = \lambda_2(\mu_4 u - v)$, the vector field points outwards perpendicularly to the line, which is pointing into the trapping region for $v \in (0, \frac{\alpha}{\eta})$. Hence, orbits flowing along the 2-dimensional $\mathcal{W}^{\mathrm{u}}(Q^-)$ at $u = a$ must enter the trapping region T_1 on $\mathcal{W}^{\mathrm{s}}(Q^+)$ and approach Q^+ in weak-stable eigendirection, see Figure 2.6.

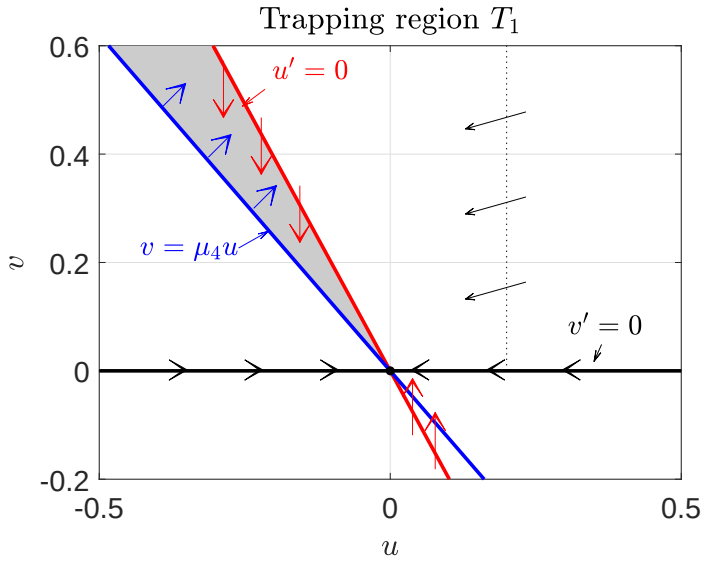

Figure 2.4: Trapping region T_1: $\lambda_2 < \lambda_4$ and $\mu_4 < 0$. The upper boundary: the nullcline of $u' = 0$ (red); the lower boundary: the weak-stable eigendirection (blue).

ii. Trapping region T_2: $\lambda_2 > \lambda_4$ and $\mu_4 > 0$. The upper boundary is the line corresponding to the strong-stable eigendirection with eigenvalue λ_4, i.e., the line $\mu_4 u - v = 0$. As the derivative of the line is given by $(\mu_4 u - v)' = \lambda_2(\mu_4 u - v)$, the vector field points outwards

perpendicularly to the line, which is pointing into the trapping region for $v \in (0, \frac{\alpha}{\eta})$. The lower boundary is given by the nullcline of $v' = 0$, i.e., the line $v = 0$, where $u' < 0$ for $u \in (0, 1)$ implies that the vector field points leftward into the trapping region; noting that $v = 0$ also represents the weak-stable eigendirection with eigenvalue λ_2. Hence, orbits flowing along the 2-dimensional $\mathcal{W}^{\mathrm{u}}(Q^-)$ at $u = a$ must enter the trapping region T_2 on $\mathcal{W}^{\mathrm{s}}(Q^+)$ and approach Q^+ in weak-stable eigendirection.

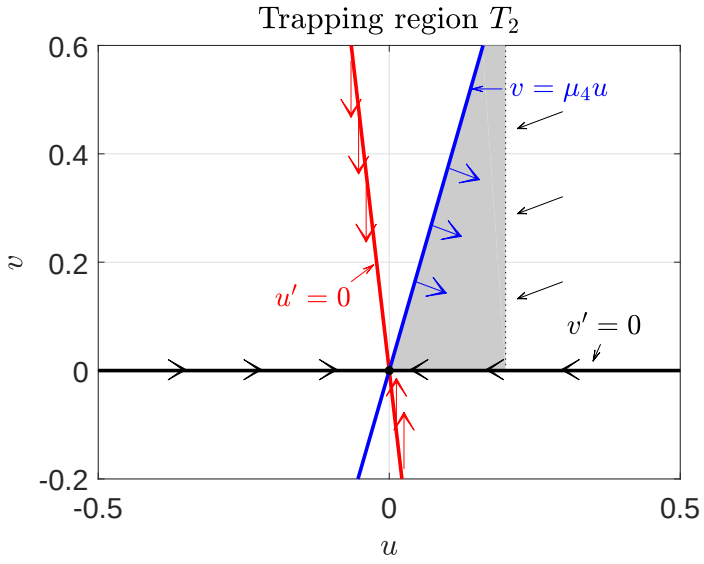

Figure 2.5: Trapping region T_2: $\lambda_2 > \lambda_4$ and $\mu_4 > 0$. The upper boundary: the strong-stable eigendirection (blue), ; the lower boundary: the nullcline of $v' = 0$ (the weak-stable eigendirection) (black).

In this chapter, we consider the case that $D \geqslant 1$, which leads to $\lambda_2 < \lambda_4$ and $\mu_4 < 0$ for all speeds c, where the trapping region is same as shown in Figure 2.4 for $c \in (0, \infty)$. Then we have

Lemma 2.2. *Orbits are connected at $u = a$ between the "outer " region and "inner" region; they leave the state Q^- and flow along the 2-dimensional unstable manifold $\mathcal{W}^{\mathrm{u}}(Q^-)$ to approach the state Q^+ along the 2-dimensional stable manifold $\mathcal{W}^{\mathrm{s}}(Q^+)$. The segment of orbits in a neighborhood of Q^+ is tangent to the weak-stable direction with eigenvalue λ_4 for all $c > 0$ with $D \geqslant 1$, where the corresponding values of the u-variable are negative.*

2.2.3 Preliminaries

By Lemma 2.2, the 2-dimensional stable manifold $\mathcal{W}^{\mathrm{s}}(Q^+)$ of Equation (2.13) is trapped in the second quadrant in (u, v)-phase space, where the value of the u-component is negative. There are two feasible choices of cut-off component: the u-component or the v-component. By setting ε small, e.g., $\varepsilon = 0.05$, we can see the affected region of a cut-off on the orbits of (2.5) in Figure 2.6, which are numerically computed by general patching solution see Appendix A.2 with speed $c = 0.1$, 0.5, 1, 1.5, and 2, .

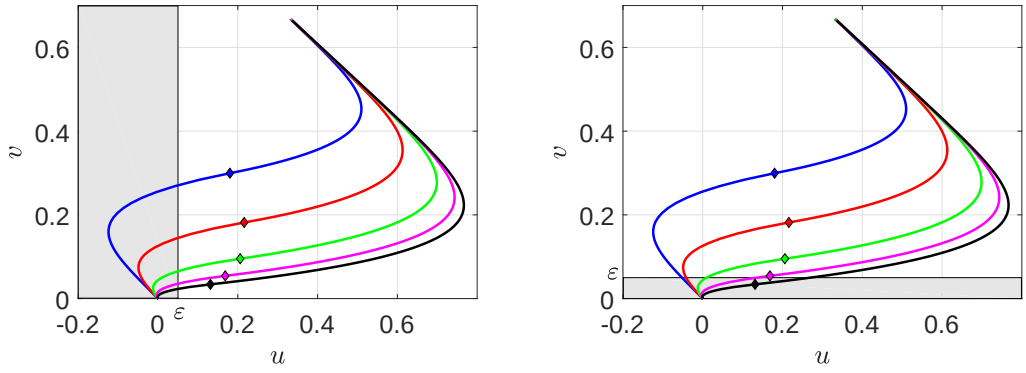

Figure 2.6: The orbits of (2.5) in (u, v)-phase space by general patching (see Appendix A.2) with speed $c = 0.1,\ 0.5,\ 1,\ 1.5,\ 2$ from top to bottom; the affected region of cut-off with $\varepsilon = 0.05$: (a)u-component, (b)v-component.

Panel (a) in Figure 2.6 displays the affected region of the u-component cut-off, i.e., $\phi = u$. For ε small, e.g. $\varepsilon = 0.05$, the values of the u-variable are of the order of ε, while the values of the v-variable vary with the speed c; for instance, when the speed $c = 0.1$ and $c = 0.5$, the corresponding values of the v-variable are much greater than 0.1, which is definitely greater than ε. In the limit as $\varepsilon \to 0$, the values of the v-variable are not as small as the u-variable, which suggests a failure in the application of the blow-up technique, as we are going to blow up in the neighborhood of the origin (Q^+). In order to approach this u-component cut-off system via geometric desingularisation, we need to make an extra condition such that the values of the (u, v)-variables are both small and inside the blown-up space; for details see Section 2.6.

Panel (b) in Figure 2.6 displays the affected region of the v-component cut-off, i.e., $\phi = v$. For ε small, e.g. $\varepsilon = 0.05$, the values of the v-variable are of the order of ε, while the values of the u-variable are negative, in particular, for the values of $c \in (0.1, 2)$, the corresponding absolute values of the u-variable seems as small as the v-variable. In the limit as $\varepsilon \to 0$, the point at the cut-off approaches Q^+, which suggests no extra restriction in the application of the blow-up technique, as the values of the (u, v)-variables remain in a neighborhood of Q^+. Hence, we mainly focus on the v-component cut-off system to showcase how a classical asymptotic analysis of cut-off reaction-diffusion dynamics can be re-interpreted within the framework of dynamical systems theory; for details see the following sections.

2.3 Geometric analysis of the v-component cut-off system

In this section, we desingularise the dynamics in a neighborhood of the origin of Equation (2.4) with $\phi = v$. To that end, we append the trivial equation $\varepsilon' = 0$ in (2.4);

$$u' = w, \tag{2.14a}$$
$$v' = z, \tag{2.14b}$$
$$w' = -cw - f(u, v)\theta(v - \varepsilon), \tag{2.14c}$$
$$z' = -\frac{c}{D}z - \frac{1}{D}g(u, v)\theta(v - \varepsilon), \tag{2.14d}$$
$$\varepsilon' = 0. \tag{2.14e}$$

The steady states of (2.14), which are denoted by Q_ε^+ and Q_ε^-, respectively, are found at $(0, 0, 0, 0, \varepsilon)$ and $(1 - \frac{\alpha}{\eta}, \frac{\alpha}{\eta}, 0, 0, \varepsilon)$ where ε is fixed and $\varepsilon \in [0, \varepsilon_0]$ with ε_0 suitably small; we also define the corresponding lines of steady states: $\ell^+ = \{(0, 0, 0, 0, \varepsilon) \,|\, \varepsilon \in [0, \varepsilon_0]\}$ and $\ell^- = \{(1 - \frac{\alpha}{\eta}, \frac{\alpha}{\eta}, 0, 0, \varepsilon) \,|\, \varepsilon \in [0, \varepsilon_0]\}$. The traveling front solution of (2.14) that connects Q_ε^- to Q_ε^+ corresponds to the connection between Q^- and Q^+ in Equation (2.4). In particular, the point

Q_ε^+ on ℓ^+ corresponding to Q^+ of Equation (2.4) is non-hyperbolic, as a double zero eigenvalue occurs due to the cut-off term $\theta(v-\varepsilon)$. Hence, we apply the blow-up technique, which can resolve the degeneracy at the point Q_ε^+ and regularize the dynamics in its neighborhood, where we can use standard dynamical system theory. We will construct a singular heteroclinic orbit Γ connecting Q_0^- and Q_0^+ in (2.14). Then, we will motivate the persistence of that orbit for ε positive and small. As mentioned before, the phase space of (2.14) is divided into three regions, I, II, and III, where the transition between regions I and III corresponds to the intermediate region II.

Therefore, the dynamics of the v-component cut-off system is best studied in an equivalent formulation of Equation (2.14) that results from a blow-up transformation of the corresponding vector field near the origin in (u,v,w,z,ε)-space. In a first step, we define the homogeneous blow-up transformation

$$u=\bar{r}\bar{u},\ v=\bar{r}\bar{v},\ w=\bar{r}\bar{w},\ z=\bar{r}\bar{z},\ \text{and}\ \varepsilon=\bar{r}\bar{\varepsilon}. \tag{2.15}$$

We will require two coordinate charts K_1 and K_2 here, which are obtained for $\bar{v}=1$ and $\bar{\varepsilon}=1$, respectively; hence, (2.15) yields

$$u=r_1u_1,\ v=r_1,\ w=r_1w_1,\ z=r_1z_1,\ \text{and}\ \varepsilon=r_1\varepsilon_1 \tag{2.16}$$

and

$$u=r_2u_2,\ v=r_2v_2,\ w=r_2w_2,\ z=r_2z_2,\ \text{and}\ \varepsilon=r_2, \tag{2.17}$$

respectively, for the coordinates in these charts. The change-of-coordinates transformation $\mathcal{K}_{12}$ between charts K_1 and K_2 is given by

$$\mathcal{K}_{12}:\ (u_1,r_1,w_1,z_1,\varepsilon_1)\mapsto\Big(\frac{u_2}{v_2},r_2v_2,\frac{w_2}{v_2},\frac{w_2}{v_2},\frac{z_2}{v_2},\frac{1}{v_2}\Big), \tag{2.18}$$

whereas its inverse $\mathcal{K}_{21}=\mathcal{K}_{12}^{-1}$ reads

$$\mathcal{K}_{21}:\ (u_2,v_2,w_2,z_2,r_2)\mapsto\Big(\frac{u_1}{\varepsilon_1},\frac{1}{\varepsilon_1},\frac{w_1}{\varepsilon_1},\frac{z_1}{\varepsilon_1},r_1\varepsilon_1\Big). \tag{2.19}$$

We define several sections for the flow of Equation (2.14) – or, rather, of the corresponding blown-up systems in charts K_1 and K_2:

$$\Sigma_1^{\text{in}}:=\Big\{(\frac{a}{\rho},\rho,w_1,z_1,\varepsilon_1)\ \Big|\ w_1\in[w_*,w^*],\ z_1\in[z_*,z^*],\ \text{and}\ \varepsilon_1\in[0,1]\Big\}, \tag{2.20a}$$

$$\Sigma_1^{\text{out}}:=\Big\{(u_1,r_1,w_1,z_1,1)\ \Big|\ u_1\in[u_*,u^*],\ r_1\in[0,v^*],\ w_1\in[w_*,w^*],\ \text{and}\ z_1\in[z_*,z^*]\Big\}, \tag{2.20b}$$

$$\Sigma_2^{\text{in}}:=\Big\{(u_2,1,w_2,z_2,r_2)\ \Big|\ u_2\in[u_*,u^*],\ w_2\in[w_*,w^*],\ z_2\in[z_*,z^*],\ \text{and}\ r_2\in[0,\varepsilon_0]\Big\}. \tag{2.20c}$$

Here, $\rho,u_*,u^*,v_*,\ v^*,\ w_*,\ w^*,\ z_*$, and z^* are suitably chosen constants; we remark that, by (2.19), the range for (u_2,w_2,z_2) may be chosen identical to that for (u_1,w_1,z_1), as $\varepsilon_1=1$ in $\Sigma_2^{\text{in}}=\mathcal{K}_{12}(\Sigma_1^{\text{out}})$. Moreover, the sections Σ_1^{in} and Σ_1^{out} clearly correspond to the respective boundaries between regions I and II and between regions II and III, when expressed in chart K_1; recall Section 2.1.

***Remark* 2.2.** For any object $\square$ given in the original (u,v,w,z,ε)-variables, we denote the corresponding blown-up object by $\bar{\square}$. Moreover, in chart K_i $(i=1,2)$, that object will be denoted by $\square_i$.

***Remark* 2.3.** The blow-up transformation defined in (2.15) is homogeneous in $\bar{r}$. In general, one may make a quasi-homogeneous Ansatz of the form $u=\bar{r}^{\alpha_1}\bar{u}$, $v=\bar{r}^{\alpha_2}\bar{v}$, $w=\bar{r}^{\alpha_3}\bar{w}$, $z=\bar{r}^{\alpha_4}\bar{z}$, and $\varepsilon=\bar{r}^{\alpha_5}\bar{\varepsilon}$, where α_i $(i=1,\dots,5)$ are positive integers; see e.g. [14]. The integers α_i are determined by finding a distinguished limit in the resulting rescaling chart, i.e.,

by balancing powers of $\bar{r}$ there. An alternative, more systematic approach is produced by the method of Newton Polygons [10]. Here, a homogeneous blow-up, with $\alpha_i = 1$ throughout, is naturally suggested by the observation that the reaction kinetics in Equation (2.4) is piecewise linear.

2.3.1 Dynamics in region I

In region I, where $a < u < 1$ and $v > \varepsilon$, the Equation (2.14) reduces to

$$u' = w, \tag{2.21a}$$
$$v' = z, \tag{2.21b}$$
$$w' = -cw + u + v - 1, \tag{2.21c}$$
$$z' = -\frac{c}{D}z + \frac{\eta}{D}v - \frac{\alpha}{D}, \tag{2.21d}$$
$$\varepsilon' = 0, \tag{2.21e}$$

as $\theta(v-\varepsilon) \equiv 1 \equiv \theta(u-a)$ in that region. Clearly, the dynamics in region I corresponds to the dynamics in the "outer" region of (2.5). Hence, the geometric analysis in this region proceeds as in Section 2.2.1.

Now, we introduce several notations for the sake of consistency and brevity. We define the section Σ^-, which represents the hyperplane $\{u = a\}$ in $(u, v, w, z, \varepsilon)$-space. The point of intersection of $\mathcal{W}^{\mathrm{u}}(Q_\varepsilon^-)$ with Σ^-, we label by P_ε. By Proposition 2.1 in Section 2.2.1, we express the point P_ε as follows:

$$P_\varepsilon = \Big(A_2 + \frac{A_1}{\mu_3} + 1 - \frac{\alpha}{\eta},\ A_1 + \frac{\alpha}{\eta},\ \lambda_1 A_2 + \frac{\lambda_3}{\mu_3}A_1,\ \lambda_3 A_1,\ \varepsilon\Big), \tag{2.22}$$

for ε fixed and small.

In the limit as $\varepsilon \to 0$, the restricted flow in region I leaves from the non-trivial steady state Q_0^- along the 2-dimensional $\mathcal{W}^{\mathrm{u}}(Q_0^-)$ and terminates at $P_0 = \big(A_2 + \frac{A_1}{\mu_3} + 1 - \frac{\alpha}{\eta}, A_1 + \frac{\alpha}{\eta}, \lambda_1 A_2 + \frac{\lambda_3}{\mu_3}A_1, \lambda_3 A_1,\, 0\big)$ in the section Σ^- , which is precisely the first portion of the singular heteroclinic orbit Γ of Equation (2.14). We label this segment of $\mathcal{W}^{\mathrm{u}}(Q_0^-)$ by Γ^u. In particular, the section Σ^- corresponds to the section Σ_1^{in} in chart K_1 via the blow-up transformation in (2.16). Meanwhile, from the definition of region I, we have $u(\xi) = a$ in Equation (2.8) in the section Σ^-; here, we take the corresponding 'time' $\xi = 0$ for the sake of simplicity. Then, we obtain a constraint throughout the rest of chapter:

$$a = A_2 + \frac{A_1}{\mu_3} + 1 - \frac{\alpha}{\eta}. \tag{2.23}$$

where A_1 and A_2 are coefficients that are as yet undetermined.

***Remark* 2.4.** In the framework of Equation (2.6) in Section 2.2.1, we clearly find that the 2-dimensional unstable manifold $\mathcal{W}^{\mathrm{u}}(Q_\varepsilon^-)$ of the point Q_ε^- at $\varepsilon = 0$ in region I is precisely the unstable manifold $\mathcal{W}^{\mathrm{u}}(Q^-)$ of Equation (2.6). Thence, we write $\mathcal{W}^{\mathrm{u}}(Q^-)$ as $\mathcal{W}^{\mathrm{u}}(Q_0^-)$ in the following. And correspondingly, the unstable manifold $\mathcal{W}^{\mathrm{u}}(\ell^-)$ of the line $\ell^- = \big\{(1 - \frac{\alpha}{\eta}, \frac{\alpha}{\eta}, 0, 0, \varepsilon) \,\big|\, \varepsilon \in [0, \varepsilon_0]\big\}$, is defined as a foliation in ε with fibers $\mathcal{W}^{\mathrm{u}}(Q_\varepsilon^-)$.

2.3.2 Dynamics in region III

In region III, $\theta(v-\varepsilon)\equiv 0$; hence, via the blow-up transformation in (2.17), Equation (2.14) reduces to

$$u_2' = w_2, \tag{2.24a}$$
$$v_2' = z_2, \tag{2.24b}$$
$$w_2' = -cw_2, \tag{2.24c}$$
$$z_2' = -\frac{c}{D}z_2, \tag{2.24d}$$
$$r_2' = 0. \tag{2.24e}$$

The steady states of (2.24) are the points on the (u_2, v_2, r_2)-sphere; however, only the points on the line $\ell_2^+ = \big\{(0,0,0,0,r_2)\,\big|\,r_2 \in [0,\varepsilon_0]\big\}$ are relevant here, which corresponds to ℓ^+ after transforming to the original (u,v,w,z,ε)-variables. We denote the points on ℓ_2^+ by $Q_{\varepsilon 2}^+$ for ε fixed. Equation (2.24) may be solved exactly: rewriting the above equations with v_2 as the independent variable and keeping in mind that $(u_2,w_2,z_2)(v_2)\big|_{v_2=0} = (0,0,0)$, we find the family of orbits $\Gamma_{\varepsilon 2}$, which correspond to the 2-dimensional stable manifold $\mathcal{W}_2^{\mathrm{s}}(Q_{\varepsilon 2}^+)$,

$$\Gamma_{\varepsilon 2}:\ \big(u_2,w_2,z_2\big)(v_2) = \Big(A_3 v_2^D, -cA_3 v_2^D, -\frac{c}{D}v_2\Big), \tag{2.25}$$

where A_3 is a coefficient that will need to be determined by matching the boundaries of the orbit in region II. For future reference, we emphasize that, since v_2 must be non-negative and decreasing, the constant A_3 will be negative. The point of intersection of $\Gamma_{\varepsilon 2}$ with the section Σ_2^{in} in (2.20), which is labeled $P_{\varepsilon 2}^{\mathrm{in}}$, is determined by taking $v_2 = 1$ in Equation (2.25), whence

$$P_{\varepsilon 2}^{\mathrm{in}} := \Big(u_2^{\mathrm{in}}, v_2^{\mathrm{in}}, w_2^{\mathrm{in}}, z_2^{\mathrm{in}}, r_2^{\mathrm{in}}\Big) = \Big(A_3, 1, -cA_3, -\frac{c}{D}, \varepsilon\Big), \tag{2.26}$$

where ε is small.

***Remark* 2.5.** The family of orbits $\Gamma_{\varepsilon 2}$ is parametrised by $r_2(=\varepsilon)$, as c and A_3 are both r_2-dependent.

As for the singular orbit Γ_2 corresponding to the 2-dimensional stable manifold $\mathcal{W}^{\mathrm{s}}(Q_{02}^+)$ in the original (u,v,w,z,ε)-variables, which is approximated by the weak-stable eigendirection for ε sufficiently small, we obtain

$$\Gamma_2:\ \big(u_2,w_2,z_2\big)(v_2) = \Big(\frac{1}{\mu_4}v_2, \frac{\lambda_4}{\mu_4}v_2, \lambda_4 v_2\Big). \tag{2.27}$$

with $P_{02}^{\mathrm{in}} := \Big(\frac{1}{\mu_4}, 1, \frac{\lambda_4}{\mu_4}, \lambda_4, 0\Big)$, by taking $v_2 = 1$.

***Remark* 2.6.** The expression for Γ_2 is obtained from the weak-stable eigenvector $\mathbf{v}_4 = \big(1, \mu_4, \lambda_4, \mu_4\lambda_4\big)^T$ of Equation (2.10) at the origin, cf. Appendix A.2.

The geometry in chart K_2 in (z_2, r_2, v_2)-space is illustrated in Figure 2.7. The projection of Γ_2 in the (v_2,z_2)-plane is the line $z_2 = \lambda_4 v_2$ with slope λ_4, which is at least as steep as the projection of $z_2 = -\frac{c}{D}v_2$ of $\Gamma_{\varepsilon 2}$ with slope $-\frac{c}{D}$, due to $|\lambda_4| > |\frac{c}{D}|$, where $\lambda_4 = \frac{1}{2D}(-c - \sqrt{c^2+4D\eta})$ by Lemma 2.1.

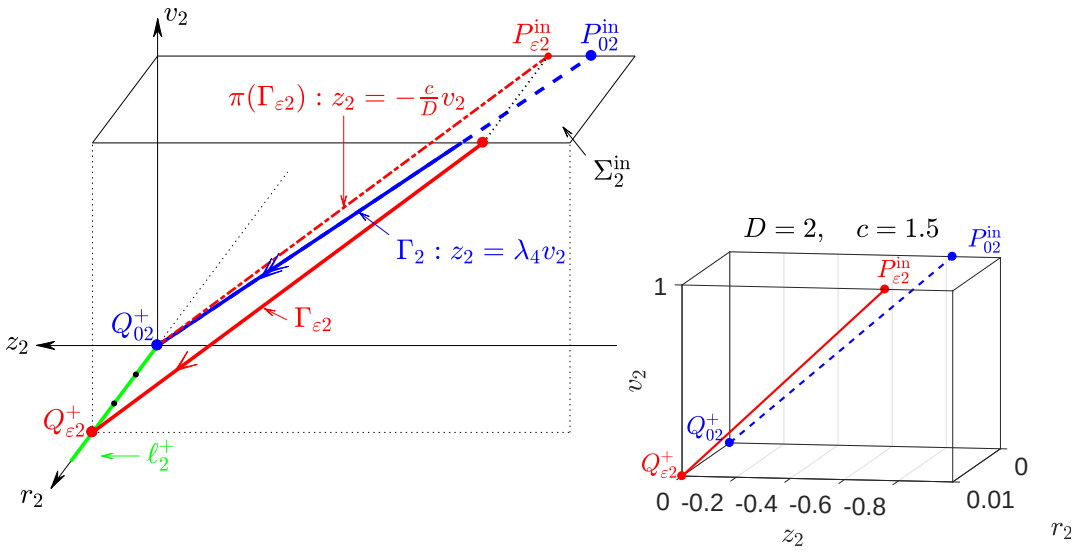

(a) (b)

Figure 2.7: The geometry of (z_2, r_2, v_2)-space in chart K_2: singular orbit Γ_2 (blue), perturbed orbit $\Gamma_{\varepsilon 2}$ (red). (a) Qualitative sketch, (b) Numerical simulation for $D = 2$, $c = 1.5$, $\varepsilon = 0.01$.

Regarding the geometry of (u_2, w_2, r_2)-space in chart K_2, there exist three distinct scenarios due to varying levels of the speed c; here, we denote these levels by low speed, intermediate speed and high speed, respectively. Here, the projection of orbit Γ_2 in the (u_2, w_2)-plane is the line $w_2 = \lambda_4 u_2$ with slope λ_4, while the projection of the perturbed line $\Gamma_{\varepsilon 2}$ is $\pi(\Gamma_{\varepsilon 2}) : w_2 = -cu_2$ with slope $-c$.

i. Low speed: $|-c| < |\lambda_4|$, i.e., $c \in (0, \sqrt{\eta(D-1)})$ by the definition. The basic local geometry is shown in panel (a) in Figure 2.8; in particular, c is small enough to ensure $u_2^{\text{in}} < 0$ in this scenario.

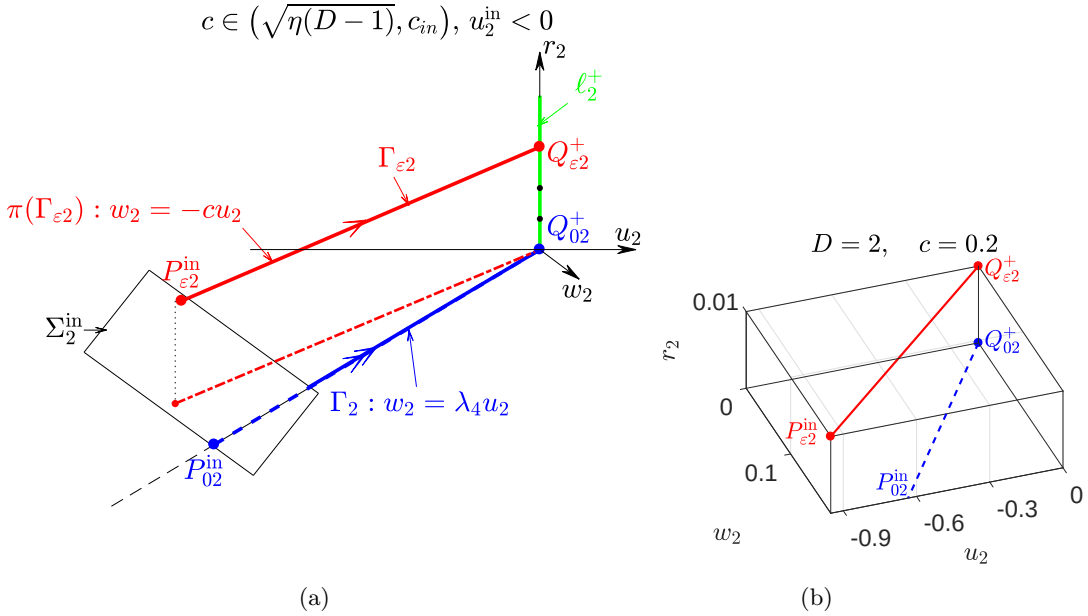

(a) (b)

Figure 2.8: The geometry of (u_2, w_2, r_2)-space: singular orbit Γ_2 (blue), perturbed orbit $\Gamma_{\varepsilon 2}$ (red). (a) Qualitative sketch with speed $c \in (0, \sqrt{\eta(D-1)})$. (b) Numerical simulation for $D = 2$, $c = 0.2$, and $\varepsilon = 0.01$.

ii. Intermediate speed: $|-c| > |\lambda_4|$ and $u_2^{\text{in}} < 0$, i.e., $c \in (\sqrt{\eta(D-1)}, c_{\text{in}})$. Here, c_{in} is determined from $u_2^{\text{in}}(c_{\text{in}}) = 0$, where u_2^{in} is defined in (2.26) for ε small. The basic local geometry is shown in panel (a) Figure 2.9.

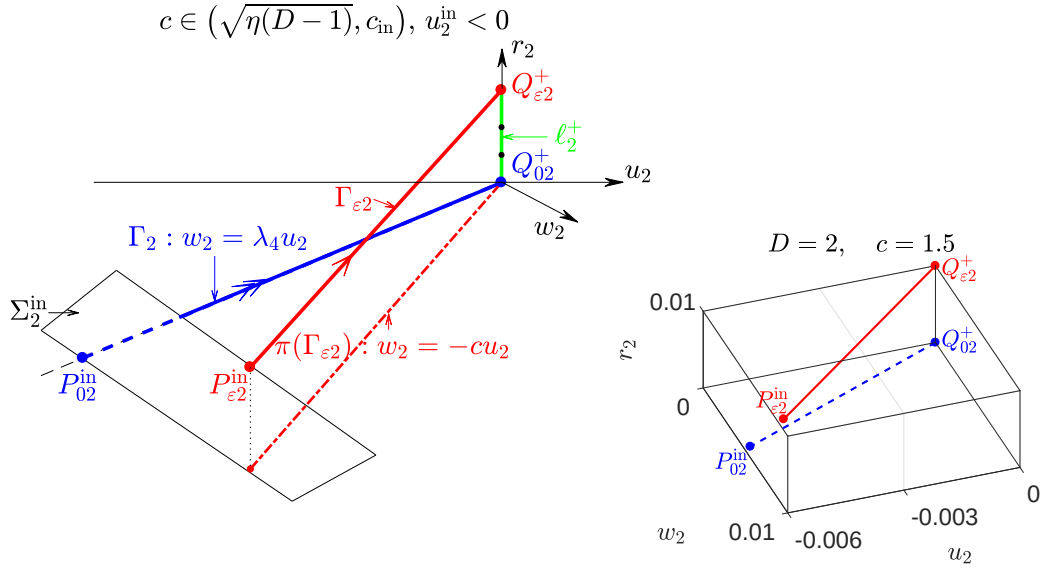

(a) (b)

Figure 2.9: The geometry of (u_2, w_2, r_2)-space: singular orbit Γ_2 (blue), perturbed orbit $\Gamma_{\varepsilon 2}$ (red). (a) Qualitative sketch with speed $c \in (\sqrt{\eta(D-1)}, c_{\text{in}})$. (b) Numerical simulation for $D = 2$, $c = 1.5$, and $\varepsilon = 0.01$.

iii. High speed: $|-c| > |\lambda_4|$ and $u_2^{\text{in}} > 0$, i.e., $c \in (c_{\text{in}}, c_{max})$. Here, c_{max} denotes the maximum of the valid front propagation speed for ε fixed and small; in particular, the speed c is unbounded in the singular case. For details, see Section 2.5. The basic local geometry is shown in panel (a) in Figure 2.10.

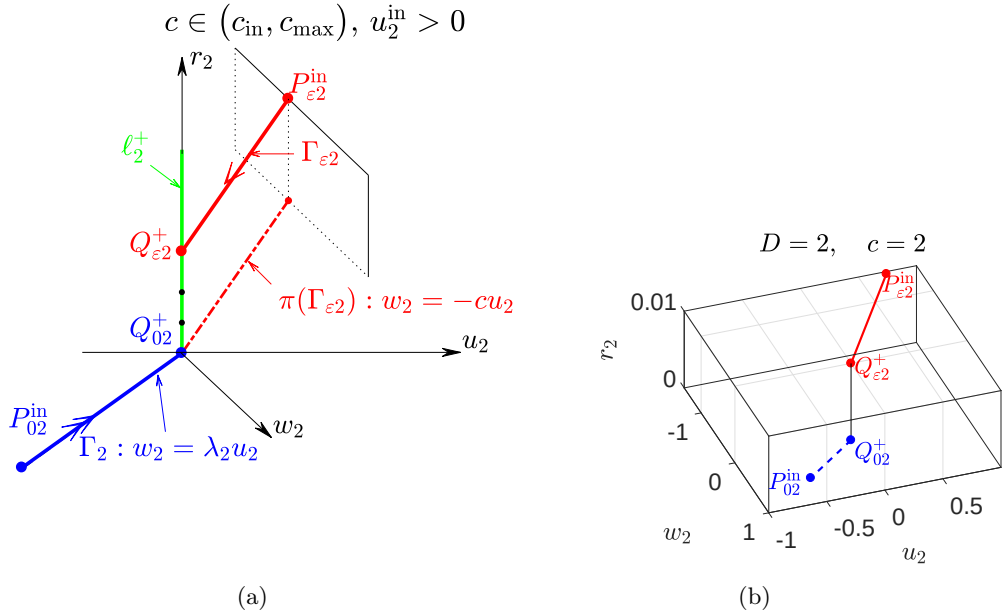

(a) (b)

Figure 2.10: The geometry of (u_2, w_2, r_2)-space: singular orbit Γ_2 (blue), perturbed orbit $\Gamma_{\varepsilon 2}$ (red). (a) Qualitative sketch with speed $c \in (c_{\text{in}}, c_{max})$. (b) Numerical simulation for $D = 2$, $c = 2$, $\varepsilon = 0.01$.

2.3.3 Dynamics in region II

The dynamics in region II is naturally described in chart K_1: substituting (2.16) into (2.14) and noting that $\theta(u-a)\equiv 0$, we find

$$u_1' = w_1 - u_1 z_1, \tag{2.28a}$$
$$r_1' = r_1 z_1, \tag{2.28b}$$
$$w_1' = -cw_1 + (1+u_1)\theta(1-\varepsilon_1) - w_1 z_1, \tag{2.28c}$$
$$z_1' = -\frac{c}{D} z_1 + \frac{\eta}{D}\theta(1-\varepsilon_1) - z_1^2, \tag{2.28d}$$
$$\varepsilon_1' = -\varepsilon_1 z_1. \tag{2.28e}$$

As we will only consider Equation (2.28) for $\varepsilon_1 \in [0,1]$, cf. the definition of the section Σ_1^{out} in (2.20), we may take $\theta(1-\varepsilon_1)\equiv 1$ in the above equations. The steady states of (2.28) are located at $P_1^+ = (\frac{1}{\mu_3}, 0, \frac{\lambda_3}{\mu_3}, \lambda_3, 0)$ and $P_1^- = (\frac{1}{\mu_4}, 0, \frac{\lambda_4}{\mu_4}, \lambda_4, 0)$. Here, $r_1 (= v)$ is monotonically decreasing in the original (u,v,w,z,ε)-space, which implies that $z_1 < 0$; recall the eigenvalues λ_3, λ_4, which are positive and negative, respectively, with $\mu_3, \mu_4 < 0$. Hence, P_1^- is relevant in our analysis as the value of the z_1-coordinate is $\lambda_4 (< 0)$. The following result is obtained via a straightforward linearisation argument:

Lemma 2.3. *The steady states $P_1^\pm$ of Equation (2.28) are hyperbolic saddle points, with eigenvalues $\lambda_2 - \lambda_3(-)$, $\lambda_3(+)$, $\lambda_1 - \lambda_3(+)$, $\lambda_4(-)$ and $-\lambda_3(-)$ for P_1^+, and eigenvalues $\lambda_1 - \lambda_4(+)$, $\lambda_4(-)$, $\lambda_2 - \lambda_4(-)$, $\lambda_3 - \lambda_4(+)$ and $-\lambda_4(+)$ for P_1^-. Both have the same eigenvectors $\mathbf{v}_i (i = 1, ..., 5)$, which are given by $\mathbf{v}_1 = (-\lambda_2, 0, 1, 0, 0)^T$, $\mathbf{v}_2 = (0, 1, 0, 0, 0)^T$, $\mathbf{v}_3 = (-\lambda_1, 0, 1, 0, 0)^T$, $\mathbf{v}_4 = (\frac{c(1-D)}{D\mu_3\mu_4}, 0, \frac{\eta - D}{D\mu_3\mu_4}, 1, 0)^T$ and $\mathbf{v}_5 = (0, 0, 0, 0, 1)^T$, respectively.*

The singular limit of $\varepsilon = 0$ in (2.4) yields two limiting systems of equations, which are obtained by setting $r_1 = 0$ and $\varepsilon_1 = 0$, respectively, in Equation (2.28):

$$\begin{aligned} u_1' &= w_1 - u_1 z_1, \\ w_1' &= -c_0 w_1 + (1+u_1) - w_1 z_1, \\ z_1' &= -\frac{c_0}{D} z_1 + \frac{\eta}{D} - z_1^2, \\ \varepsilon_1' &= -\varepsilon_1 z_1 \end{aligned}$$

and

$$\begin{aligned} r_1' &= r_1 z_1, \\ u_1' &= w_1 - u_1 z_1, \\ w_1' &= -c_0 w_1 + (1+u_1) - w_1 z_1, \\ z_1' &= -\frac{c_0}{D} z_1 + \frac{\eta}{D} - z_1^2; \end{aligned}$$

here, $c_0 = c(\varepsilon)\big|_{\varepsilon=0}$.

In the invariant plane $\{\varepsilon_1 = 0\}$, we define the orbit Γ_1^-, which is passing through P_{01}^{in}, and is attracted to P_1^-. We note here, that Γ_1^- corresponds to the 2-dimensional stable manifold $\mathcal{W}^{\text{s}}(Q_0^+)$ after transformation to chart K_1. To that end, we focus on orbits entering at P_0 in the section Σ^-, where the 2-dimensional unstable manifold $\mathcal{W}^{\text{u}}(Q_0^-)$ in region I ends. We have the following representation of P_{01}^{in}:

$$P_{01}^{\text{in}} := \left(u_1^{\text{in}}, r_1^{\text{in}}, w_1^{\text{in}}, z_1^{\text{in}}, 0\right) = \left(\frac{A_2 + \frac{A_1}{\mu_3} + 1 - \frac{\alpha}{\eta}}{A_1 + \frac{\alpha}{\eta}}, A_1 + \frac{\alpha}{\eta}, \frac{\lambda_1 A_2 + \frac{\lambda_3}{\mu_3} A_1}{A_1 + \frac{\alpha}{\eta}}, \frac{\lambda_3 A_1}{A_1 + \frac{\alpha}{\eta}}, 0\right) \tag{2.29}$$

where $z_1^{\text{in}} < 0$ as r_1 should be decreasing. Recalling the eigenvectors $\mathbf{v}_i$ $(i = 1, ..., 5)$ defined in Lemma 2.3, $\mathbf{v}_2$ and $\mathbf{v}_3$ correspond to the negative eigenvalues λ_4 and $\lambda_2 - \lambda_4$, respectively; we easily find that $z_1^{\text{in}} = \lambda_4$, which is exactly the z_1-coordinate value of P_1^-, i.e. $z_1' = 0$. Then we

obtain one constraint on Γ_1^- as

$$\frac{\lambda_3 A_1}{A_1+\frac{\alpha}{\eta}}=\lambda_4, \tag{2.30}$$

which implies $A_1=\frac{\alpha}{\eta}\frac{\lambda_4}{\lambda_3-\lambda_4}$.

Moreover, the $(u_1^{\rm in},w_1^{\rm in})$-coordinates of $P_{01}^{\rm in}$ should stay on the stable manifold $\mathcal{W}^{\rm s}(P_1^-)$of P_1^-, i.e., on the projection of the stable eigendirection $\mathbf{v}_3$ onto the (u_1,w_1)-plane with direction vector $(-\lambda_1,1)^T$; here, the projection of the stable manifold $\mathcal{W}^{\rm s}(P_1^-)$ is represented by the line $u_1-\frac{1}{\mu_4}+\lambda_1(w_1-\frac{\lambda_4}{\mu_4})=0$. Hence, the $(u_1^{\rm in},w_1^{\rm in})$-coordinates should satisfy this line equation. Then, we obtain another constraint on Γ_1^- as

$$\frac{A_2+\frac{A_1}{\mu_3}+1-\frac{\alpha}{\eta}}{A_1+\frac{\alpha}{\eta}}-\frac{1}{\mu_4}=-\lambda_1\left(\frac{\lambda_1A_2+\frac{\lambda_3}{\mu_3}A_1}{A_1+\frac{\alpha}{\eta}}-\frac{\lambda_4}{\mu_4}\right) \tag{2.31}$$

which implies $A_2=\frac{\lambda_2}{\lambda_1-\lambda_2}(1-\frac{\alpha}{\eta})-\frac{\alpha}{\eta}\frac{\lambda_2}{(\lambda_1-\lambda_2)(\lambda_3-\lambda_4)}\Big[\frac{\lambda_3}{\mu_4}(1+\lambda_1\lambda_4)-\frac{\lambda_4}{\mu_3}(1+\lambda_1\lambda_3)\Big]$.

Combining the above expressions for A_1 and A_2, substituting into $a=A_2+\frac{A_1}{\mu_3}+1-\frac{\alpha}{\eta}$ in (2.23), we finally obtain the sought-after relation between c and a

$$a_0(c_0)=\Big(1-\frac{\alpha}{\eta}\Big)\frac{\lambda_1}{\lambda_1-\lambda_2}-\frac{\alpha}{\eta}\frac{1}{(\lambda_1-\lambda_2)(\lambda_3-\lambda_4)}\left[\frac{\lambda_3}{\mu_4}(\lambda_2-\lambda_4)-\frac{\lambda_4}{\mu_3}(\lambda_1-\lambda_3)\right] \tag{2.32}$$

and the representation of Γ_1^-

$$\begin{aligned}\Gamma_1^- :=&\big(u_1,r_1,w_1,z_1\big)(\xi)\\ =&\Big(\big(u_1^{\rm in}-\frac{1}{\mu_4}\big)\mathrm{e}^{(\lambda_2-\lambda_4)\xi}+\frac{1}{\mu_4},\, r_1^{\rm in}\mathrm{e}^{\lambda_4\xi},\, \big(w_1^{\rm in}-\frac{\lambda_4}{\mu_4}\big)\mathrm{e}^{(\lambda_2-\lambda_4)\xi}+\frac{\lambda_4}{\mu_4},\, \lambda_4\Big)\end{aligned} \tag{2.33}$$

where $(u_1^{\rm in},r_1^{\rm in},w_1^{\rm in})$ are as defined in (2.29).

Similarly, in the invariant plane $\{r_1=0\}$, the orbit passing through $P_{01}^{\rm out}=(\frac{1}{\mu_4},\,0,\,\frac{\lambda_4}{\mu_4},\,\lambda_4,\,1)$, which is labeled Γ_1^+, is attracted to P_1^- in backward "time", for $\xi\to-\infty$:

$$\Gamma_1^+ :=\big(u_1,w_1,z_1,\varepsilon_1\big)(\xi)=\Big(\frac{1}{\mu_4},\frac{\lambda_4}{\mu_4},\,\lambda_4,\,\mathrm{e}^{-\lambda_4\xi}\Big) \tag{2.34}$$

***Remark* 2.7.** The points $P_{01}^{\rm in}$ and $P_{01}^{\rm out}$ correspond to the points $P_0=\big(A_2+\frac{A_1}{\mu_3}+1-\frac{\alpha}{\eta},A_1+\frac{\alpha}{\eta},\lambda_1A_2+\frac{\lambda_3}{\mu_3}A_1,\lambda_3A_1,\,0\big)$ in (2.22) and $P_{02}^{\rm in}=\big(\frac{1}{\mu_4},1,\frac{\lambda_4}{\mu_4},\lambda_4,0\big)$, under the transformation in (2.16) and $\mathcal{K}_{12}$ in (2.18), respectively.

Thus, The orbit Γ_1 in chart K_1 consists of the union of Γ_1^- and Γ_1^+. The local geometry in chart K_1 in (z_1,ε_1,r_1)-space is illustrated in panel (a) in Figure 2.11; numerical simulation for $D=2$, $c=1.5$, and $\varepsilon=0.01$, see panel (b).

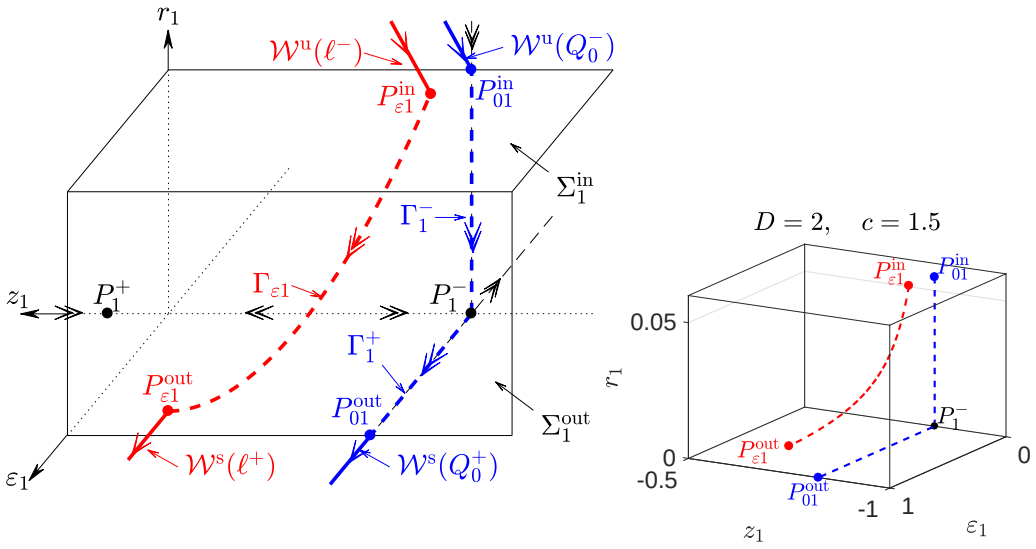

(a) (b)

Figure 2.11: The geometry of $(z_1, \varepsilon_1, r_1)$-space: singular orbit Γ_1 (blue), perturbed orbit $\Gamma_{\varepsilon 1}$ (red); (a) Qualitative sketch. (b) Numerical simulation for $D = 2$, $c = 1.5$, $\varepsilon = 0.01$.

The local geometry in chart K_1 in $(u_1, w_1, \varepsilon_1)$-space is illustrated in panel (a) in Figure 2.12. Note that, as there are three distinct geometric scenarios in chart K_2, cf. Section 2.3.2, we should have three corresponding local geometries in chart K_1 as well; however, for the sake of simplicity, we only show the qualitative sketch of the intermediate speed here; numerical simulation for $D = 2$, $c = 1.5$, and $\varepsilon = 0.01$, see panel (b).

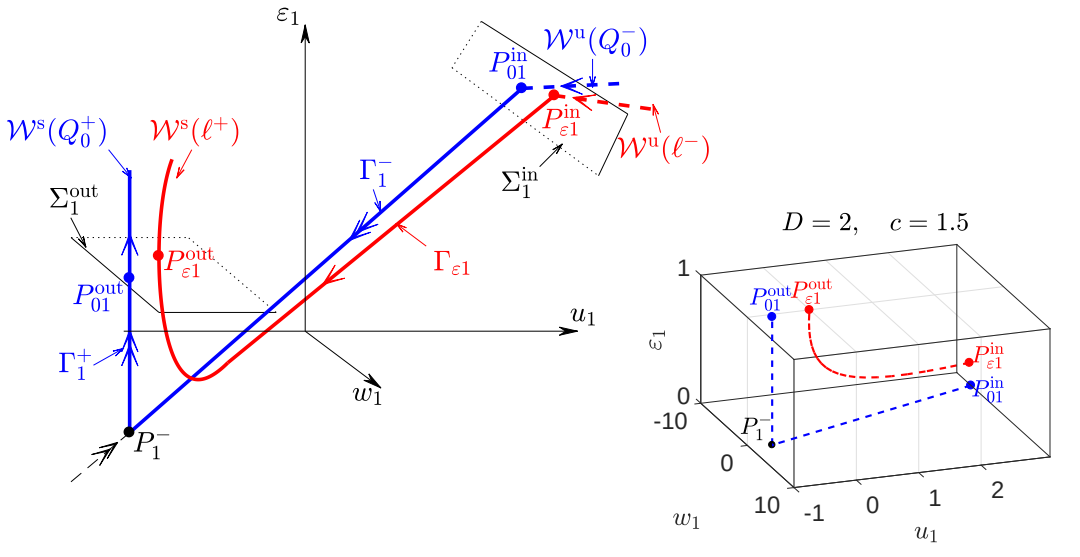

(a) (b)

Figure 2.12: The geometry of $(u_1, w_1, \varepsilon_1)$-space: singular orbit Γ_1 (blue), perturbed orbit $\Gamma_{\varepsilon 1}$ (red); (a) Qualitative sketch. (b) Numerical simulation for $D = 2$, $c = 1.5$, $\varepsilon = 0.01$.

***Remark* 2.8.** We note that Equation (2.28) is derived from the linear system in (2.14) in region II, which can be solved explicitly in terms of the independent variable ξ; for details see Appendix A.1.1, where an explicit solution is given in Equation (A.3). Transforming that solution to chart K_1, via the transformation in (2.16), we obtain $r_1 = v_{g_2}(\xi)$, $u_1 = u_{g_2}(\xi)/v_{g_2}(\xi)$,

$w_1 = w_{g_2}(\xi)/v_{g_2}(\xi)$, $z_1 = z_{g_2}(\xi)/v_{g_2}(\xi)$.

2.3.4 Global geometry in blow-up space

To summarize, the singular heteroclinic orbit Γ connecting the equilibria Q_0^- and Q_0^+ is defined as the union of the orbits obtained in the above sections, $\bar{\Gamma}^u$, $\bar{\Gamma}^-$ and $\bar{\Gamma}^+$ as well as of the singularities at the points $\bar{P}_1^-$ and $\bar{P}_0^{\text{in}}$. The global geometry in blown-up coordinates in $(\bar{z}, \bar{\varepsilon}, \bar{v})$-space is illustrated in Figure 2.13, where the scenario is independent of the value of speed; for details see Section 2.3.2.

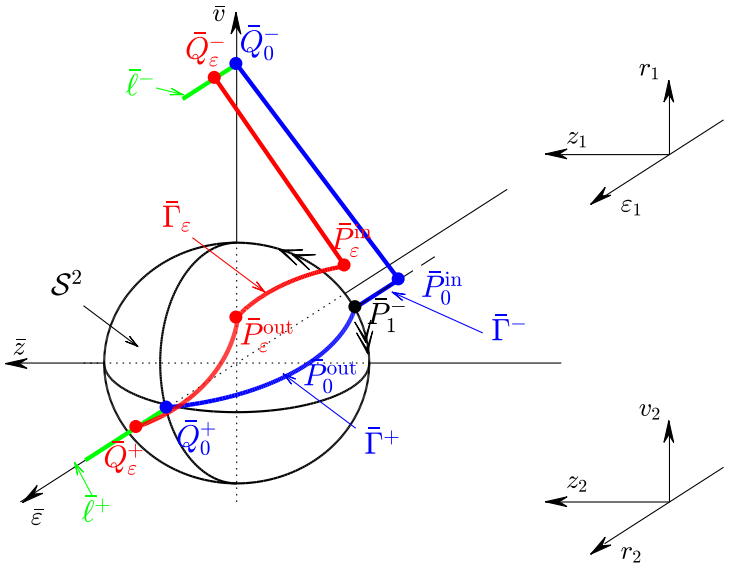

Figure 2.13: The geometry of $(\bar{z}, \bar{\varepsilon}, \bar{v})$ in blow-up space. Qualitative sketch: singular orbit (blue), perturbed orbit (red).

The geometry in $(\bar{u}, \bar{w}, \bar{\varepsilon})$-space varies with different speeds: the singular orbit $\bar{\Gamma}_1^-$ seems to cut through the blown-up sphere due to the choice of coordinates in $(\bar{u}, \bar{w}, \bar{\varepsilon})$-space, and is attracted by $\bar{P}_1^-$, before approaching $\bar{Q}_0^+$ on $\bar{\Gamma}_1^+$; in particular, the perturbed orbits persist on each side of the singular orbit Γ corresponding to the low speed $c \in (0, \sqrt{\eta(D-1)})$ and intermediate speed $c \in (\sqrt{\eta(D-1)}, c_{\text{in}})$, respectively, see Figure 2.14 and Figure 2.15; however, for high speeds $c \in (c_{\text{in}}, c_{max})$ in Figure 2.16, the perturbed orbit is not shown to be cutting through the blown-up sphere, as $u_2^{\text{in}} > 0$ is defined in chart K_2; for details see chart K_2 in Section 2.3.2. We will also discuss how speeds change the orbit in the original (u, v)-phase space in Section 2.5.4.

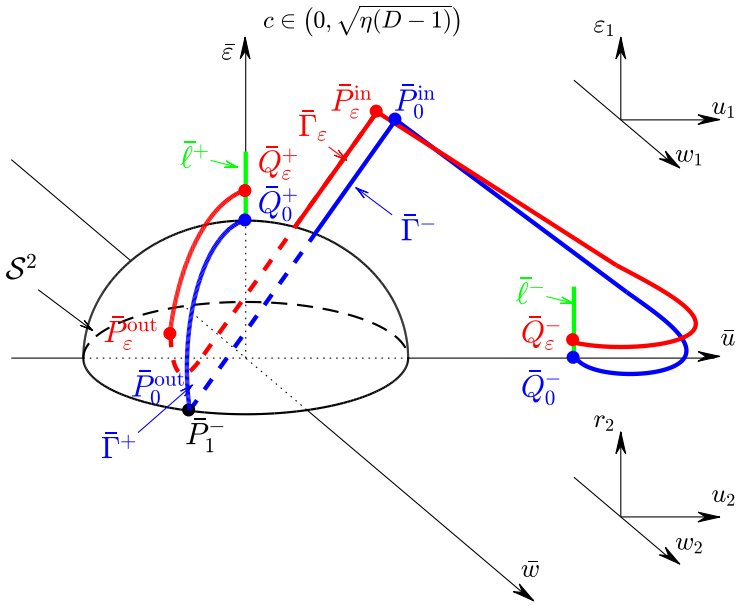

Figure 2.14: The geometry of $(\bar{u}, \bar{w}, \bar{\varepsilon})$ in blow-up space with low speed $c \in (0, \sqrt{\eta(D-1)})$. Qualitative sketch: singular orbit (blue), perturbed orbit (red).

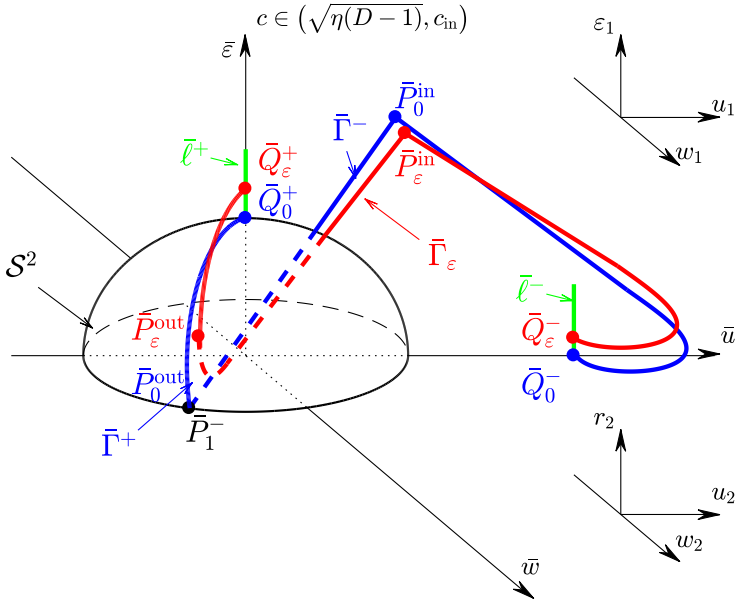

Figure 2.15: The geometry of $(\bar{u}, \bar{w}, \bar{\varepsilon})$ in blow-up space with intermediate speed $c \in (\sqrt{\eta(D-1)}, c_{\text{in}})$. Qualitative sketch: singular orbit (blue), perturbed orbit (red).

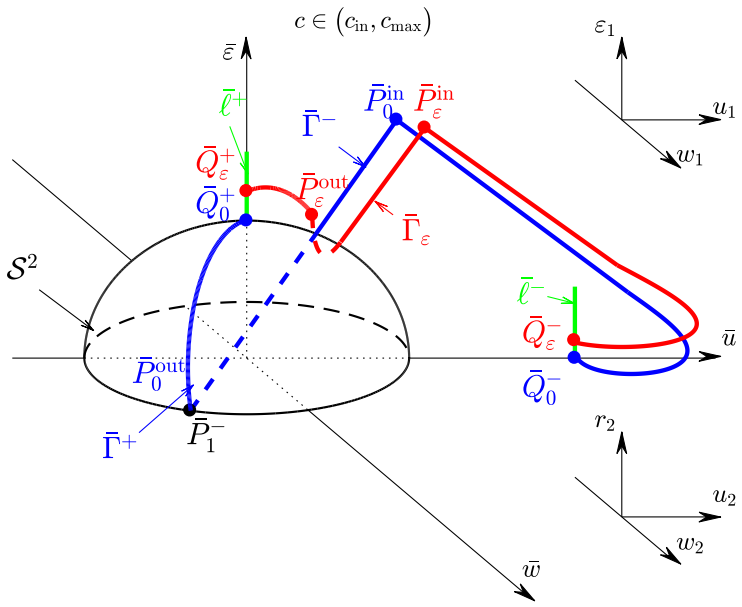

Figure 2.16: The geometry of $(\bar{u}, \bar{w}, \bar{\varepsilon})$ in blow-up space with high speed $c \in (c_{\text{in}}, c_{max})$. Qualitative sketch: singular orbit (blue), perturbed orbit (red).

2.4 Existence and asymptotics of $a_\varepsilon(c)$

In this section, we motivate the persistence of the singular heteroclinic orbit Γ, which is constructed in the previous section, for ε positive and sufficiently small. To that end, we combine the dynamics in the three regions obtained in Section 2.3.2.

In region I, the orbit Γ^u corresponds to the unstable manifold $\mathcal{W}^{\text{u}}(Q_0^-)$ of the point Q_0^- will persist as the unstable manifold $\mathcal{W}^{\text{u}}(Q_\varepsilon^-)$ of Q_ε^-. The manifold $\mathcal{W}^{\text{u}}(\ell^-)$ of the line ℓ^- is then defined as a foliation in $\varepsilon \in [0, \varepsilon_0]$, with fibers $\mathcal{W}^{\text{u}}(Q_\varepsilon^-)$.

Similarly, in region III, the orbit Γ_2 corresponds to the stable manifold $\mathcal{W}_2^{\text{s}}(Q_{02}^+)$ of Q_{02}^+ will perturb smoothly for $r_2 > 0$ small and $u_2 \leqslant 1$, to the manifold $\mathcal{W}_2^{\text{s}}(Q_{\varepsilon 2}^+)$ of $Q_{\varepsilon 2}^+$. And the stable manifold $\mathcal{W}^{\text{s}}(\ell_2^+)$ of the line ℓ_2^+ is then given by $\bigcup_{\varepsilon\in[0,\varepsilon_0]} \mathcal{W}^{\text{s}}(Q_{\varepsilon 2}^+)$. Next, we need to show the existence of Γ_1, which connects Γ^u and Γ_2 in the region II, where we use the patching method at the corresponding boundaries. The argument will be carried out entirely in region II, i.e., in chart K_1. To that end, we firstly recall the definition of the two sections Σ_1^{in} and Σ_1^{out} for the flow of (2.28) defined in (2.20) and we label the corresponding patching points by $P_{\varepsilon 1}^{\text{in}}$ and $P_{\varepsilon 1}^{\text{out}}$, respectively. In particular, the section Σ_1^{in} and the point $P_{\varepsilon 1}^{\text{in}}$ correspond to the section Σ^- and the point P_ε defined in Section 2.3.1, respectively, after blow-up transformation to chart K_1. Similarly, the section Σ_1^{out} and the point $P_{\varepsilon 1}^{\text{out}}$ correspond to the section Σ_2^{in} and the point $P_{\varepsilon 2}^{\text{in}}$ of (2.26) in chart K_2 in Section 2.3.2, respectively, under the change-of-coordinates $\mathcal{K}_{12}$. In other words, the section Σ_1^{in} defines the boundary between regions II and I, while Σ_1^{out} defines the boundary between regions II and III; in particular, the corresponding patching points are represented as

$$P_{\varepsilon 1}^{\text{in}} := \big(u_1^{\text{in}}, r_1^{\text{in}}, w_1^{\text{in}}, z_1^{\text{in}}, \varepsilon_1^{\text{in}}\big) \tag{2.35a}$$
$$= \left(\frac{A_2 + \frac{A_1}{\mu_3} + 1 - \frac{\alpha}{\eta}}{A_1 + \frac{\alpha}{\eta}}, A_1 + \frac{\alpha}{\eta}, \frac{\lambda_1 A_2 + \frac{\lambda_3}{\mu_3} A_1}{A_1 + \frac{\alpha}{\eta}}, \frac{\lambda_3 A_1}{A_1 + \frac{\alpha}{\eta}}, \frac{\varepsilon}{A_1 + \frac{\alpha}{\eta}}\right),$$
$$P_{\varepsilon 1}^{\text{out}} := \big(u_1^{\text{out}}, r_1^{\text{out}}, w_1^{\text{out}}, z_1^{\text{out}}, \varepsilon_1^{\text{out}}\big) = \big(A_3, \varepsilon, -cA_3, -\frac{c}{D}, 1\big). \tag{2.35b}$$

Next, we aim to approximate the transition map $\Pi_1 : \Sigma_1^{\text{in}} \to \Sigma_1^{\text{out}}$ that yields the corre-

sponding portion of the persistent heteroclinic orbit that lies in this region II.

2.4.1 Transition map Π_1

To approximate the transition map for the flow of Equation (2.28) between the two sections Σ_1^{in} and Σ_1^{out} defined in (2.20), we begin by dividing out a factor of $-z_1$ from (2.28), which corresponds to a transformation of the independent variable that leaves the corresponding phase portrait unchanged. (We note that $-z_1$ is positive and, hence, that the direction of the flow is unaltered, since we are restricting to a neighbourhood of P_1^- here.) Then, we shift P_1^- to the origin in chart K_1 by defining the new variables (U, W, Z) via $u_1 = \frac{1}{\mu_4} + U$, $w_1 = \frac{\lambda_4}{\mu_4} + W$ and $z_1 = \lambda_4 + Z$. In sum, we hence obtain the transformed system of equations

$$U' = \frac{1}{\mu_4} + U - \frac{\frac{\lambda_4}{\mu_4} + W}{\lambda_4 + Z}, \tag{2.36a}$$

$$r_1' = -r_1, \tag{2.36b}$$

$$W' = -\frac{-c(\frac{\lambda_4}{\mu_4} + W) + (1 + \frac{1}{\mu_4} + U)}{\lambda_4 + Z} + \frac{\lambda_4}{\mu_4} + W, \tag{2.36c}$$

$$Z' = \frac{c}{D} - \frac{\eta}{D(\lambda_4 + Z)} + \lambda_4 + Z, \tag{2.36d}$$

$$\varepsilon_1' = \varepsilon_1. \tag{2.36e}$$

where the prime now denotes differentiation with respect to the new independent time τ .

The principal equilibrium of Equation (2.36) is now located at the origin. A standard linearisation argument yields:

Lemma 2.4. *The origin is a hyperbolic saddle point for* (2.36)*, with eigenvalues* $\delta_1 = -\frac{\lambda_1}{\lambda_4} + 1$ (+)*,* -1*,* $\delta_2 = -\frac{\lambda_2}{\lambda_4} + 1$ (−)*,* $\delta_3 = -\frac{\lambda_3}{\lambda_4} + 1$ (+)*, and* 1*.*

We observe that resonances between the eigenvalues of the linearisation of (2.36) about the origin exists if and only if $D = 1$. However, as the (U, W, Z)-subsystem in {(2.36a),(2.36c), (2.36d)} is decoupled, i.e., independent of (r_1, ε_1), these resonances are not realised. Hence, Equation (2.36) may be linearised to any order in $(U, r_1, W, Z, \varepsilon_1)$ via a sequence of near-identity transformations that only involve (U, W, Z); in particular, it follows that the former will be defined on $(r_1, \varepsilon_1) \in [0, a] \times [0, 1]$, as no restriction has to be made on the two variables r_1 and ε_1. In fact, we can easily solve Equations (2.36b) and (2.36e) to find $r_1 = (A_1 + \frac{\alpha}{\eta})\mathrm{e}^{-\tau}$ and $\varepsilon_1 = \frac{\varepsilon}{A_1 + \frac{\alpha}{\eta}}\mathrm{e}^{\tau}$, respectively; by patching the (r_1, ε_1)-coordinates at the boundaries, i.e., $r_1^{\text{in}}(\tau_1) = A_1 + \frac{\alpha}{\eta}$, $r_1^{\text{out}}(\tau_2) = \varepsilon$, $\varepsilon_1^{\text{in}}(\tau_1) = \frac{\varepsilon}{A_1 + \frac{\alpha}{\eta}}$ and $\varepsilon_1^{\text{out}}(\tau_2) = 1$; here, we choose $\tau_1 = 0$ for simplicity, then determine the corresponding value $\tau_2 = \tau^* = \ln \frac{A_1 + \frac{\alpha}{\eta}}{\varepsilon}$.

In a first step, we expand the common denominator in Equation (2.36) via

$$\frac{1}{\lambda_4 + Z} = \frac{1}{\lambda_4}\Big[1 - \frac{1}{\lambda_4} Z + \frac{1}{\lambda_4^2} Z^2 + \mathcal{O}(Z^3)\Big],$$

keeping in mind that we assume $|Z|$ to be small. Substituting into (2.36), we find that Equations {(2.36a),(2.36c),(2.36d)} become

$$U' = U - \frac{1}{\lambda_4} W + \frac{1}{\mu_4 \lambda_4} Z + \frac{1}{\lambda_4^2} WZ - \frac{1}{\mu_4 \lambda_4^2} Z^2 + \mathcal{O}(3), \tag{2.37a}$$

$$W' = -\frac{1}{\lambda_4} U + \Big(\frac{c}{\lambda_4} + 1\Big) W + \frac{1}{\mu_4} Z + \frac{1}{\lambda_4^2} UZ - \frac{c}{\lambda_4^2} WZ - \frac{1}{\mu_4 \lambda_4} Z^2 + \mathcal{O}(3), \tag{2.37b}$$

$$Z' = \Big(\frac{\eta}{D}\frac{1}{\lambda_4^2} + 1\Big) Z + \frac{\eta}{D}\frac{1}{\lambda_4^2} Z^2 + \mathcal{O}(3), \tag{2.37c}$$

where $\mathcal{O}(3)$ denotes terms of order 3 and upwards in (U, W, Z).

2.4.2 Formal linearisation

In this subsection, we consider a formal linearisation of Equation (2.36) which is linear of (2.37), in the corresponding new variables $(\widehat{U}, \widehat{W}, \widehat{Z})$:

$$\widehat{U}' = \widehat{U} - \frac{1}{\lambda_4}\widehat{W} + \frac{1}{\mu_4\lambda_4}\widehat{Z}, \tag{2.38a}$$

$$\widehat{W}' = -\frac{1}{\lambda_4}\widehat{U} + \Big(\frac{c}{\lambda_4} + 1\Big)\widehat{W} + \frac{1}{\mu_4}\widehat{Z}, \tag{2.38b}$$

$$\widehat{Z}' = \Big(\frac{\eta}{D}\frac{1}{\lambda_4^2} + 1\Big)\widehat{Z}. \tag{2.38c}$$

The eigenvalues of Equation (2.38) at the origin are given by $\delta_i = -\frac{\lambda_i}{\lambda_4} + 1$ $(i = 1, 2, 3)$, as defined in Lemma 2.4, where $\delta_2 < 0$, with corresponding eigenvectors $\mathbf{v}_1 = \big(-\lambda_2, 1, 0\big)^T$, $\mathbf{v}_2 = \big(-\lambda_1, 1, 0\big)^T$, and $\mathbf{v}_3 = \big(\frac{c(1-D)}{D\mu_3\mu_4}, \frac{\eta - D}{D\mu_3\mu_4}, 1\big)^T$. Defining the change-of-variable matrix $\mathbf{P} = [\mathbf{v_1}|\mathbf{v_2}|\mathbf{v_3}]$, we write $\mathbf{w} = (\widehat{U}, \widehat{W}, \widehat{Z})^T = \mathbf{P}\mathbf{x}$, and $\mathbf{x} = (x_1, x_2, x_3)^T$; then, Equation (2.38) becomes $\mathbf{x}' = \mathrm{diag}(\delta_1, \delta_2, \delta_3)\mathbf{x}$, which has the following general solution for $\mathbf{x}$: $x_i = C_i\mathrm{e}^{\delta_i\tau}$, with undetermined coefficients C_i $(i = 1, 2, 3)$. It follows that the general solution for $\mathbf{w}$ can be written as

$$\widehat{U} = -\lambda_2 C_1\mathrm{e}^{\delta_1\tau} - \lambda_1 C_2\mathrm{e}^{\delta_2\tau} + \frac{c(1-D)}{D\mu_3\mu_4}C_3\mathrm{e}^{(\delta_3\tau)}, \tag{2.39a}$$

$$\widehat{W} = C_1\mathrm{e}^{\delta_1\tau} + C_2\mathrm{e}^{\delta_2\tau} + \frac{\eta - D}{D\mu_3\mu_4}C_3\mathrm{e}^{\delta_3\tau}, \tag{2.39b}$$

$$\widehat{Z} = C_3\mathrm{e}^{\delta_3\tau}. \tag{2.39c}$$

Here, we can denote the approximation to the general solution of (2.36) by the formal linearisation in (2.39) as $\widehat{\Gamma}_1$, noting that we have obtained the explicit solutions for $r_1 = (A_1 + \frac{\alpha}{\eta})\mathrm{e}^{-\tau}$ and $\varepsilon_1 = \frac{\varepsilon}{A_1 + \frac{\alpha}{\eta}}\mathrm{e}^{\tau}$. We convert the patching points $P_{\varepsilon 1}^{\mathrm{in}}$ and $P_{\varepsilon 1}^{\mathrm{out}}$ at the boundaries in (2.35) into the new variables $(\widehat{U}, \widehat{W}, \widehat{Z})$ by the formal linearisation, which yields

$$\begin{aligned}\widehat{P}_{\varepsilon 1}^{\mathrm{in}} :=& \big(\widehat{U}^{\mathrm{in}},\, r_1^{\mathrm{in}},\, \widehat{W}^{\mathrm{in}},\, \widehat{Z}^{\mathrm{in}},\, \varepsilon_1^{\mathrm{in}}\big) \qquad (2.40a)\\ =& \left(\frac{A_2 + \frac{A_1}{\mu_3} + 1 - \frac{\alpha}{\eta}}{A_1 + \frac{\alpha}{\eta}} - \frac{1}{\mu_4},\, A_1 + \frac{\alpha}{\eta},\, \frac{\lambda_1 A_2 + \frac{\lambda_3}{\mu_3}A_1}{A_1 + \frac{\alpha}{\eta}} - \frac{\lambda_4}{\mu_4},\, \frac{\lambda_3 A_1}{A_1 + \frac{\alpha}{\eta}} - \lambda_4,\, \frac{\varepsilon}{A_1 + \frac{\alpha}{\eta}}\right) \text{at } \tau = 0,\\ \widehat{P}_{\varepsilon 1}^{\mathrm{out}} :=& \big(\widehat{U}^{\mathrm{out}},\, r_1^{\mathrm{out}},\, \widehat{W}^{\mathrm{out}},\, \widehat{Z}^{\mathrm{out}},\, \varepsilon_1^{\mathrm{out}}\big) \qquad (2.40b)\\ =& \Big(A_3 - \frac{1}{\mu_4},\, \varepsilon,\, -cA_3 - \frac{\lambda_4}{\mu_4},\, -\frac{c}{D} - \lambda_4,\, 1\Big) \text{ at } \tau^* = \ln\frac{A_1 + \frac{\alpha}{\eta}}{\varepsilon},\end{aligned}$$

2.4.2.1 Patching at boundaries of (2.40)

We can determine all coefficients A_i, C_i $(i = 1, 2, 3)$ by patching the general solution between the two sections $\widehat{\Sigma}_1^{\mathrm{in}}$ and $\widehat{\Sigma}_1^{\mathrm{out}}$ at the points of intersection $\widehat{P}_{\varepsilon 1}^{\mathrm{in}}$ and $\widehat{P}_{\varepsilon 1}^{\mathrm{out}}$, i.e., we solve the particular solution with specific boundary condition (2.40) in $(\widehat{U}, \widehat{W}, \widehat{Z})$, which completes the

construction of the orbit $\widehat{\Gamma}_1$ in chart K_1; we have the patching equations as follows:

$$\frac{A_2 + A_1/\mu_3 + 1 - \frac{\alpha}{\eta}}{A_1 + \frac{\alpha}{\eta}} - \frac{1}{\mu_4} = -\lambda_2 C_1 - \lambda_1 C_2 + \frac{c(1-D)}{D\mu_3\mu_4} C_3, \tag{2.41a}$$

$$\frac{\lambda_1 A_2 + \lambda_3/\mu_3 A_1}{A_1 + \frac{\alpha}{\eta}} - \frac{\lambda_4}{\mu_4} = C_1 + C_2 + \frac{\eta - D}{D\mu_3\mu_4} C_3, \tag{2.41b}$$

$$\frac{\lambda_3 A_1}{A_1 + \frac{\alpha}{\eta}} - \lambda_4 = C_3, \tag{2.41c}$$

$$A_3 - \frac{1}{\mu_4} = -\lambda_2 C_1 \mathrm{e}^{\delta_1 \tau^*} - \lambda_1 C_2 \mathrm{e}^{\delta_2 \tau^*} + \frac{c(1-D)}{D\mu_3\mu_4} C_3 \mathrm{e}^{\delta_3 \tau^*}, \tag{2.41d}$$

$$-cA_3 - \frac{\lambda_4}{\mu_4} = C_1 \mathrm{e}^{\delta_1 \tau^*} + C_2 \mathrm{e}^{\delta_2 \tau^*} + \frac{\eta - D}{D\mu_3\mu_4} C_3 \mathrm{e}^{\delta_3 \tau^*}, \tag{2.41e}$$

$$-\frac{c}{D} - \lambda_4 = C_3 \mathrm{e}^{\delta_3 \tau^*}. \tag{2.41f}$$

From the above equations, we cannot find explicit solutions for all the coefficients A_i and C_i in dependence of the speed c and the cut-off threshold ε. Instead, we obtain two simplified equations with A_1 and A_2 remaining, denoted $F_i(A_1, A_2, c, \varepsilon) = 0\,(i = 1, 2)$:

$$F_1 := \frac{\lambda_3 A_1}{A_1 + \frac{\alpha}{\eta}} - \lambda_4 - \lambda_3 \Big(\frac{\varepsilon}{A_1 + \frac{\alpha}{\eta}}\Big)^{\delta_3}, \tag{2.42a}$$

$$\begin{aligned} F_2 :=& \frac{c(D-1)}{D\mu_3\mu_4\lambda_2^2} \Big(\frac{\varepsilon}{A_1 + \frac{\alpha}{\eta}}\Big)^{\delta_1} + \frac{(\eta - D)\lambda_3}{D\mu_3\mu_4} \Big(\frac{\varepsilon}{A_1 + \frac{\alpha}{\eta}}\Big)^{\delta_3} - \frac{\mu_3\lambda_1 A_2 + \lambda_3 A_1}{\mu_3(A_1 + \frac{\alpha}{\eta})} + \frac{\lambda_4}{\mu_4} \\ &+ \left[\frac{\lambda_3(D\lambda_1^2 + c\lambda_1 - \eta)}{D\mu_3\mu_4} \Big(\frac{\varepsilon}{A_1 + \frac{\alpha}{\eta}}\Big)^{\delta_3} + \frac{(\lambda_3 - \lambda_1)A_1 - \mu_3\lambda_1(1 - \frac{\alpha}{\eta})}{\mu_3(A_1 + \frac{\alpha}{\eta})} + \frac{\lambda_1 - \lambda_4}{\mu_4} \right] \\ &\times \left[\frac{1}{1 + \lambda_1^2} - \frac{\lambda_1^2}{\lambda_2^2(1 + \lambda_1^2)} \Big(\frac{\varepsilon}{A_1 + \frac{\alpha}{\eta}}\Big)^{\delta_1 - \delta_2} \right], \end{aligned} \tag{2.42b}$$

where $\delta_1, \delta_3 > 0$, $\delta_1 - \delta_2 > 0$, $a \in (0, 1 - \frac{\alpha}{\eta})$ and $\varepsilon \in (0, A_1 + \frac{\alpha}{\eta})$, which is necessary for the existence of a front connecting the two steady states as mentioned in Section 2.1. Then, we can calculate the values A_1 and A_2 numerically by solving $F_i = 0\,(i = 1, 2)$ for given small ε. Recalling the constraint in (2.23), after substituting the results of A_1 and A_2, we obtain

$$a_\varepsilon(c) = A_2 + \frac{A_1}{\mu_3} + 1 - \frac{\alpha}{\eta}, \tag{2.43}$$

which is the desired c-a relation formulae by formal linearisation patching. We will discuss the numerical simulation of Equation (2.43) in Section 2.5.

***Remark* 2.9.** To clarify, the coefficients $A_i\,(i = 1, 2, 3)$ and $C_i\,(i = 1, 2, 3)$ depend on the speed c and the cut-off threshold ε, i.e. $A_i = A_i(c, \varepsilon)\,(i = 1, 2, 3)$ and $C_i = C_i(c, \varepsilon)\,(i = 1, 2, 3)$, but we may suppress the dependence by A_i and C_i for short. Similarly, the equations $F_i\,(i = 1, 2)$ depend on $(A_1, A_2, c, \varepsilon)$, i.e. $F_i = F_i\,(A_1, A_2, c, \varepsilon)$.

2.4.2.2 Existence and uniqueness

In the singular case of $\varepsilon = 0$ in $F_i(A_1, A_2, c_0, 0) = 0\,(i = 1, 2)$ in (2.42), we obtain the corresponding singular limit of the speed relation as $a_0(c_0)$, which gives us an explicit expression for a as a function of c:

$$a_0(c_0) = \Big(1 - \frac{\alpha}{\eta}\Big) \frac{\lambda_1}{\lambda_1 - \lambda_2} - \frac{\alpha}{\eta} \frac{1}{(\lambda_1 - \lambda_2)(\lambda_3 - \lambda_4)} \left[\frac{\lambda_3}{\mu_4}(\lambda_2 - \lambda_4) - \frac{\lambda_4}{\mu_3}(\lambda_1 - \lambda_3) \right] \tag{2.44}$$

which corresponds to the existence of the singular orbit Γ, and can be verified by the general patching method of Equation (2.4) without cut-off; for details see Appendix A.2 or [74].

For $\varepsilon = 0$, we know that we have an unique solution of the speed c-a relation by solving A_1, A_2 in (2.42a)-(2.42b), cf. Equation (2.44). Now the proof of the existence of $a_0(c_0)$, which is equivalent to proving that we can get the unique solution from the two constraints $F_i(c_0, 0) = 0\,(i = 1, 2)$ by applying the Implicit Function Theorem. According to the Implicit Function Theorem, we consider the Jacobian matrix with respect to A_1 and A_2 at $(c, \varepsilon) = (c_0, 0)$ for the singular case, where $\big(A_1, A_2\big)|_{(c_0,0)}$ is the only one pair of solutions satisfying constraints (2.42a)-(2.42b). Now, the general Jacobian J_ε for this two-equation system yields

$$J_\varepsilon = \begin{bmatrix} \frac{\partial F_1}{\partial A_1} & \frac{\partial F_1}{\partial A_2} \\ \frac{\partial F_2}{\partial A_1} & \frac{\partial F_2}{\partial A_2} \end{bmatrix} = \begin{bmatrix} \frac{\alpha}{\eta}\frac{\lambda_3}{(A_1+\frac{\alpha}{\eta})^2} + \frac{\lambda_3\delta_3}{A_1+\frac{\alpha}{\eta}}\Big(\frac{\varepsilon}{A_1+\frac{\alpha}{\eta}}\Big)^{\delta_3} & 0 \\ \frac{\partial F_2}{\partial A_1} & -\frac{\lambda_1}{A_1+\frac{\alpha}{\eta}}. \end{bmatrix} \tag{2.45}$$

In the singular case $\varepsilon = 0$, note that, $A_1 = \frac{\alpha}{\eta}\frac{\lambda_4}{\lambda_3-\lambda_4}$ is obtained by Equation (2.30), the corresponding determinant of J_0 is

$$Det(J_0)\big|_{(c_0,0)} = -\frac{\eta}{\alpha D} \times \frac{2c_0^2 + 8D\eta + D\sqrt{c_0^2+4D\eta}\big(c_0 - \sqrt{c_0^2+4}\big)}{c_0 - \sqrt{c_0^2+4D\eta}}. \tag{2.46}$$

It is obvious that $Det(J_0)$ is nonzero as the numerator is nonzero with the well-defined denominator. Then, we can say that there exists a unique solution A_1 and A_2 such that equations $F_i = 0\,(i = 1, 2)$ in (2.42) for ε and $|c - c_0|$ sufficiently small, which is equivalent to the existence of $a_\varepsilon(c)$ in Equation (2.43), i.e., to the persistence of $a_0(c_0)$ for ε positive and small by the Implicit Function Theorem.

***Remark* 2.10.** For ε small, the same procedure as above shows that the determinant of J_ε has the form

$$Det(J_\varepsilon)\Big|_{(c,\varepsilon)} = \frac{\alpha}{\eta}\frac{\lambda_3}{(A_1+\frac{\alpha}{\eta})^2} - \frac{\lambda_1}{A_1+\frac{\alpha}{\eta}} + \frac{\lambda_3\delta_3\varepsilon^{\delta_3}}{(A_1+\frac{\alpha}{\eta})^{\delta_3+1}}, \tag{2.47}$$

which is nonzero.

2.4.2.3 Valid speed range

From the results of formal linearisation patching, we observe that there exists a maximum value of the speed c for ε nonzero. In particular, we find an explicit expression via the obtained two constraints $F_i\,(i = 1, 2)$, as the value of r_1 at $\widehat{P}^{\text{in}}_{\varepsilon 1}$ is at least greater or equal to the value at $\widehat{P}^{\text{out}}_{\varepsilon 1}$, the transition map exists for $A_1 + \frac{\alpha}{\eta} \geqslant \varepsilon$ with transition time $\tau \geqslant 0$. From the numerical simulation in Section 2.2.3, see Figure 2.6, the value of the v-variable at $u = a$ is decreasing as c increases, i.e., $\widehat{P}^{\text{in}}_{\varepsilon 1}$ approaches $\widehat{P}^{\text{out}}_{\varepsilon 1}$. Region II is eliminated with the transition time $\tau = 0$ by setting $\frac{A_1+\frac{\alpha}{\eta}}{\varepsilon} \equiv 1$ in (2.42a). Hence, we can obtain the maximum speed c_{max} expressed by the formula

$$c_{max} = (\alpha - \eta\varepsilon)\sqrt{\frac{D}{\alpha\varepsilon}}. \tag{2.48}$$

2.4.3 The bifurcation scenarios

According to the numerical simulation of the speed relation $a_0(c)$, cf. Figure.2 in [74], we observe that there exists one saddle-node bifurcation for a certain value of D, which is obtained by the equation $\frac{da_0(c)}{dc} = 0$:

$$\begin{aligned} \frac{da_0(c)}{dc}\Big|_{c=c_0} =& -\frac{2}{(c^2+4)^{\frac{3}{2}}}(1-\frac{\alpha}{\eta}) + \frac{\alpha}{\eta}\frac{2Dc(c^2+2D\eta+c)}{(c^2+4)^{\frac{3}{2}}(c^2+4D\eta)^{\frac{3}{2}}}\left[\frac{\lambda_3}{\mu_4}(\lambda_2-\lambda_4) - \frac{\lambda_4}{\mu_3}(\lambda_1-\lambda_3)\right] \\ & - \frac{\alpha}{\eta}\frac{1}{(c^2+4)^{\frac{1}{2}}(c^2+4D\eta)^{\frac{1}{2}}}\left[\frac{\lambda_3}{\mu_4}(\lambda_2-\lambda_4) - \frac{\lambda_4}{\mu_3}(\lambda_1-\lambda_3)\right]', \end{aligned} \tag{2.49}$$

where $'$ denotes the derivative with respect to c. When ε is positive and small, it is too complicated to get explicit expressions for A_1 and A_2 so that we cannot express $a_\varepsilon(c)$ as a function of the speed c explicitly. Hence, the bifurcation points may not be produced straightforwardly by solving $\frac{da_\varepsilon(c)}{dc} = 0$, and can be evaluated numerically as in Section 2.5 below.

Panel (a) in Figure 2.17 shows the number of bifurcation points in the c-a relation curve, where one bifurcation exists on the left-hand curve with $D < D^* \approx 5.1287$, i.e., one solution of the speed c such that $\frac{da_0(c)}{dc} = 0$. Between the two branches of curves for $D \in (D^*, 22)$, there exists a single speed for each suitable value of a , while the right-hand curve allows two bifurcation points with $D > 22$ approximately, which we do not discuss in detail here, as for large D, the factor $\frac{1}{D}$ will play a role as another small parameter. More results on the effect of varying the values of the parameters α, η, D can be found in [74]. In panel (b) of Figure 2.17, we plot the numerical simulation of $a_0(c_0)$ with $D = 2, 4, 6, 8, 10$; we can clearly find the change of bifurcation scenarios.

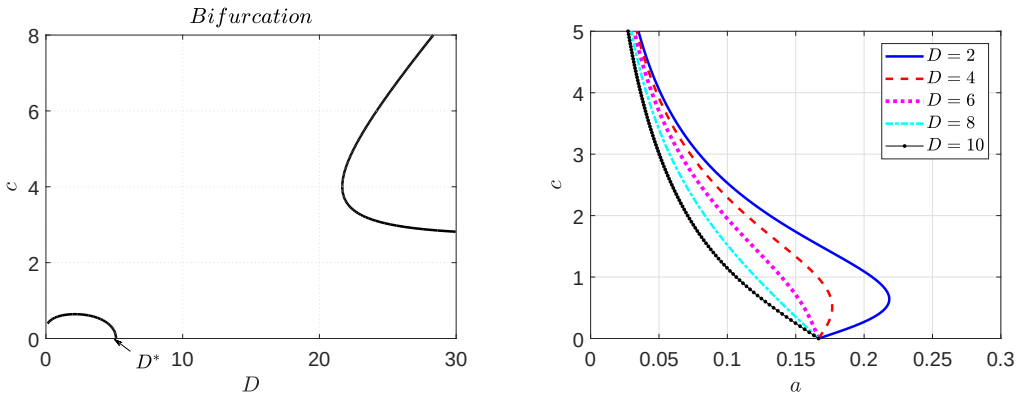

(a) (b)

Figure 2.17: (a) The bifurcation behavior in the singular case for $D \in (0, 30)$ and $c \in (0, 8)$. (b) The bifurcation of $a_0(c_0)$, with $D = 2, 4, 6, 8, 10$.

Let's take $D = 2$ for example; then, the critical value (a_b, c_b) at the bifurcation, is found where $\frac{da_0(c_b)}{dc} = 0$. When $a > a_b$, there is no solution for the speed here, which indicates that there does not exist a heteroclinic orbit connecting Q_0^- and Q_0^+; when $a = a_b$, we have a unique speed c_b, which corresponds to the existence of an unique orbit at $c = c_b$, while for $0 < a < a_b$, there exists two possible values of the speed that lead to two possible orbit constructions, where the upper branch corresponds to the stable speed and the lower branch refers to the unstable speed; for details see [57, 75].

To investigate the geometry of such bifurcation behavior, we recall the transition map Π_1, recall Section 2.4.1; there we have shifted P_1^- to the origin, with shifted boundaries (2.40). We discuss how the discontinuity position a is involved in the construction of a singular orbit, keeping the constraint (2.23)$\big(a = A_2 + \frac{A_1}{\mu_3} + 1 - \frac{\alpha}{\eta}\big)$ in mind, we can explore the orbit construction via two aspects, as we can solve the expression of either coefficient A_1 or A_2 in terms of a, i.e., express A_1 with respect to (a, A_2) or A_2 with respect to (a, A_1). Meanwhile, one of the constraints $F_i(c, 0) = 0, (i = 1, 2)$ is satisfied, which corresponds to patching the pair of variables $(\widehat{U}, \widehat{W})$ or $(r_1, \widehat{Z})$ at the boundaries, recall (2.40), with the other pair undetermined. Note that, since the variables r_1 and ε_1 are decoupled in (2.36) and solved explicitly, the (r_1, ε_1)-variables are patched automatically.

2.4.3.1 Variables $(\widehat{U}, \widehat{W})$ are patched and $(r_1, \widehat{Z})$ varies

We have patched the pair of variables $(\widehat{U}, \widehat{W})$ at the boundaries in $\widehat{P}_{\varepsilon 1}^{\text{in}}$ of (2.35), i.e. we have $F_2(c, 0) = 0$, with the expression A_1 obtained from the constraint (2.23), which means the front solution in the original (u, w)-variables have been completed for all speeds c while the front solution in the (v, z)-variables are to be determined with a certain speed. The resulting

equations are given as follows

$$A_1 = \mu_3\Big(a - 1 + \frac{\alpha}{\eta} - A_2\Big), \tag{2.50}$$

$$\frac{a}{A_1 + \frac{\alpha}{\eta}} - \frac{1}{\mu_4} = -\lambda_1 \left(\frac{\lambda_1 A_2 + \frac{\lambda_3}{\mu_3} A_1}{A_1 + \frac{\alpha}{\eta}} - \frac{\lambda_4}{\mu_4}\right). \tag{2.51}$$

By solving the above equations, we obtain the solution A_1, A_2 in dependence of (a, c), that is

$$A_1(a,c) = \mu_3 \left(\frac{(\lambda_1^2+1)a - \lambda_1^2(1-\frac{\alpha}{\eta}) - \frac{\alpha}{\eta}\frac{1+\lambda_1\lambda_4}{\mu_4}}{\lambda_1^2 - \lambda_1\lambda_3 + \frac{\mu_3(1+\lambda_1\lambda_4)}{\mu_4}}\right), \tag{2.52}$$

$$A_2(a,c) = \frac{\frac{\alpha}{\eta}\frac{1+\lambda_1\lambda_4}{\mu_4} - a - (a - 1 + \frac{\alpha}{\eta})\Big(\lambda_1\lambda_3 - \frac{\mu_3(1+\lambda_1\lambda_4)}{\mu_4}\Big)}{\lambda_1^2 - \lambda_1\lambda_3 + \frac{\mu_3(1+\lambda_1\lambda_4)}{\mu_4}}. \tag{2.53}$$

To complete the patching in $(r_1, \widehat{Z})$-variables, we substitute the above $A_1(a,c)$ and $A_2(a,c)$ into the boundary condition in (2.40) that $r_1^{\text{in}} = A_1(a,c) + \frac{\alpha}{\eta}$ and $\widehat{Z}^{\text{in}} = \frac{\lambda_3 A_1(a,c)}{A_1(a,c)+\frac{\alpha}{\eta}} - \lambda_4$, the singular orbit exists iff $\widehat{Z}^{\text{in}} = 0$, corresponding to the constraint $F_1(c,0) = 0$, i.e. there should be intersection between the $(r_1^{\text{in}}, \widehat{Z}^{\text{in}})$-curve and $\widehat{Z}^{\text{in}} = 0$ at a certain value of c; local geometry can be found in Figure 2.11. After computing the numerical values depending on varying positive speeds for a fixed value of a, we have the following Figure 2.18: when $a = 0.21 < a_b$, there are two intersections of the $(r_1^{\text{in}}, \widehat{Z}^{\text{in}})$-curve with $\widehat{Z}^{\text{in}} = 0$ in the $(r_1^{\text{in}}, \widehat{Z}^{\text{in}})$-phase plane, which implies two speeds to construct the orbit, while for $a = 0.22 > a_b$, there is no intersection, i.e., $\widehat{Z}^{\text{in}} < 0$ for all $c > 0$ with $r_1^{\text{in}} > 0$, which implies the fact that for $a > a_b$ no heteroclinic orbits exist; see Figure 2.18. Note that, a_b denotes the value of a at the bifurcation.

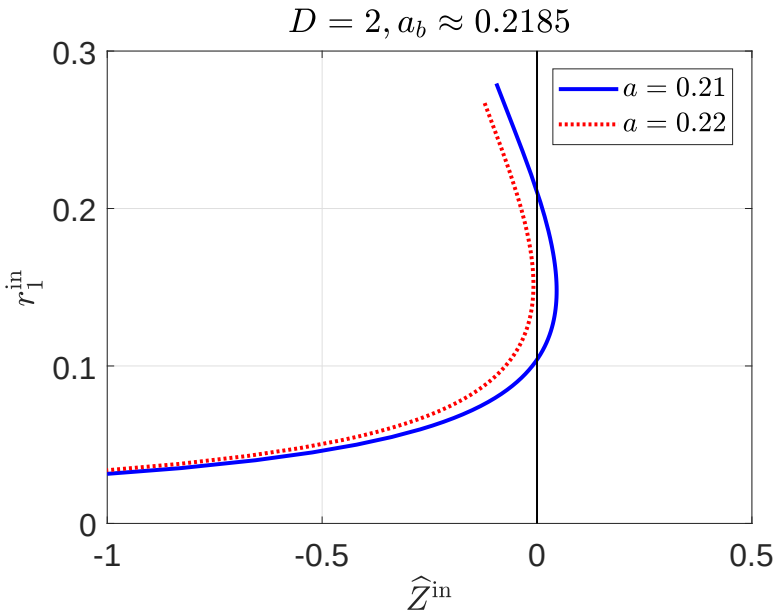

Figure 2.18: The evaluated $(r_1^{\text{in}}, \widehat{Z}^{\text{in}})$-curve for fixed $a = 0.21$ (solid blue), and $a = 0.22$ (dotted red); with $D = 2$ and $\varepsilon = 0$, the bifurcation value evaluates to $a_b \approx 0.2185$.

2.4.3.2 Variables $(r_1, \widehat{Z})$ are patched and $(\widehat{U}, \widehat{W})$ varies

We have patched the pair of variables $(r_1, \widehat{Z})$ of the boundaries in $\widehat{P}_{\varepsilon 1}^{\text{in}}$ of (2.40), i.e. $F_1(c,0) = 0$, with the expression A_2 obtained from the constraint (2.23), which means the front solution in the original (v, z)-variables have been completed for all speeds c while the front solution in the

(u, w)-variables are to be determined completed with a certain speed. The resulting equations are given as following

$$A_2 = a - \Big(\frac{A_1}{\mu_3} + 1 - \frac{\alpha}{\eta}\Big), \tag{2.54}$$

$$\frac{\lambda_3 A_1}{A_1 + \frac{\alpha}{\eta}} - \lambda_4 = 0. \tag{2.55}$$

By solving the above equations, we obtain the solution of A_1, A_2 in dependence of (a,c), that is

$$A_1(a,c) = \frac{\alpha}{\eta}\frac{\lambda_4}{\lambda_3 - \lambda_4}, \tag{2.56}$$

$$A_2(a,c) = a - 1 + \frac{\alpha}{\eta} - \frac{\alpha}{\eta}\frac{\lambda_4}{\mu_3(\lambda_3 - \lambda_4)}. \tag{2.57}$$

To complete the patching in $(\widehat{U}, \widehat{W})$-variables, we substitute the above $A_1(a,c)$ and $A_2(a,c)$ into the boundary condition in (2.40) that $\widehat{U}^{\text{in}} = \frac{a}{A_1(a,c)+\frac{\alpha}{\eta}} - \frac{1}{\mu_4}$ and $\widehat{W}^{\text{in}} = \frac{\lambda_1 A_2(a,c) + \frac{\lambda_3}{\mu_3} A_1(a,c)}{A_1(a,c)+\frac{\alpha}{\eta}} - \frac{\lambda_4}{\mu_4}$. We evaluate the shortest distance between the point $(\widehat{U}^{\text{in}}, \widehat{W}^{\text{in}})$ of $\widehat{P}_{01}^{\text{in}}$ in (2.40) and the projected line $\ell : \widehat{U} + \lambda_1 \widehat{W} = 0$ in the $(\widehat{U}, \widehat{W})$-plane, which corresponds to Γ_1^- as defined in (2.33) in Section 2.3.3:

$$Dist = \frac{1}{1+\lambda_1^2}\left|\left\{\frac{\eta}{\alpha}\frac{\lambda_3 - \lambda_4}{\lambda_3}\Big[(\lambda_1^2+1)a - \lambda_1^2(1-\frac{\alpha}{\eta})\Big] - \frac{\lambda_1\lambda_4(\lambda_1 - \lambda_3)}{\mu_3\lambda_3} - \frac{1+\lambda_1\lambda_4}{\mu_4}\right\}\right| \tag{2.58}$$

An orbit exists iff $Dist = 0$, corresponding to the constraint $F_2(c, 0) = 0$, i.e. there should be zeros of $Dist$ at some positive speed. We compute the numerical values of $Dist$ over a range of positive speeds, see Figure 2.19. When $a = 0.21 < a_b$, there are two roots with $Dist = 0$-axis, which leads to two feasible orbits, while for $a = 0.22 > a_b$, there is no intersection, i.e., $Dist > 0$ for all $c > 0$, which implies the fact that for $a > a_b$ no orbits exist.

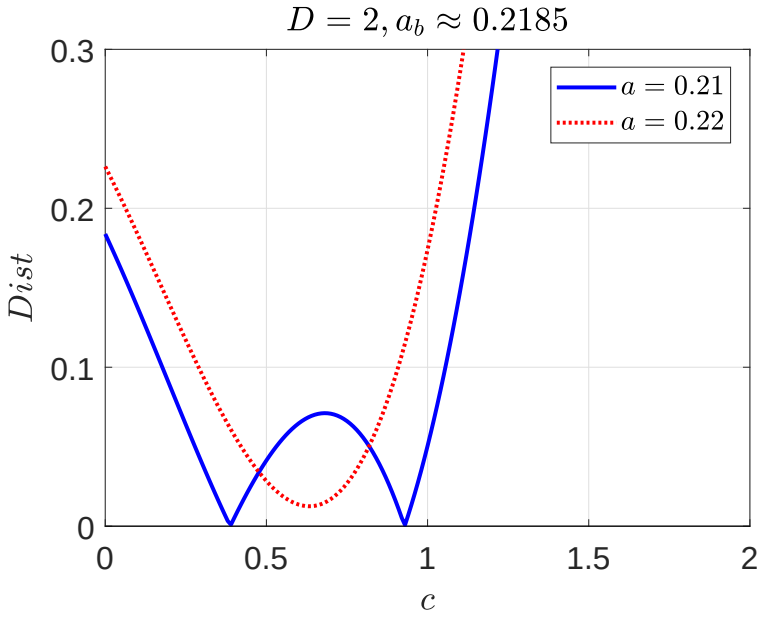

Figure 2.19: The evaluated $Dist$ between $\widehat{P}_{01}^{\text{in}}$ and the line ℓ of in $(\widehat{U}, \widehat{W})$-plane, for fixed $a = 0.21$(solid blue) and $a = 0.22$ (dotted red); with $D = 2$, the bifurcation value evaluates to $a_b \approx 0.2185$.

In Figure 2.20, we illustrate the geometric position of the point $(\widehat{U}^{\text{in}}, \widehat{W}^{\text{in}})$ and the line ℓ in

$(\widehat{U}, \widehat{W}, \widehat{Z})$-space as well as the projection into the $(\widehat{U}, \widehat{W})$-plane, with $c = 0.2$.

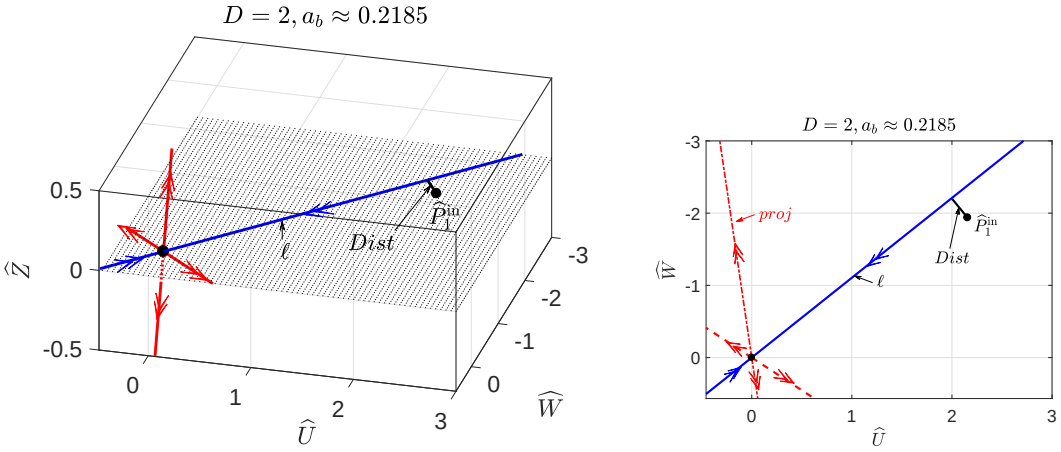

(a) (b)

Figure 2.20: (a) The approximated position of $\widehat{P}_{01}^{\text{in}}$ in $(\widehat{U}, \widehat{W}, \widehat{Z})$-space and the line ℓ (solid blue) with the corresponding unstable manifold (dashed red). (b) The position of $\widehat{P}_{01}^{\text{in}}$ and the line ℓ in the $(\widehat{U}, \widehat{W})$-plane with projected unstable manifold labeled *proj* (dash-dotted red).

***Remark* 2.11.** The stable manifold and one of the two unstable directions lie in the plane $\{\widehat{Z} = 0\}$ of $(\widehat{U}, \widehat{W}, \widehat{Z})$-space, and the other unstable direction is shown projected in Figure 2.20. The 3-dimensional plot is computed with $D = 2$ and $c = 0.2$; as the actual position varies with the speed, we only show one case here.

2.4.3.3 Summary

Both results of the above two aspects in our geometric construction agree with each other, in that, for $a > a_b$, there is no valid singular orbit between Q_0^- and Q_0^+, and for $a = a_b$, there is an unique orbit, while for $0 < a < a_b$, there exist two solutions, one stable wave and one unstable wave. In addition, for $\varepsilon > 0$ small, we may find similar results for fixed $a_\varepsilon(c)$ in the same manner as above, which will not be studied explicitly due to the complex expression for $a_\varepsilon(c)$ obtained in Section 2.4.

2.4.4 Second-order normal form

In the formal linearisation of Equation (2.37), we only considered the linear terms, neglecting higher order terms. Next, we perform a normal form transformation, which will allow us to eliminate rigorously the quadratic terms from Equation (2.37):

Proposition 2.3. *Let*

$$\beta = D^2{\lambda_4}^4 - cD^2{\lambda_4}^3 - D^2{\lambda_4}^2 + 4D\eta{\lambda_4}^2 - 2cD\eta\lambda_4 + 4\eta^2;$$

then, the near-identity transformation

$$\begin{aligned}
U &= \tilde{u} + \frac{D\big[(\lambda_4+1)(2\eta^2 - Dc\eta\lambda_4) - \beta\big]}{\beta\mu_4\left(D{\lambda_4}^2 + \eta\right)}\tilde{z}^2 + \frac{D}{D\lambda_4^2+\eta}\tilde{w}\tilde{z},\\
W &= \tilde{w} - \frac{D\lambda_4\big[\beta - (\lambda_4+1)(2\eta^2 + D\eta\lambda_4^2 - D\eta)\big]}{\beta\mu_4\left(D{\lambda_4}^2 + \eta\right)}\tilde{z}^2 + \frac{D}{D\lambda_4^2+\eta}\tilde{u}\tilde{z} - \frac{cD}{D\lambda_4^2+\eta}\tilde{w}\tilde{z},\\
Z &= \tilde{z} + \frac{\eta}{D\lambda_4^2+\eta}\tilde{z}^2
\end{aligned}$$

transforms Equation (2.37) *into*

$$\tilde{u}' = \tilde{u} - \frac{1}{\lambda_4}\tilde{w} + \frac{1}{\mu_4\lambda_4}\tilde{z} + \mathcal{O}(3), \tag{2.59a}$$

$$\tilde{w}' = -\frac{1}{\lambda_4}\tilde{u} + \Big(\frac{c}{\lambda_4} + 1\Big)\tilde{w} + \frac{1}{\mu_4}\tilde{z} + \mathcal{O}(3), \tag{2.59b}$$

$$\tilde{z}' = \Big(\frac{\eta}{D}\frac{1}{\lambda_4^2} + 1\Big)\tilde{z} + \mathcal{O}(3). \tag{2.59c}$$

Proof. We make the Ansatz

$$\begin{aligned} U &= \tilde{u} \ + \alpha_1\tilde{u}^2 + \alpha_2\tilde{w}^2 + \alpha_3\tilde{z}^2 + \alpha_4\tilde{u}\tilde{w} + \alpha_5\tilde{u}\tilde{z} + \alpha_6\tilde{w}\tilde{z}, \\ W &= \tilde{w} + \beta_1\tilde{u}^2 \ + \beta_2\tilde{w}^2 + \beta_3\tilde{z}^2 + \beta_4\tilde{u}\tilde{w} + \beta_5\tilde{u}\tilde{z} + \beta_6\tilde{w}\tilde{z}, \\ Z &= \tilde{z} \ + \gamma_1\tilde{u}^2 \ + \gamma_2\tilde{w}^2 + \gamma_3\tilde{z}^2 \ + \gamma_4\tilde{u}\tilde{w} + \gamma_5\tilde{u}\tilde{z} + \gamma_6\tilde{w}\tilde{z}, \end{aligned}$$

which we differentiate with respect to the independent variable. Thus, for instance, we find

$$U' = (1 + 2\alpha_1\tilde{u} + \alpha_4\tilde{w} + \alpha_5\tilde{z})\tilde{u}' + (\alpha_4\tilde{u} + 2\alpha_2\tilde{w} + \alpha_6\tilde{z})\tilde{w}' + (\alpha_5\tilde{u} + \alpha_6\tilde{w} + 2\alpha_3\tilde{z})\tilde{z}',$$

which we equate to (2.37a), rewritten in terms of $(\tilde{u}, \tilde{w}, \tilde{z})$:

$$\begin{aligned} U' =& \big(\tilde{u} + \alpha_1\tilde{u}^2 + \alpha_2\tilde{w}^2 + \alpha_3\tilde{z}^2 + \alpha_4\tilde{u}\tilde{w} + \alpha_5\tilde{u}\tilde{z} + \alpha_6\tilde{w}\tilde{z}\big) \\ &- \frac{1}{\lambda_4}\big(\tilde{w} + \beta_1\tilde{u}^2 \ + \beta_2\tilde{w}^2 + \beta_3\tilde{z}^2 + \beta_4\tilde{u}\tilde{w} + \beta_5\tilde{u}\tilde{z} + \beta_6\tilde{w}\tilde{z}\big) \\ &+ \frac{1}{\mu_4\lambda_4}\big(\tilde{z} + \gamma_1\tilde{u}^2 + \gamma_2\tilde{w}^2 + \gamma_3\tilde{z}^2 + \gamma_4\tilde{u}\tilde{w} + \gamma_5\tilde{u}\tilde{z} + \gamma_6\tilde{w}\tilde{z}\big) \\ &+ \frac{1}{\lambda_4^2}\big[\tilde{w}\tilde{z} + \mathcal{O}(3)\big] - \frac{1}{\mu_4\lambda_4^2}\big[\tilde{z}^2 + \mathcal{O}(3)\big] \end{aligned}$$

Collecting terms in like powers of $(\tilde{u}, \tilde{w}, \tilde{z})$, substituting in for $\tilde{w}' = -\frac{1}{\lambda_4}\tilde{u} + \big(\frac{c}{\lambda_4} + 1\big)\tilde{w} + \frac{1}{\mu_4}\tilde{z} + \mathcal{O}(2)$ and $\tilde{z}' = \big(\frac{\eta}{D}\frac{1}{\lambda_4^2} + 1\big)\tilde{z} + \mathcal{O}(2)$ from (2.37), expanding $(1 + 2\alpha_1\tilde{u} + \alpha_4\tilde{w} + \alpha_5\tilde{z})^{-1}$ and solving for $\tilde{u}$, we find the transformation for u, as claimed. The argument for $\tilde{w}$ and $\tilde{z}$ is similar. □

The second-order normal from transformation obtained in Proposition 2.3 allows us to eliminate the quadratic terms from Equation (2.37), which improves the accuracy of the approximation to the c-a relation $a_\varepsilon(c)$; recall Equation (2.43). The derivation in second-order normal form follows the same process as the formal linearisation patching in Section 2.4.2.

Firstly, we invert the transformation as follows

$$\begin{aligned} \tilde{u} &= U - \frac{D\big[(\lambda_4 + 1)(2\eta^2 - Dc\eta\lambda_4) - \beta\big]}{\beta\mu_4(D{\lambda_4}^2 + \eta)}Z^2 - \frac{D}{D\lambda_4^2 + \eta}WZ + \mathcal{O}(3), \\ \tilde{w} &= W + \frac{D\lambda_4\big[\beta - (\lambda_4 + 1)(2\eta^2 + D\eta\lambda_4^2 - D\eta)\big]}{\beta\mu_4(D{\lambda_4}^2 + \eta)}Z^2 - \frac{D}{D\lambda_4^2 + \eta}UZ + \frac{cD}{D\lambda_4^2 + \eta}WZ + \mathcal{O}(3), \\ \tilde{z} &= Z - \frac{\eta}{D\lambda_4^2 + \eta}Z^2 + \mathcal{O}(3). \end{aligned}$$

Noting that we have obtained the explicit solutions for $r_1 = (A_1 + \frac{\alpha}{\eta})\mathrm{e}^{-\tau}$ and $\varepsilon_1 = \frac{\varepsilon}{A_1 + \frac{\alpha}{\eta}}\mathrm{e}^{\tau}$. Then, we transform the boundary conditions at $P_{\varepsilon 1}^{\mathrm{in}}$ and $P_{\varepsilon 1}^{\mathrm{out}}$ of (2.35) in section Σ_1^{in} and Σ_1^{out} into $\tilde{P}_{\varepsilon 1}^{\mathrm{in}}$ and $\tilde{P}_{\varepsilon 1}^{\mathrm{out}}$ in section $\tilde{\Sigma}_1^{\mathrm{in}}$ and $\tilde{\Sigma}_1^{\mathrm{out}}$ for our second-order normal form patching:

$$\tilde{P}_{\varepsilon 1}^{\mathrm{in}} := \Big(\tilde{u}^{\mathrm{in}}, r_1^{\mathrm{in}}, \tilde{w}^{\mathrm{in}}, \tilde{z}^{\mathrm{in}}, \varepsilon_1^{\mathrm{in}}\Big) \quad \text{at } \tau = 0, \tag{2.60a}$$

$$\tilde{P}_{\varepsilon 1}^{\mathrm{out}} := \Big(\tilde{u}^{\mathrm{out}}, r_1^{\mathrm{out}}, \tilde{w}^{\mathrm{out}}, \tilde{z}^{\mathrm{out}}, \varepsilon_1^{\mathrm{out}}\Big) \quad \text{at } \tau^* = \ln\frac{A_1 + \frac{\alpha}{\eta}}{\varepsilon}, \tag{2.60b}$$

where the corresponding transformed values at the boundaries in the $(\tilde{u}, \tilde{w}, \tilde{z})$-variables are

detailed in Appendix A.1.2, after eliminating higher order terms .

Patching at boundaries (2.60)

We can determine the related new coefficients A_i, C_i $(i = 1, 2, 3)$ in the general solution of Equation (2.59) with the $\mathcal{O}(3)$-terms omitted, by patching at the boundaries between the two sections $\widetilde{\Sigma}_1^{\text{in}}$ and $\widetilde{\Sigma}_1^{\text{out}}$ at the points of intersection $\widetilde{P}_{\varepsilon 1}^{\text{in}}$ and $\widetilde{P}_{\varepsilon 1}^{\text{out}}$, i.e., we solve the particular solution with specific boundary condition (2.60) in $(\tilde{u}, \tilde{w}, \tilde{z})$, which completes the construction of the orbit $\widetilde{\Gamma}_1$ in chart K_1; here, $\widetilde{\Gamma}_1$ denotes the approximation to the portion of the heteroclinic orbit Γ_1 in chart K_1 in region II by the second-order normal form patching; for details on the patching process, see Appendix A.1.2.

We obtain two simplified equations containing A_1 and A_2, are defined as $\widetilde{F}_i(A_1, A_2, c, \varepsilon) = 0\,(i = 1, 2)$,

$$\widetilde{F}_1 := \Big(\frac{\lambda_3 A_1}{A_1 + \frac{\alpha}{\eta}} - \lambda_4\Big) - \frac{\eta}{D\lambda_4^2 + \eta}\Big(\frac{\lambda_3 A_1}{A_1 + \frac{\alpha}{\eta}} - \lambda_4\Big)^2 - \Big(\lambda_3 - \frac{\eta\lambda_3^2}{D\lambda_4^2 + \eta}\Big)\Big(\frac{\varepsilon}{A_1 + \frac{\alpha}{\eta}}\Big)^{\delta_3}, \tag{2.61}$$

$$\begin{aligned}
\widetilde{F}_2 := {} & \left[\lambda_3^2\alpha_3 + \frac{(D\lambda_4^2 - D\lambda_3\lambda_4 + \eta)}{\mu_4(D\lambda_4^2 + \eta)}\right]\Big(c(D\lambda_4^2 + Dc\lambda_3 + \eta) + D\lambda_3\Big) \\
& + \left[\lambda_3^2\beta_3 + \frac{\lambda_4}{\mu_4} - \frac{D\lambda_3(1 - c\lambda_4)}{\mu_4(D\lambda_4^2 + \eta)}\right]\Big(D\lambda_4^2 + Dc\lambda_3 + \eta\Big) \\
& + \frac{(D\lambda_4^2 + Dc\lambda_3 + \eta)(1 - c\lambda_2) - D\lambda_2\lambda_3}{(\lambda_1 - \lambda_2)}\Big(\tilde{u}^{\text{in}} + \lambda_1\tilde{w}^{\text{in}} - \frac{D\lambda_2 + \eta\lambda_1 + c}{D\mu_3\mu_4}\tilde{z}^{\text{in}}\Big)\Big(\frac{\varepsilon}{A_1 + \frac{\alpha}{\eta}}\Big)^{-\delta_1} \\
& + \frac{(D\lambda_4^2 + Dc\lambda_3 + \eta)(1 - c\lambda_1) - D\lambda_1\lambda_3}{(\lambda_2 - \lambda_1)}\Big(\tilde{u}^{\text{in}} + \lambda_2\tilde{w}^{\text{in}} - \frac{D\lambda_1 + \eta\lambda_2 + c}{D\mu_3\mu_4}\tilde{z}^{\text{in}}\Big)\Big(\frac{\varepsilon}{A_1 + \frac{\alpha}{\eta}}\Big)^{-\delta_2} \\
& + \left[\frac{c\lambda_3(1 - D)}{\mu_3\mu_4} + (D\lambda_4^2 + Dc\lambda_3 + \eta)\frac{c^2(1 - D) + (\eta - D)}{D\mu_3\mu_4}\right]\tilde{z}^{\text{in}}\Big(\frac{\varepsilon}{A_1 + \frac{\alpha}{\eta}}\Big)^{-\delta_3}
\end{aligned} \tag{2.62}$$

Then, we can calculate the values of A_1 and A_2 by solving $\widetilde{F}_i = 0\,(i = 1, 2)$ numerically for given ε small, then substituting into the constraint of the c-a relation curve:

$$\tilde{a}_\varepsilon(c) = A_2 + \frac{A_1}{\mu_3} + 1 - \frac{\alpha}{\eta}. \tag{2.63}$$

Note that, we suppress the dependence on c and ε here for simplicity, i.e. $A_i = A_i(c, \varepsilon)$, $C_i = C_i(c, \varepsilon)$, and $\widetilde{F}_i = \widetilde{F}_i(A_1, A_2, c, \varepsilon)$. The proof of the existence of $\tilde{a}_\varepsilon(c)$ follows the same procedure as for $a_\varepsilon(c)$ in Section 2.4, which is equivalent to proving that we can get the unique solution from the two constraints $\widetilde{F}_i = 0, (i = 1, 2)$ by the Implicit Function Theorem. We find analogous results numerically as well, i.e., the persistence will be obtained by the Implicit Function Theorem.

2.5 Numerical simulations

In this section, we present the numerical simulations of the obtained speed relation $a_\varepsilon(c)$ and $\tilde{a}_\varepsilon(c)$ defined in (2.43) and (2.63), respectively, by formal linearisation and the second-order normal form in Sections 2.4.2 and 2.4.4, respectively. We also display the c-a relation obtained by the general patching, labeled $a(c, \varepsilon)$, are obtained by matching the general solution at the patching points: connecting regions I and II, and regions II and III, respectively, for the sake of the continuity of the general solution in each region in the original ODE system; for details we refer to Appendix A.1.1.

***Remark* 2.12.** We use the notation $a(c, \varepsilon)$ representing the speed c-a relation obtained by general patching, which is not an explicit formula for a depending on (c, ε).

***Remark* 2.13.** The parameters $\alpha(= 0.08)$ and $\eta(= 0.12)$ are fixed in the numerical computations throughout this chapter. Other choices of α and η give qualitatively similar results, which are not shown here.

2.5.1 Simulation of $a_\varepsilon(c)$

We first compute the result of $a_\varepsilon(c)$ obtained by formal linearisation in Section 2.4.2, in a range of values for the cut-off threshold ε in Figure 2.21, where $\varepsilon = 0.1$, 0.05, 0.01, 0.001 and $\varepsilon = 0$ for the values of $D = 1, 2, 5$ and 10. In the limit as $\varepsilon = 0$ (thin solid black), the upper branches of the curves show that the speed c grows as a decreases and may reach infinity when $a \to 0$; in particular, for $D = 1$, 2 and 5, one saddle-node bifurcation occurs in agreement with the study of bifurcation scenarios in Section 2.4.3, which admit the existence of a neutrally stable front at the bifurcation [57]. Moreover, we find the curves would cross the horizontal a-axis to negative values of the speed c, which should be considered in a symmetric situation; here, we only consider $c > 0$.

For D fixed, e.g., $D = 1$, the valid range of the speed c becomes wider as $\varepsilon \to 0$, i.e., the value of c_{max} increases by decreasing ε; the same phenomenon occurs for $D = 2$, 5, 10, in agreement with the definition of c_{max} in Equation (2.48) in Section 2.4.2.3. The fit of the perturbed curves to the singular curve improves as ε decreases; in particular, for ε sufficiently small, e.g. $\varepsilon = 0.01$ (dashed cyan) and $\varepsilon = 0.001$ (dotted magenta), the perturbed curves are close to the corresponding singular one, while for $\varepsilon = 0.1$ (solid blue) and $\varepsilon = 0.05$ (dash-dotted red), the numerical simulations suggest that these values of the cut-off threshold are too large.

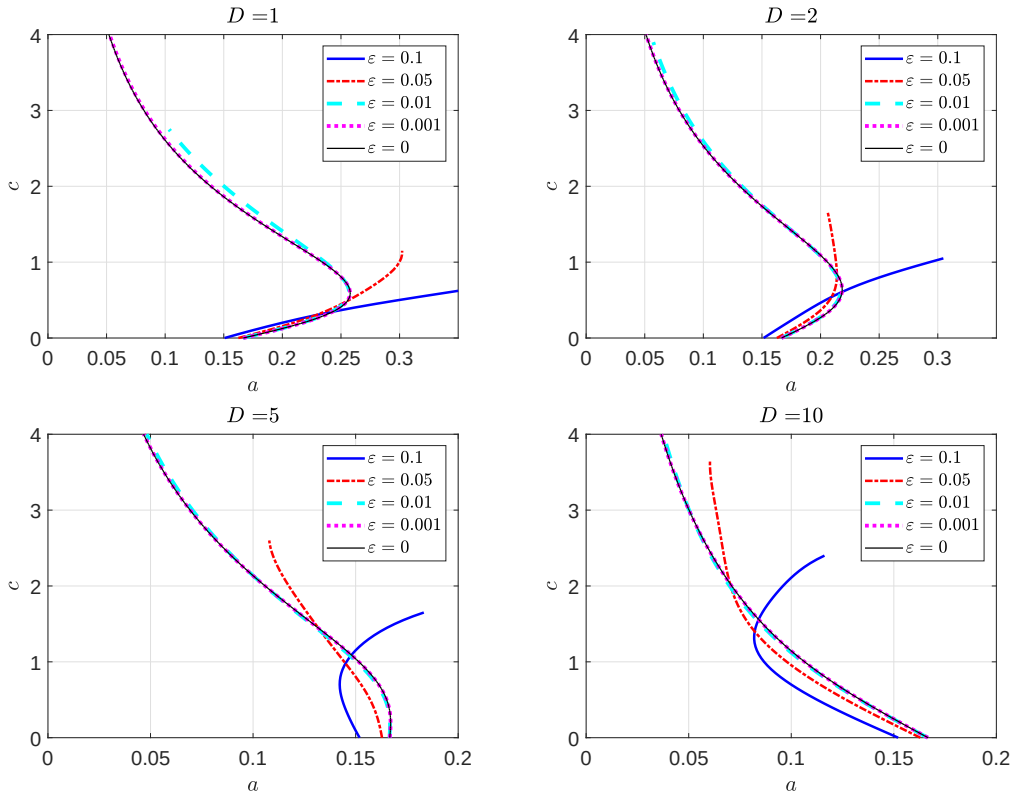

Figure 2.21: Speed relation obtained by formal linearisation patching $a_\varepsilon(c)$, for $D = 1, 2, 5, 10$, with $\varepsilon = 0.1, 0.05, 0.01, 0.001$ and $\varepsilon = 0$, for fixed $\eta = 0.12$, $\alpha = 0.08$.

.

We approximately compute the values of (a_b, c_b) at bifurcation points for $\varepsilon = 0.01$ and $\varepsilon = 0.001$; see Table 2.1. For $D = 1, 2$ and 5, we find that the perturbed bifurcation point approaches the corresponding singular one as $\varepsilon \to 0$; note that, no bifurcation exists for $D = 10$.

Table 2.1: Approximated bifurcation points (a_b, c_b) obtained by formal linearisation patching $a_\varepsilon(c)$, for $D = 1, 2, 5$ with $\varepsilon = 0.01, 0.001$ and 0, for fixed $\eta = 0.12$, $\alpha = 0.08$.

ε	0.01	0.001	0
$D = 1$	(0.2570, 0.5983)	(0.2578, 0.5914)	(0.2579, 0.5915)
$D = 2$	(0.2174, 0.6396)	(0.2184, 0.6403)	(0.2185, 0.6407)
$D = 5$	(0.1667, 0.1577)	(0.1671, 0.1946)	(0.1671, 0.1957)

2.5.2 Comparison of $a_\varepsilon(c)$ and $a(c, \varepsilon)$

In this section, we compare the results of $a_\varepsilon(c)$ and $a(c, \varepsilon)$, which are obtained by formal linearisation patching and general patching with $D = 1, 2, 5, 10$ and $\varepsilon = 0.01, 0.001$; see Figure 2.22. The solid red curves correspond to the results of $a_\varepsilon(c)$ by formal linearisation patching; the dash-dotted blue curves describe the results of $a(c, \varepsilon)$ by general patching; while the thin black curves represent the corresponding singular solutions. The small rectangular area along the curves is zoomed-in to the bottom left axes.

For fixed values of D , e.g. $D = 1$, we observe that the fit of the formal linearistion patching method improves as ε decreases, and the error of formal linearisation and the singular limit is about $\mathcal{O}(\varepsilon)$; the same phenomenon is found for $D = 2, 5$ and 10. For ε small and fixed, e.g. $\varepsilon = 0.01$, the fit also improves as D increases, which suggests that the value of $\frac{1}{D}$ plays a role of an additional "small" parameters such that the accuracy of formal linearisation patching improves; the same phenomenon is found for $\varepsilon = 0.001$.

Moreover, the red hexagram along the curve denotes the intersection of the curves, obtained by formal linearisation patching and in the singular limit; the corresponding speed at the intersection is labeled by c_{crit}. The value of c_{crit} increases as ε decreases for D fixed; also, it grows with the value of D for ε small and fixed.

For $c < c_{crit}$, the perturbed curve lies inside of the singular curve, i.e., the value of $a_\varepsilon(c)$ is less than $a_0(c)$; while for $c > c_{crit}$, the perturbed curve lies outside of the singular curve, i.e., the value of $a_\varepsilon(c)$ is greater than $a_0(c)$ in its valid speed range. When one bifurcation occurs, i.e., for $D = 1, 2$ and 5, the cut-off speed ($\varepsilon > 0$) remains higher than the singular speed below the bifurcation and above the critical intersection at c_{crit}; while the cut-off speed stays below the singular speed in the range of speeds between the bifurcation and intersection c_{crit}. In addition, for $D = 10$, i.e., when no bifurcation occurs, the cut-off speed stays above the singular speed for $c > c_{crit}$, while it remains below it for $c < c_{crit}$.

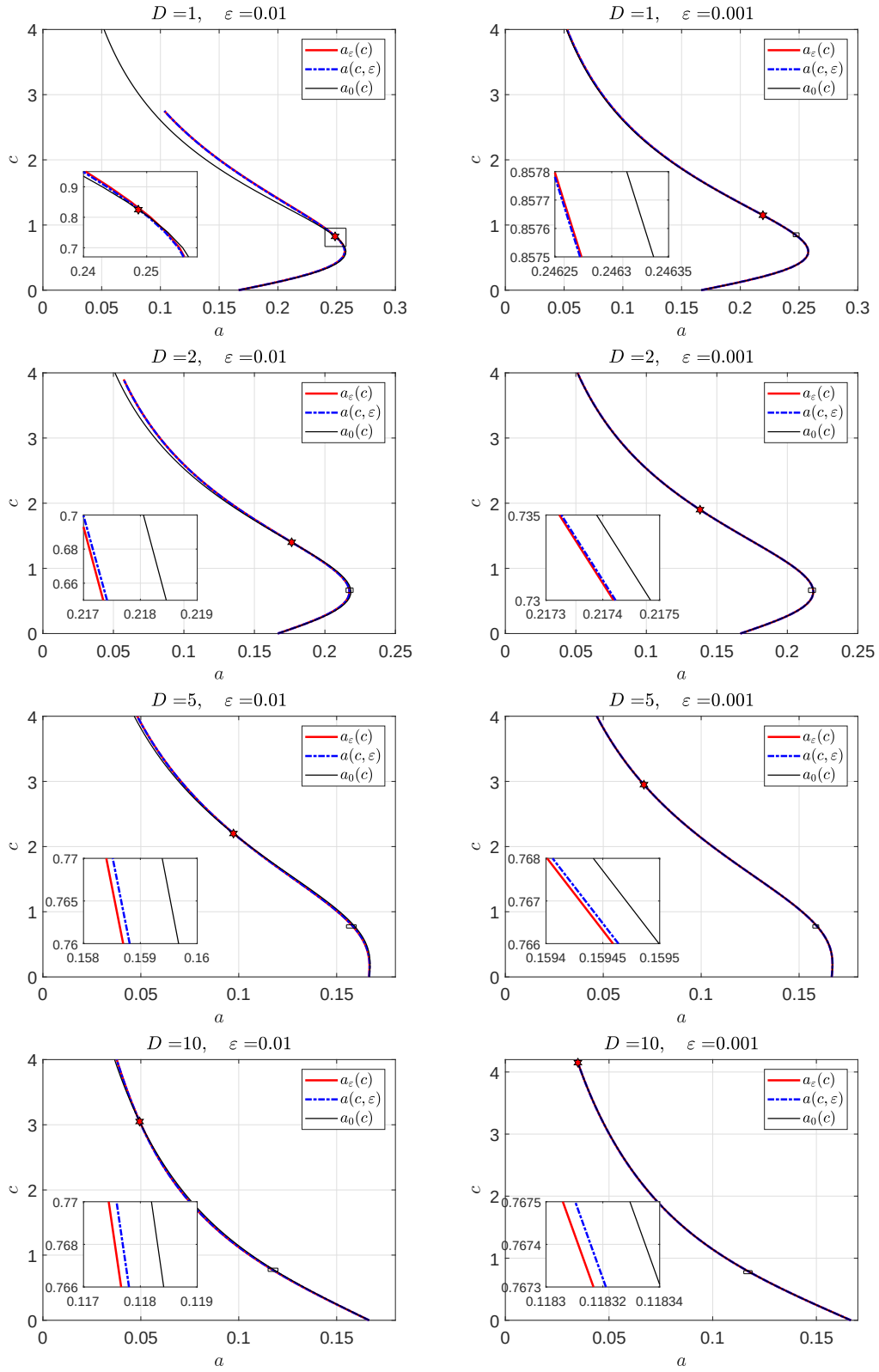

Figure 2.22: Speed relation obtained by formal linearisation patching $a_\varepsilon(c)$ (solid red), general patching $a(c,\varepsilon)$ (dash-dotted blue) and the singular limit $a_0(c)$ (thin solid black), for $D = 1, 2, 5, 10$ with $\varepsilon = 0.01, 0.001$ and $\varepsilon = 0$, for fixed $\eta = 0.12, \alpha = 0.08$; here, c_{crit} (red hexagram), the small rectangular area is zoomed-in to the bottom left axes.

2.5.3 Simulation of $\tilde{a}_\varepsilon(c)$

Now, we compare the error of the two blow-up patching approaches with general patching. We define the error $\Delta\tilde{a}_\varepsilon$, which is obtained from the results of second-order normal form patching and general patching, i.e., $\Delta\tilde{a}_\varepsilon = \tilde{a}_\varepsilon(c) - a(c,\varepsilon)$. Similarly, the error Δa_ε is obtained by the results of the formal linearisation patching and general patching, i.e., $\Delta a_\varepsilon = a_\varepsilon(c) - a(c,\varepsilon)$. Note that, the computations are carried out by prescribing the numerical values for the speed c and D.

In Figure 2.23, we display the error Δa_ε (solid red) for $\varepsilon = 0.1$ with $D = 1, 2, 5$ and 10; there, we observe that the order of the error Δa_ε is $\mathcal{O}(\varepsilon^2)$, which is better than the expected $\mathcal{O}(\varepsilon)$ by formal linearisation. Likewise, we simulate the error for $\varepsilon = 0.01$ and $\varepsilon = 0.001$, in Figure 2.24 and Figure 2.25, respectively; here, we find the same performance as that we have observed an order of $\mathcal{O}(\varepsilon^2)$ by formal linearisation. In order to explain this unexpected performance of the order $\mathcal{O}(\varepsilon^2)$ by formal linearisation, we recall Equations (2.37) in Section 2.4.2; there, we find that the Z-variable is decoupled, and the plane $\{Z = 0\}$ is invariant. Hence, the solution obtained for the Z-variable in Equation (2.38) is actually the exact solution, which enhances the accuracy of the formal linearisation patching.

As for the error $\Delta\tilde{a}_\varepsilon$ (dash-dotted magenta), which is illustrated in Figure 2.23 through Figure 2.25 for $\varepsilon = 0.1$, 0.01 and $\varepsilon = 0.001$, with $D = 1, 2, 5$ and 10, we observe that an accuracy of the order of $\mathcal{O}(\varepsilon^2)$ is provided by second-order normal form patching, which is in agreement with the accuracy expected from the second-order normal form transformation. Moreover, as we have observed that both formal linearisation and second-order normal form patching have an accuracy of the order $\mathcal{O}(\varepsilon^2)$, the latter still performs slightly better than the former.

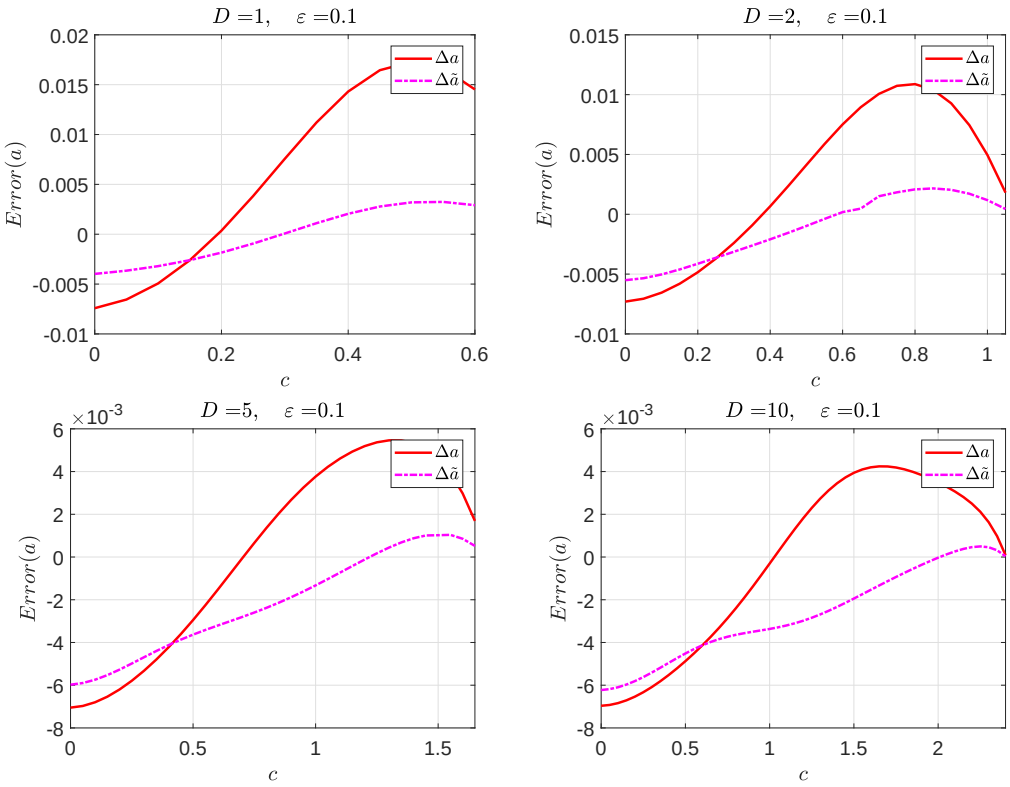

Figure 2.23: Numerical simulation of Δa_ε (solid red) and $\Delta\tilde{a}_\varepsilon$ (dash-dotted magenta), for $c \in [0, c_{max}]$, with $D = 1, 2, 5, 10$ and $\varepsilon = 0.1$, and $\eta = 0.12, \alpha = 0.08$ fixed.

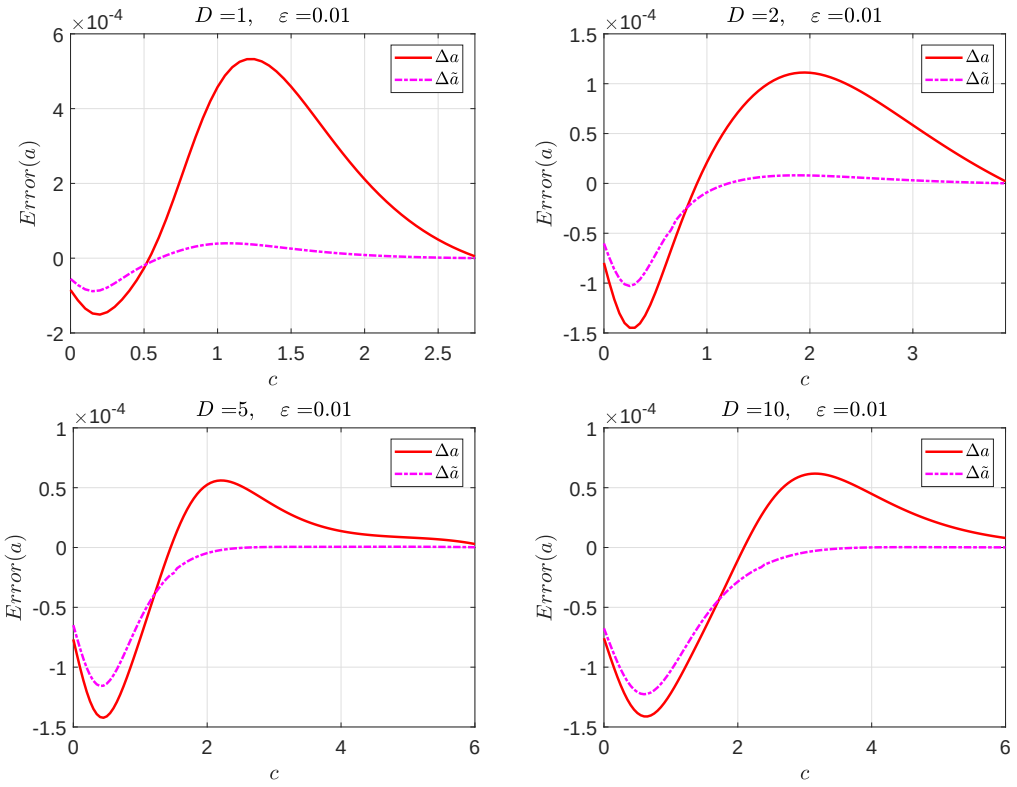

Figure 2.24: Numerical simulation of Δa_ε (solid red) and $\Delta\tilde{a}_\varepsilon$ (dash-dotted magenta), for $c \in [0, c_{max}]$, with $D = 1, 2, 5, 10$ and $\varepsilon = 0.01$, and $\eta = 0.12, \alpha = 0.08$ fixed.

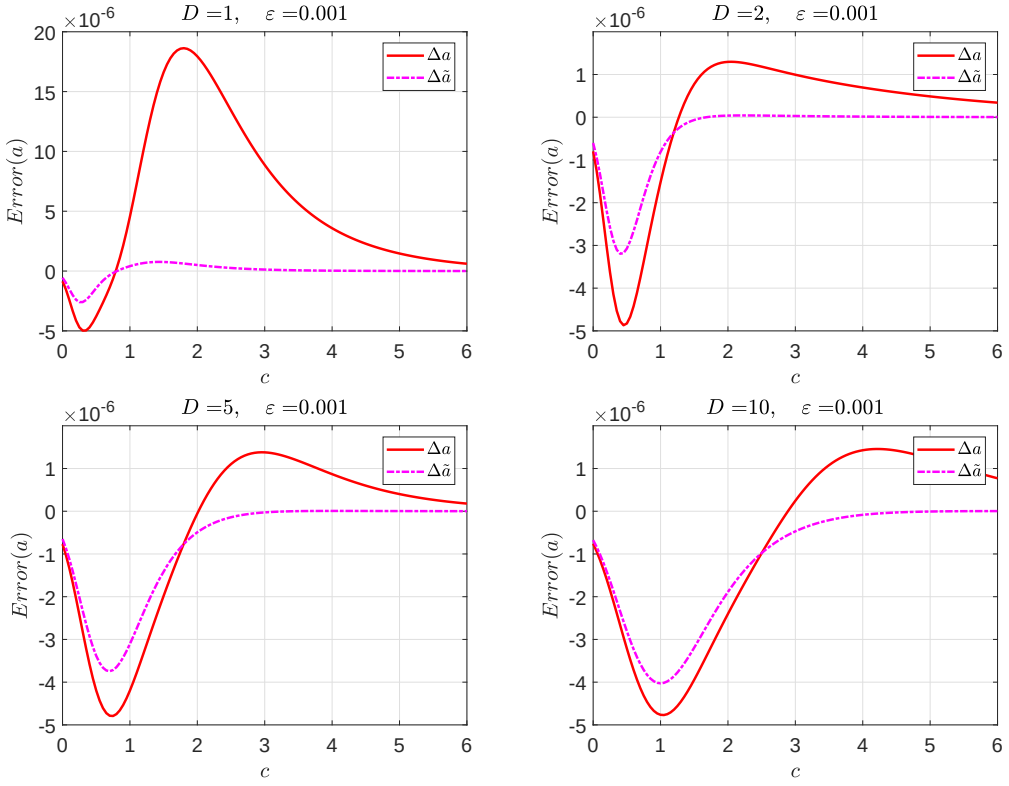

Figure 2.25: Numerical simulation of Δa_ε (solid red) and $\Delta\tilde{a}_\varepsilon$ (dash-dotted magenta), for $c \in [0, c_{max}]$, with $D = 1, 2, 5, 10$ and $\varepsilon = 0.001$, and $\eta = 0.12, \alpha = 0.08$ fixed.

In addition, the accuracy is improved with the value of D, which is in agreement of our suggestion in Section 2.5.2 that the factor $\frac{1}{D}$ plays role of a "small" parameter.

We have observed that the formal linearisation patching method has provided an accuracy of order $\mathcal{O}(\varepsilon)$ in Section 2.5.2, which fits well with the singular limit. We then represent the error $\tilde{a}_\varepsilon(c) - a_0(c)$, which is obtained by the results of the second-order normal form patching and the singular limit, see Figure 2.26. For $\varepsilon = 0.01$ (a) and $\varepsilon = 0.001$ (b), with $D = 1, 2, 5$ and 10, we observe that $\tilde{a}_\varepsilon(c) - a_0(c)$ is approximately of the order of $\mathcal{O}(\frac{\varepsilon}{D})$, where we have combined the factor of $\frac{1}{D}$ with the order $\mathcal{O}(\varepsilon)$ observed in Section 2.5.1; meanwhile, $\tilde{a}_\varepsilon(c) - a_0(c)$ has a root at $c = \tilde{c}_{crit}$, where $\tilde{c}_{crit}$ corresponds to the intersection of the results by second-order normal form patching and the singular limit; recall the definition of c_{crit}, which is defined in Section 2.5.2 for the formal linearisation, i.e., by $a_\varepsilon(c) - a_0(c)|_{c=c_{crit}} = 0$.

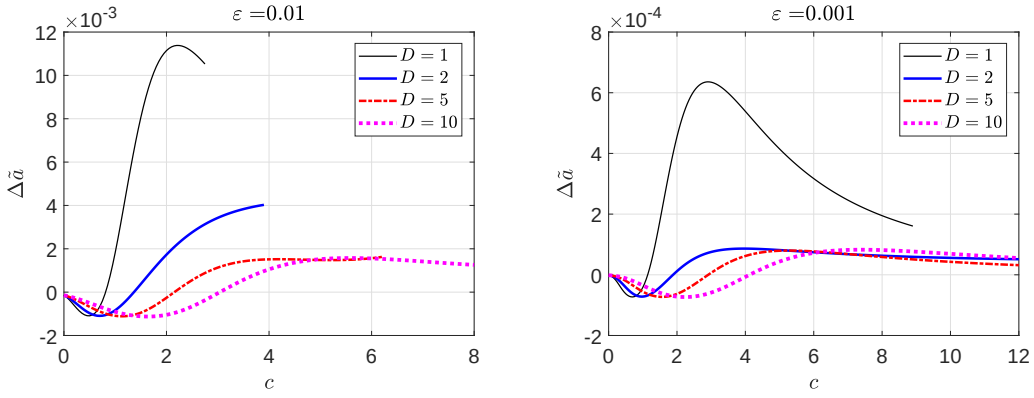

Figure 2.26: Numerical calculation of $\tilde{a}_\varepsilon(c) - a_0(c)$ in the valid speed range, with $D = 1, 2, 5, 10$ and (a) $\varepsilon = 0.01$ and (b) $\varepsilon = 0.001$, for $\eta = 0.12, \alpha = 0.08$ fixed .

***Remark* 2.14.** We may proceed to a higher-order normal form transformation in the study of the transition through chart K_1, in order to obtain a higher accuracy. However, the formal linearisation patching seems to provide a good approximation to our general solution with $\mathcal{O}(\varepsilon^2)$ accuracy. While the second-order normal form improves the accuracy of patching in blown-up space slightly within the order of $\mathcal{O}(\varepsilon^2)$, we do not proceed to a third-order normal form and further in this thesis.

2.5.4 Simulation of the orbits

Recalling the basic properties of Equation (2.5), the four eigenvalues $\lambda_i\,(i = 1...4)$ depend on c and D. The values of the strong/weak eigenvalues vary as well, although the strong/weak eigenvectors do not switch as we consider $D \geqslant 1$ here. This will lead to interesting behavior in that the patching position varies at the cut-off threshold. And the shape of the orbit in (u, v)-phase space will change depending on the speed as well. For example, for $D = 2$ and $\varepsilon = 0.01$, here, we recall the numerical c-a relation for $D = 2$ and $\varepsilon = 0.01$ in Figure 2.27.

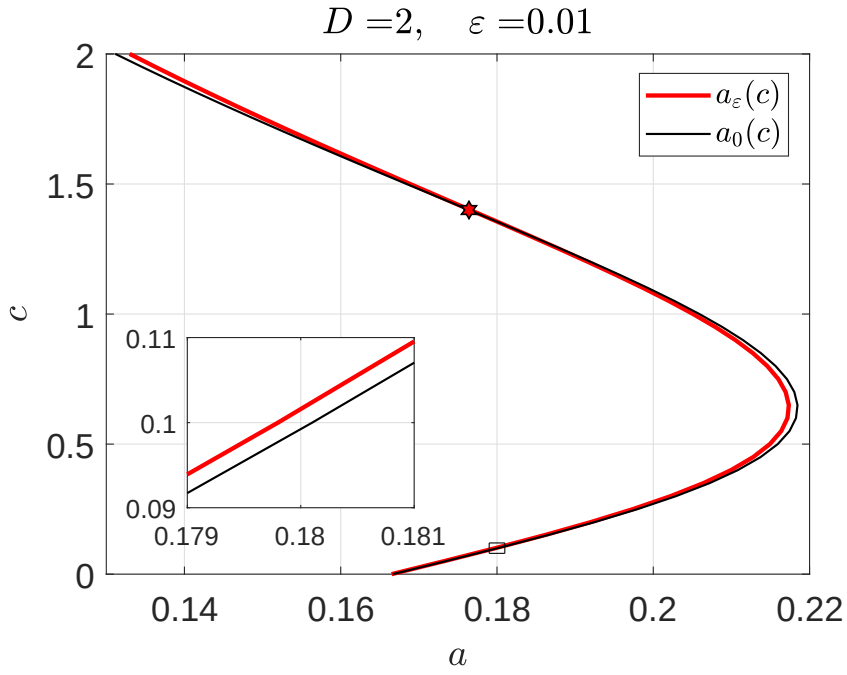

Figure 2.27: Speed relation obtained by formal linearisation patching $a_\varepsilon(c)$ (solid red) and the singular limit $a_0(c)$ (thin solid black); for $D = 2$ and $\varepsilon = 0.01$; $\eta = 0.12, \alpha = 0.08$ fixed.

We simulate the front solution at different speeds numerically, and plot the corresponding orbit in (u, v)-coordinates; see Figures 2.28 through 2.30. The perturbed orbit (dash-dotted diamond) obtained from the front solution by formal linearisation patching consists of three segments, which are divided by two red dots corresponding to the discontinuity position and the cut-off threshold, respectively. The singular orbit is indicated by a dashed blue line with the "outer" region and the "inner" region separated by the corresponding discontinuity position (blue diamond). In addition, we zoom in to the parts of the orbits around the origin (top left axes) and the discontinuity position (bottom right axes).

i. Low speed: Here, we take $c = 0.05$ as the example for the low speed case. We find that the perturbed orbit follows a similar path as the singular orbit in region I and region II until reaching the cut-off threshold ε; here, we take $\varepsilon = 0.01$ for example. For $v \in (0, \varepsilon)$ in region III, where the reaction term is switched off, the corresponding values of u in the perturbed orbit are greater than those in the singular orbit, and u stays negative in that range; Meanwhile, this perturbation of the orbit agrees with the behavior of the c-a relation, where for $c = 1 \in (0, c_b)$, the value of $a_\varepsilon(c)|_{c=1}$ is less than $a_0(c)|_{c=1}$; see Figure 2.28. The local geometric structure in the equivalent blown-up space can be found in Section 2.3.2; see Figures 2.7 and 2.8.

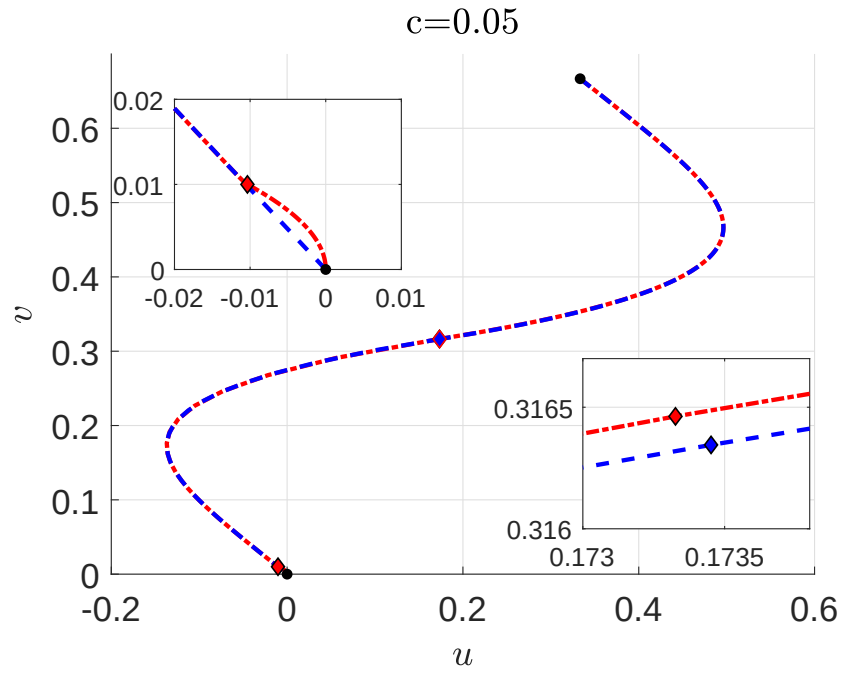

Figure 2.28: The orbits in (u, v)-phase space: perturbed orbit (dash-dotted red) and singular orbit (dashed blue), with discontinuity position and cut-off threshold (colored diamond), at speed $c = 0.05$, for $D = 2$ with $\varepsilon = 0.01$, and $\eta = 0.12$, $\alpha = 0.08$ fixed.

ii. Intermediate speed: Here, we take $c = 1$ and $c = 1.55$ as two examples for the intermediate speed case. We find that the perturbed orbit follows a similar path as the singular orbit in region I and the most part of region II. However, around the cut-off threshold in region II, e.g., for $v \in (\varepsilon, 2\varepsilon)$, the corresponding values of u in the perturbed orbit are greater than those in the singular orbit. Likewise, in region III, i.e. for $v \in (0, \varepsilon)$, the corresponding values of u in the perturbed orbit are greater than those in the singular orbit and u stays negative; see Figure 2.29; The local geometric structure in the equivalent blown-up space can be found in Section 2.3.2, see Figure 2.7 and 2.9. Meanwhile, this perturbation of the orbit agrees with the behavior of the c-a relation, where for $c = 1 \in (c_b, c_{crit})$, the value of $a_\varepsilon(c) - a_0(c)|_{c=1} < 0$; for $c = 1.55 \in (c_{crit}, c_{max})$, the value of $a_\varepsilon(c) - a_0(c)|_{c=1.55} > 0$; see the numerical simulation in Figure 2.22.

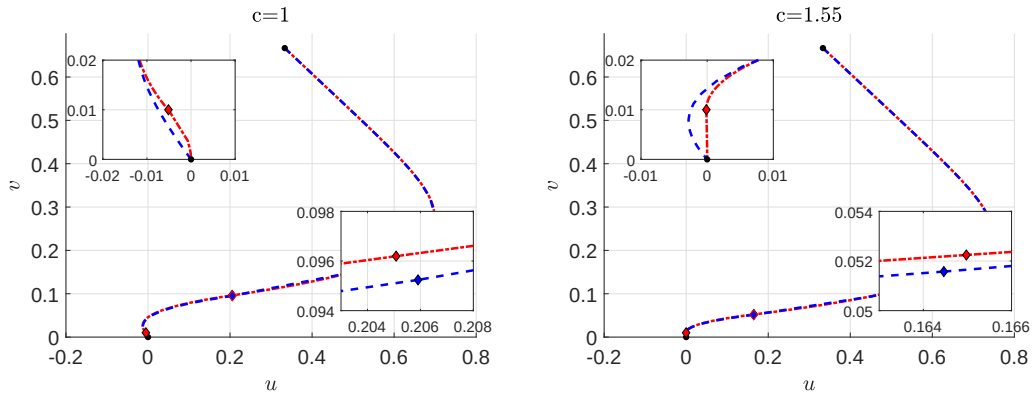

Figure 2.29: The orbits in (u, v)-phase space: perturbed orbit (dash-dotted red) and singular orbit (dashed blue), with discontinuity position and cut-off threshold (colored diamond), at speed $c = 1$ and $c = 1.55$, for $D = 2$ with $\varepsilon = 0.01$, and $\eta = 0.12$, $\alpha = 0.08$ fixed.

iii. High speed: Here, we take $c = 2$ as the example for the high speed case. We find that the

perturbed orbit follows the similar path as a singular limit orbit in region I and the most part of region II. However, around the cut-off threshold in region II, e.g., for $v \in (\varepsilon, 2\varepsilon)$, the corresponding values of u in the perturbed orbit are greater than those in the singular orbit. Likewise, in region III, i.e. for $v \in (0, \varepsilon)$, the corresponding values of u in the perturbed orbit are much greater than those in the singular orbit and u stays positive; see Figure 2.30; The local geometric structure in the equivalent blown-up space can be found in Section 2.3.2, see Figure 2.7 and 2.10. Meanwhile, this perturbation of a front solution agrees with the behavior of the c-a relation, for $c = 2 \in (c_{crit}, c_{max})$, the value of $a_\varepsilon(c)$ is greater than $a_0(c)$; moreover, the error of $a_\varepsilon(c) - a_0(c)|_{c=2} (\approx 0.01)$ is greater than $a_\varepsilon(c) - a_0(c)|_{c=1.55} (\approx 0.005)$; see the numerical simulation in Figure 2.22.

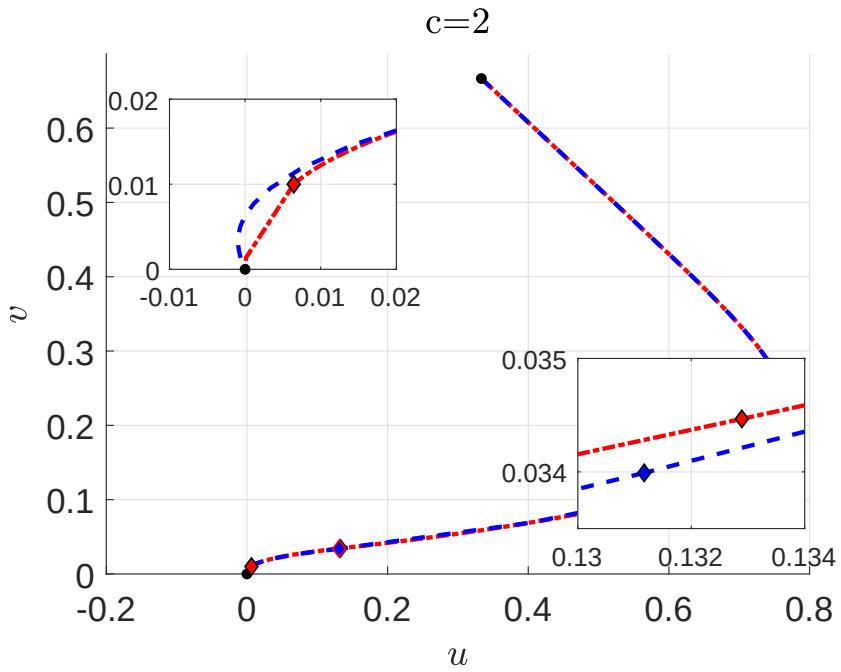

Figure 2.30: The orbits in (u, v)-phase space: perturbed orbit (dash-dotted red) and singular orbit (dashed blue), with discontinuity position and cut-off threshold (colored diamond), at speed $c = 2$, for $D = 2$ with $\varepsilon = 0.01$, and $\eta = 0.12$, $\alpha = 0.08$ fixed.

The observations around the discontinuity position $u = a$: for $c = 0.05$ and 1, i.e., $c < c_{crit}$, we clearly find that the values of the u-coordinate of the patching points $a_\varepsilon(c)$ are to the left of the singular patching point $a_0(c)$, i.e., $a_\varepsilon(c) - a_0(c)|_{c=0.05,c=1} < 0$, which agrees with our numerical observation of a_ε and a_0 in Figure 2.27; there, the perturbed $a_\varepsilon(c)$ curve stays slightly inside the singular limit of $a_0(c)$. For $c = 1.55$ and 2, i.e., for $c > c_{crit}$, we clearly find that the values of the u-coordinate of patching points $a_\varepsilon(c)$ are to the right of the singular patching point $a_0(c)$, i.e., $a_\varepsilon(c) - a_0(c)|_{c=1.55,c=2} > 0$, which agrees with our numerical observation of a_ε and a_0 in Figure 2.27; there, the perturbed curve $a_\varepsilon(c)$ stays slightly outside the singular limit of $a_0(c)$.

When one bifurcation scenario occurs, i.e., for $D \in (1, D^*)$ as defined in Section 2.4.3, with ε positive and small, the cut-off accelerates the front corresponding to the singular one in a range of speed $c \in \{(0, c_b) \cup (c_{crit}, c_{max})\}$, i.e., the cut-off accelerates the unstable speed and top part of the stable speed. By contrast, in a range of $c \in (c_b, c_{crit})$, the cut-off slows down the related stable fronts. When we take $D \in (D^*, 22)$, no bifurcation occurs in the c-a relation, then, the perturbed speed is slightly lower than the singular speed in a range of $c \in (0, c_{crit})$, while it is higher in $c \in (c_{crit}, c_{max})$.

We can also find such a shift in the cut-off speed in the numerical simulation of the second-order normal form patching, see Figure 2.26, where the sign of $\tilde{a}_\varepsilon(c) - a_0(c)$ changes at $c = \tilde{c}_{crit}$; note that, the value of $\tilde{c}_{crit}$ is similar to c_{crit} within the order of $\mathcal{O}(\varepsilon^2)$, hence, the observations

corresponding to the critical speed $\tilde{c}_{crit}$ by second-order normal form are omitted here, which are in agreement with those for c_{crit} by formal linearisation.

To summarize the effect of a cut-off on the (u, v) orbits of our two-component reaction-diffusion systems (2.4), the local curvature of the perturbed orbits around the origin changes depending on the value of ε and the speed c; in particular, the perturbed orbits are restricted in the first quadrant in the (u, v)-phase space in a specified range of the values of (c, ε), i.e., the cut-off could prevent the u-variable reacting in the negative area, which makes the corresponding system more realistic biologically. Moreover, for ε sufficiently small, the perturbed speed may stay below the singular speed in a particular speed range, e.g., $c \in (c_b, c_{crit})$ and $c \in (0, c_{crit})$ for one bifurcation and no bifurcation, respectively, which performs similarly to the recent research on the FKPP equation with a cut-off; there a logarithmic term was subtracted from the minimum speed obtained in the absence of a cut-off; for details see [9, 15].

2.6 Speed condition in u-component cut-off system

The dynamics of the u-component cut-off system is best studied in an equivalent formulation of Equation (2.4) with $\phi = u$ that results from a blow-up transformation of the corresponding vector field near the origin in $(u, v, w, z, \varepsilon)$-space. The approach follows the same procedure as that we followed for the v-component cut-off system. Hence, we do repeat the analysis; for details see Appendix A.3. Note that, we also keep the symbols for the basic notation for the sake of simplicity, e.g., we reuse A_i, C_i $(i = 1, 2, 3)$ denoting the corresponding coefficients in the analysis of u-component cut-off system.

As we have observed in Section 2.2.3, we require an extra condition on applying the blow-up technique so that the value of v stays in a neighborhood of the origin. To that end, we define a valid range of the speed consisting of a maximum and a minimum speed.

The maximum speed c follows the same idea as we have given in the v-component cut-off; see Section 2.4.2.3. Recall the definition of the region II, i.e., $u \in (\varepsilon, a)$, and $a \in (\varepsilon, 1 - \frac{\alpha}{\eta})$; where the restriction on a is necessary for the existence of a front connecting the two steady states as mentioned in Section 2.1. We can approximate the maximum speed by setting $\frac{a}{\varepsilon} \equiv 1$ in the c-a relation F_ε in Equation (A.42), which is an explicit formula obtained by formal linearisation patching, i.e., the region II is eliminated and the transition time given by $\tau = \tau^* = 0$. Then we obtain an equation $F_{c1} = \varepsilon$, where

$$F_{c1} := \frac{\alpha c}{4\eta^2} \frac{(c - \sqrt{c^2+4})(c - \sqrt{c^2+4D\eta})(c - Dc + D\sqrt{c^2+4} - \sqrt{c^2+4D\eta})}{c(D-1)(c - \sqrt{c^2+4D\eta}) - 2D\eta + 2D^2} + \frac{1}{4}(1 - \frac{\alpha}{\eta})(c - \sqrt{c^2+4})^2, \tag{2.64}$$

where the value of c_{max} satisfies $F_{c1}|_{c=c_{max}} = \varepsilon$.

The minimum speed is defined to ensure the value of v stays in a neighborhood around the origin. Here, we define a "small" quantity σ, which is a constant or a function in dependence on ε; if the value of v at the cut-off threshold $u = \varepsilon$ satisfies the inequality $v|_{u=\varepsilon} \leqslant \sigma$, then we treat this point of $(u, v)|_{u=\varepsilon}$ as a neighborhood of the origin. Transferring this inequality into the equivalent blown-up space in chart K_1, i.e. $v = v_1 r_1$ with $u = r_1$, we obtain that $v_1^{\text{out}} r_1^{\text{out}} \leqslant \sigma$; note that, $v_1^{\text{out}} = -\frac{D}{c} A_3$ is defined in Σ_1^{out} of (A.40), and the solution of A_3 is given in (A.41). Hence, the desired formula for $v\,(= v_1^{\text{out}} r_1^{\text{out}})$ is labeled by $F_{c2} = \sigma$:

$$F_{c2} := -\frac{D\,\alpha}{c\sqrt{c^2 + 4\,D\,\eta}} \left(\frac{\left(c - \sqrt{c^2 + 4\,D\,\eta}\right)^4}{16\,D^3\,\eta^2} - 1 \right) \left(\frac{\varepsilon}{a}\right)^{\frac{c+\sqrt{c^2+4\,D\,\eta}}{D\,(c+\sqrt{c^2+4})}}, \tag{2.65}$$

where the values of c and a are obtained by the corresponding speed relation $F_\varepsilon = 0$ in (A.41).

The minimum speed c_{min} satisfies the above equation $F_{c2} = \sigma$; the speed in a range of $c \geqslant c_{min}$ will support the application of the blow-up technique in the u-component cut-off system.

In all, the valid speed range for the u-component cut-off system via the blow-up technique is represented by $(c_{min},\, c_{max})$, where $F_{c1}|_{c=c_{max}} = \varepsilon$ and $F_{c2}|_{c=c_{min}} = \sigma$ with $F_\varepsilon = 0$.

For a more extensive discussion and numerical results, we refer to Appendix A.3.

Some numerical results

Here, we approximate the values of c_{min} and c_{max} by setting $\sigma = \varepsilon$ for ease of computation, for the corresponding valid speed range see Table 2.2.

Table 2.2: Approximated valid speed range (c_{min}, c_{max}), for $D = 1, 2, 5$ and 10 with $\varepsilon = 0.01,\ 0.05,\ 0.01$, and $\sigma = \varepsilon$, for fixed $\eta = 0.12$, $\alpha = 0.08$

ε	0.1	0.05	0.01
$D = 1$	(0.5050, 2.8136)	(0.6302, 4.2291)	(0.8766, 9.8919)
$D = 2$	(0.8677, 2.8005)	(1.1870, 4.2191)	(2.1936, 9.8878)
$D = 5$	(1.6132, 2.7507)	(2.4080, 4.1885)	(5.5943, 9.8755)
$D = 10$	(2.4176, 2.6570)	(3.6717, 4.1349)	(8.7047, 9.8548)

Then, we present the comparison of the results of formal linearisation patching (F_ε) and the general patching solution (G_ε) with $D = 1, 2, 5, 10$ and $\varepsilon = 0.05$; see Figure 2.31. We find that the fit varies with different D: the fit is good for $D = 1$ and 2, while for D large, e.g. $D = 5$ or 10, the fit is bad in the range of the speed $c \in (0, 1)$, which suggests the valid speed range of $\big(c_{min}, c_{max}\big)$ as mentioned above. For instance, when $D = 5$, $c_{min} = 2.4080$, we find the fit is good above the minimum valid speed; the same phenomenon occurs for $D = 10$.

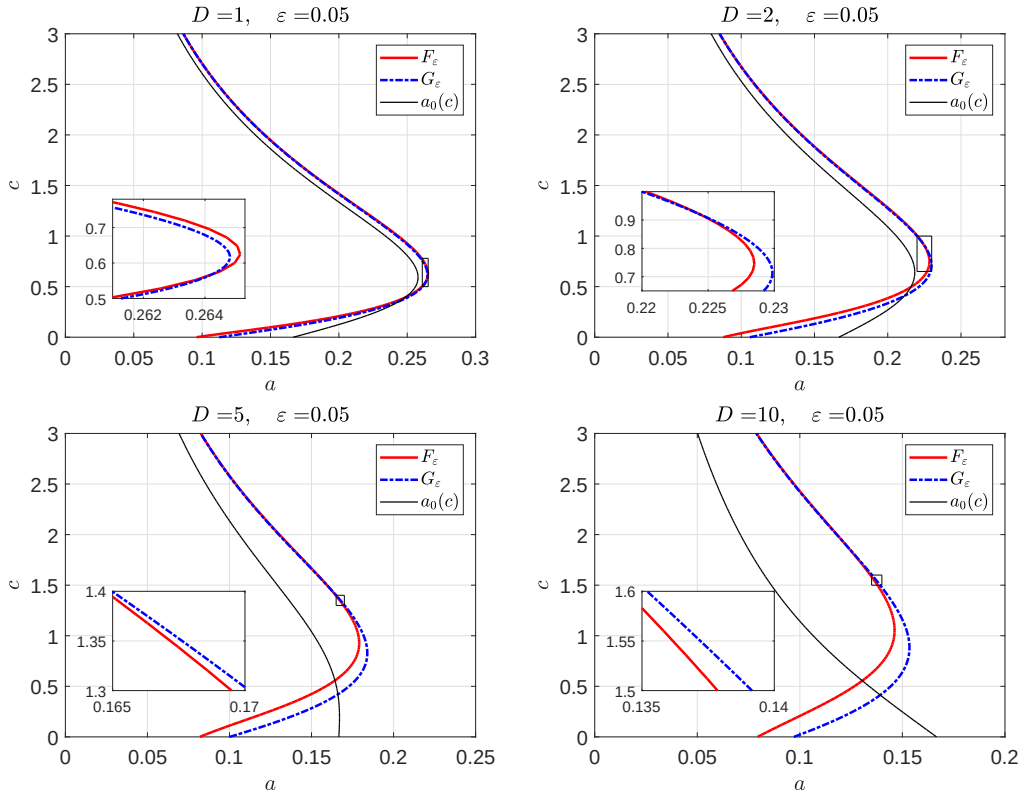

Figure 2.31: Speed relation obtained by formal linearisation patching F_ε, general patching G_ε and the singular limit $a_0(c)$, for $D = 1, 2, 5, 10$ with $\varepsilon = 0.05$, for fixed $\eta = 0.12, \alpha = 0.08$; here, the small rectangular area is zoomed-in to the bottom left axes.

2.7 Conclusions

Originally, the two-component system with Tonnelier-Gerstner reaction kinetics is one example of the Morris-Lecar model, which is used to illustrate oscillations in the giant muscle fiber of barnacles [67]. Due to its biophysical meaning and the fact that parameters are measurable, it has received increasing attention in the computational neuroscience community [74]. In this chapter, we have discussed the two component reaction-diffusion system with Tonnelier-Gerstner kinetics with a cut-off by a combination of geometric analysis and numerical simulations.

For v-component cut-off system,

- We display the local and global structure of the singular and perturbed orbits in the blown-up space; in particular, there exist three distinct scenarios of orbits in $(\bar{u}, \bar{w}, \bar{\varepsilon})$-space: low, intermediate and high speed, which are determined by the position of corresponding P_2^{in} in chart K_2.

- The existence of the singular orbit Γ is equivalent to the existence of the transition in chart K_1, where we observe the bifurcation behavior in the c-a speed relation. Then we perform a formal linearisation and derive second-order normal form to obtain the corresponded relation $a_\varepsilon(c)$ and $\tilde{a}_\varepsilon(c)$, respectively; and the formal linearisation patching provides good accuracy between $a_\varepsilon(c)$ and $a(c, \varepsilon)$.

- The maximum speed c_{max} is obtained by the criteria that region II vanishes via by formal linearisation analysis, and c_{max} will tend to ∞ as $\varepsilon \to 0$; there also exists a critical value of speed c_{crit} represents the intersection of the curves of $a_\varepsilon(c)$ and $a_0(c)$.

- For ε sufficiently small, the cut-off will affect the propagating speed in different speed range: accelerate the front or slow it down. In other words, cut-off pushes down the discontinuity position a corresponding to the singular front solution for $c \in (0, c_{crit})$, pulls up the position in $c \in (c_{crit}, c_{max})$.

For u-component cut-off system, the approach follows the same procedure as that we followed for the v-component cut-off system. Due to the specific situation as we have discussed in Section 2.2.3, extra speed condition is required to ensure that the solution stays in the neighborhood of the origin, hence

- We define a valid range of the speed by (c_{min}, c_{max}), c_{min} is defined to ensure the value of v stays in a neighborhood around the origin, c_{max} follows the same idea as we have given in the v-component cut-off that region II vanishes.

- We perform a formal linearisation and derive second-order normal form to obtain the corresponded relation, see Appendix A.3; and the formal linearisation patching alos provides good accuracy for the speed in its valid range (c_{min}, c_{max}), c_{min}.

- The cut-off could prevent the u-variable from becoming negative, which makes the corresponding system more realistic biologically.

For further work, as our analysis is not fully rigorous, but as there is no resonance in the underlying system, we do not consider the effect of higher order terms of the system in our transition in chart K_1, one may use more accurate normal form transformation and estimate the effect of more terms on the related system to proceed a more accurate approach.

Chapter 3

Oscillations in a cAMP signaling model for cell aggregation

3.1 Introduction

In the present chapter, we perform a geometric analysis of a singularly perturbed model for a cyclic AMP (cAMP) signaling system that controls aggregation of the amoeboid microorganism *Dictyostelium discoideum*. The life cycle of Dd contains many basic processes throughout the development of biology, in particular, the Dd cells, which are randomly located, will secrete cAMP transferring information in the media through cell membrane. The extracellular cAMP will activate the production of cAMP from intracellular ATP by binding the activate state of the receptor. There exist the transitions between the activate state and the desensitized state via a conformational change. The concentration of intracellular cAMP should remain within some concentration level so that the cells can function normally, when concentration of intracellular cAMP exceeds some limit, then cells secrete cAMP. The propagation of cAMP performs the wavelike biological pattern formation, which has been studied for many different mathematical models.

The periodic synthesis of pulses of cAMP constitutes an example of a biochemical oscillation of clear physiological significance [24]. Two main types of dynamic behaviour are observed in cAMP signaling systems: autonomous oscillation [23, 24, 26] and relay of super-threshold pulses [59, 63]. The model of cAMP signaling due to Goldbeter and Segel [27, 28] shows that both types of dynamics are caused by the auto-catalytic regulation of adenylate cyclase, the latter enzyme being activated on the binding of extracellular cAMP to the cell receptor [25, 58]. Moreover, relay behaviour has been linked with autonomous oscillation, which represents the excitability of the system. In the model by Goldbeter and Segel, the substrate ATP plays a role in the oscillation and relay response; however, it has been shown experimentally that intracellular ATP remains constant during the oscillation [60], and that the relay results from the absence of ATP consumption when the cAMP receptor is uncoupled from adenylate cyclase upon incubation with caffeine [66]. These observations were made under the assumption that adenylate cyclase is an allosteric enzyme; moreover, significant variation is required in the concentration of ATP. Goldbeter and Martiel considered another situation, whereby the mechanism is based on desensitisation of the cAMP receptor to extracellular cAMP, see Figure 3.1.

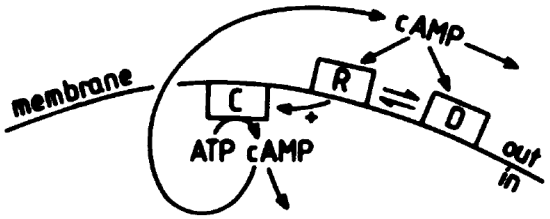

Figure 3.1: Model of the cAMP signaling system [46]

The full model proposed by Martiel and Goldbeter, which consists of seven differential equations, can be reduced to the three-variable system

$$\frac{d\rho_T}{dt} = -f_1(\gamma)\rho_T - f_2(\gamma)(1-\rho_T), \tag{3.1a}$$

$$\frac{d\beta}{dt} = q\sigma\phi(\rho_T,\gamma) - (k_i+k_t)\beta, \tag{3.1b}$$

$$\frac{d\gamma}{dt} = \frac{k_t}{h}\beta - k_e\gamma, \tag{3.1c}$$

with

$$f_1(\gamma) = \frac{k_1+k_2\gamma}{1+\gamma}, \quad f_2(\gamma) = \frac{k_1L_1+k_2L_2\gamma}{1+c\gamma}, \tag{3.2a}$$

$$\phi(\rho_T,\gamma) = \frac{\alpha(\lambda\theta+\epsilon Y^2)}{1+\alpha\theta+\epsilon Y^2(1+\alpha)}, \quad \text{and} \quad Y = \frac{\rho_T\gamma}{1+\gamma}. \tag{3.2b}$$

Here, ρ_T represents the total fraction of receptor in the active state, while β and γ denote intracellular and extracellular concentrations, respectively, of cAMP. Moreover, c, α, λ, θ, ϵ, σ, h, k_i, k_t, k_e, k_j, L_j $(j=1,2)$, and q are suitably defined parameters; details can be found in [46]. Equation (3.1) can be reduced further to a two-variable system for sufficiently large value of the parameters q, k_i, and k_t, which allows a quasi-steady-state assumption to be made for β: Equation (3.1b) implies $\beta = q\sigma\frac{\phi(\rho_T,\gamma)}{(k_i+k_t)}$. Therefore, the effective dynamics is then characterised by the following planar system of nonlinear ordinary differential equations (ODEs),

$$\frac{d\rho_T}{dt} = -f_1(\gamma)\rho_T - f_2(\gamma)(1-\rho_T), \tag{3.3a}$$

$$\frac{d\gamma}{dt} = \frac{q\sigma k_t}{h(k_i+k_t)}\phi(\rho_T,\gamma) - k_e\gamma. \tag{3.3b}$$

While experiments [46] indicate that $q \gg 1$, whereas k_i and k_t are of the order 1, and hence lower than what is expected for a quasi-steady-state assumption, numerical simulation shows that the planar system in (3.3) provides a reasonably good approximation for the three-variable system in (3.1). Therefore, (3.3) can be considered as the core mechanism in the cAMP signaling system, allowing for a phase plane analysis for relay and oscillation due to the simplicity of the governing equations.

With these observations in mind, we now introduce the singular perturbation problem considered in the present chapter, which is based on a model that was proposed by Lițcanu and Velázquez in [43] as a rescaled version of the three-variable Martiel-Goldbeter model, Equation (3.1):

$$R_\tau(\tilde{x},\tau) = \kappa(U+\mathcal{P}\varepsilon)\left[\frac{\mu(U+\varepsilon)-(U+d\varepsilon)R}{(U+\frac{\varepsilon}{c})(U+\varepsilon)}\right], \tag{3.4a}$$

$$W_\tau(\tilde{x},\tau) = \frac{b\varepsilon(U+\varepsilon)^2+\Theta R^2U^2}{(U+\varepsilon)^2+\Lambda R^2U^2} - W, \tag{3.4b}$$

$$U_\tau(\tilde{x},\tau) = U_{\tilde{x}\tilde{x}} + \Gamma[W-U]. \tag{3.4c}$$

The state variables, which are now denoted by R, W, and U, correspond to the total proportion of receptors in the active state ρ_T, the concentration of intracellular cAMP β, and the concentration of extracellular cAMP γ, respectively; the model parameters are defined in Table 3.1, with $\tau = (k_i+k_t)t$ and $x = \sqrt{\frac{D}{k_i+k_t}}\tilde{x}$. In particular, Equation (3.4) incorporates an extracellular cAMP diffusion term, as introduced in [69]; correspondingly, R, W, and U are functions of both space $\tilde{x}$ and time τ. The main result of [43] is a proof for the existence of traveling pulse solutions of (3.4) in one spatial dimension on the basis of singular perturbation theory, under the assumption that the parameters κ and ε are small, cf. again Table 3.1; moreover, asymptotic formulae are derived for these pulse solutions in a number of relevant scaling regimes.

Here, we study oscillatory dynamics in Equation (3.4) in the absence of diffusion. Imposing

a quasi-steady-state assumption on W, as was done for (3.1) above, and noting that R, W, and U now depend on τ only, we first reduce the model to the two-variable system

$$R_\tau = \kappa(U + \mathcal{P}\varepsilon)\frac{\mu(U+\varepsilon) - (U + d\varepsilon)R}{(U + \frac{\varepsilon}{c})(U+\varepsilon)}, \tag{3.5a}$$

$$U_\tau = \frac{b\varepsilon(U+\varepsilon)^2 + \Theta R^2U^2}{(U+\varepsilon)^2 + \Lambda R^2U^2} - U. \tag{3.5b}$$

Given the definition of the parameters κ and ε in [43], which are both assumed to be small, (3.5) is singularly perturbed. Here, we emphasise that the impact of these two parameters on the dynamics of (3.5) manifests very differently: while the parameter κ is a "conventional" singular perturbation parameter that reflects the separation of scales between the slow variable R and the fast variable U, the parameter ε induces a different type of singular perturbation which affects mainly the geometry of the corresponding critical manifold $\mathcal{S}_{00}$ and which is reflected by the non-uniformity of the limit as $\varepsilon \to 0$ in Equation (3.5); specifically, that limit will depend fundamentally on whether $U \gg \varepsilon$ or $U = \mathcal{O}(\varepsilon)$ therein. Correspondingly, the limit as $\kappa \to 0$ in Equation (3.5) can be studied using Fenichel's geometric singular perturbation theory [19], while the structure of the resulting asymptotics in ε can be resolved rigorously via the blow-up technique [14]. For an introduction to geometric singular perturbation theory and blow-up in the context of the present family of problems, the reader is referred to Appendix A of [41].

Our analysis of Equation (3.5) is, in fact, motivated by the study of the Goldbeter-Lefever model [61] in [41]; there, the critical manifold was found to consist of two non-hyperbolic lines and one normally hyperbolic line. The blow-up method was then applied to obtain a complete desingularisation of the flow near that manifold, allowing the authors to prove the occurrence of relaxation oscillation in the system.

While Equation (3.5) shares some characteristics of the Goldbeter-Lefever model studied in [41], it is slightly more degenerate: as will turn out, the critical manifold here is the union of one non-hyperbolic line in the "inner" region and one normally hyperbolic curve in the "outer" region, which meet in a degenerate steady state at the origin. Moreover, the U-variable has to be scaled with the singular parameter ε due to the presence of the term $(U+\varepsilon)^2 + \Lambda R^2U^2$ in (3.5b), as ε cannot be eliminated by a simple change-of-coordinates, which represents the major conceptual difference to the model considered in [41]. Therefore, the resulting singularly perturbed structure of Equation (3.4) is novel; our resolution of that structure, and in particular of the highly degenerate dynamics near the origin in (R, U, ε)-space, results in improved understanding of the oscillatory dynamics that is observed in the reformulated singular perturbation problem of cAMP signaling, Equation (3.5).

Motivated by [41], and in accordance with the numerical values given in Table 3.1, we rescale the parameters $\mu = \tilde{\mu}\varepsilon^{\frac{1}{2}}$, $d = \tilde{d}\varepsilon^{\frac{1}{2}}$, and $b = \tilde{b}\varepsilon$ in (3.5). These scalings broadly agree with assumptions made in [43], where $\mu \sim d$, $\mu \simeq \varepsilon$, and $b \ll 1$ were considered; however, we rescale μ and d with $\varepsilon^{\frac{1}{2}}$ instead of with ε here, which is consistent with the basic geometry of oscillation found in [46] for the three-dimensional system, Equation (3.1). Moreover, we rewrite the resulting equations in the equivalent form

$$R' = \kappa(U + \mathcal{P}\varepsilon)\frac{(U+\varepsilon)^2 + \Lambda R^2U^2}{(U+\varepsilon)(U+\frac{\varepsilon}{c})}\big[\tilde{\mu}\varepsilon^{\frac{1}{2}}(U+\varepsilon) - (U + \tilde{d}\varepsilon^{\frac{3}{2}})R\big], \tag{3.6a}$$

$$U' = \tilde{b}\varepsilon^2(U+\varepsilon)^2 + \Theta R^2U^2 - U\big[(U+\varepsilon)^2 + \Lambda R^2U^2\big], \tag{3.6b}$$

which is obtained by formally multiplying the right-hand sides in (3.5) with a factor of $(U + \varepsilon)^2 + \Lambda R^2U^2$. (Since that factor is non-negative, the corresponding transformation of time does not change the direction of the flow.) Here, the prime now denotes differentiation with respect to the new, rescaled time.

The following is the main result of our analysis:

Theorem 3.1. *Let $(\kappa, \varepsilon) \in (0, \kappa_0) \times (0, \varepsilon_0)$, with κ_0 and ε_0 positive and sufficiently small. Then, there exists a unique family of attracting periodic cycles $\Gamma_{\kappa\varepsilon}$ for Equation (3.6), which tends to $\Gamma_{0\varepsilon}$ as $\kappa \to 0$ uniformly for $\varepsilon \in (0, \varepsilon_0]$, and to the singular cycle Γ_{00} as $(\kappa, \varepsilon) \to (0, 0)$.*

A visualisation of the assertions of Theorem 3.1 can be found in Figure 3.2, where the

Table 3.1: Definition and numerical values, with orders of magnitude, of the parameters in (3.4); cf. [43], where the quantities in the second column are defined.

Parameter	Definition	Order of magnitude	Numerical value
κ	$\frac{k_2(1+L_2)}{k_i+k_t}$	$\ll 1$	0.0023
μ	$\frac{m+d}{m+1}$	$\ll 1 \sim d$	0.1274
ε	M^{-1}	$\ll 1$	0.1258
d	$\frac{1+L_1}{c+L_1}$	$\ll 1$	0.1
b	$\frac{\alpha q \sigma k_t}{(k_i+k_t)h} \frac{\lambda\theta}{1+\alpha\theta}$	$\ll 1$	0.01587
Γ	$\frac{k_e}{k_i+k_t}$	$\simeq 1$	2.1052
Λ	$(A\mu^2)^{-1}$	$\simeq 1$	0.2966
Θ	$\Lambda B \varepsilon$	$\simeq 1$ or $\gg 1$	1.5087
c		$\gg 1$	100
$\mathcal{P}$	$\frac{k_1}{k_2}$	$\gg 1$	100

singular cycle $\Gamma_{0\varepsilon}$ is sketched in addition to the nullclines of Equation (3.6) and a sample cycle $\Gamma_{\kappa\varepsilon}$ which was obtained numerically. Here, the values of the relevant parameters are as specified in Table 3.1, with the exception of $\kappa(= 0.00023)$, $\mu(= 0.13)$, and $d(= 0.071)$; the latter two are chosen such that the unique equilibrium in the system is shifted to the middle upper branch of the U-nullcline with a restriction for $\varepsilon < \varepsilon_{max}(\approx 0.2)$, thus allowing for excitability and, hence, oscillatory dynamics.

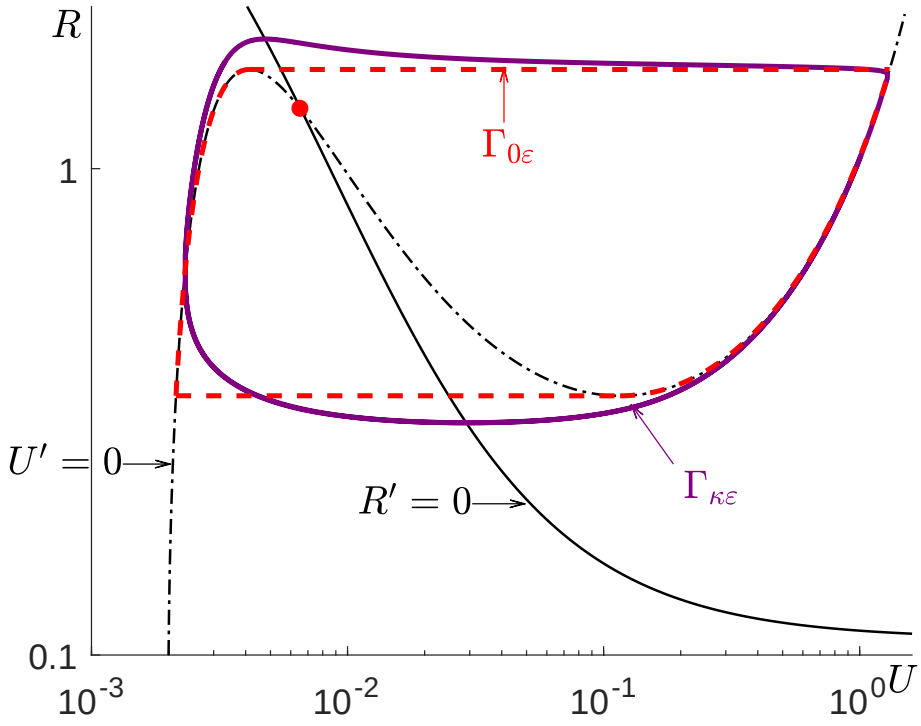

Figure 3.2: Nullclines and periodic cycles for Equation (3.6): R-nullcline (solid black); U-nullcline (dot-dashed black); periodic cycle $\Gamma_{0\varepsilon}$ (dashed red); numerically computed periodic cycle $\Gamma_{\kappa\varepsilon}$ (solid purple), with $\kappa = 0.00023$, $\mu = 0.13$, $d = 0.071$, and $\varepsilon = 0.1258$, other parameters see Table 3.1; equilibrium (red dot). Log scale for U-axis.

In the remainder of the chapter, we will prove Theorem 3.1 by constructing a family of periodic (relaxation-type) cycles for Equation (3.6); as is common in singular perturbation

theory, we will first identify a singular cycle when $\kappa = 0 = \varepsilon$, where the cubic-shape of slow manifold $\mathcal{S}_{0\varepsilon}$ vanishes to the critical manifold $\mathcal{S}_{00}$, where the fold points vanish as well, see Figure 3.3 and Figure 3.4 . Subsequently, we will show the persistence of that cycle for κ and ε positive, but small. Our analysis follows that of Kosiuk and Szmolyan [41] in spirit, subject to the appropriate modifications due to differences in the singular structure of (3.6); in particular, our focus is on the resulting asymptotics in ε, which is discussed in detail, whereas the relatively standard perturbation analysis with respect to κ is treated in a more cursory fashion.

3.2 Singular dynamics

For $\varepsilon > 0, as Equation\ (3.6) represents a slow-fast system in standard form$, with singular perturbation parameter κ, we rewrite the corresponding flow on the slow time-scale to obtain the equivalent formulation

$$\dot{R} = (U + \mathcal{P}\varepsilon)\frac{(U+\varepsilon)^2 + \Lambda R^2 U^2}{(U+\varepsilon)(U+\frac{\varepsilon}{c})}\big[\tilde{\mu}\varepsilon^{\frac{1}{2}}(U+\varepsilon) - (U + \tilde{d}\varepsilon^{\frac{3}{2}})R\big], \tag{3.7a}$$

$$\kappa\dot{U} = \tilde{b}\varepsilon^2(U+\varepsilon)^2 + \Theta R^2 U^2 - U\big[(U+\varepsilon)^2 + \Lambda R^2 U^2\big]. \tag{3.7b}$$

In our analysis, we hence first consider the singular limit of $\kappa = 0$ in Equations (3.6) and (3.7). The small ε dynamics in that limit will be studied separately in different regimes $\mathcal{R}_j$ $(j = 1, 2, 3)$, which are defined in Section 3.3 below.

3.2.1 Slow-fast analysis for $\kappa = 0$ and $\varepsilon > 0$

Setting $\kappa = 0$ in Equations (3.6) and (3.7) for fixed, positive ε defines two limiting systems, the "layer problem"

$$R' = 0, \tag{3.8a}$$

$$U' = \tilde{b}\varepsilon^2(U+\varepsilon)^2 + \Theta R^2 U^2 - U\big[(U+\varepsilon)^2 + \Lambda R^2 U^2\big] \tag{3.8b}$$

and the "reduced problem"

$$\dot{R} = (U + \mathcal{P}\varepsilon)\frac{(U+\varepsilon)^2 + \Lambda R^2 U^2}{(U+\varepsilon)(U+\frac{\varepsilon}{c})}\big[\tilde{\mu}\varepsilon^{\frac{1}{2}}(U+\varepsilon) - (U + \tilde{d}\varepsilon^{\frac{3}{2}})R\big], \tag{3.9a}$$

$$0 = \tilde{b}\varepsilon^2(U+\varepsilon)^2 + \Theta R^2 U^2 - U\big[(U+\varepsilon)^2 + \Lambda R^2 U^2\big]. \tag{3.9b}$$

The critical manifold $\mathcal{S}_{0\varepsilon}$, which is defined by (3.9b), is precisely the U-nullcline in Equation (3.6). The manifold $\mathcal{S}_{0\varepsilon}$ is S-shaped; For $\forall\, \varepsilon \in (0, \varepsilon_0]$, there exists a folded structure that $\mathcal{S}_{0\varepsilon} = \mathcal{S}^{a-}_{0\varepsilon} \cup \mathcal{S}^{r}_{0\varepsilon} \cup \mathcal{S}^{a+}_{0\varepsilon}$, see Figure 3.3 for an illustration; linearisation of the layer problem, Equation (3.8), about $\mathcal{S}_{0\varepsilon}$ gives

$$\frac{\partial U'}{\partial U} = 2\tilde{b}\varepsilon^2(U+\varepsilon) + 2\Theta R^2 U - \big[(U+\varepsilon)^2 + \Lambda R^2 U^2\big] - 2U\big[(U+\varepsilon) + \Lambda R^2 U\big],$$

which has zeroes at $U = U^A_{0\varepsilon} = \mathcal{O}(\varepsilon^2)$ and $U = U^C_{0\varepsilon} = \frac{2}{3}\frac{\Theta R^2}{1+\Lambda R^2} - \frac{4}{3(1+\Lambda R^2)}\varepsilon + \mathcal{O}(\varepsilon^2)$. Hence, $\mathcal{S}_{0\varepsilon}$ consists of three branches, which are separated by the two fold points $A_{0\varepsilon} : \big(U^A_{0\varepsilon}, R^A_{0\varepsilon}\big)$ and $C_{0\varepsilon} : \big(U^C_{0\varepsilon}, R^C_{0\varepsilon}\big)$; the left branch $\mathcal{S}^{a-}_{0\varepsilon}$ and the right branch $\mathcal{S}^{a+}_{0\varepsilon}$ are attracting under the layer flow of Equation (3.6), while the middle branch $\mathcal{S}^{r}_{0\varepsilon}$ is repelling. (Here, the R-coordinates of $A_{0\varepsilon}$ and $C_{0\varepsilon}$ are found by solving (3.9b), evaluated at $U^A_{0\varepsilon}$ and $U^C_{0\varepsilon}$, respectively, with $R^A_{0\varepsilon} = \sqrt{\frac{1-\tilde{b}}{\Theta}} + \sqrt{\frac{1-\tilde{b}}{\Theta}}\varepsilon + \mathcal{O}(\varepsilon^2)$ and $R^C_{0\varepsilon} = \sqrt{\frac{6}{\Theta}}\varepsilon^{\frac{1}{2}} + \mathcal{O}(\varepsilon).$) In particular, we can apply the results of the extended geometric singular perturbation theory to the fold points in our proof of Theorem 3.1, for details see [42].

We denote the unique equilibrium of (3.6), which is found in the intersection of the R-nullcline with $\mathcal{S}_{0\varepsilon}$, by $E_{0\varepsilon}$; see Figure 3.3. (Due to our assumptions on the parameters d, μ, and Θ, $E_{0\varepsilon}$ is, in fact, located on the middle branch $\mathcal{S}^{r}_{0\varepsilon}$ of $\mathcal{S}_{0\varepsilon}$.) Analysis of the reduced

flow on $\mathcal{S}_{0\varepsilon}$ shows that R increases below the point $A_{0\varepsilon}$ on $\mathcal{S}^{a-}_{0\varepsilon}$, while it decreases on $\mathcal{S}^{a+}_{0\varepsilon}$. (The direction of the flow on $\mathcal{S}^{r}_{0\varepsilon}$, as indicated in Figure 3.3, is determined by the sign of the term $[\tilde{\mu}\varepsilon^{\frac{1}{2}}(U+\varepsilon)-(U+\tilde{d}\varepsilon^{\frac{3}{2}})R]$ in (3.9a).) Hence, we obtain the following standard singular relaxation-type dynamics for $\kappa = 0$ and fixed, positive ε: orbits starting on $\mathcal{S}^{a-}_{0\varepsilon}$ jump at the fold point $A_{0\varepsilon}$ and reach a point $D_{0\varepsilon}$ on $\mathcal{S}^{a+}_{0\varepsilon}$ along the 1-dimensional stable manifold thereof; they then follow the reduced dynamics on $\mathcal{S}^{a+}_{0\varepsilon}$ until they reach the fold point at $C_{0\varepsilon}$, from where they jump back to a point $B_{0\varepsilon}$ on $\mathcal{S}^{a-}_{0\varepsilon}$ along the 1-dimensional stable manifold thereof; finally, they follow the reduced dynamics on $\mathcal{S}^{a-}_{0\varepsilon}$ until they reach $A_{0\varepsilon}$, at which point the above dynamics repeats. Correspondingly, we define the singular cycle $\Gamma_{0\varepsilon}$, which consists of the heteroclinic orbit $\Gamma^{AD}_{0\varepsilon}$ connecting $A_{0\varepsilon}$ to $D_{0\varepsilon}$ under the layer flow of (3.8), the segment $\Gamma^{DC}_{0\varepsilon}$ of $\mathcal{S}^{a+}_{0\varepsilon}$ from $D_{0\varepsilon}$ to $C_{0\varepsilon}$, the heteroclinic orbit $\Gamma^{CB}_{0\varepsilon}$ connecting $C_{0\varepsilon}$ to $B_{0\varepsilon}$ under the layer flow, and the segment $\Gamma^{BA}_{0\varepsilon}$ of $\mathcal{S}^{a-}_{0\varepsilon}$ between $B_{0\varepsilon}$ and $A_{0\varepsilon}$; cf. again Figure 3.3.

***Remark* 3.1.** Here and in the following, reduced dynamics is depicted in blue, while the corresponding layer flow is shown in green; double arrows indicate hyperbolicity, while non-hyperbolic dynamics is indicated with single arrows.

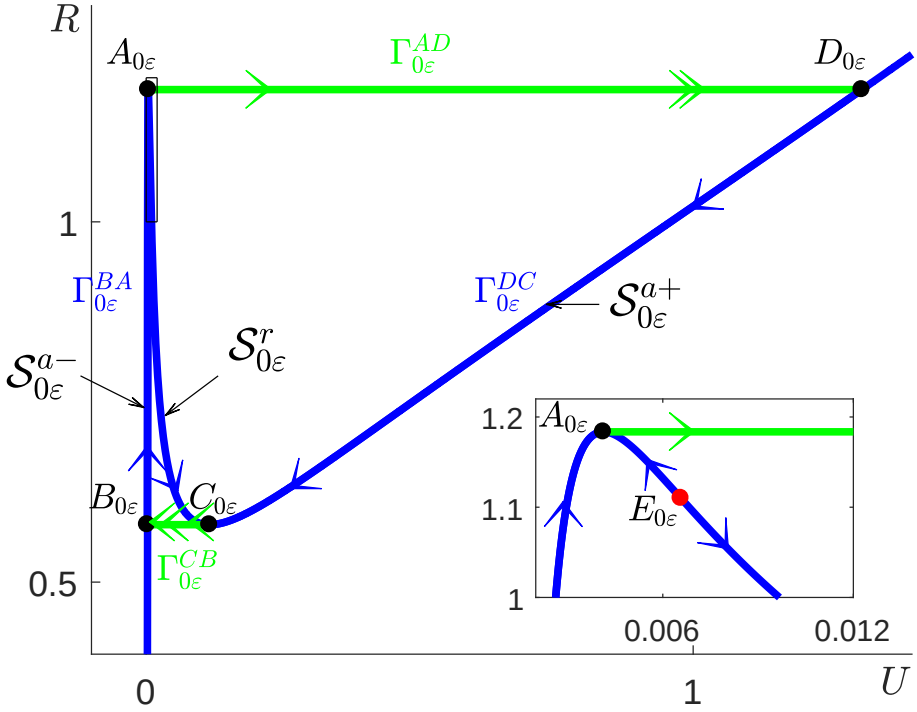

Figure 3.3: Critical manifold $\mathcal{S}_{0\varepsilon}$ for Equation (3.8).

As Equation (3.6) constitutes a two-parameter singular perturbation problem, we are interested in the double limit as κ and ε tend to zero simultaneously.

3.2.2 Slow-fast analysis for $\kappa = 0 = \varepsilon$

As will turn out, the limit as $(\kappa, \varepsilon) \to (0,0)$ in Equation (3.6) is significantly more singular for fixed ε than the limit of $\kappa \to 0$ considered in the previous subsection.

For $(\kappa, \varepsilon) = (0,0)$, (3.6) yields the seemingly simple layer problem

$$R' = 0, \tag{3.10a}$$

$$U' = \Theta R^2 U^2 - U\big(U^2 + \Lambda R^2 U^2\big), \tag{3.10b}$$

which corresponds precisely to the system that is obtained from (3.8) for $\varepsilon = 0$. Equation (3.10) admits the critical manifold $\mathcal{S}_{00}$, which consists of the curves $\mathcal{S}_{00}^{r} = \{(R,0) \,|\, R > 0\}$ and $\mathcal{S}_{00}^{\mathrm{a}+} = \{(U,R) \,|\, U = \frac{\Theta R^2}{1+\Lambda R^2},\ R > 0\}$, which meet in the origin Q. Linearisation of Equation (3.10) about $\mathcal{S}_{00}$ shows that the curve $\mathcal{S}_{00}^{\mathrm{a}+}$ is normally hyperbolic, while $\mathcal{S}_{00}^{r}$ – the R-axis – and the point Q are non-hyperbolic; see Figure 3.4 for an illustration.

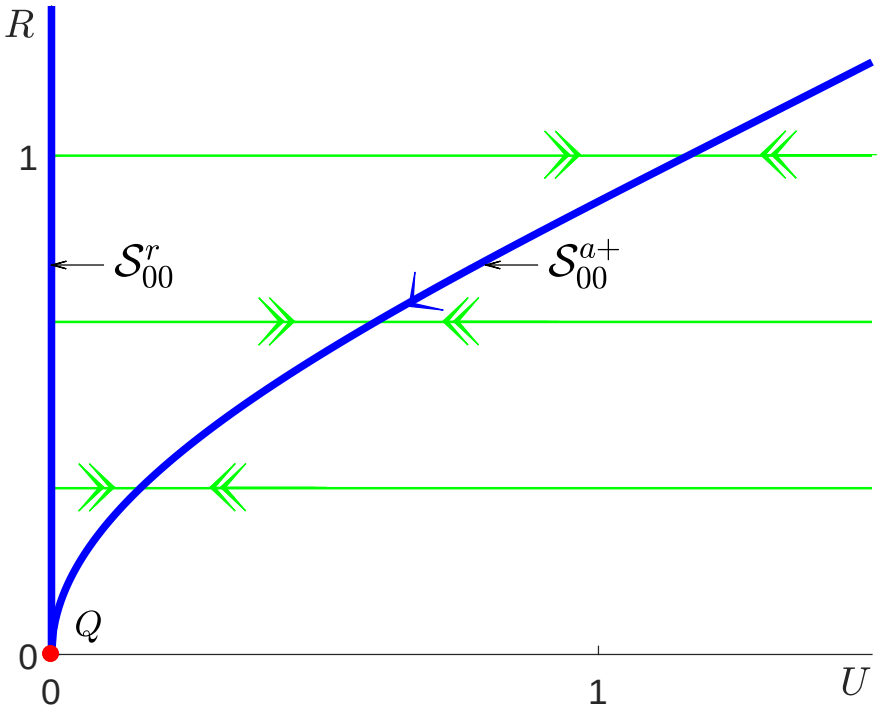

Figure 3.4: Critical manifold $\mathcal{S}_{00}$ for Equation (3.10).

In particular, it follows that, for U and R bounded away from zero, the critical manifold $\mathcal{S}_{0\varepsilon}^{\mathrm{a}+}$ introduced in the previous subsection is a regular perturbation (in ε) of the manifold $\mathcal{S}_{00}^{\mathrm{a}+}$ defined above. Hence, standard theory [19] can be applied to show the persistence of $\mathcal{S}_{00}^{\mathrm{a}+}$ for κ and ε positive and small in that case:

Proposition 3.1. *Let $\varepsilon \in [0, \varepsilon_0]$ be fixed, and let $\kappa \in [0, \kappa_0)$, with ε_0 and κ_0 positive and sufficiently small. Moreover, let $U \in [\alpha, 1]$ and $R \in [\beta, 1]$, with α and β positive and small, but independent of (κ, ε). Then, the following statements hold:*

1. *For $\kappa = 0$, Equation (3.8) admits the critical manifold*

$$\mathcal{S}_{0\varepsilon}^{a+} = \{(R,U) \,|\, R \in [\beta, 1],\ U = \Phi_{0\varepsilon}\}; \tag{3.11}$$

here, the function $\Phi_{0\varepsilon}$ satisfies

$$\Phi_{0\varepsilon} = \frac{\Theta R^2}{1+\Lambda R^2} + \frac{\tilde{b}}{1+\Lambda R^2}\varepsilon^2 + \mathcal{O}(\varepsilon^3). \tag{3.12}$$

2. *The manifold $\mathcal{S}_{0\varepsilon}^{a+}$ is normally attracting, with a single negative eigenvalue $-\frac{\Theta^2 R^4}{1+\Lambda R^2}$.*

3. *The reduced flow on $\mathcal{S}_{0\varepsilon}^{a+}$ is given by*

$$\dot{R} = -\frac{\Theta^2 R^5}{1+\Lambda R^2} + \frac{\Theta^2 R^4 \tilde{\mu}}{1+\Lambda R^2}\sqrt{\varepsilon} + \mathcal{O}(\varepsilon),$$

which implies, in particular, $\dot{R} < 0$ *for* ε *sufficiently small.*

4. *For* κ *positive and small, the manifold* $\mathcal{S}^{a+}_{0\varepsilon}$ *perturbs to a manifold*

$$\mathcal{S}^{a-}_{\kappa\varepsilon} = \big\{(R,U)\,\big|\,R \in [\beta,1],\ U = \Phi_{\kappa\varepsilon}\big\}, \tag{3.13}$$

where $\Phi_{\kappa\varepsilon} = \Phi_{0\varepsilon} + \mathcal{O}(\kappa)$ *is regular in* (κ,ε) *to any order therein.*

***Remark* 3.2.** Comparison of Figures 3.3 and 3.4 shows that the manifolds $\mathcal{S}^{a-}_{0\varepsilon}$ and $\mathcal{S}^{r}_{0\varepsilon}$ merge into $\mathcal{S}^{r}_{00}$ in the limit as $\varepsilon \to 0$, this makes $\mathcal{S}^{r}_{00}$ degenerate; in other words, the left attracting branch of the critical manifold $\mathcal{S}_{0\varepsilon}$ vanishes. Correspondingly, the points $B_{0\varepsilon}$ and $C_{0\varepsilon}$ coalesce into the origin Q in that limit.

3.3 Scaling regimes

The discussion in Section 3.2 indicates that, for $\varepsilon = 0$, essential portions of the sought-after relaxation cycle $\Gamma_{\kappa\varepsilon}$ for Equation (3.6) are "hidden" in the non-hyperbolic line $\mathcal{S}^{r}_{00}$ and the point Q; specifically, it is intuitively clear that $\mathcal{S}^{a-}_{0\varepsilon}$ and $\mathcal{S}^{r}_{0\varepsilon}$ merge into $\mathcal{S}^{r}_{00}$ in that limit, while the fold point $C_{0\varepsilon}$ converges to the point Q, the origin. Appropriate rescalings of R and U are required in order to make these aspects of the dynamics visible in different scaling regimes. These regimes are denoted by $\mathcal{R}_j$ $(j = 1,2,3)$, and are defined as follows:

1. Regime $\mathcal{R}_1$: $U = \mathcal{O}(\varepsilon^2)$, $R = \mathcal{O}(1)$;
2. Regime $\mathcal{R}_2$: $U = \mathcal{O}(\varepsilon)$, $R = \mathcal{O}(\varepsilon^{\frac{1}{2}})$;
3. Regime $\mathcal{R}_3$: $U = \mathcal{O}(1)$, $R = \mathcal{O}(1)$.

In particular, the "outer" and "inner" regions, which are mentioned in the Section 3.1, are covered by Regime $\mathcal{R}_3$ and Regimes $\mathcal{R}_j$ $(j = 1,2)$, respectively; see Figure 3.5.

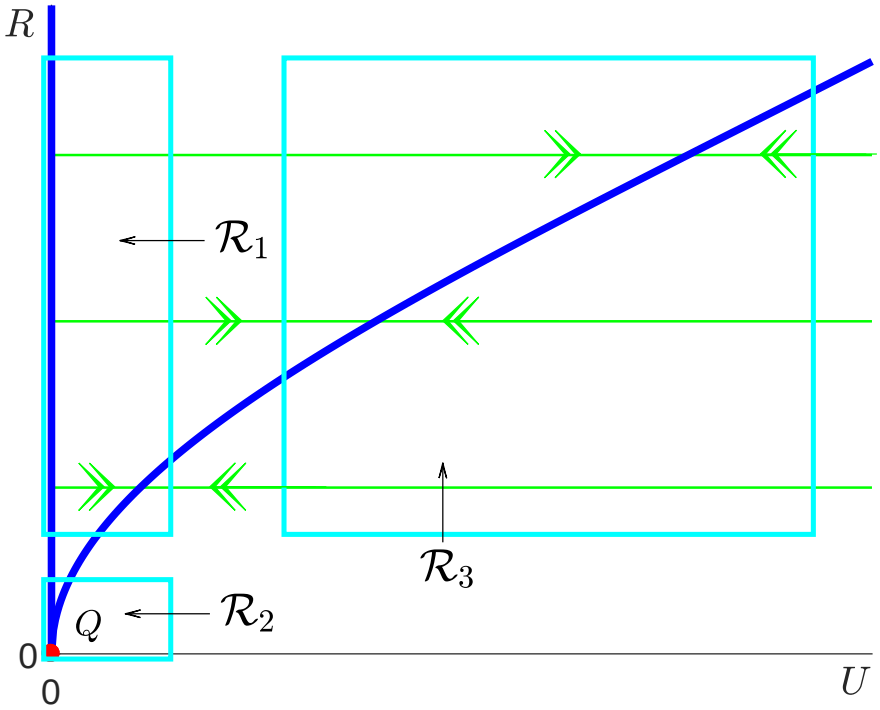

Figure 3.5: The scaling regimes $\mathcal{R}_1$, $\mathcal{R}_2$, and $\mathcal{R}_3$

The above scalings in U – which then imply the corresponding scalings of R – can be substantiated via the method of Newton polygons [10]. In particular, it shows that the parameter b is of the order $\mathcal{O}(\varepsilon)$ is needed, as assumed above. In this section, we will discuss the geometry in the above regimes in turn to motivate how the "full" singular dynamics of Equation (3.6) can be desingularised to allow for a description of the resulting, global oscillation. Our discussion will be substantiated, and made fully rigorous, in subsequent sections, where a desingularisation will be achieved via the blow-up technique. In particular, as the three regimes introduced above do not overlap, it is not *a priori* evident how to match them; here, we will show that matching can be accomplished in various coordinate charts after blow-up, as was also done in [41]. (We emphasise that these charts are not covered by the scaling regimes themselves, but that they are found by our blow-up analysis.)

3.3.1 Regime $\mathcal{R}_1$: $U = \mathcal{O}(\varepsilon^2)$, $R = \mathcal{O}(1)$

Regime $\mathcal{R}_1$ covers a neighbourhood of the R-axis that is, however, bounded away from the origin Q. Correspondingly, we introduce the scaling

$$R = R_1 \quad \text{and} \quad U = \varepsilon^2 U_1 \tag{3.14}$$

in that regime. For the sake of definiteness, we assume that $U_1 \in [0, \bar{\alpha}_1]$ and $R_1 \in [\underline{\beta}_1, \bar{\beta}_1]$, where $\underline{\beta}_1$ is small, $\bar{\beta}_1$ is $\mathcal{O}(1)$ and $\bar{\alpha}_1$ is large, corresponding to our assumption that the original variables U and R satisfy $U = \mathcal{O}(\varepsilon^2)$ and $R = \mathcal{O}(1)$; see Figure 3.6.

After dividing out the factor ε^2, we obtain the following system of equations from Equation (3.6):

$$R_1' = \kappa\varepsilon^{\frac{1}{2}}(\varepsilon U_1 + \mathcal{P})\frac{(\varepsilon U_1 + 1)^2 + \Lambda R_1^2\varepsilon^2 U_1^2}{(\varepsilon U_1 + 1)(\varepsilon U_1 + \frac{1}{c})}\big[\tilde{\mu}(\varepsilon U_1 + 1) - (\varepsilon^{\frac{1}{2}} U_1 + \tilde{d})R_1\big], \tag{3.15a}$$

$$U_1' = \tilde{b}(\varepsilon U_1 + 1)^2 + \Theta R_1^2 U_1^2 - U_1\big[(\varepsilon U_1 + 1)^2 + \Lambda R_1^2\varepsilon^2 U_1^2\big], \tag{3.15b}$$

which represents a slow-fast system in standard form for κ small.

When $\kappa = 0$, Equation (3.15) yields the layer problem

$$R_1' = 0, \tag{3.16a}$$

$$U_1' = \tilde{b}(\varepsilon U_1 + 1)^2 + \Theta R_1^2 U_1^2 - U_1\big[(\varepsilon U_1 + 1)^2 + \Lambda R_1^2\varepsilon^2 U_1^2\big]; \tag{3.16b}$$

considering the limit of $\varepsilon = 0$ in (3.16), we obtain

$$R_1' = 0, \tag{3.17a}$$

$$U_1' = \tilde{b} + \Theta R_1^2 U_1^2 - U_1. \tag{3.17b}$$

The critical manifold for Equation (3.17) – which follows from the corresponding reduced problem – is defined by equation $\tilde{b} + \Theta R_1^2 U_1^2 - U_1 = 0$; we denote that manifold as $\mathcal{S}_{00_1}$. The manifold $\mathcal{S}_{00_1}$ consists of a left attracting branch $\mathcal{S}_{00_1}^{a-}$, where $U_1 < 2\tilde{b}$, and a right repelling branch $\mathcal{S}_{00_1}^{r}$ with $U_1 > 2\tilde{b}$; these two branches are separated by a fold point at $A_{00_1} : \big(\frac{1}{2\sqrt{\Theta\tilde{b}}}, 2\tilde{b}\big)$. The branch $\mathcal{S}_{00_1}^{r}$ is asymptotic to the U_1-axis as $U_1 \to \infty$, while the branch $\mathcal{S}_{00_1}^{a-}$ intersects the U_1-axis in the point B_{00_1} is at $(0, \tilde{b})$. Orbits starting close to the U_1-axis are rapidly attracted to $\mathcal{S}_{00_1}^{a-}$; they then follow the reduced dynamics until they reach the fold point at A_{00_1}, where they jump in the positive U_1-direction along an orbit of the layer problem, Equation (3.16), which we denote by $\Gamma_{00_1}^{A}$. The geometry in regime $\mathcal{R}_1$ is summarised in Figure 3.6; for details on the passage past a singularly perturbed planar fold, the reader is referred to [42], as well as to the summary in Appendix A of [41].

***Remark* 3.3.** We note that the steady state E_{0_ε} is not visible in regime $\mathcal{R}_1$: given our choice of μ and d, with $\frac{\tilde{\mu}}{\tilde{d}} > \frac{1}{2\sqrt{\Theta\tilde{b}}}$, the equation $\{\tilde{b} + \Theta R_1^2 U_1^2 - U_1 = 0\}\big|_{\{R_1 = \frac{\tilde{\mu}}{\tilde{d}}\}}$ admits no real solutions for U_1. In particular, it follows that the reduced flow in the R_1-variable is directed upwards to A_{00_1} on $\mathcal{S}_{00_1}$.

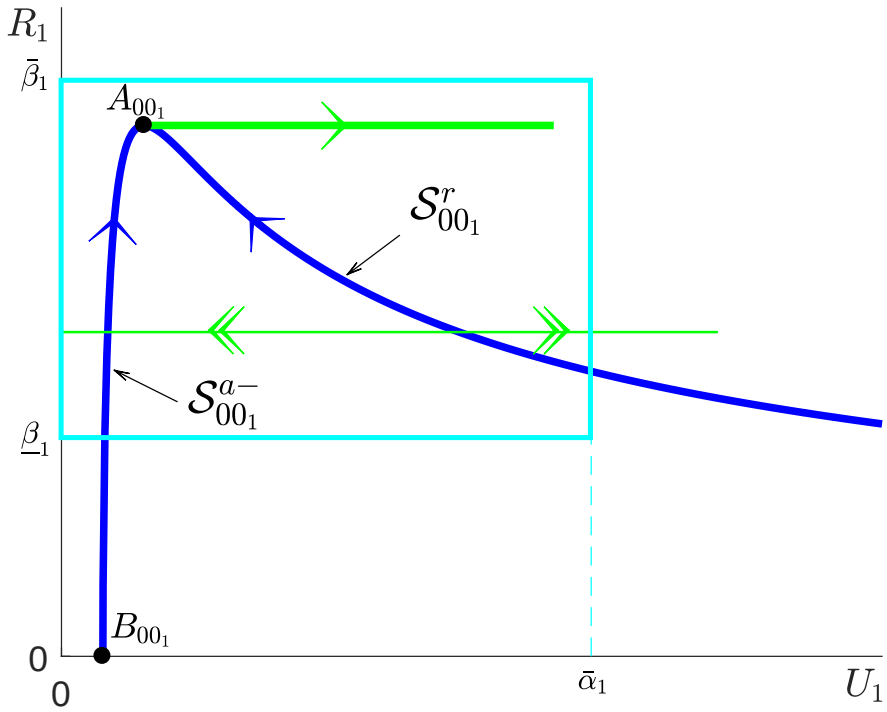

Figure 3.6: Critical manifold $\mathcal{S}_{00_1}$ and fast dynamics in Regime $\mathcal{R}_1$

***Remark* 3.4.** The critical manifold $\mathcal{S}_{00_1}$ corresponds to appropriately specified portions of $\mathcal{S}^{a-}_{0\varepsilon}$ and $\mathcal{S}^r_{0\varepsilon}$, as defined in Section 3.2.1, in the limit as $\varepsilon \to 0$, while the fold point at A_{00_1} corresponds to $A_{0\varepsilon}$ in that limit. In some sense, which is to be specified later, the point $C_{0\varepsilon}$ is retrieved for $U_1 \to \infty$ on $\mathcal{S}^r_{0\varepsilon_1}$ in the limit as $\varepsilon \to 0$.

3.3.2 Regime $\mathcal{R}_2$: $U = \mathcal{O}(\varepsilon)$, $R = \mathcal{O}(\varepsilon^{\frac{1}{2}})$

Regime $\mathcal{R}_2$ covers a neighbourhood of the origin Q; recall Figure 3.5. We introduce the scaling

$$R = \varepsilon^{\frac{1}{2}} R_2 \quad \text{and} \quad U = \varepsilon U_2; \tag{3.18}$$

here, we assume that $U_2 \in [0, \bar{\alpha}_2]$ and $R_2 \in [0, \bar{\beta}_2]$, where $\bar{\alpha}_2$ and $\bar{\beta}_2$ are large, corresponding to our assumption that the original variables U and R satisfy $U = \mathcal{O}(\varepsilon)$ and $R = \mathcal{O}(\varepsilon^{\frac{1}{2}})$, respectively.

After division through a factor of ε^2, Equation (3.6) becomes

$$R_2' = \kappa(U_2 + \mathcal{P}) \frac{(U_2+1)^2 + \Lambda\varepsilon R_2^2 U_2^2}{(U_2+1)(U_2+\frac{1}{c})} \big[\tilde{\mu}(U_2+1) - \big(U_2 + \tilde{d}\varepsilon^{\frac{1}{2}}\big) R_2\big], \tag{3.19a}$$

$$U_2' = \tilde{b}\varepsilon(U_2+1)^2 + \Theta R_2^2 U_2^2 - U_2\big[(U_2+1)^2 + \Lambda\varepsilon R_2^2 U_2^2\big], \tag{3.19b}$$

which again represents a slow-fast system for κ small.

The layer problem obtained for $\kappa = 0$ now reads

$$R_2' = 0, \tag{3.20a}$$

$$U_2' = \tilde{b}\varepsilon(U_2+1)^2 + \Theta R_2^2 U_2^2 - U_2\big[(U_2+1)^2 + \Lambda\varepsilon R_2^2 U_2^2\big]; \tag{3.20b}$$

setting $\varepsilon = 0$ in (3.20), we find the simplified system

$$R_2' = 0, \tag{3.21a}$$
$$U_2' = \Theta R_2^2 U_2^2 - U_2(U_2+1)^2; \tag{3.21b}$$

the corresponding critical manifold, which is denoted as $\mathcal{S}_{00_2}$, is defined by equation $\Theta R_2^2 U_2^2 - U_2(U_2+1)^2 = 0$. The manifold $\mathcal{S}_{00_2}$ consists of a left attracting branch $\mathcal{S}_{00_2}^{a-}$, corresponding to $\{U_2 = 0\}$, a middle repelling branch $\mathcal{S}_{00_2}^{r}$, with $0 < U_2 < 1$, and a right attracting branch $\mathcal{S}_{00_2}^{a+}$, where $U_2 > 1$. The branches $\mathcal{S}_{00_2}^{r}$ and $\mathcal{S}_{00_2}^{a+}$ are separated by a fold point $C_{00_2} : \left(\frac{2}{\sqrt{\Theta}}, 1\right)$. Orbits follow the slow flow on the branch $\mathcal{S}_{00_2}^{a+}$ until they reach the fold point at C_{00_2}, where they jump to a point B_{00_2} on $\mathcal{S}_{00_2}^{a-}$ and then follow the slow flow on $\mathcal{S}_{00_2}^{a-}$; see Figure 3.7 for an illustration. We note that the fold point at $A_{0\varepsilon}$ – and, hence, the fast jump to $D_{0\varepsilon}$ – is not visible in this regime. Finally, by our assumptions on the parameters d and μ, the steady state at $E_{00_2} : \left(\Theta\tilde{\mu}^2, \tilde{\mu} + \frac{1}{\Theta\tilde{\mu}}\right)$ is located on the upper middle repelling branch $\mathcal{S}_{00_2}^{r}$. (That state is is found in the intersection of $\mathcal{S}_{00_2}$ with the R_2-nullcline $\left\{R_2 = \frac{\tilde{\mu}(U_2+1)}{U_2}\right\}$.)

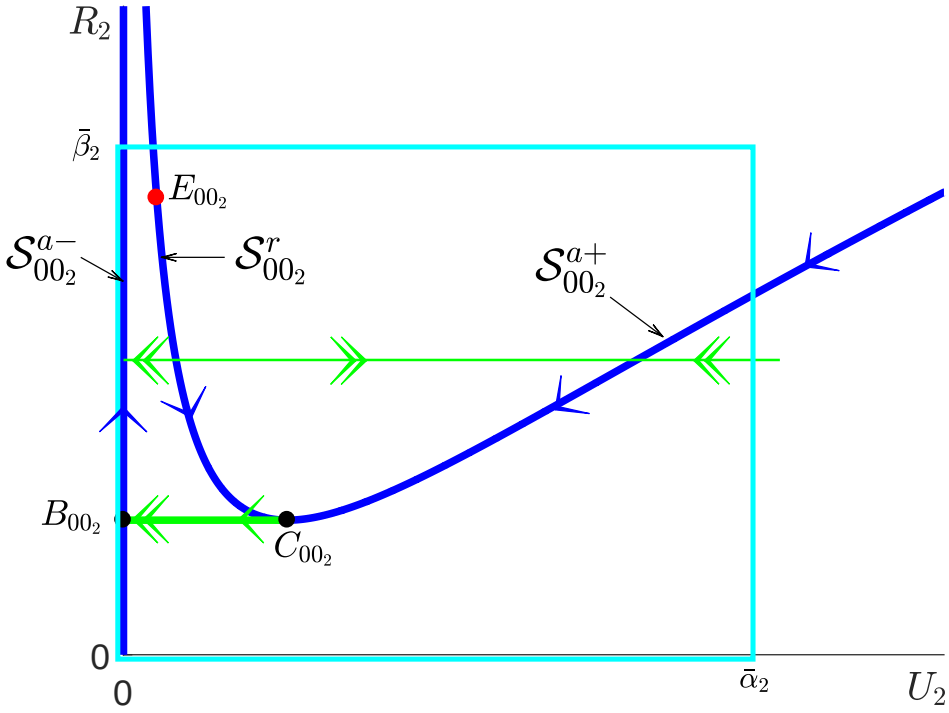

Figure 3.7: Critical manifold $\mathcal{S}_{00_2}$ and fast dynamics in Regime $\mathcal{R}_2$

***Remark* 3.5.** The critical manifold $\mathcal{S}_{00_2}$ corresponds to appropriately specified portions of $\mathcal{S}_{0\varepsilon}^{a-}$, $\mathcal{S}_{0\varepsilon}^{r}$, and $\mathcal{S}_{0\varepsilon}^{a+}$, as defined in Section 3.2.1, in the limit as $\varepsilon \to 0$. In particular, the fold point at C_{00_2} corresponds to $C_{0\varepsilon}$, in that limit, while the point B_{00_2} is referring to $B_{0\varepsilon}$. The jump point at $D_{0\varepsilon}$ corresponds to the limit as $U_2 \to \infty$ on $\mathcal{S}_{0\varepsilon_2}^{a+}$, while the fold point at $A_{0\varepsilon}$ is found in the limit as $R_2 \to \infty$ on $\mathcal{S}_{0\varepsilon_2}^{a-}$ in the limit of $\varepsilon \to 0$.

3.3.3 Regime $\mathcal{R}_3$: $U = \mathcal{O}(1)$, $R = \mathcal{O}(1)$

In regime $\mathcal{R}_3$, Equation (3.6) depends on ε in a regular fashion. We consider $U_3 \in [\underline{\alpha}_3, \bar{\alpha}_3]$, and $R_3 \in [\underline{\beta}_3, \bar{\beta}_3]$, where $\underline{\alpha}_3$ and $\underline{\beta}_3$ are positive and small, with $\bar{\alpha}_3$ and $\bar{\beta}_3$ are $\mathcal{O}(1)$, corresponding to our assumption that the original variables U and R satisfy $U = \mathcal{O}(1)$ and $R = \mathcal{O}(1)$, respectively.

For $\kappa = 0$ in (3.6), we obtain the layer problem given in (3.16), while the limit of $\varepsilon = 0$ yields the singular layer problem

$$R_3' = 0, \tag{3.22a}$$
$$U_3' = \Theta R_3^2 U_3^2 - U_3^3(1 + \Lambda R_3^2). \tag{3.22b}$$

The critical manifold for Equation (3.22), which we denote as $\mathcal{S}^{a+}_{00_3}$, is defined by equation $\Theta R_3^2 - U_3(1 + \Lambda R_3^2) = 0$, and is normally attracting. The reduced flow on $\mathcal{S}^{a+}_{00_3}$ for $\varepsilon = 0$ has the form

$$\dot{R}_3 = -U_3^2 R_3(1 + \Lambda R_3^2); \tag{3.23}$$

hence, R_3 is decreasing on $\mathcal{S}^{a+}_{00_3}$; see Figure 3.8.

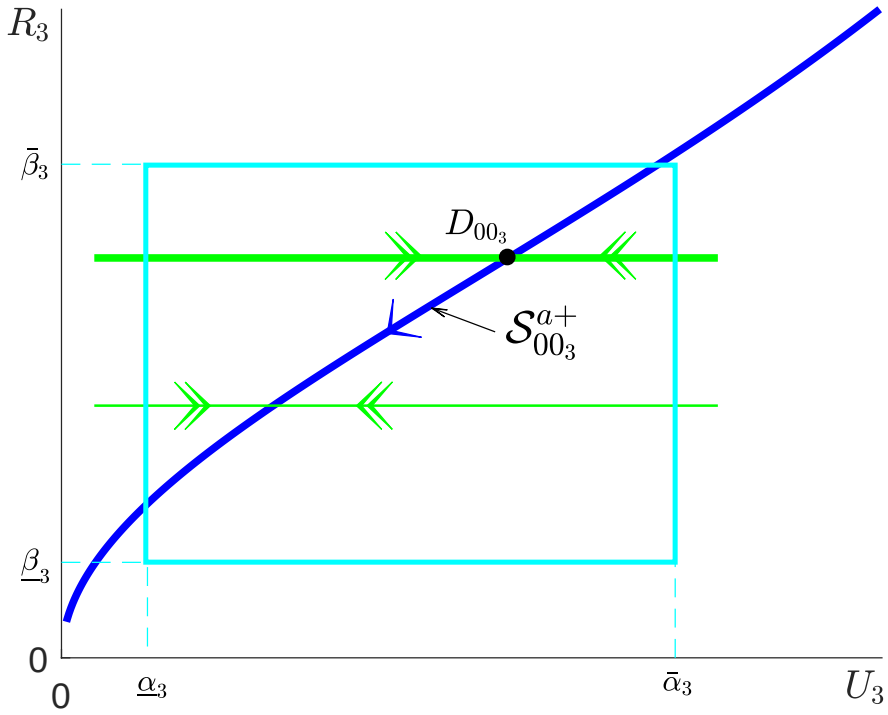

Figure 3.8: Critical manifold $\mathcal{S}^{a+}_{00_3}$ and fast dynamics in Regime $\mathcal{R}_3$

For $\varepsilon > 0$, the curve $\mathcal{S}^{a+}_{00_3}$ perturbs regularly to the analogue, in regime $\mathcal{R}_3$, of the family of the saddle-type critical manifolds that was denoted by $\mathcal{S}^{a+}_{0\varepsilon}$ in Section 3.2.1. Standard theory [19] implies that orbits to the left of the critical manifold $\mathcal{S}^{a+}_{00_3}$ are rapidly attracted by the slow manifold corresponding to $\mathcal{S}^{a+}_{00_3}$; they then follow the slow flow on that manifold.

***Remark* 3.6.** In the limit as $\varepsilon \to 0$, the critical manifold $\mathcal{S}^{a+}_{00_3}$ corresponds to the portion of $\mathcal{S}^{a+}_{0\varepsilon}$ where U_3 and R_3 are $\mathcal{O}(1)$. The point $D_{00_3} \in \mathcal{S}^{a+}_{00_3}$ corresponds to the point $D_{0\varepsilon} \in \mathcal{S}^{a+}_{0\varepsilon}$ in that limit, while the singular orbit connecting the point A_{00_3} – which is not visible in this regime – to D_{00_3} corresponds to the saddle-type fibre of the point D_{0_ε} in the limit as $\varepsilon \to 0$.

3.3.4 Summary

To summarise our discussion of the three regimes $\mathcal{R}_j$ $(j = 1, 2, 3)$, we define the singular cycle Γ_{00} for Equation (3.6) in the limit of $(\kappa, \varepsilon) = (0, 0)$ as

$$\Gamma_{00} = \Gamma_{00}^{AD} \cup \Gamma_{00}^{DQ} \cup \Gamma_{00}^{QA},$$

where the orbit Γ_{00}^{AD} corresponds to the fast fibre of (3.8) that connects the points A_{00} : $\left(\frac{1}{2\sqrt{\Theta\tilde{b}}}, 0\right)$ and D_{00} : $\left(\frac{1}{2\sqrt{\Theta\tilde{b}}}, \frac{\Theta}{4\Theta\tilde{b}+\Lambda}\right)$, the orbit Γ_{00}^{DQ} is the segment of the critical manifold $\mathcal{S}_{00}^{a+}$ between the points Q_{00} : $(0, 0)$ and D_{00}, and Γ_{00}^{QA} is the segment of the critical manifold $\mathcal{S}_{00}^{r}$ between the points Q_{00} and A_{00}; see Figure 3.9. We emphasise again that the flow on $\mathcal{S}_{00}^{r}$ is not defined, i.e., that the segment Γ_{00}^{QA} is degenerate; that degeneracy will be partially resolved by blow-up.

For $(\kappa, \varepsilon) \to (0, 0)$, regime $\mathcal{R}_1$ collapses to the non-hyperbolic line $\mathcal{S}_{00}^{r}$, while regime $\mathcal{R}_2$ collapses to the non-hyperbolic origin; in particular, the points B_{00} and C_{00} coincide in the double singular limit as Q_{00}, as the fast fibre connecting them vanishes. In regime $\mathcal{R}_3$, on the other hand, that limit is regular, as can be seen from the fact that the manifold $\mathcal{S}_{00}^{a+}$ remains normally attracting.

In conclusion, the degenerate geometry of Γ_{00} has hence been locally resolved in the scaling regimes $\mathcal{R}_j$ $(j = 1, 2, 3)$; however, to obtain a global picture, we need to investigate the transition between these regimes via blow-up in order to achieve a uniformly valid, geometric description of the oscillation in the two-parameter singular perturbation problem, Equation (3.6).

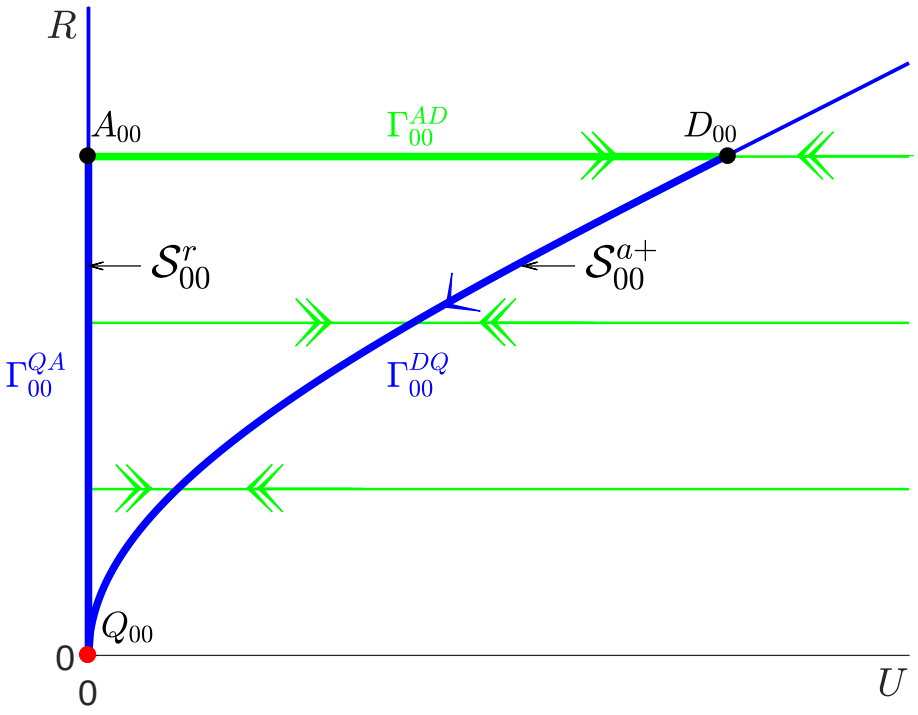

Figure 3.9: Critical manifold $\mathcal{S}_{00}$ for Equation (3.10) and the singular cycle Γ_{00}.

3.4 Blow-up analysis

Given the highly singular nature of Equation (3.6) in Regimes $\mathcal{R}_1$ and $\mathcal{R}_2$, we apply the blow-up technique to desingularise the dynamics in a neighbourhood of the non-hyperbolic R-axis, with a particular focus on the degenerate equilibrium at the origin. To that end, we consider the

augmented vector field that is obtained by appending the trivial equation $\varepsilon' = 0$ in (3.6):

$$R' = \kappa(U + \mathcal{P}\varepsilon)\frac{(U+\varepsilon)^2 + \Lambda R^2 U^2}{(U+\varepsilon)(U+\frac{\varepsilon}{c})}\big[\tilde{\mu}\varepsilon^{\frac{1}{2}}(U+\varepsilon) - (U + \tilde{d}\varepsilon^{\frac{3}{2}})R\big], \tag{3.24a}$$

$$U' = \tilde{b}\varepsilon^2(U+\varepsilon)^2 + \Theta R^2 U^2 - U\big[(U+\varepsilon)^2 + \Lambda R^2 U^2\big], \tag{3.24b}$$

$$\varepsilon' = 0. \tag{3.24c}$$

Our analysis will proceed in two steps: first, we will blow up the origin in the extended (R, U, ε)-space, which will allow us to give a rigorous description of the dynamics in Regime $\mathcal{R}_2$; the non-hyperbolic line $\mathcal{S}^r_{00}$ – which corresponds to Regime $\mathcal{R}_1$ – will be recovered in one of the phase-directional charts in that blow up, and will be desingularised via a second (cylindrical) blow-up transformation. The dynamics that is obtained in the various coordinate charts, post blow-up, will then be combined into a global description of the flow of Equation (3.6) near the degenerate R-axis that is uniformly valid in both κ and ε.

***Remark* 3.7.** Recall Section 3.2.1, we here label the family of critical manifolds of system (3.24) by $\mathcal{S}_{0\varepsilon}$, where $\mathcal{S}_{0\varepsilon} = \mathcal{S}^{a-}_{0\varepsilon} \cup \mathcal{F}^A_{0\varepsilon} \cup \mathcal{S}^r_{0\varepsilon} \cup \mathcal{F}^C_{0\varepsilon} \cup \mathcal{S}^{a+}_{0\varepsilon}$ for $\varepsilon \in [0, \varepsilon_0]$, with fold curves $\mathcal{F}^A_{0\varepsilon} := \big\{(A_{0\varepsilon}, \varepsilon)\,\big|\,\varepsilon \in [0, \varepsilon_0]\big\}$ and $\mathcal{F}^C_{0\varepsilon} := \big\{(C_{0\varepsilon}, \varepsilon)\,\big|\,\varepsilon \in [0, \varepsilon_0]\big\}$.

3.4.1 Blow-up of the non-hyperbolic origin

We recall that Regime $\mathcal{R}_2$ is specified by $U = \mathcal{O}(\varepsilon)$ and $R = \mathcal{O}(\varepsilon^{\frac{1}{2}})$ in Section 3.3.2. In reflection of these scalings, we introduce the following quasi-homogeneous blow-up transformation of the origin in Equation (3.24):

$$R = \bar{\rho}\bar{r}, \quad U = \bar{\rho}^2\bar{u}, \quad \text{and} \quad \varepsilon = \bar{\rho}^2\bar{\varepsilon}, \tag{3.25}$$

with $(\bar{r}, \bar{u}, \bar{\varepsilon}) \in \mathbb{S}^2$. In other words, the degenerate origin corresponding to $\bar{\rho} = 0$ in Equation (3.25) is blown up to the 2-sphere in $\mathbb{R}^3$. We will require two coordinate charts in our analysis, which we denote by K_1 and K_2; these charts are obtained for $\bar{r} = 1$ and $\bar{\varepsilon} = 1$, respectively, which implies

$$R = \rho_1, \quad U = \rho_1^2 u_1, \quad \text{and} \quad \varepsilon = \rho_1^2\varepsilon_1 \tag{3.26}$$

and

$$R = \rho_2 r_2, \quad U = \rho_2^2 u_2, \quad \text{and} \quad \varepsilon = \rho_2^2, \tag{3.27}$$

respectively, for the coordinates in these charts.

***Remark* 3.8.** For any object $\square_{\kappa\varepsilon}$ given in the original (R, U, ε)-variables, we denote the corresponding blown-up object by $\overline{\square}_\kappa$. Moreover, in chart K_i, that object will be denoted by $\square_{\kappa_i}$.

Lemma 3.1. *The change-of-coordinates transformation $\mathcal{K}_{12}$ between charts K_1 and K_2 is given by*

$$\mathcal{K}_{12} : (\rho_1, u_1, \varepsilon_1) \mapsto \left(\rho_2 r_2, \frac{u_2}{r_2^2}, \frac{1}{r_2^2}\right); \tag{3.28}$$

its inverse $\mathcal{K}_{21} = \mathcal{K}_{12}^{-1}$ reads

$$\mathcal{K}_{21} : (r_2, u_2, \rho_2) \mapsto \left(\frac{1}{\sqrt{\varepsilon_1}}, \frac{u_1}{\varepsilon_1}, \rho_1\sqrt{\varepsilon_1}\right). \tag{3.29}$$

We will first consider the dynamics in the "rescaling" chart K_2; then, we will study the flow in the "phase-directional" chart K_1; in particular, the latter will allow us to describe the transition between the "outer" and "inner" regions, which correspond to Regimes $\mathcal{R}_1$ and $\mathcal{R}_2$, respectively, in Section 3.3.

3.4.2 Dynamics in chart K_2

In chart K_2, the blow-up transformation defined in (3.25) is expressed as in (3.27); substituting into Equation (3.24), we find

$$r_2' = \kappa\rho_2^4(u_2+\mathcal{P})\frac{(u_2+1)^2+\Lambda\rho_2^2r_2^2u_2^2}{(u_2+1)(u_2+\frac{1}{c})}\big[\tilde{\mu}(u_2+1)-(u_2+\tilde{d}\rho_2)r_2\big], \tag{3.30a}$$

$$u_2' = \rho_2^4\Big\{\tilde{b}\rho_2^2(u_2+1)^2+\Theta r_2^2u_2^2-u_2\big[(u_2+1)^2+\Lambda\rho_2^2r_2^2u_2^2\big]\Big\}, \tag{3.30b}$$

$$\rho_2' = 0. \tag{3.30c}$$

By dividing out a factor of ρ_2^4 from the right-hand sides in Equation (3.30), we obtain the desingularised dynamics in chart K_2:

$$r_2' = \kappa(u_2+\mathcal{P})\frac{(u_2+1)^2+\Lambda\rho_2^2r_2^2u_2^2}{(u_2+1)(u_2+\frac{1}{c})}\big[\tilde{\mu}(u_2+1)-(u_2+\tilde{d}\rho_2)r_2\big], \tag{3.31a}$$

$$u_2' = \tilde{b}\rho_2^2(u_2+1)^2+\Theta r_2^2u_2^2-u_2\big[(u_2+1)^2+\Lambda\rho_2^2r_2^2u_2^2\big], \tag{3.31b}$$

$$\rho_2' = 0, \tag{3.31c}$$

which is a slow-fast system in standard form, with the (small) singular perturbation parameter κ; correspondingly, the variable r_2 is slow, while u_2 is fast. We observe that K_2 corresponds precisely to Regime $\mathcal{R}_2$, as Equation (3.31) is equivalent to (3.19), with $(R_2,U_2)=(r_2,u_2)$, $\varepsilon=\rho_2^2$, and the (trivial) equation $\rho_2'=0$ appended. Hence, the geometric singular perturbation analysis in chart K_2 proceeds as in Section 3.3.2; the relevant dynamics in blow-up space is again illustrated in Figure 3.7.

We first consider the flow of Equation (3.31) in the invariant plane $\{\rho_2=0\}$, which is governed by

$$r_2' = \kappa(u_2+\mathcal{P})\frac{u_2+1}{u_2+\frac{1}{c}}\big[\tilde{\mu}(u_2+1)-u_2r_2\big], \tag{3.32a}$$

$$u_2' = \Theta r_2^2u_2^2-u_2(u_2+1)^2, \tag{3.32b}$$

$$\rho_2' = 0. \tag{3.32c}$$

Equation (3.32) is again a slow-fast system in standard form, with singular perturbation parameter κ; correspondingly, the variable r_2 is slow, while u_2 is fast. The corresponding layer problem reads

$$r_2' = 0, \tag{3.33a}$$

$$u_2' = \Theta r_2^2u_2^2-u_2(u_2+1)^2, \tag{3.33b}$$

$$\rho_2' = 0. \tag{3.33c}$$

It follows immediately from Section 3.3.2 that the critical manifold for Equation (3.33) consists of the three branches $\mathcal{S}_{0_2}^{a-}$, $\mathcal{S}_{0_2}^{r}$, and $\mathcal{S}_{0_2}^{a+}$; the former equals a segment of the r_2-axis, and is normally attracting under the flow of (3.33). The manifold $\mathcal{S}_{0_2}^{r}\cup\mathcal{S}_{0_2}^{a+}$ is parabolic in shape; in particular, $\mathcal{S}_{0_2}^{r}$ is normally repelling, while $\mathcal{S}_{0_2}^{a+}$ is normally attracting, outside of a neighbourhood of the fold point at $C_{0_2}:\ \big(\frac{2}{\sqrt{\Theta}},1,0\big)$ at which hyperbolicity is lost. See again Figure 3.7 for an illustration. (Here, we note that the notation $\square_{0_2}$ in chart K_2 is equivalent to $\square_{00_2}$ in Regime $\mathcal{R}_2$.)

3.4.3 Dynamics in Chart K_1

In chart K_1, the blow-up transformation defined in Equation (3.25) is given as in (3.26). Substituting into Equation (3.24), we obtain the equivalent system of equations

$$\rho_1' = \kappa\rho_1^5(u_1+\mathcal{P}\varepsilon_1)\frac{(u_1+\varepsilon_1)^2+\Lambda\rho_1^2u_1^2}{(u_1+\varepsilon_1)(u_1+\frac{\varepsilon_1}{c})}\Big[\tilde{\mu}\varepsilon_1^{\frac{1}{2}}(u_1+\varepsilon_1)-\Big(u_1+\tilde{d}\rho_1\varepsilon_1^{\frac{3}{2}}\Big)\Big], \tag{3.34a}$$

$$\begin{aligned} u_1' = {}& \rho_1^4\Big\{\tilde{b}\rho_1^2\varepsilon_1^2(u_1+\varepsilon_1)^2+\Theta u_1^2-u_1\big[(u_1+\varepsilon_1)^2+\Lambda\rho_1^2u_1^2\big]\Big\},\\ & -2\kappa\rho_1^4u_1(u_1+\mathcal{P}\varepsilon_1)\frac{(u_1+\varepsilon_1)^2+\Lambda\rho_1^2u_1^2}{(u_1+\varepsilon_1)(u_1+\frac{\varepsilon_1}{c})}\Big[\tilde{\mu}\varepsilon_1^{\frac{1}{2}}(u_1+\varepsilon_1)-\Big(u_1+\tilde{d}\rho_1\varepsilon_1^{\frac{3}{2}}\Big)\Big], \end{aligned} \tag{3.34b}$$

$$\varepsilon_1' = -2\kappa\rho_1^4\varepsilon_1(u_1+\mathcal{P}\varepsilon_1)\frac{(u_1+\varepsilon_1)^2+\Lambda\rho_1^2u_1^2}{(u_1+\varepsilon_1)(u_1+\frac{\varepsilon_1}{c})}\Big[\tilde{\mu}\varepsilon_1^{\frac{1}{2}}(u_1+\varepsilon_1)-\Big(u_1+\tilde{d}\rho_1\varepsilon_1^{\frac{3}{2}}\Big)\Big]. \tag{3.34c}$$

Dividing out a factor of ρ_1^4 from the above equations and setting dividing out a factor of ρ_1^4 from the resulting equations, as before, and setting

$$F_1(\rho_1,u_1,\varepsilon_1) = (u_1+\mathcal{P}\varepsilon_1)\frac{(u_1+\varepsilon_1)^2+\Lambda\rho_1^2u_1^2}{(u_1+\varepsilon_1)(u_1+\frac{\varepsilon_1}{c})}\Big[\tilde{\mu}\varepsilon_1^{\frac{1}{2}}(u_1+\varepsilon_1)-\Big(u_1+\tilde{d}\rho_1\varepsilon_1^{\frac{3}{2}}\Big)\Big],$$

we obtain the system

$$\rho_1' = \kappa\rho_1F_1(\rho_1,u_1,\varepsilon_1), \tag{3.35a}$$

$$u_1' = \tilde{b}\rho_1^2\varepsilon_1^2(u_1+\varepsilon_1)^2+\Theta u_1^2-u_1\big[(u_1+\varepsilon_1)^2+\Lambda\rho_1^2u_1^2\big]-2\kappa u_1F_1(\rho_1,u_1,\varepsilon_1), \tag{3.35b}$$

$$\varepsilon_1' = -2\kappa\varepsilon_1F_1(\rho_1,u_1,\varepsilon_1), \tag{3.35c}$$

which is a slow-fast system with singular perturbation parameter κ; correspondingly, the variables ρ_1 and ε_1 are slow, while u_1 is fast.

***Remark* 3.9.** *A priori*, it may seem that the denominator $(u_1+\varepsilon_1)(u_1+\frac{\varepsilon_1}{c})$ in $F_1(\rho_1,u_1,\varepsilon_1)$ may cause non-uniformity in the limit as $(u_1,\varepsilon_1)\to(0,0)$. However, one can show that F_1 at $(u_1,\varepsilon_1)=(0,0)$ vanishes at least to the order $\mathcal{O}(2)$; hence, the vector field in (3.35) is $\mathcal{C}^3$-smooth in u_1 and ε_1, which is sufficient for our purposes.

Setting $\kappa=0$ in Equation (3.35) gives the layer problem

$$\rho_1' = 0, \tag{3.36a}$$

$$u_1' = \tilde{b}\rho_1^2\varepsilon_1^2(u_1+\varepsilon_1)^2+\Theta u_1^2-u_1\Big[(u_1+\varepsilon_1)^2+\Lambda\rho_1^2u_1^2\Big], \tag{3.36b}$$

$$\varepsilon_1' = 0, \tag{3.36c}$$

The corresponding critical manifold $\mathcal{S}_{0_1}$ is the hypersurface in $(\rho_1,u_1,\varepsilon_1)$-space defined by the set

$$\tilde{b}\rho_1^2\varepsilon_1^2(u_1+\varepsilon_1)^2+\Theta u_1^2-u_1\big[(u_1+\varepsilon_1)^2+\Lambda\rho_1^2u_1^2\big]=0. \tag{3.37}$$

The flow in the invariant plane $\{\rho_1=0\}$ is governed by

$$u_1' = \Theta u_1^2-u_1(u_1+\varepsilon_1)^2-2\kappa u_1F_1(0,u_1,\varepsilon_1), \tag{3.38a}$$

$$\varepsilon_1' = -2\kappa\varepsilon_1F_1(0,u_1,\varepsilon_1), \tag{3.38b}$$

with

$$F_1(0,u_1,\varepsilon_1) = (u_1+\mathcal{P}\varepsilon_1)\frac{u_1+\varepsilon_1}{u_1+\frac{\varepsilon_1}{c}}\Big[\tilde{\mu}\varepsilon_1^{\frac{1}{2}}(u_1+\varepsilon_1)-u_1\Big].$$

(One can show that the expansions of both $u_1F_1(0,u_1,\varepsilon_1)$ and $\varepsilon_1F_1(0,u_1,\varepsilon_1)$ in (u_1,ε_1) vanish at least to $\mathcal{O}(2)$; recall Remark 3.9.) Setting $\kappa=0$ in Equation (3.38), we obtain the layer

problem

$$u_1' = \Theta u_1^2 - u_1(u_1+\varepsilon_1)^2, \tag{3.39a}$$
$$\varepsilon_1' = 0. \tag{3.39b}$$

The critical manifold of Equation (3.39), which is denoted by $\hat{\mathcal{S}}_{0_1}$, is the set $\{u_1\big[\Theta u_1 - (u_1+\varepsilon_1)^2 = 0\big]\}$; it consists of a normally attracting left branch $\hat{\mathcal{S}}_{0_1}^{a-}$ corresponding to the invariant line $\{u_1 = 0\}$ with ε_1 positive, a normally repelling middle branch $\hat{\mathcal{S}}_{0_1}^{r}$ that corresponds to $u_1 \in (0, \frac{\Theta}{4})$, and a normally attracting right branch $\hat{\mathcal{S}}_{0_1}^{a+}$ corresponding to $u_1 \in (\frac{\Theta}{4}, \Theta]$. The branches $\hat{\mathcal{S}}_{0_1}^{r}$ and $\hat{\mathcal{S}}_{0_1}^{a+}$ are separated by the fold point $C_{0_1} : \big(0, \frac{\Theta}{4}, \frac{\Theta}{4}\big)$; the equilibrium $E_{0_1} : \Big(0, \frac{\Theta^3\tilde{\mu}^4}{(\Theta\tilde{\mu}^2+1)^2}, \frac{\Theta^2\tilde{\mu}^2}{(\Theta\tilde{\mu}^2+1)^2}\Big)$, which is easily obtained from (3.37), lies on $\hat{\mathcal{S}}_{0_1}^{r}$ due to our assumptions on the parameters μ and Θ, while $\hat{\mathcal{S}}_{0_1}^{a-}$ and $\hat{\mathcal{S}}_{0_1}^{r}$ intersect in the non-hyperbolic point $P_1 : (0,0,0)$. (We note that, clearly, all three branches of $\hat{\mathcal{S}}_{0_1}$ are intersections of $\mathcal{S}_{0_1}$ with the plane $\{\rho_1 = 0\}$.) From the corresponding reduced problem, we see that ε_1 increases above E_{0_1} on $\hat{\mathcal{S}}_{0_1}^{r}$ and on $\hat{\mathcal{S}}_{0_1}^{a+}$, while it decreases below E_{0_1} on $\hat{\mathcal{S}}_{0_1}^{r}$ and on $\hat{\mathcal{S}}_{0_1}^{a-}$. Hence, orbits follow the slow manifold $\hat{\mathcal{S}}_{0_1}^{a+}$ until they reach the fold point at C_{0_1}, where they jump to the point $B_{0_1} : \big(0, 0, \frac{\Theta}{4}\big) \in \hat{\mathcal{S}}_{0_1}^{a-}$.

In the invariant plane $\{\varepsilon_1 = 0\}$, $F_1(\rho_1, u_1, 0) = -u_1^2(1+\Lambda\rho_1^2)$ implies

$$\rho_1' = -\kappa\rho_1 u_1^2(1+\Lambda\rho_1^2), \tag{3.40a}$$
$$u_1' = u_1^2\big[\Theta - u_1(1+\Lambda\rho_1^2)\big] + 2\kappa u_1^3(1+\Lambda\rho_1^2), \tag{3.40b}$$

which, for $\kappa = 0$, yields the layer problem

$$\rho_1' = 0, \tag{3.41a}$$
$$u_1' = u_1^2\big[\Theta - u_1(1+\Lambda\rho_1^2)\big]. \tag{3.41b}$$

The critical manifold for Equation (3.41), which is denoted by $\check{\mathcal{S}}_{0_1}$, is defined by equation $u_1^2\big[\Theta - u_1(1+\Lambda\rho_1^2)\big] = 0$. A straightforward calculation shows that $\check{\mathcal{S}}_{0_1}$ consists of a right attracting branch $\check{\mathcal{S}}_{0_1}^{a+}$ corresponding to the invariant curve $u_1 = \frac{\Theta}{1+\Lambda\rho_1^2}$ and the non-hyperbolic line $\check{\mathcal{S}}_{0_1}^{r}$, given by $\{u_1 = 0\}$. Both branches of $\check{\mathcal{S}}_{0_1}$ are intersections of the critical manifold $\mathcal{S}_{0_1}$ for Equation (3.36) with the plane $\{\varepsilon_1 = 0\}$. From the corresponding reduced problem, we find that ρ_1 is decreasing on $\check{\mathcal{S}}_{0_1}^{a+}$. Finally, the curves $\check{\mathcal{S}}_{0_1}^{a+}$ and $\hat{\mathcal{S}}_{0_1}^{a+}$ intersect on the u_1-axis at the point $Q_1 : (0, \Theta, 0)$; see Figure 3.10 for an illustration.

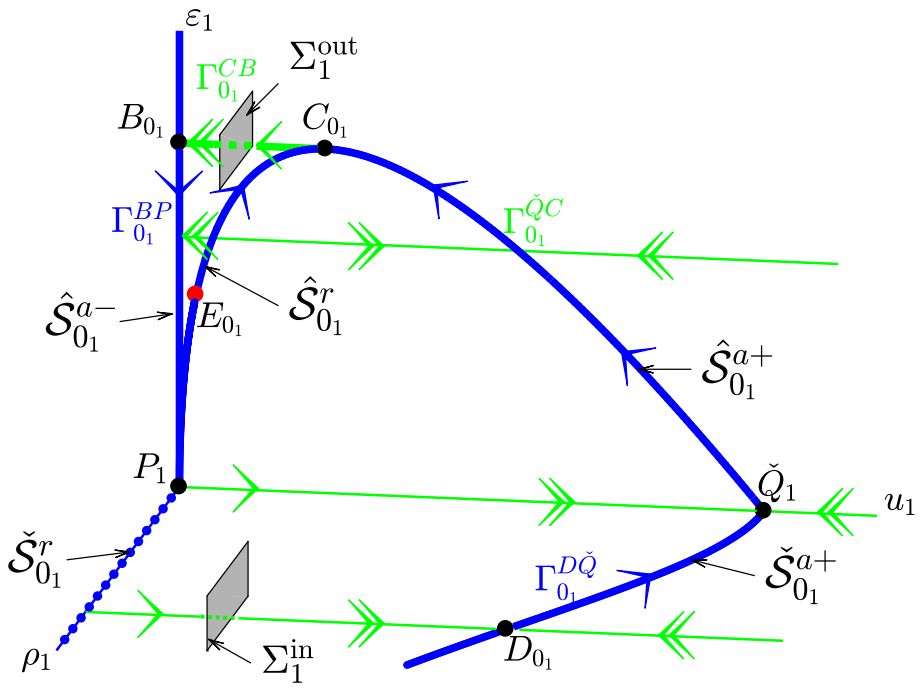

Figure 3.10: The geometry in chart K_1: critical manifolds and reduced flows in blue; orbits of layer problem in green.

We may summarise the above discussion as follows:

Lemma 3.2. *For ρ_1 or ε_1 sufficiently small, the critical manifold $\mathcal{S}_{0_1}$ for Equation (3.37) has the following properties:*

i. The manifold $\mathcal{S}_{0_1} = \mathcal{S}_{0_1}^{a-} \cup \mathcal{S}_{0_1}^{r} \cup \mathcal{F}_{0_1}^{C} \cup \mathcal{S}_{0_1}^{a+}$ is smooth away from the line $\check{\mathcal{S}}_{0_1}^{r}$.

ii. The manifold $\mathcal{S}_{0_1}$ has a folded structure; specifically, it is divided by the fold curve $\mathcal{F}_{0_1}^{C}$ into two branches $\mathcal{S}_{0_1}^{r}$ and $\mathcal{S}_{0_1}^{a+}$, whereas the branches $\mathcal{S}_{0_1}^{a-}$ and $\mathcal{S}_{0_1}^{r}$ intersect cusp-like along $\check{\mathcal{S}}_{0_1}^{r}$.

iii. The branches $\mathcal{S}_{0_1}^{a-}$ and $\mathcal{S}_{0_1}^{a+}$ are attracting under the layer flow of Equation (3.36), while the branch $\mathcal{S}_{0_1}^{r}$ is repelling.

iv. The restriction of $\mathcal{S}_{0_1}^{a-}$, $\mathcal{S}_{0_1}^{r}$, and $\mathcal{S}_{0_1}^{a+}$ to the invariant hyperplane $\{\rho_1 = 0\}$ corresponds to $\hat{\mathcal{S}}_{0_1}^{a-}$, $\hat{\mathcal{S}}_{0_1}^{r}$, and $\hat{\mathcal{S}}_{0_1}^{a+}$, respectively; correspondingly, the fold curve $\mathcal{F}_{0_1}^{C}$ reduces to the point C_{0_1}.

v. In the invariant hyperplane $\{\varepsilon_1 = 0\}$, $\mathcal{S}_{0_1}^{a-}$ and $\mathcal{S}_{0_1}^{r}$ coalesce into $\check{\mathcal{S}}_{0_1}^{r}$, while $\mathcal{S}_{0_1}^{a+}$ corresponds to $\check{\mathcal{S}}_{0_1}^{a+}$ in that limit.

Proof. The proof follows from the Implicit Function Theorem, in combination with the structural stability of folds; see [41] and the references therein for details. In particular, the geometric singular perturbation theory has been extended to the fold point by Krupa and Szmolyan [42], where they present a detailed geometric approach for a generic fold in the planar case of system. For more analysis of the fold curve in $\mathbb{R}^3$, we refer to the results of [65]. □

Summing up we have the following situation in chart K_1: the segment $\Gamma_{0_1}^{D\check{Q}}$ of the singular orbit is initialised close to the point $D_{0_1} : \left(\frac{1}{2\sqrt{\Theta\tilde{b}}}, \frac{4\Theta^2\tilde{b}}{4\Theta\tilde{b}+\Lambda}, 0\right)$, which is obtained in chart K_4 in the following section; the orbit is attracted to $\check{\mathcal{S}}_{0_1}^{a+}$ and then follows the slow flow on $\check{\mathcal{S}}_{0_1}^{a+}$ until

it reaches the point $\check{Q}_1$; the continuation of $\Gamma_{0_1}^{D\check{Q}}$ past $\check{Q}_1$ is given by the orbit $\Gamma_{0_1}^{\check{Q}C}$ along the slow flow on $\hat{\mathcal{S}}_{0_1}^{a+}$ to the fold point at C_{0_1}, where the orbit $\Gamma_{0_1}^{CB}$ represents the jump along the fast flow to the point B_{0_1} on $\hat{\mathcal{S}}_{0_1}^{a-}$; the orbit $\Gamma_{0_1}^{B\check{P}}$ then follows the slow flow on $\hat{\mathcal{S}}_{0_1}^{a-}$ to the origin P_1. The continuation of the orbit is located on the degenerate (non-hyperbolic) line $\check{\mathcal{S}}_{0_1}^{r}$; to resolve that degeneracy, we require a further blow-up transformation, which is introduced in the subsequent subsection.

3.4.4 Blow-up of the non-hyperbolic line

To analyse the dynamics in a neighbourhood of the non-hyperbolic line $\check{\mathcal{S}}_{0_1}^{r}$ recovered in chart K_1, we introduce the quasi-homogeneous, cylindrical blow-up transformation

$$\rho_1 = \bar{r}, \quad u_1 = \bar{\delta}^2\bar{u}, \quad \text{and} \quad \varepsilon_1 = \bar{\delta}\bar{\varepsilon}. \tag{3.42}$$

We will require the coordinate charts K_3 and K_4, which are obtained for $\bar{\varepsilon} = 1$ and $\bar{u} = 1$, respectively; hence, we have

$$\rho_1 = r_3, \quad u_1 = \delta_3^2 u_3, \quad \text{and} \quad \varepsilon_1 = \delta_3 \tag{3.43}$$

and

$$\rho_1 = r_4, \quad u_1 = \delta_4^2, \quad \text{and} \quad \varepsilon_1 = \delta_4\varepsilon_4, \tag{3.44}$$

respectively, for the coordinates in these charts.

Lemma 3.3. *The change-of-coordinates transformation $\mathcal{K}_{34}$ between charts K_3 and K_4 is given by*

$$\mathcal{K}_{34} : (r_3, u_3, \delta_3) \mapsto \left(r_4, \frac{1}{\varepsilon_4^2}, \delta_4\varepsilon_4\right); \tag{3.45}$$

its inverse $\mathcal{K}_{43} = \mathcal{K}_{34}^{-1}$ reads

$$\mathcal{K}_{43} : (r_4, \delta_4, \varepsilon_4) \mapsto \left(r_3, \delta_3\sqrt{u_3}, \frac{1}{\sqrt{u_3}}\right). \tag{3.46}$$

3.4.5 Dynamics in chart K_3

In chart K_3, the blow-up transformation defined by $\bar{\varepsilon} = 1$ in Equation (3.42) is given as in (3.43). Substituting into Equation (3.35), we obtain the equivalent system of equations

$$r_3' = \kappa r_3\delta_3^{\frac{5}{2}}(\delta_3 u_3 + \mathcal{P})\frac{(\delta_3 u_3+1)^2 + \Lambda r_3^2\delta_3^2 u_3^2}{(\delta_3 u_3+1)(\delta_3 u_3 + \frac{1}{c})}\Big[\tilde{\mu}(\delta_3 u_3 + 1) - \Big(\delta_3^{\frac{1}{2}} u_3 + \tilde{d} r_3\Big)\Big], \tag{3.47a}$$

$$\begin{aligned} u_3' = {} & \delta_3^2\Big\{\tilde{b} r_3^2(\delta_3 u_3+1)^2 + \Theta u_3^2 - u_3\big[(\delta_3 u_3+1)^2 + \Lambda r_3^2\delta_3^2 u_3^2\big]\Big\} \\ & + 2\kappa\delta_3^{\frac{5}{2}} u_3(\delta_3 u_3 + \mathcal{P})\frac{(\delta_3 u_3+1)^2 + \Lambda r_3^2\delta_3^2 u_3^2}{(\delta_3 u_3+1)(\delta_3 u_3 + \frac{1}{c})}\Big[\tilde{\mu}(\delta_3 u_3 + 1) - \Big(\delta_3^{\frac{1}{2}} u_3 + \tilde{d} r_3\Big)\Big], \end{aligned} \tag{3.47b}$$

$$\delta_3' = -2\kappa\delta_3^{\frac{7}{2}}(\delta_3 u_3 + \mathcal{P})\frac{(\delta_3 u_3+1)^2 + \Lambda r_3^2\delta_3^2 u_3^2}{(\delta_3 u_3+1)(\delta_3 u_3 + \frac{1}{c})}\Big[\tilde{\mu}(\delta_3 u_3 + 1) - \Big(\delta_3^{\frac{1}{2}} u_3 + \tilde{d} r_3\Big)\Big]. \tag{3.47c}$$

Dividing out the factor δ_3^2 and defining dividing out the factor δ_3^2 from the resulting equations, and defining

$$\begin{aligned} F_3(r_3, u_3, \delta_3)(= F_1(r_3, \delta_3^2 u_3, \delta_3)\delta_3^{-2}) = {} & \delta_3^{\frac{1}{2}}(\delta_3 u_3 + \mathcal{P})\frac{(\delta_3 u_3+1)^2 + \Lambda r_3^2\delta_3^2 u_3^2}{(\delta_3 u_3+1)(\delta_3 u_3 + \frac{1}{c})} \\ & \times \Big[\tilde{\mu}(\delta_3 u_3 + 1) - \Big(\delta_3^{\frac{1}{2}} u_3 + \tilde{d} r_3\Big)\Big], \end{aligned}$$

we obtain the system

$$r_3' = \kappa r_3 F_3(r_3, u_3, \delta_3), \tag{3.48a}$$
$$u_3' = \tilde{b} r_3^2 (\delta_3 u_3 + 1)^2 + \Theta u_3^2 - u_3\big[(\delta_3 u_3 + 1)^2 + \Lambda r_3^2 \delta_3^2 u_3^2\big] + 2\kappa u_3 F_3(r_3, u_3, \delta_3), \tag{3.48b}$$
$$\delta_3' = -2\kappa \delta_3 F_3(r_3, u_3, \delta_3), \tag{3.48c}$$

which is a slow-fast system in standard form, with singular perturbation parameter κ; correspondingly, the variables r_3 and δ_3 are slow, while u_3 is fast. Here, the prime now denotes differentiation with respect to a new time variable. For $\kappa = 0$ in (3.48), one obtains the layer problem

$$r_3' = 0, \tag{3.49a}$$
$$u_3' = \tilde{b} r_3^2 (\delta_3 u_3 + 1)^2 + \Theta u_3^2 - u_3\big[(\delta_3 u_3 + 1)^2 + \Lambda r_3^2 \delta_3^2 u_3^2\big], \tag{3.49b}$$
$$\delta_3' = 0. \tag{3.49c}$$

The corresponding critical manifold $\mathcal{S}_{0_3}$ is described by a hypersurface in $\{(r_3, u_3, \delta_3)\}$-space that is defined by the set

$$\tilde{b} r_3^2 (\delta_3 u_3 + 1)^2 + \Theta u_3^2 - u_3\big[(\delta_3 u_3 + 1)^2 + \Lambda r_3^2 \delta_3^2 u_3^2\big] = 0. \tag{3.50}$$

The flow of Equation (3.48) in the invariant plane $\{r_3 = 0\}$ is governed by

$$u_3' = \Theta u_3^2 - u_3(\delta_3 u_3 + 1)^2 + 2\kappa u_3 F_3(0, u_3, \delta_3), \tag{3.51a}$$
$$\delta_3' = -2\kappa \delta_3 F_3(0, u_3, \delta_3), \tag{3.51b}$$

with

$$F_3(0, u_3, \delta_3) = \delta_3^{\frac{1}{2}} (\delta_3 u_3 + \mathcal{P}) \frac{\delta_3 u_3 + 1}{\delta_3 u_3 + \frac{1}{c}} \Big[\tilde{\mu}(\delta_3 u_3 + 1) - \delta_3^{\frac{1}{2}} u_3\Big],$$

which is again a slow-fast system with respect to κ; correspondingly, the variable ε_3 is slow, while u_3 is a fast variable. Setting $\kappa = 0$, we obtain the layer problem

$$u_3' = \Theta u_3^2 - u_3(\delta_3 u_3 + 1)^2, \tag{3.52a}$$
$$\delta_3' = 0. \tag{3.52b}$$

The critical manifold in the plane $\{r_3 = 0\}$, which we denote by $\hat{\mathcal{S}}_{0_3}$, is defined by equation $u_3\big[\Theta u_3 - (\delta_3 u_3 + 1)^2\big] = 0$. It consists of an attracting left branch $\hat{\mathcal{S}}_{0_3}^{a-}$ – the δ_3-axis, a repelling middle branch $\hat{\mathcal{S}}_{0_3}^{r}$, and an attracting right branch $\hat{\mathcal{S}}_{0_3}^{a+}$. The branches $\hat{\mathcal{S}}_{0_3}^{r}$ and $\hat{\mathcal{S}}_{0_3}^{a+}$ are separated by a fold point at $C_{0_3} : \big(0, \frac{4}{\Theta}, \frac{\Theta}{4}\big)$; here, we note that the equilibrium $E_{0_3} : \Big(0, \frac{(\Theta\tilde{\mu}^2+1)^2}{\Theta}, \frac{\Theta^2\tilde{\mu}^2}{(\Theta\tilde{\mu}^2+1)^2}\Big)$ lies in $\hat{\mathcal{S}}_{0_3}^{r}$. Moreover, $\hat{\mathcal{S}}_{0_3}^{a-}$ and $\hat{\mathcal{S}}_{0_3}^{r}$ intersect the u_3-axis in the points $\hat{P}_3 : (0,0,0)$ and $\hat{Q}_3 : (0, \frac{1}{\Theta}, 0)$, respectively. All three branches of $\hat{\mathcal{S}}_{0_3}$ are intersections of $\mathcal{S}_{0_3}$ with the plane $\{r_3 = 0\}$. From the corresponding reduced problem, we conclude that δ_3 is increasing on $\hat{\mathcal{S}}_{0_3}^{r}$ above E_{0_3} and on $\hat{\mathcal{S}}_{0_3}^{a+}$, while it is decreasing on $\hat{\mathcal{S}}_{0_3}^{r}$ below E_{0_3} and on $\hat{\mathcal{S}}_{0_3}^{a-}$. Hence, orbits follow the slow manifold $\hat{\mathcal{S}}_{0_3}^{a+}$ until they reach the fold point at C_{0_3}, where they jump to the point $B_{0_3} : \big(0, 0, \frac{\Theta}{4}\big) \in \hat{\mathcal{S}}_{0_3}^{a-}$.

Next, we consider the flow of Equation (3.48) in the invariant plane $\{\delta_3 = 0\}$, which is governed by

$$r_3' = 0, \tag{3.53a}$$
$$u_3' = \tilde{b} r_3^2 + \Theta u_3^2 - u_3. \tag{3.53b}$$

The corresponding critical manifold, which is denoted by $\check{\mathcal{S}}_{0_3}$, is defined by equation $\tilde{b} r_3^2 + \Theta u_3^2 - u_3 = 0$; it consists of a left attracting branch $\check{\mathcal{S}}_{0_3}^{a-}$ corresponding to $u_3 \in \big[0, \frac{1}{2\Theta}\big)$ and a right repelling branch $\check{\mathcal{S}}_{0_3}^{a+}$ which corresponds to $u_3 \in \big(\frac{1}{2\Theta}, \frac{1}{\Theta}\big]$. The two branches are separated

by a fold point at A_{0_3} : $\left(\frac{1}{2\sqrt{\Theta\tilde{b}}}, \frac{1}{2\Theta}, 0\right)$. Both branches are intersections of $\mathcal{S}_{0_3}$ with the plane $\{\delta_3 = 0\}$. The geometry in chart K_3 is summarised in Figure 3.11. Due to $F_3(r_3, u_3, 0) = 0$, the reduced flow in $\delta_3 = 0\}$ is degenerate; however, for δ_3 positive and small, orbits follow the corresponding sheet $\mathcal{S}^a_{0_3}$ of S_{0_3} until they reach the fold curve $\mathcal{F}^A_{0_3}$ and then jump forward to a point D_{0_3}, which is not visible in this chart.

***Remark* 3.10.** When δ_3 is small, given our choice of μ and d, with $\frac{\tilde{\mu}}{\tilde{d}} > \frac{1}{2\sqrt{\Theta\tilde{b}}}$, the term $\left[\tilde{\mu}(\delta_3 u_3 + 1) - \left(\delta_3^{\frac{1}{2}} u_3 + \tilde{d} r_3\right)\right]$ in $F_3(r_3, u_3, \delta_3)$, rewritten as $\left[(\tilde{\mu} - \tilde{d} r_3) - u_3 \delta_3^{\frac{1}{2}} + \tilde{\mu} u_3 \delta_3\right]$, admits the positive sign of r_3' for $r_3 \leqslant \frac{1}{2\sqrt{\Theta\tilde{b}}}$, and it follows that the reduced flow in the r_3-variable is directed upwards to A_{0_3} on $\mathcal{S}^a_{0_3}$; recall Remark 3.3.

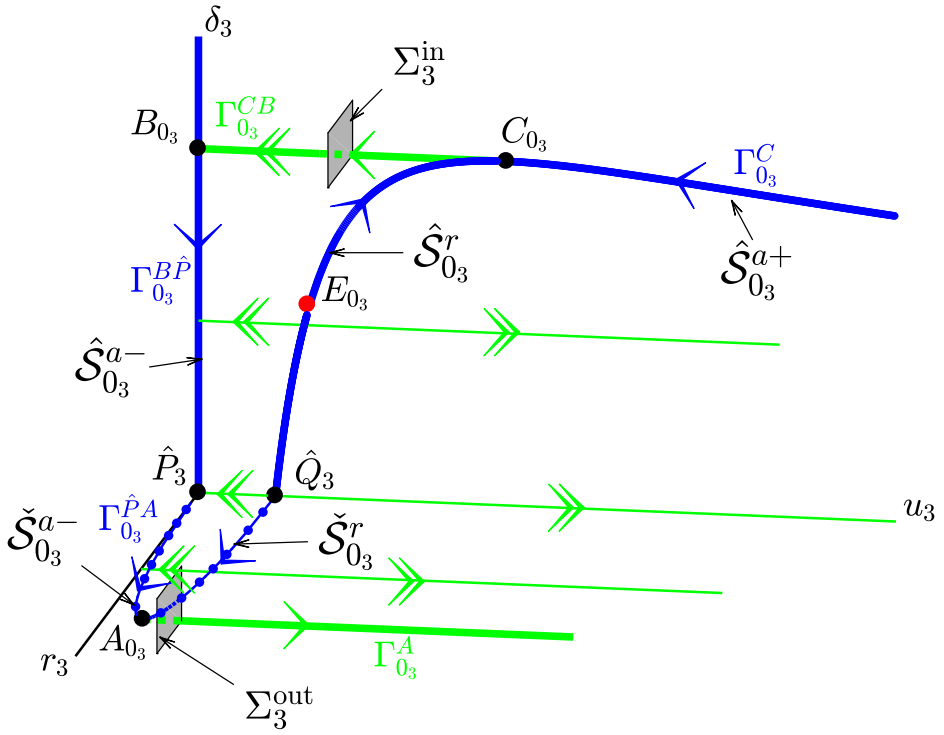

Figure 3.11: The geometry in chart K_3.

We conclude with the following result, the proof of which is analogous to that of Lemma 3.2:

Lemma 3.4. *For r_3 or δ_3 sufficiently small, the critical manifold $\mathcal{S}_{0_3}$ for Equation* (3.50) *has the following properties:*

i. The manifold $\mathcal{S}_{0_3} = \mathcal{S}^{a-}_{0_3} \cup \mathcal{F}^A_{0_3} \cup \mathcal{S}^r_{0_3} \cup \mathcal{F}^C_{0_3} \cup \mathcal{S}^{a+}_{0_3}$ is smooth.

ii. The manifold $\mathcal{S}_{0_3}$ has a folded structure; in particular, the branches $\mathcal{S}^{a-}_{0_3}$ and $\mathcal{S}^r_{0_3}$ are separated by the fold curve $\mathcal{F}^A_{0_3}$, while $\mathcal{S}^r_{0_3}$ and $\mathcal{S}^{a+}_{0_3}$ are separated by the fold curve $\mathcal{F}^C_{0_3}$.

iii. The branches $\mathcal{S}^{a-}_{0_3}$ and $\mathcal{S}^{a+}_{0_3}$ are attracting under the layer flow of Equation (3.49)*, while the branch $\mathcal{S}^r_{0_3}$ is repelling.*

iv. The restriction of $\mathcal{S}^{a-}_{0_3}$, $\mathcal{S}^r_{0_3}$ and $\mathcal{S}^{a+}_{0_3}$ to the invariant hyperplane $\{r_3 = 0\}$ corresponds to $\hat{\mathcal{S}}^{a-}_{0_3}$, $\hat{\mathcal{S}}^r_{0_3}$ and $\hat{\mathcal{S}}^{a+}_{0_3}$, respectively. Correspondingly, the fold curve $F^C_{0_3}$ reduces to the point C_{0_3}.

v. In the invariant hyperplane $\{\delta_3 = 0\}$, $\mathcal{S}^{a-}_{0_3}$ and $\mathcal{S}^r_{0_3}$ reduce to $\check{\mathcal{S}}^{a-}_{0_3}$ and $\check{\mathcal{S}}^r_{0_3}$, respectively. The fold curve $\mathcal{F}^A_{0_3}$ tends to the point A_{0_3} in that limit.

In summary, the segment $\Gamma_{0_3}^{C}$ of the singular orbit follows the slow flow on $\hat{\mathcal{S}}_{0_3}^{a+}$ to the fold point C_{0_3}; the orbit $\Gamma_{0_3}^{CB}$ represents the jump along the fast flow to the point B_{0_3}. The segment $\Gamma_{0_3}^{B\hat{P}}$ then follows the slow flow on $\hat{\mathcal{S}}_{0_3}^{a-}$ until it reaches the origin $\hat{P}_3$, continuing with the orbit $\Gamma_{0_3}^{\hat{P}A}$ that corresponds to the segment of $\check{\mathcal{S}}_{0_3}^{a-}$ between $\hat{P}_3$ and the fold point A_{0_3}; finally, the orbit jumps along the fast flow to the right for u_3 large. We label the corresponding segment by $\Gamma_{0_3}^{A}$. The large-u_3 dynamics of Equation (3.48) is then naturally studied in chart K_4.

3.4.6 Dynamics in chart K_4

In chart K_4, the blow-up transformation defined by $\bar{u}_1 = 1$ in Equation (3.42) is given as in (3.44). Substituting into Equation (3.35), we obtain the equivalent system of equations

$$r_4' = \kappa r_4 \delta_4^{\frac{5}{2}}(\delta_4 + \mathcal{P}\varepsilon_4)\frac{(\delta_4+\varepsilon_4)^2 + \Lambda r_4^2\delta_4^2}{(\delta_4+\varepsilon_4)(\delta_4+\frac{\varepsilon_4}{c})}\Big[\tilde{\mu}\varepsilon_4^{\frac{1}{2}}(\delta_4+\varepsilon_4) - \Big(\delta_4^{\frac{1}{2}} + \tilde{d}r_4\varepsilon_4^{\frac{3}{2}}\Big)\Big], \tag{3.54a}$$

$$\begin{aligned}\delta_4' = {}& \frac{1}{2}\delta_4^3\Big\{\tilde{b}r_4^2\varepsilon_4^2(\delta_4+\varepsilon_4)^2 + \Theta - \big[(\delta_4+\varepsilon_4)^2 + \Lambda r_4^2\delta_4^2\big]\Big\},\\ & - \kappa\delta_4^{\frac{7}{2}}(\delta_4 + \mathcal{P}\varepsilon_4)\frac{(\delta_4+\varepsilon_4)^2 + \Lambda r_4^2\delta_4^2}{(\delta_4+\varepsilon_4)(\delta_4+\frac{\varepsilon_4}{c})}\Big[\tilde{\mu}\varepsilon_4^{\frac{1}{2}}(\delta_4+\varepsilon_4) - \Big(\delta_4^{\frac{1}{2}} + \tilde{d}r_4\varepsilon_4^{\frac{3}{2}}\Big)\Big],\end{aligned} \tag{3.54b}$$

$$\begin{aligned}\varepsilon_4' = {}& -\frac{1}{2}\delta_4^2\varepsilon_4\Big\{\tilde{b}r_4^2\varepsilon_4^2(\delta_4+\varepsilon_4)^2 + \Theta - \big[(\delta_4+\varepsilon_4)^2 + \Lambda r_4^2\delta_4^2\big]\Big\}\\ & - \kappa\varepsilon_4\delta_4^{\frac{5}{2}}(\delta_4 + \mathcal{P}\varepsilon_4)\frac{(\delta_4+\varepsilon_4)^2 + \Lambda r_4^2\delta_4^2}{(\delta_4+\varepsilon_4)(\delta_4+\frac{\varepsilon_4}{c})}\Big[\tilde{\mu}\varepsilon_4^{\frac{1}{2}}(\delta_4+\varepsilon_4) - \Big(\delta_4^{\frac{1}{2}} + \tilde{d}r_4\varepsilon_4^{\frac{3}{2}}\Big)\Big].\end{aligned} \tag{3.54c}$$

By dividing out the factor δ_4^2 and defining dividing out a factor of δ_4^2, and defining

$$\begin{aligned}F_4(r_4,\delta_4,\varepsilon_4)(= F_1(r_4,\delta_4^2,\delta_4\varepsilon_4)\delta_4^{-2}) = {}& \delta_4^{\frac{1}{2}}(\delta_4+\mathcal{P}\varepsilon_4)\frac{(\delta_4+\varepsilon_4)^2+\Lambda r_4^2\delta_4^2}{(\delta_4+\varepsilon_4)(\delta_4+\frac{\varepsilon_4}{c})}\\ & \times\Big[\tilde{\mu}\varepsilon_4^{\frac{1}{2}}(\delta_4+\varepsilon_4) - \Big(\delta_4^{\frac{1}{2}} + \tilde{d}r_4\varepsilon_4^{\frac{3}{2}}\Big)\Big],\end{aligned}$$

we obtain the simplified system

$$r_4' = \kappa r_4 F_4(r_4,\delta_4,\varepsilon_4), \tag{3.55a}$$

$$\delta_4' = \frac{1}{2}\delta_4\Big\{\tilde{b}r_4^2\varepsilon_4^2(\delta_4+\varepsilon_4)^2 + \Theta - \big[(\delta_4+\varepsilon_4)^2 + \Lambda r_4^2\delta_4^2\big]\Big\} - \kappa\delta_4 F_4(r_4,\delta_4,\varepsilon_4), \tag{3.55b}$$

$$\varepsilon_4' = -\frac{1}{2}\varepsilon_4\Big\{\tilde{b}r_4^2\varepsilon_4^2(\delta_4+\varepsilon_4)^2 + \Theta - \big[(\delta_4+\varepsilon_4)^2 + \Lambda r_4^2\delta_4^2\big]\Big\} - \kappa\varepsilon_4 F_4(r_4,\delta_4,\varepsilon_4), \tag{3.55c}$$

which is a slow-fast system with singular perturbation parameter κ; correspondingly, the variable r_4 is slow, while δ_4 and ε_4 are fast. Here, the prime now denotes differentiation with respect to ξ.

***Remark* 3.11.** The denominator $(\delta_4+\varepsilon_4)(\delta_4+\frac{\varepsilon_4}{c})$ in $F_4(r_4,\delta_4,\varepsilon_4)$ may be expected to render the limit as $(\delta_4,\varepsilon_4)\to(0,0)$ in (3.55) non-uniform; recall Remark 3.9. Since, however, the expansion of F_4 at $(\delta_4,\varepsilon_4)=(0,0)$ vanishes at least to the order $\mathcal{O}(2)$, one again has at least $\mathcal{C}^2$-smoothness in δ_4 and ε_4.

Setting $\kappa = 0$ in (3.55), we obtain the layer problem

$$r_4' = 0, \tag{3.56a}$$

$$\delta_4' = \frac{1}{2}\delta_4\Big\{\tilde{b}r_4^2\varepsilon_4^2(\delta_4+\varepsilon_4)^2 + \Theta - \big[(\delta_4+\varepsilon_4)^2 + \Lambda r_4^2\delta_4^2\big]\Big\}, \tag{3.56b}$$

$$\varepsilon_4' = -\frac{1}{2}\varepsilon_4\Big\{\tilde{b}r_4^2\varepsilon_4^2(\delta_4+\varepsilon_4)^2 + \Theta - \big[(\delta_4+\varepsilon_4)^2 + \Lambda r_4^2\delta_4^2\big]\Big\}. \tag{3.56c}$$

The corresponding critical manifold $\mathcal{S}_{0_4}$ is described by the hypersurface in $\{(r_4,\delta_4,\varepsilon_4)\}$-space

that is defined by the set

$$\tilde{b}r_4^2\varepsilon_4^2(\delta_4+\varepsilon_4)^2+\Theta-\big[(\delta_4+\varepsilon_4)^2+\Lambda r_4^2\delta_4^2\big]=0 \quad \text{or} \quad \delta_4=0=\varepsilon_4. \tag{3.57}$$

We consider the flow of Equation (3.56) in the invariant plane $\{\delta_4=0\}$, which is governed by

$$r_4'=0, \tag{3.58a}$$
$$\varepsilon_4'=-\frac{1}{2}\varepsilon_4\big(\tilde{b}r_4^2\varepsilon_4^4+\Theta-\varepsilon_4^2\big). \tag{3.58b}$$

The corresponding critical manifold is defined by

$$\tilde{b}r_4^2\varepsilon_4^4+\Theta-\varepsilon_4^2=0 \quad \text{or} \quad \varepsilon_4=0;$$

it consists of a lower repelling branch $\check{\mathcal{S}}_{0_4}^r$ corresponding to $\varepsilon_4\in[\sqrt{\Theta},\sqrt{2\Theta})$ and an upper attracting branch $\check{\mathcal{S}}_{0_4}^{a-}$ with $\varepsilon_4\in(\sqrt{2\Theta},\infty)$, which are separated by the fold point $A_{0_4}:\big(\frac{1}{2\sqrt{\Theta\tilde{b}}},0,\sqrt{2\Theta}\big)$, as well as of the attracting r_4-axis, which we denote by $\mathcal{S}_{0_4}^r$. All three branches are found in the intersection of $\mathcal{S}_{0_4}$ with the plane $\{\delta_4=0\}$. Orbits follow the slow manifold $\check{\mathcal{S}}_{0_4}^{a-}$ until they reach the fold point at A_{0_4}, where they jump forward to the point $\check{P}_4:(\frac{1}{2\sqrt{\Theta\tilde{b}}},0,0)\in\mathcal{S}_{0_4}^r$.

In the invariant plane $\{\varepsilon_4=0\}$, Equation (3.56) reduces to

$$r_4'=-\kappa r_4\delta_4^2(1+\Lambda r_4^2), \tag{3.59a}$$
$$\delta_4'=\frac{1}{2}\delta_4\big[\Theta-\delta_4^2(1+\Lambda r_4^2)\big]+\kappa\delta_4^3(1+\Lambda r_4^2), \tag{3.59b}$$

as $F_4(r_4,\delta_4,0)=-\delta_4^2(1+\Lambda r_4^2)$ then. The corresponding layer problem is obtained for $\kappa=0$,

$$r_4'=0, \tag{3.60a}$$
$$\delta_4'=\frac{1}{2}\delta_4\big[\Theta-\delta_4^2(1+\Lambda r_4^2)\big], \tag{3.60b}$$

which implies that the critical manifold satisfies

$$\Theta-\delta_4^2(1+\Lambda r_4^2)=0 \quad \text{or} \quad \delta_4=0;$$

that manifold consists of a right attracting branch $\check{\mathcal{S}}_{0_4}^{a+}$, which intersects the δ_4-axis in the point $\check{Q}_4=(0,\sqrt{\Theta},0)$, and the repelling r_4-axis, which we again denote by $\mathcal{S}_{0_4}^r$. Orbits starting close to $\check{P}_4\in\mathcal{S}_{0_4}^r$ leave along the unstable manifold thereof and jump to the point $D_{0_4}:\big(\frac{1}{2\sqrt{\Theta\tilde{b}}},\frac{2\Theta\sqrt{\tilde{b}}}{\sqrt{4\Theta\tilde{b}+\Lambda}},0\big)$ in $\check{\mathcal{S}}_{0_4}^{a+}$; then, they follow the slow manifold $\check{\mathcal{S}}_{0_4}^{a+}$ until they reach the point $\check{Q}_4$. An illustration of the resulting geometry can be found in Figure 3.12.

Similarly, in the invariant plane $\{r_4=0\}$, the flow of Equation (3.56) is governed by

$$\delta_4'=\frac{1}{2}\delta_4\big[\Theta-(\delta_4+\varepsilon_4)^2\big]-\kappa\delta_4F_4(0,\delta_4,\varepsilon_4), \tag{3.61a}$$
$$\varepsilon_4'=-\frac{1}{2}\varepsilon_4\big[\Theta-(\delta_4+\varepsilon_4)^2\big]-\kappa\varepsilon_4F_4(0,\delta_4,\varepsilon_4), \tag{3.61b}$$

where

$$F(0,\delta_4,\varepsilon_4)=\delta_4^{\frac{1}{2}}(\delta_4+\mathcal{P}\varepsilon_4)\frac{\delta_4+\varepsilon_4}{\delta_4+\frac{\varepsilon_4}{c}}\big[\tilde{\mu}\varepsilon_4^{\frac{1}{2}}(\delta_4+\varepsilon_4)-\delta_4^{\frac{1}{2}}\big].$$

(Again, one can conclude $\mathcal{C}^3$-smoothness of the vector field in (3.61) as $(\delta_4,\varepsilon_4)\to(0,0)$ due to the fact that the expansions of $\delta_4F_4(0,\delta_4,\varepsilon_4)$ and $\varepsilon_4F_4(0,\delta_4,\varepsilon_4)$ in (δ_4,ε_4) vanish at least to

$\mathcal{O}(2)$; recall Remark 3.11.) Setting $\kappa = 0$, we obtain the layer problem

$$\delta_4' = \frac{1}{2}\delta_4\big[\Theta - (\delta_4 + \varepsilon_4)^2\big], \tag{3.62a}$$

$$\varepsilon_4' = -\frac{1}{2}\varepsilon_4\big[\Theta - (\delta_4 + \varepsilon_4)^2\big]; \tag{3.62b}$$

the corresponding critical manifold, which is denoted by $\hat{\mathcal{S}}_{0_4}$, is defined by the set

$$\Theta - (\delta_4 + \varepsilon_4)^2 = 0\big\} \quad \text{or} \quad \{\delta_4 = 0 = \varepsilon_4.$$

The branch obtained from the first condition above is a line that consists of an attracting right segment $\hat{\mathcal{S}}^{a+}_{0_4}$ connecting the point $\check{Q}_4$ to the fold point at C_{0_4} : $\big(0, \frac{\sqrt{\Theta}}{2}, \frac{\sqrt{\Theta}}{2}\big)$ and a repelling left segment connecting the point $\hat{Q}_4$: $(0, 0, \sqrt{\Theta})$ to C_{0_4}; the corresponding equilibrium E_{0_4} : $\big(0, \frac{\Theta^{\frac{3}{2}}\tilde{\mu}^2}{\Theta\tilde{\mu}^2+1}, \frac{\Theta}{\Theta\tilde{\mu}^2+1}\big)$ lies in $\hat{\mathcal{S}}^r_{0_4}$. The reduced flow on $\hat{\mathcal{S}}^r_{0_4}$ is increasing above E_{0_4}, while it decreases below E_{0_4} until it reaches the fold point at C_{0_4}.

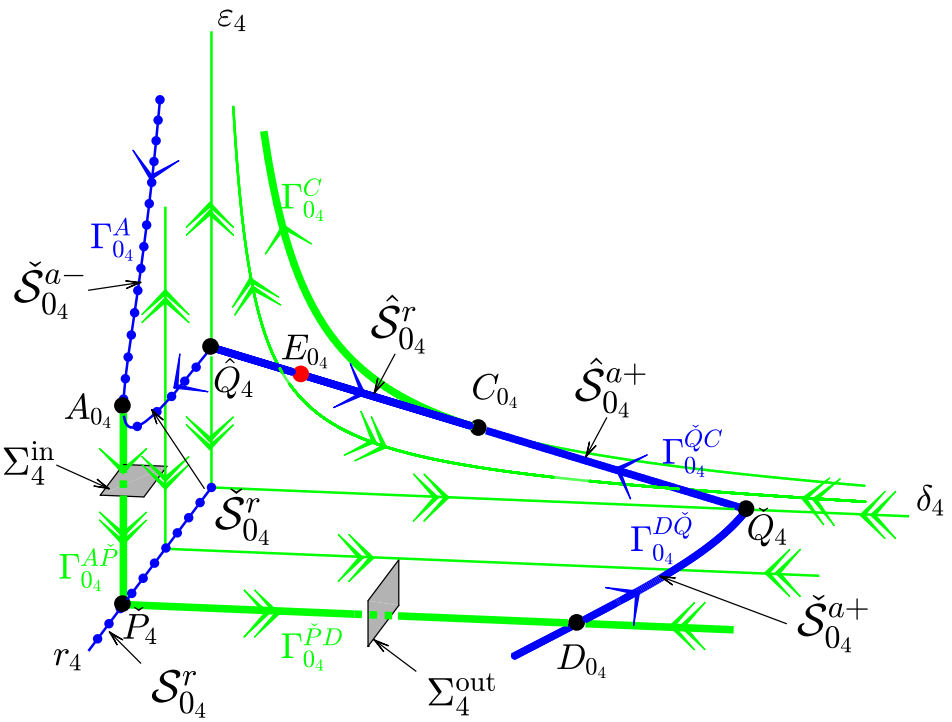

Figure 3.12: Singular geometry in chart K_4.

In conclusion, we have the following result:, the proof of which is again analogous to that of Lemma 3.2:

Lemma 3.5. *For r_4, δ_4, or ε_4 sufficiently small, the critical manifold $\mathcal{S}_{0_4}$ for Equation* (3.57) *has the following properties:*

i. The manifold $\mathcal{S}_{0_4} = \mathcal{S}^{a-}_{0_4} \cup \mathcal{F}^A_{0_4} \cup \mathcal{S}^r_{0_4} \cup \mathcal{F}^C_{0_4} \cup \mathcal{S}^{a+}_{0_4}$ is smooth away from line $\mathcal{S}^r_{0_4}$.

ii. $\mathcal{S}_{0_4}$ has a folded structure; in particular, the branches $\mathcal{S}^{a-}_{0_4}$ and $\mathcal{S}^r_{0_4}$ are separated by the fold curve $\mathcal{F}^A_{0_4}$, while $\mathcal{S}^r_{0_4}$ and $\mathcal{S}^{a+}_{0_4}$ are separated by the fold curve $\mathcal{F}^C_{0_4}$.

iii. The branches $\mathcal{S}^{a-}_{0_4}$ and $\mathcal{S}^{a+}_{0_4}$ are attracting under the layer flow of Equation (3.56)*, while the branch $\mathcal{S}^r_{0_4}$ is repelling.*

iv. The restriction of $\mathcal{S}^r_{0_4}$ *and* $\mathcal{S}^{a+}_{0_4}$ *to the invariant hyperplane* $\{r_4 = 0\}$ *corresponds to* $\hat{\mathcal{S}}^r_{0_4}$ *and* $\hat{\mathcal{S}}^{a+}_{0_4}$*, respectively. Correspondingly, the fold curve* $\mathcal{F}^C_{0_4}$ *reduces to the point* C_{0_4}*.*

v. In the invariant hyperplane $\{\delta_4 = 0\}$*,* $\mathcal{S}^{a-}_{0_4}$ *and* $\mathcal{S}^r_{0_4}$ *reduce to* $\check{\mathcal{S}}^{a-}_{0_4}$ *and* $\check{\mathcal{S}}^r_{0_4}$*, respectively. The fold curve* $\mathcal{F}^A_{0_4}$ *tends to the point* A_{0_4} *in that limit.*

vi. The restriction of $\mathcal{S}^{a+}_{0_4}$ *to the invariant hyperplane* $\{\varepsilon_4 = 0\}$ *corresponds to* $\check{\mathcal{S}}^{a+}_{0_4}$*.*

vii. The manifold $\mathcal{S}^r_{0_4}$ *consists of equilibria for Equation* (3.55)*, with* 1*-dimensional stable manifold in the hyperplane* $\{\delta_4 = 0\}$ *and* 1*-dimensional unstable manifold in the hyperplane* $\{\varepsilon_4 = 0\}$

To summarise, the segment $\Gamma^{A\check{P}}_{0_4}$ of the singular cycle is initiated close to the fold point at A_{0_4} and is attracted to $\check{\mathcal{S}}^{a-}_{0_4}$, where it jumps forward along the fast flow to the point $\check{P}_4$; the orbit $\Gamma^{\check{P}D}_{0_4}$ then leaves along the unstable manifold and is attracted by $\check{\mathcal{S}}^{a+}_{0_4}$ connecting to the point D_{0_4}; the orbit $\Gamma^{D\check{Q}}_{0_4}$ follows the slow flow $\check{\mathcal{S}}^{a+}_{0_4}$ to the point $\check{Q}_4$ and continues as the orbit $\Gamma^{\check{Q}C}_{0_4}$ along the slow flow on $\hat{\mathcal{S}}^{a+}_{0_4}$ until it reaches the point C_{0_4}, where the orbit $\Gamma^C_{0_4}$ represents the jump back which is, however, not visible in chart K_4, but is discussed in K_3 already.

3.4.7 Global geometry in blow-up space

We now summarise the global geometry of the blow-up space, which we label $\overline{M}_\kappa$; the above analysis implies that $\overline{M}_\kappa$ consists of the sphere M_U and the cylinder M_R, which are obtained by the blow-up transformation in (3.25) at the origin Q in (R, U, ε)-space and the blow-up in (3.42) of the non-hyperbolic line $\check{\mathcal{S}}^r_{0_1}$ in chart K_1 of the former, respectively; see Figure 3.14.

Lemma 3.6. *The critical manifold of system* (3.24) *in blow-up space* $\overline{M}_0$ *is defined as*

$$\bar{\mathcal{S}}_0 = \bar{\mathcal{S}}^{a-}_0 \cup \bar{\mathcal{F}}^A_0 \cup \bar{\mathcal{S}}^r_0 \cup \bar{\mathcal{F}}^C_0 \cup \bar{\mathcal{S}}^{a+}_0;$$

here, the branches $\bar{\mathcal{S}}^{a-}_0$ *and* $\bar{\mathcal{S}}^{a+}_0$ *are attracting under the layer flow that is induced by Equation* (3.8) *after blow-up, while the branch* $\bar{\mathcal{S}}^r_0$ *is repelling. Moreover,* $\bar{\mathcal{S}}^{a-}_0$ *and* $\bar{\mathcal{S}}^{a+}_0$ *are separated by the fold curve* $\bar{\mathcal{F}}^A_0$*, while* $\bar{\mathcal{S}}^r_0$ *and* $\bar{\mathcal{S}}^{a+}_0$ *are separated by the fold curve* $\bar{\mathcal{F}}^C_0$*. Recall Remark 3.8, the notation of* $\bar{\square}_\kappa$ *corresponding to the original object* $\square_{\kappa\varepsilon}$ *after blow-up.*

Lemma 3.7. *The singular cycle* $\bar{\Gamma}_{00}$ *is defined by*

$$\bar{\Gamma}_{00} = \bar{\Gamma}^{A\check{P}}_{00} \cup \bar{\Gamma}^{\check{P}D}_{00} \cup \bar{\Gamma}^{D\check{Q}}_{00} \cup \bar{\Gamma}^{\check{Q}C}_{00} \cup \bar{\Gamma}^{CB}_{00} \cup \bar{\Gamma}^{B\hat{P}}_{00} \cup \bar{\Gamma}^{\hat{P}A}_{00}. \tag{3.63}$$

Here, the heteroclinic orbit $\bar{\Gamma}^{A\check{P}}_{00}$ *is located on the cylinder* M_R *and represents the fast jump from the point* $\bar{A}_0$ *to the point* $\check{P} \in \bar{\mathcal{S}}^r_0$*; the heteroclinic orbit* $\bar{\Gamma}^{\check{P}D}_{00}$ *lies in the plane* $\{\bar{\varepsilon} = 0\}$*, connecting* $\check{P}$ *to the point* $\bar{D}_0 \in \bar{\mathcal{S}}^{a+}_0$*; and* $\bar{\Gamma}^{D\check{Q}}_{00}$ *represents the transition on* $\bar{\mathcal{S}}^{a+}_0$ *from* $\bar{D}_0$ *to the point* $\check{Q}$*. On the sphere* M_U*, the segment* $\bar{\Gamma}^{\check{Q}C}_{00}$ *on* $\bar{\mathcal{S}}^{a+}_0$ *connects the point* $\check{Q}$ *to the fold point at* $\bar{C}_0$*;* $\bar{\Gamma}^{CB}_{00}$ *denotes the heteroclinic connection from* $\bar{C}_0$ *to the point* $\bar{B}_0 \in \bar{\mathcal{S}}^{a-}_0$*, followed by the orbit* $\bar{\Gamma}^{B\hat{P}}_{00}$ *from* $\bar{B}_0$ *to the point* $\hat{P}$*. The final part* $\bar{\Gamma}^{\hat{P}A}_{00}$ *is located on the cylinder* M_R*, and denotes the transition on* $\bar{\mathcal{S}}^{a-}_0$ *from* $\hat{P}$ *to the fold point at* $\bar{A}_0$*. (Here, we label the orbits in blow-up space by* $\bar{\Gamma}_{\kappa\varepsilon}$ *for clarify, with the singular cycle* $\bar{\Gamma}_{00}$ *defined by* $(\kappa, \varepsilon) \to (0, 0)$*.)*

An illustration of $\bar{\Gamma}_{00}$ and $\bar{\Gamma}_{0\varepsilon}$ can be found in Figure 3.14 and the corresponding charts K_i $(i = 1, ..., 4)$ in Figure 3.13.

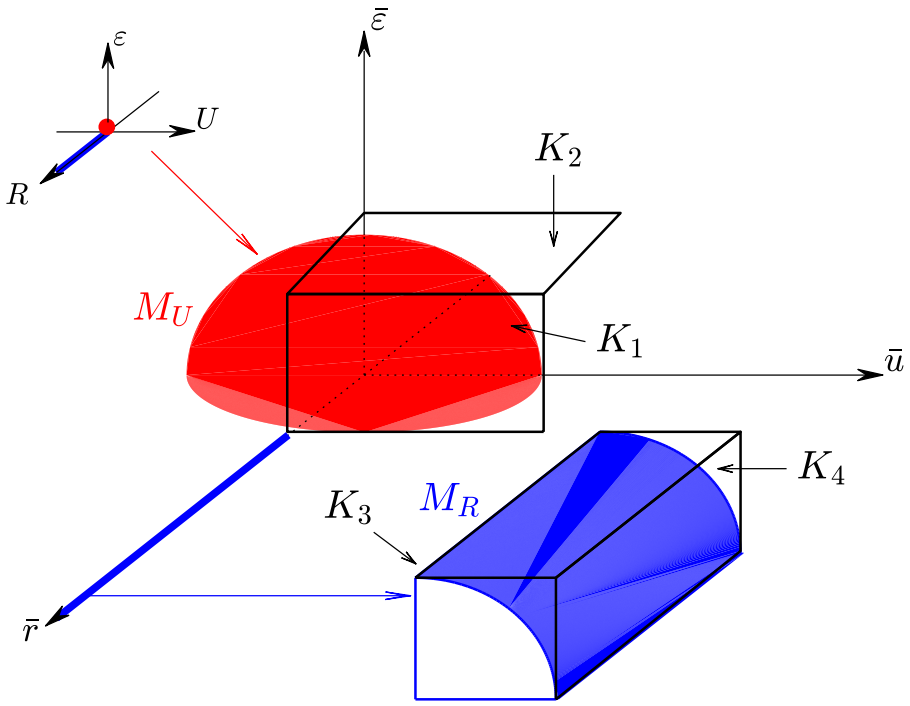

Figure 3.13: The charts K_i $(i = 1, \ldots, 4)$ in blow-up space $\overline{M}_0$.

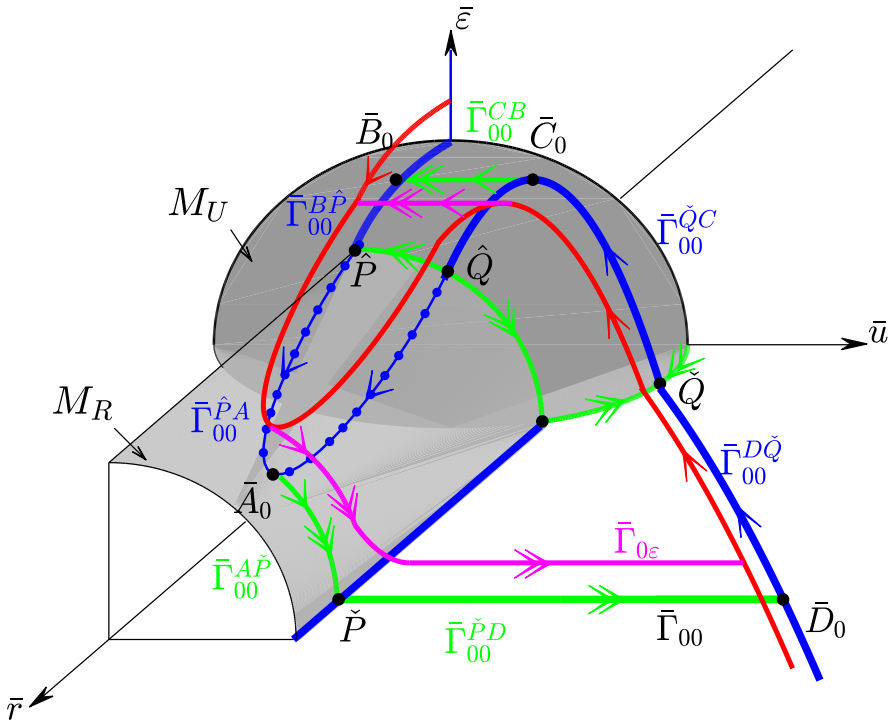

Figure 3.14: Geometry in blow-up space $\overline{M}_0$: the singular cycle $\bar{\Gamma}_{00}$ and the orbit $\bar{\Gamma}_{0\varepsilon}$.

3.5 Poincaré map and existence

To prove the persistence of the singular cycle $\bar{\Gamma}_{00}$ for κ and ε sufficiently small, we construct a Poincaré map in the neighborhood of $\bar{\Gamma}_{00}$ which is obtained through the concatenation of three transition maps Π_i, $i = 1, 3, 4$, between the specific sections for the flow in blow-up space $\overline{M}_\kappa$; see Figure 3.15.

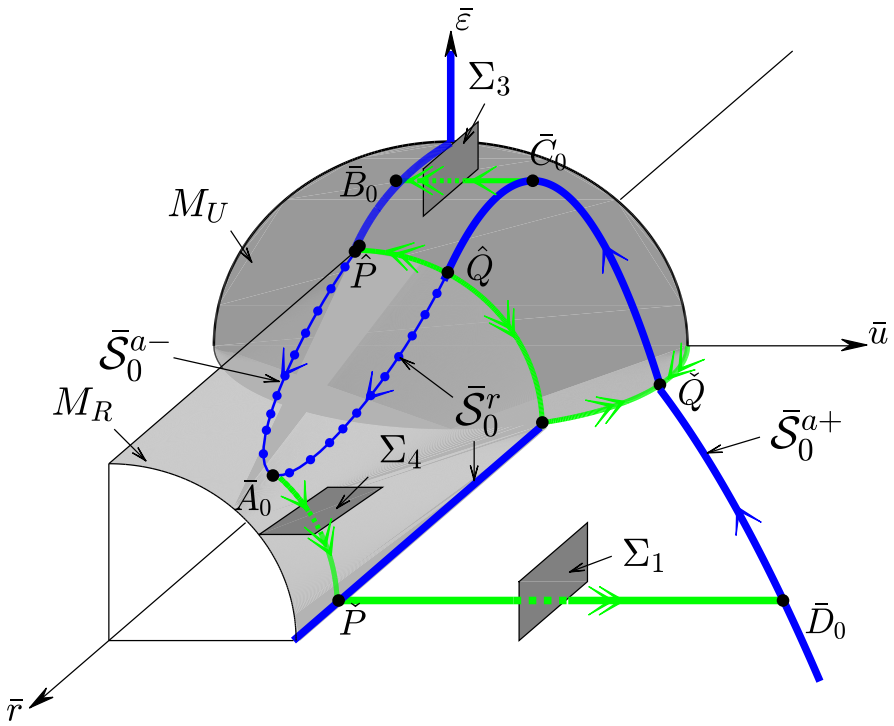

Figure 3.15: The sections of the Poincaré map

i. The transition map $\Pi_1 : \Sigma_1 \to \Sigma_3$ is initialised in a section Σ_1; the corresponding flow is attracted to the slow manifold $\bar{\mathcal{S}}_\kappa^{a+}$, which it follows up to the non-hyperbolic fold curve $\bar{\mathcal{F}}_0^C$, where it jumps along the heteroclinic connection $\bar{\Gamma}_{00}^{CB}$ to reach a section Σ_3.

ii. The transition map $\Pi_3 : \Sigma_3 \to \Sigma_4$ is initialised in a section Σ_3; the corresponding flow is attracted to the slow manifold $\bar{\mathcal{S}}_\kappa^{a-}$, which it follows up to the non-hyperbolic fold curve $\bar{\mathcal{F}}_0^A$, where it jumps along the heteroclinic connection $\bar{\Gamma}_{00}^{A\check{P}}$ to reach a section Σ_4.

iii. The transition map $\Pi_4 : \Sigma_4 \to \Sigma_1$ is initialised in a section Σ_4; it then follows the heteroclinic $\bar{\Gamma}_{00}^{A\check{P}}$, passing through the hyperbolic line $\bar{\mathcal{S}}_0^r$ and along the heteroclinic $\bar{\Gamma}_{00}^{\check{P}D}$ to reach a section Σ_1.

The Poincaré map $\Pi : \Sigma_1 \to \Sigma_1$, which is a global return map, is now defined as the composition $\Pi = \Pi_4 \circ \Pi_3 \circ \Pi_1$. Here, we note that the maps Π_i $(i = 1, 3, 4)$ are constructed in charts K_i, respectively; details can be found in the following subsections.

***Remark* 3.12.** The sections Σ_1, Σ_3, and Σ_4 are defined so that they are transversal to the heteroclinic orbits $\bar{\Gamma}_{00}^{\check{P}D}$, $\bar{\Gamma}_{00}^{CB}$, and $\bar{\Gamma}_{00}^{A\check{P}}$, respectively; see again Figure 3.15.

3.5.1 Transition map Π_1

The transition map Π_1 is constructed in chart K_1 as a mapping between the sections Σ_1 and Σ_3. To that end, we define these sections in chart K_1 as

$$\Sigma_1^{\text{in}} := \left\{ (\rho_1, \tfrac{\Theta}{4}, \varepsilon_1) \,\middle|\, \rho_1 - \tfrac{1}{2\sqrt{\Theta\tilde{b}}} \in [\rho_*, \rho^*], \varepsilon_1 \in [\varepsilon_*, \varepsilon^*] \right\} \quad \text{and} \tag{3.64a}$$

$$\Sigma_1^{\text{out}} := \left\{ (\rho_1, \tfrac{\Theta}{8}, \varepsilon_1) \,\middle|\, \rho_1 \in [\rho_*, \rho^*], \varepsilon_1 - \tfrac{\Theta}{4} \in [\varepsilon_*, \varepsilon^*] \right\}, \tag{3.64b}$$

respectively. (Here, ρ_*, ρ^*, ε_*, and ε^* are suitably chosen constants.)

Lemma 3.8. *For $(\kappa, \varepsilon) \in (0, \kappa_0] \times (0, \varepsilon_0]$ with κ_0 and ε_0 positive and sufficiently small, the transition map Π_1 is a contraction with contraction rate $\mathcal{O}(\mathrm{e}^{-\nu/\kappa})$, where ν is a positive constant. The restriction of Π_1 to the leaf $\{\varepsilon \equiv \text{constant}\}$ satisfies $\varepsilon_1 \approx 4\Theta\tilde{b}\varepsilon$ in Σ_1^{in} and $\rho_1 \approx \sqrt{\frac{4}{\Theta}\varepsilon}$ in Σ_1^{out}.*

Proof. The passage past a regular fold point is studied in detail in [42]; in particular, it follows from the analysis therein that orbits initiated in Σ_1^{in} are attracted by the extended slow manifold $\bar{\mathcal{S}}_\kappa^{a+}$ at a contraction rate of the order $\mathcal{O}(\mathrm{e}^{-\nu/\kappa})$, while the distance between the intersection of that extended manifold with Σ_1^{out} to the singular cycle $\bar{\Gamma}_{00}$ is of the order $\mathcal{O}(\kappa^{2/3})$. For ε fixed, we make use of the fact that $\varepsilon = \rho_1^2\varepsilon_1$ in chart K_1 to conclude that $\varepsilon_1 \approx 4\Theta\tilde{b}\varepsilon$ in Σ_1^{in} and $\rho_1 \approx \sqrt{\frac{4}{\Theta}\varepsilon}$ in Σ_1^{out}. □

***Remark* 3.13.** While our approximation of the transition map Π_1 is performed in chart K_1, the dynamics in that chart can also be recovered in Regime $\mathcal{R}_2$. Hence, the results of [42] on passage past a singularly perturbed planar fold can be applied to Equation (3.19). For a more detailed analysis in chart K_1, we refer to [65], where folds in $\mathbb{R}^3$ are studied.

3.5.2 Transition map Π_3

The transition map Π_3 is constructed in chart K_3 as a mapping between the sections Σ_3 and Σ_4. Then, the section Σ_3 is obtained by transformation of the section Σ_1^{out} defined in (3.64) from chart K_1 into chart K_3 via (3.43); the section Σ_4 is defined directly in chart K_3, which yields

$$\Sigma_3^{\text{in}} := \left\{ (r_3, \tfrac{2}{\Theta}, \delta_3) \,\middle|\, r_3 \in [r_*, r^*], \delta_3 - \tfrac{\Theta}{4} \in [\delta_*, \delta^*] \right\} \quad \text{and} \tag{3.65a}$$

$$\Sigma_3^{\text{out}} := \left\{ (r_3, \tfrac{1}{\Theta}, \delta_3) \,\middle|\, r_3 - \tfrac{1}{2\sqrt{\Theta\tilde{b}}} \in [r_*, r^*], \delta_3 \in [\delta_*, \delta^*] \right\}, \tag{3.65b}$$

respectively. (Here, r_*, r^*, δ_*, and δ^* are suitably chosen constants, as before.)

We have the following result, the proof of which is analogous to that of Lemma 3.8:

Lemma 3.9. *For $(\kappa, \varepsilon) \in (0, \kappa_0] \times (0, \varepsilon_0]$ with κ_0 and ε_0 positive and sufficiently small, the transition map Π_3 is a contraction with contraction rate $\mathcal{O}(\mathrm{e}^{-\nu/\kappa})$, where ν is a positive constant. The restriction of Π_3 to the leaf $\{\varepsilon \equiv \text{constant}\}$ satisfies $r_3 \approx \sqrt{\frac{4}{\Theta}\varepsilon}$ in Σ_3^{in} and $\delta_3 \approx 4\Theta\tilde{b}\varepsilon$ in Σ_3^{out}.*

***Remark* 3.14.** Again, the map Π_3 can alternatively be approximated in Regime $\mathcal{R}_1$, i.e., by reference to Equation (3.15), to which the results of [42] apply. A more detailed analysis in chart K_3 can be based on [65].

3.5.3 Transition map Π_4

The transition map Π_4 is constructed in chart K_4 as a mapping between the sections Σ_4 and Σ_1. Here, Σ_4 is obtained as the image of the section Σ_3^{out} from chart K_3 in chart K_4 via the

transformation $\mathcal{K}_{43}$ defined in (3.46), while the section Σ_1 is the image of the section Σ_1^{in} from chart K_1 in chart K_4 under the following transformation $\mathcal{K}_{41}$,

$$\mathcal{K}_{41}:\ (r_4,\delta_4,\varepsilon_4)\mapsto\big(\rho_1,u_1^{\frac{1}{2}},\varepsilon_1 u_1^{-\frac{1}{2}}\big). \tag{3.66}$$

Hence, the sections Σ_4 and Σ_1 in chart K_4 are represented as

$$\Sigma_4^{\text{in}}:=\Big\{(r_4,\delta_4,\sqrt{\Theta})\,\Big|\,r_4-\tfrac{1}{2\sqrt{\Theta\tilde{b}}}\in[r_*,r^*],\delta_4\in[\delta_*,\delta^*]\Big\}\quad\text{and} \tag{3.67a}$$

$$\Sigma_4^{\text{out}}:=\Big\{(r_4,\tfrac{\sqrt{\Theta}}{2},\varepsilon_4)\,\Big|\,r_4-\tfrac{1}{2\sqrt{\Theta\tilde{b}}}\in[r_*,r^*],\varepsilon_4\in[\varepsilon_*,\varepsilon^*]\Big\}, \tag{3.67b}$$

where the constants r_*, r^*, δ_*, δ^*, ε_*, and ε^* are defined as above.

Lemma 3.10. *For $(\kappa,\varepsilon)\in(0,\kappa_0]\times(0,\varepsilon_0]$ with κ_0 and ε_0 positive and sufficiently small, the transition map $\Pi_4:\ \Sigma_4\to\Sigma_1$ satisfies*

$$(r_4^{\text{in}},\delta_4^{\text{in}},\sqrt{\Theta})\mapsto\big(r_4^{\text{out}},\tfrac{\sqrt{\Theta}}{2},\varepsilon_4^{\text{out}}\big),$$

with $\delta_4\approx 4\sqrt{\Theta}\,\tilde{b}\varepsilon$ in Σ_4^{in} and $\varepsilon_4\approx 8\sqrt{\Theta}\,\tilde{b}\varepsilon$ in Σ_4^{out}. In particular, as the restriction of Π_4 to a leaf $\{\varepsilon\equiv\text{constant}\}$ satisfies

$$r_4^{\text{out}}=r_4^{\text{in}}+\mathcal{O}(\kappa\ln\varepsilon),$$

the map Π_4 is at mostly weakly expanding.

Proof. Recall the governing equations in chart K_4, as given in Equation (3.55); by dividing out the factor $\frac{1}{2}\Big\{\tilde{b}r_4^2\varepsilon_4^2(\delta_4+\varepsilon_4)^2+\Theta-\big[(\delta_4+\varepsilon_4)^2+\Lambda r_4^2\delta_4^2\big]\Big\}$, we obtain the new system

$$r_4'=\kappa r_4\tilde{F}_4(r_4,\delta_4,\varepsilon_4) \tag{3.68a}$$

$$\delta_4'=\delta_4-\kappa\delta_4\tilde{F}_4(r_4,\delta_4,\varepsilon_4), \tag{3.68b}$$

$$\varepsilon_4'=-\varepsilon_4-\kappa\varepsilon_3\tilde{F}_4(r_4,\delta_4,\varepsilon_4), \tag{3.68c}$$

where $\tilde{F}_4(r_4\delta_4,\varepsilon_4)$ is smooth and $\mathcal{O}(1)$. Since the corresponding linear system is given by

$$\begin{aligned}r_4'&=0,\\ \delta_4'&=\delta_4,\\ \varepsilon_4'&=-\varepsilon_4,\end{aligned}$$

we can approximate the transition for ε constant by noting that $\delta_4\approx 4\sqrt{\Theta}\,\tilde{b}\varepsilon$ in Σ_4^{in} and $\varepsilon_4\approx 8\sqrt{\Theta}\,\tilde{b}\varepsilon$ in Σ_4^{out} due to $\varepsilon=r_4^2\delta_4\varepsilon_4$ in chart K_4. Next, we approximate the transition time T_4 under Π_4, which is of the order $\mathcal{O}(-\ln\varepsilon)$. Finally, as r_4 is $\mathcal{O}(1)$, we can approximate r_4 by $r_4'=\kappa\mathcal{O}(1)$, from which the statement of the lemma follows. □

3.5.4 Proof of Theorem 3.1

To conclude the proof of Theorem 3.1, we combine the above asymptotics of the transition maps Π_i $(i=1,3,4)$ into the Poincaré map Π, which yields

Theorem 3.2. *For $(\kappa,\varepsilon)\in(0,\kappa_0]\times(0,\varepsilon_0]$ with κ_0 and ε_0 positive and sufficiently small, there exists a unique family of attracting periodic cycles $\bar{\Gamma}_{\kappa\varepsilon}$ in the blown-up vector field $\overline{M}_\kappa$. That family tends to $\bar{\Gamma}_{0\varepsilon}$ as $\kappa\to 0$ uniformly for $\varepsilon\in(0,\varepsilon_0]$, and converges to the singular cycle $\bar{\Gamma}_{00}$ as $(\kappa,\varepsilon)\to(0,0)$.*

Proof. The proof follows from a combination of Lemmas 3.8, 3.9, and 3.10. □

Theorem 3.1 is a direct consequence of Theorem 3.2 after blow-down.

3.6 Discussion

In the present article, we have performed a geometric analysis of a singularly perturbed two-variable model for a cyclic AMP (cAMP) signaling system. The model is obtained from a scaling of the three-variable Martiel-Goldbeter model [46] which is due to Lit̨canu and Velázquez [43]. The planar system resulting from a quasi-steady state assumption, Equation (3.5), represents a two-parameter singular perturbation problem; the presence of two parameters in the model manifests in a highly degenerate, and non-standard, singular limit which is resolved via a combination of geometric singular perturbation theory and the desinbgularisation technique known as blow-up. In particular,

- Our approach allows us to describe in detail the global geometry of the problem in the limit as both model parameters tend to zero;
- The underlying critical manifold which is desingularised in the process consists of one non-hyperbolic line in the "inner" region and one normally hyperbolic curve in the "outer" region which meet at a degenerate equilibrium at the origin.
- Our resolution allows us to construct a family of periodic (relaxation-type) cycles for Equation (3.4), thus shedding light on a novel singular perturbation problem and improving our understanding of the corresponding oscillatory dynamics.

In future, we intend to extend our analysis to the three-variable reaction-diffusion system (3.4) [43], which incorporates an extracellular cAMP diffusion term, as introduced in [69]. Correspondingly, R, W, and U are functions of both space $\tilde{x}$ and time τ, with $x = \sqrt{\frac{D}{k_i+k_t}}\tilde{x}$; cf. again Table 3.1.The main result of [43] is a proof for the existence of traveling pulse solutions to (3.4) in one spatial dimension on the basis of singular perturbation theory, under the assumption that the parameters κ and ε are small; moreover, asymptotic formulae are derived for these pulse solutions in a number of relevant scaling regimes. We expect that a geometric construction of these solutions can be based on the framework established here, in the context of our simplified two-variable Equation (3.5). However, in preliminary work, we have not managed to find a scaling for regime $\mathcal{R}_1$ that allows us to establish an overlap with $\mathcal{R}_3$; recall our discussion in Section 3.4. That failing may, in fact, suggest that Equation (3.5) is ill-posed in some sense, and is reflected in the fact that a key non-linear eigenvalue problem in Section 4.1.2 of [43] has to be solved numerically to allow for the calculation of the unique velocity of travelling pulses. Hence, we believe that further investigation is warranted.

Bibliography

[1] Kolmogorov A., Petrovskii I., and Piskunov N. A study of the diffusion equation that is related to the growth of a quality of matter and its application to a biological problem. *Moscow University Mathematics Bulletin*, 1(1-26), 1937.

[2] María Jesús Álvarez, Antoni Ferragut, and Xavier Jarque. A survey on the blow up technique. *International Journal of Bifurcation and Chaos*, 21(11):3103–3118, nov 2011.

[3] D. G. Aronson and H. F. Weinberger. Nonlinear diffusion in population genetics, combustion, and nerve pulse propagation. In *Lecture Notes in Mathematics*, pages 5–49. Springer Berlin Heidelberg, 1975.

[4] D.G Aronson and H.F Weinberger. Multidimensional nonlinear diffusion arising in population genetics. *Advances in Mathematics*, 30(1):33–76, oct 1978.

[5] R. D. Benguria and M. C. Depassier. Speed of pulled fronts with a cutoff. *Physical Review E*, 75(5), may 2007.

[6] Egbert Brieskorn and Horst Knrrer. *Plane Algebraic Curves*. Number 370-383. Springer Basel, 2012.

[7] N. F. Britton. *Reaction-Diffusion Equations and Their Applications to Biology*. Academic Press, 1986.

[8] Marco Brunella and Massimo Miari. Topological equivalence of a plane vector field with its principal part defined through newton polyhedra. *Journal of Differential Equations*, 85(2):338–366, jun 1990.

[9] Eric Brunet and Bernard Derrida. Shift in the velocity of a front due to a cutoff. *Physical Review E*, 56(3):2597–2604, sep 1997.

[10] Alexander D. Bruno. *Local Methods in Nonlinear Differential Equations: Part I The Local Method of Nonlinear Analysis of Differential Equations Part II The Sets of ... (Springer Series in Soviet Mathematics)*. Springer, 2011.

[11] Jack Carr. *Applications of Centre Manifold Theory*. Springer US, 1981.

[12] Earl A. Coddington and Norman Levinson. *Theory of Ordinary Differential Equations*. Krieger Pub Co, 1984.

[13] Freddy Dumortier. Singularities of vector fields on the plane. *Journal of Differential Equations*, 23(1):53–106, jan 1977.

[14] Freddy Dumortier. Techniques in the theory of local bifurcations: Blow-up, normal forms, nilpotent bifurcations, singular perturbations. In *Bifurcations and Periodic Orbits of Vector Fields*, pages 19–73. Springer Netherlands, 1993.

[15] Freddy Dumortier, Nikola Popović, and Tasso J Kaper. The critical wave speed for the fisher–kolmogorov–petrowskii–piscounov equation with cut-off. *Nonlinearity*, 20(4):855–877, mar 2007.

[16] Freddy Dumortier, Nikola Popović, and Tasso J. Kaper. A geometric approach to bistable front propagation in scalar reaction–diffusion equations with cut-off. *Physica D: Nonlinear Phenomena*, 239(20-22):1984–1999, oct 2010.

[17] Freddy Dumortier and Robert Roussarie. Canard cycles and center manifolds. *Memoirs of the American Mathematical Society*, 121(577):0–0, 1996.

[18] Freddy Dumortier, Robert Roussarie, and Jorge Sotomayor. Bifurcations of cuspidal loops. *Nonlinearity*, 10(6):1369–1408, nov 1997.

[19] Neil Fenichel. Geometric singular perturbation theory for ordinary differential equations. *Journal of Differential Equations*, 31(1):53–98, jan 1979.

[20] John A. Feroe. Existence and stability of multiple impulse solutions of a nerve equation. *SIAM Journal on Applied Mathematics*, 42(2):235–246, apr 1982.

[21] P. C. Fife. *Mathematical Aspects of Reacting and Diffusing Systems (Lecture Notes in Biomathematics)*. Springer, 1979.

[22] R. A. Fisher. The wave of advance of advantagous genes. *Annals of Eugenics*, 7(4):355–369, jun 1937.

[23] G. Gerisch and B. Hess. Cyclic-AMP-controlled oscillations in suspended dictyostelium cells: Their relation to morphogenetic cell interactions. *Proceedings of the National Academy of Sciences*, 71(5):2118–2122, may 1974.

[24] G. Gerisch and U. Wick. Intracellular oscillations and release of cyclic AMP from dictyostelium cells. *Biochemical and Biophysical Research Communications*, 65(1):364–370, jul 1975.

[25] Günther Gerisch and Dieter Malchow. Cyclic amp receptors and the control of cell aggregation in dictyostelium. *Advances in cyclic nucleotide research*, 7:49–68, 1976.

[26] Günther Gerisch, Dieter Malchow, Werner Roos, and U Wick. Oscillations of cyclic nucleotide concentrations in relation to the excitability of dictyostelium cells. *The Journal of experimental biology*, 81:33–47, 1979.

[27] A. Goldbeter and L. A. Segel. Unified mechanism for relay and oscillation of cyclic AMP in dictyostelium discoideum. *Proceedings of the National Academy of Sciences*, 74(4):1543–1547, apr 1977.

[28] A. Goldbeter and L.A. Segel. Control of developmental transitions in the cyclic AMP signalling system of dictyostelium discoideum. *Differentiation*, 17(1-3):127–135, dec 1980.

[29] Johan Grasman. *Asymptotic Methods for Relaxation Oscillations and Applications*. Springer New York, 1987.

[30] Peter Grinrod. *The Theory and Applications of Reaction Diffusion Equations : Patterns and Waves*. Clarendon Press, 1996.

[31] John Guckenheimer and Philip Holmes. *Nonlinear Oscillations, Dynamical Systems, and Bifurcations of Vector Fields (Applied Mathematical Sciences)*. Springer, 2002.

[32] Geertje Hek. Geometric singular perturbation theory in biological practice. *Journal of Mathematical Biology*, 60(3):347–386, apr 2009.

[33] Daniel Henry. *Geometric Theory of Semilinear Parabolic Equations*. Springer Berlin Heidelberg, 1981.

[34] Morris W. Hirsch and Stephen Smale. *Differential Equations, Dynamical Systems, and Linear Algebra (Pure and Applied Mathematics)*. Academic Press, 1974.

[35] Christopher K. R. T. Jones. *Dynamical Systems: Lectures Given at the 2nd Session of the Centro Internazionale Matematico Estivo (C.I.M.E.) held in Montecatini Terme, Italy, June 13–22, 1994*, chapter Geometric singular perturbation theory, pages 44–118. Springer Berlin Heidelberg, Berlin, Heidelberg, 1995.

[36] Tasso J. Kaper. An introduction to geometric methods and dynamical systems theory for singular perturbation problems, 1999.

[37] Raymond Kapral and Kenneth Showalter, editors. *Chemical Waves and Patterns*. Springer Netherlands, 1995.

[38] J. P. Keener. Waves in excitable media. *SIAM J. Appl. Math.*, 39(3):528–548, dec 1980.

[39] Evelyn F. Keller and Garrett M. Odell. Necessary and sufficient conditions for chemotactic bands. *Mathematical Biosciences*, 27(3-4):309–317, jan 1975.

[40] Evelyn F. Keller and Lee A. Segel. Traveling bands of chemotactic bacteria: A theoretical analysis. *Journal of Theoretical Biology*, 30(2):235–248, feb 1971.

[41] Ilona Kosiuk and Peter Szmolyan. Scaling in singular perturbation problems: Blowing up a relaxation oscillator. *SIAM Journal on Applied Dynamical Systems*, 10(4):1307–1343, jan 2011.

[42] M. Krupa and P. Szmolyan. Extending geometric singular perturbation theory to nonhyperbolic points—fold and canard points in two dimensions. *SIAM Journal on Mathematical Analysis*, 33(2):286–314, jan 2001.

[43] Gabriela Lit̨canu and Juan J. L. Velázquez. Singular perturbation analysis of cAMP signalling in dictyostelium discoideum aggregates. *Journal of Mathematical Biology*, 52(5):682–718, mar 2006.

[44] Robert Luther. Propagation of chemical reactions in space. *Journal of Chemical Education*, 64(9):740, sep 1987. English translation by Arnold,R. and Showalter, K. and Tyson, J.J.

[45] J. E. Marsden and M. McCracken. *The Hopf Bifurcation and Its Applications (Applied Mathematical Sciences)*. Springer, 1976.

[46] J L Martiel and A. Goldbeter. A model based on receptor desensitization for cyclic AMP signaling in dictyostelium cells. *Biophysical Journal*, 52(5):807–828, nov 1987.

[47] H.P McKean. Nagumo's equation. *Advances in Mathematics*, 4(3):209–223, jun 1970.

[48] E. F. Mishchenko and N. Kh. Rozov. *Differential Equations with Small Parameters and Relaxation Oscillations*. Springer US, 1980.

[49] James D. Murray. *Mathematical Biology: I. An Introduction (Interdisciplinary Applied Mathematics) (Pt. 1)*. Springer, 2007.

[50] James D. Murray. *Mathematical Biology II: Spatial Models and Biomedical Applications (Interdisciplinary Applied Mathematics) (v. 2)*. Springer, 2011.

[51] P.C. Newell. Attraction and adhesion in the slime mold dictyostelium. *In Fungal Differentiation: A Contemporary Synthesis (ed. J.E. Smith)*, pages pp. 43–71., 1983. Marcel Dekker, New York.

[52] Henri Poincaré. *Les méthodes nouvelles de la mécanique céleste, Volume 3*. Gauthier-Villars, Paris, 1899.

[53] L. S. Pontryagin. Asymptotic behavior of solutions of systems of differential equations with a small parameter in the derivatives of highest order. *(Russian) Izv. Akad. Nauk SSSR. Ser. Mat.*, 21:605626, 1957.

[54] Nikola Popović. A geometric analysis of front propagation in a family of degenerate reaction-diffusion equations with cutoff. *Zeitschrift fr angewandte Mathematik und Physik*, 62(3):405–437, feb 2011.

[55] Nikola Popović. A geometric analysis of front propagation in an integrable nagumo equation with a linear cut-off. *Physica D: Nonlinear Phenomena*, 241(22):1976–1984, nov 2012.

[56] John Rinzel and Joseph B. Keller. Traveling wave solutions of a nerve conduction equation. *Biophysical Journal*, 13(12):1313–1337, dec 1973.

[57] John Rinzel and David Terman. Propagation phenomena in a bistable reaction-diffusion system. *SIAM J. Appl. Math.*, 42(5):1111–1137, oct 1982.

[58] W. Roos and G. Gerisch. Receptor-mediated adenylate cyclase activation in Dictyostelium discoideum. *FEBS(Fed. Eur. Biochem. Soc.) Letters*, 68(2):170–172, oct 1976.

[59] W. Roos, V. Nanjundiah, D. Malchow, and G. Gerisch. Amplification of cyclic-AMP signals in aggregating cells ofDictyostelium discoideum. *FEBS Letters*, 53(2):139–142, may 1975.

[60] W. Roos, C. Scheidegger, and G. Gerisch. Adenylate cyclase activity oscillations as signals for cell aggregation in dictyostelium discoideum. *Nature*, 266(5599):259–261, mar 1977.

[61] Lee Segel and Albert Goldbeter. Scaling in biochemical kinetics: dissection of a relaxation oscillator. *Journal of Mathematical Biology*, 32(2):147–160, jan 1994.

[62] A. Seidenberg. Reduction of singularities of the differential equation ady = bdx. *American Journal of Mathematics*, 90(1):248, jan 1968.

[63] B. M. Shaffer. Secretion of cyclic AMP induced by cyclic AMP in the cellular slime mould dictyostelium discoideum. *Nature*, 255(5509):549–552, jun 1975.

[64] Kenneth Showalter and John J. Tyson. Luther's 1906 discovery and analysis of chemical waves. *Journal of Chemical Education*, 64(9):742, sep 1987.

[65] P. Szmolyan and M. Wechselberger. Relaxation oscillations in r3. *Journal of Differential Equations*, 200(1):69–104, jun 2004.

[66] A. Theibert. Cyclic 3', 5'-AMP relay in dictyostelium discoideum: adaptation is independent of activation of adenylate cyclase. *The Journal of Cell Biology*, 97(1):173–177, jul 1983.

[67] Arnaud Tonnelier and Wulfram Gerstner. Piecewise linear differential equations and integrate-and-fire neurons: Insights from two-dimensional membrane models. *Physical Review E*, 67(2), feb 2003.

[68] A. M. Turing. The chemical basis of morphogenesis. *Philosophical Transactions of the Royal Society B: Biological Sciences*, 237(641):37–72, aug 1952.

[69] John J. Tyson, Kevin A. Alexander, V.S. Manoranjan, and J.D. Murray. Spiral waves of cyclic amp in a model of slime mold aggregation. *Physica D: Nonlinear Phenomena*, 34(1-2):193–207, jan 1989.

[70] John J. Tyson and Paul C. Fife. Target patterns in a realistic model of the belousov–zhabotinskii reaction. *The Journal of Chemical Physics*, 73(5):2224–2237, sep 1980.

[71] John J. Tyson and James P. Keener. Singular perturbation theory of traveling waves in excitable media (a review). *Physica D: Nonlinear Phenomena*, 32(3):327–361, dec 1988.

[72] S. Wiggins. *Introduction to Applied Nonlinear Dynamical Systems and Chaos (Texts in Applied Mathematics, Vol 2)*. Springer-Verlag, 1996.

[73] A. N. Zaikin and A. M. Zhabotinsky. Concentration wave propagation in two-dimensional liquid-phase self-oscillating system. *Nature*, 225(5232):535–537, feb 1970.

[74] E. P. Zemskov, K. Kassner, M. A. Tsyganov, and I. R. Epstein. Speed of traveling fronts in a sigmoidal reaction-diffusion system. *Chaos*, 21(1):013115, 2011.

[75] E. P. Zemskov and V. Méndez. Propagation of fronts in activator-inhibitor systems with a cutoff. *The European Physical Journal B*, 48(1):81–86, nov 2005.

Appendix A

Cut-off front propagation

A.1 Dynamics of the v-component cut-off system

Recall the Equation (2.14) of the v-component cut-off system:

$$u' = w, \tag{A.1a}$$
$$v' = z, \tag{A.1b}$$
$$w' = -cw - f(u,v)\theta(v-\varepsilon), \tag{A.1c}$$
$$z' = -\frac{c}{D}z - \frac{1}{D}g(u,v)\theta(v-\varepsilon). \tag{A.1d}$$

The steady states $Q^+ = (0,0,0,0)$ and $Q^- = (1-\frac{\alpha}{\eta}, \frac{\alpha}{\eta}, 0, 0)$ of Equation (A.1) in the absence of cut-off are hyperbolic saddle points. Both have eigenvalues $\lambda_i\,(i = 1, ..., 4)$, with $\lambda_1 = \frac{1}{2}(-c + \sqrt{c^2+4})\,(+)$, $\lambda_2 = \frac{1}{2}(-c - \sqrt{c^2+4})\,(-)$, $\lambda_3 = \frac{1}{2D}(-c + \sqrt{c^2+4D\eta})\,(+)$ and $\lambda_4 = \frac{1}{2D}(-c - \sqrt{c^2+4D\eta})\,(-)$, here the eigenvalues λ_1 and λ_3 are positive, while λ_2 and λ_4 are negative. The corresponding eigenvectors $\mathbf{v}_1 = \big(1, 0, \lambda_1, 0\big)^T$, $\mathbf{v}_2 = \big(1, 0, \lambda_2, 0\big)^T$, $\mathbf{v}_3 = \big(1, \mu_3, \lambda_3, \mu_3\lambda_3\big)^T$ and $\mathbf{v}_4 = \big(1, \mu_4, \lambda_4, \mu_4\lambda_4\big)^T$, respectively, where $\mu_j = \lambda_j^2 + c\lambda_j - 1$, $(j = 3, 4)$.

A.1.1 General patching

We consider the travelling front solutions propagating from Q^- when $\xi \to -\infty$ to Q^+ when $\xi \to +\infty$. The general solutions for this problem in the regions can be written as follows:
In region I: $u \geqslant a$ and $v \geqslant \varepsilon$, for $\xi \leqslant \xi_0$

$$u_{g_1}(\xi) = A_2 e^{\lambda_1\xi} + \frac{A_1}{\mu_3}e^{\lambda_3\xi} + 1 - \alpha/\eta, \tag{A.2a}$$
$$v_{g_1}(\xi) = A_1 e^{\lambda_3\xi} + \alpha/\eta, \tag{A.2b}$$
$$w_{g_1}(\xi) = \lambda_1 A_2 e^{\lambda_1\xi} + \frac{\lambda_3}{\mu_3}A_1 e^{\lambda_3\xi}, \tag{A.2c}$$
$$z_{g_1}(\xi) = \lambda_3 A_1 e^{\lambda_3\xi}. \tag{A.2d}$$

In region II: $u \leqslant a$ and $v \geqslant \varepsilon$, for $\xi_0 \leqslant \xi \leqslant \xi^*$

$$u_{g_2}(\xi) = A_{21}e^{\lambda_1\xi} + A_{22}e^{\lambda_2\xi} + \frac{B_{23}}{\mu_3}e^{\lambda_3\xi} + \frac{B_{24}}{\mu_4}e^{\lambda_4\xi}, \tag{A.3a}$$
$$v_{g_2}(\xi) = B_{23}e^{\lambda_3\xi} + B_{24}e^{\lambda_4\xi}, \tag{A.3b}$$
$$w_{g_2}(\xi) = \lambda_1 A_{21}e^{\lambda_1\xi} + \lambda_2 A_{22}e^{\lambda_2\xi} + \frac{\lambda_3}{\mu_3}B_{23}e^{\lambda_3\xi} + \frac{\lambda_4}{\mu_4}B_{24}e^{\lambda_4\xi}, \tag{A.3c}$$
$$z_{g_2}(\xi) = \lambda_3 B_{23}e^{\lambda_3\xi} + \lambda_4 B_{24}e^{\lambda_4\xi}. \tag{A.3d}$$

In region III: $u \leqslant a$ and $v \leqslant \varepsilon$, for $\xi \geqslant \xi^*$

$$u_{g_3}(\xi) = A_0 e^{-c\xi}, \tag{A.4a}$$
$$v_{g_3}(\xi) = B_0 e^{-\frac{c}{D}\xi}, \tag{A.4b}$$
$$w_{g_3}(\xi) = -cA_0 e^{-c\xi}, \tag{A.4c}$$
$$z_{g_3}(\xi) = -\frac{c}{D} B_0 e^{-\frac{c}{D}\xi}, \tag{A.4d}$$

where $\lambda_{1,2} = \frac{-c \pm \sqrt{c^2+4}}{2}, \lambda_{3,4} = \frac{-c \pm \sqrt{c^2+4D\eta}}{2D}$, and $\mu_j = \lambda_j^2 + c\lambda_j - 1 \, (j = 3, 4)$.

Then we can solve for all coefficients A_{ij}, B_{ij} by patching the three regions together, using the conditions for continuity of functions. We obtain the front solutions explicitly, by choosing $\xi_0 = 0$ for the sake of simplicity.

We have all the coefficients written as

$$B_{24} = \frac{\alpha/\eta}{1 - \frac{\lambda_4}{\lambda_3}}, \tag{A.5a}$$
$$B_{23} = -\frac{\lambda_3}{\lambda_4} e^{(\lambda_4 - \lambda_3)\xi^*} \frac{\alpha/\eta}{1 - \frac{\lambda_4}{\lambda_3}}, \tag{A.5b}$$
$$A_1 = -\alpha/\eta - \frac{\lambda_3}{\lambda_4} e^{(\lambda_4 - \lambda_3)\xi^*} \frac{\alpha/\eta}{1 - \frac{\lambda_4}{\lambda_3}} + \frac{\alpha/\eta}{1 - \frac{\lambda_4}{\lambda_3}}, \tag{A.5c}$$
$$B_0 = -\frac{\alpha}{\eta} \frac{\lambda_3}{\lambda_4} e^{-\lambda_3 \xi^*}, \tag{A.5d}$$
$$A_{22} = \frac{\lambda_1}{\lambda_1 - \lambda_2}(1 - \frac{\alpha}{\eta}) + \frac{\alpha/\eta}{(\lambda_1 - \lambda_2)(\lambda_3 - \lambda_4)} \Big[\frac{\lambda_4(\lambda_1 - \lambda_3)}{\mu_3} - \frac{\lambda_3(\lambda_1 - \lambda_4)}{\mu_4} \Big], \tag{A.5e}$$
$$A_{21} = -\frac{\lambda_1}{\lambda_2} A_{22} e^{(\lambda_2 - \lambda_1)\xi^*} + \frac{1}{\lambda_2 \lambda_4} \big(\frac{1}{\mu_4} - \frac{1}{\mu_3} \big) \frac{\alpha/\eta}{1 - \frac{\lambda_4}{\lambda_3}} e^{(\lambda_4 - \lambda_1)\xi^*}, \tag{A.5f}$$
$$A_2 = -1 + \frac{\alpha}{\eta} \Big[1 + \frac{1}{\mu_3} + \big(\frac{1}{\mu_4} - \frac{1}{\mu_3} \big) \frac{1}{1 - \frac{\lambda_4}{\lambda_3}} \Big] + A_{21} + A_{22}, \tag{A.5g}$$
$$A_0 = e^{c\xi^*} \Big[A_{21} e^{\lambda_1 \xi^*} + A_{22} e^{\lambda_2 \xi^*} + \big(-\frac{\lambda_3}{\lambda_4 \mu_3} + \frac{1}{\mu_4} \big) \frac{\alpha/\eta}{1 - \frac{\lambda_4}{\lambda_3}} e^{\lambda_4 \xi^*} \Big]. \tag{A.5h}$$

And two constraints $u_{g_2}(\xi_0) = a$, $v_{g_2}(\xi^*) = \varepsilon$, which are obtained at the patching points, are expressed as equations $G_i(a, \xi^*, c, \varepsilon) = 0 \, (i = 1, 2)$:

$$G_1(a, \xi^*, c, \varepsilon) := A_{21} + A_{22} - \frac{1}{\mu_3} \frac{\lambda_3}{\lambda_4} \mathrm{e}^{(\lambda_4 - \lambda_3)\xi^*} \frac{\alpha/\eta}{1 - \frac{\lambda_4}{\lambda_3}} + \frac{1}{\mu_4} \frac{\alpha/\eta}{1 - \frac{\lambda_4}{\lambda_3}} - a, \tag{A.6a}$$
$$G_2(a, \xi^*, c, \varepsilon) := \frac{\alpha}{\eta} \frac{\lambda_3}{\lambda_4} e^{\lambda_4 \xi^*} + \varepsilon. \tag{A.6b}$$

here, the c-a relation is labeled by $a(c, \varepsilon)$.

Existence and uniqueness

In the singular limit defined as $\varepsilon = 0$ and $\xi^* \to \infty$ in Equation(A.6), we can obtain an explicit expression of singular limit $a(c_0, 0)$,

$$a(c_0, 0) = (1 - \frac{\alpha}{\eta}) \frac{\lambda_1}{\lambda_1 - \lambda_2} - \frac{\alpha}{\eta} \frac{1}{(\lambda_1 - \lambda_2)(\lambda_3 - \lambda_4)} \Big[\frac{\lambda_3}{\mu_4}(\lambda_2 - \lambda_4) - \frac{\lambda_4}{\mu_3}(\lambda_1 - \lambda_3) \Big] \tag{A.7}$$

which is also the result of the general patching method for the singular system, for details see Appendix A.2 or [74]. In particular, the denominators $(\lambda_1 - \lambda_2)$, $(\lambda_3 - \lambda_3)$, μ_3 and μ_4 are well-defined; the existence of $a_0(c_0)$ has been proved in Section 2.4 as well.

For ε small, we know that we have an unique solution of the speed c-a relation by solving a, ξ^* in (A.6a)-(A.6b). To that end, we prove that there exists a unique solution from the two

constraints $G_i(c_0, 0) = 0\,(i = 1, 2)$ by applying the Implicit Function Theorem. We consider the Jacobian matrix with respect to a and ξ^* at $(c, \varepsilon) = (c, \varepsilon)$,

$$J = \begin{bmatrix} \frac{\partial G_1}{\partial a} & \frac{\partial G_1}{\partial \xi^*} \\ \frac{\partial G_2}{\partial a} & \frac{\partial G_2}{\partial \xi^*} \end{bmatrix} = \begin{bmatrix} -1 & \frac{\partial G_1}{\partial \xi^*} \\ 0 & \frac{\alpha}{\eta}\lambda_3 \mathrm{e}^{\lambda_4 \xi^*} \end{bmatrix}, \text{ and } Det(J)\big|_{(c,\varepsilon)} = -\frac{\alpha}{\eta}\lambda_3 \mathrm{e}^{\lambda_4 \xi^*}$$

It is clear that $Det(J)$ is nonzero as λ_3 is nonzero and ξ^* is bounded for ε positive and small. Then, we can say that there exists a unique solution a and ξ^* such that equations $G_i|_{(c,\varepsilon)} = 0\,(i = 1, 2)$ in (A.6), which is equivalent to the existence of $a(c, \varepsilon)$, i.e., to the persistence of $a(c, \varepsilon)$ for ε positive and small by the Implicit Function Theorem.

Numerical simulation

For the bifurcation result, we solve the two constraints (A.6) numerically and obtain the relation between speed c and discontinuity position a for the cut-off sigmoidal system, plotted with $D = 1, 2, 5, 10$ with $\varepsilon = 0.1, 0.05, 0.01, 0.001$, see Figure A.1.

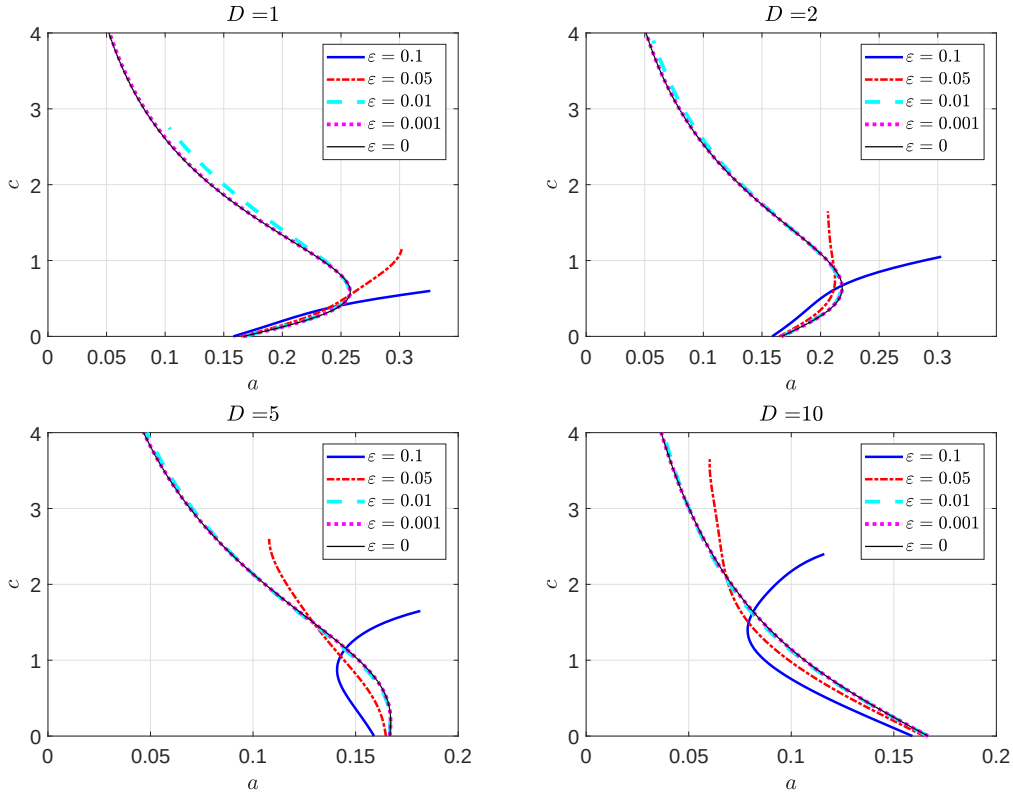

Figure A.1: Speed relation obtained by general patching $a(c, \varepsilon)$, for $D = 1, 2, 5, 10$, with $\varepsilon = 0.1, 0.05, 0.01, 0.001$ and $\varepsilon = 0$, for fixed $\eta = 0.12$, $\alpha = 0.08$.

A.1.2 Second-order normal form of the v-component cut-off system

Recalling Proposition 2.3 in Section 2.4.4, we invert the transformation as follows

$$\tilde{u} = U - \frac{D\big[(\lambda_4+1)(2\eta^2 - Dc\eta\lambda_4) - \beta\big]}{\beta\mu_4\left(D{\lambda_4}^2+\eta\right)}Z^2 - \frac{D}{D\lambda_4^2+\eta}WZ + \mathcal{O}(3), \tag{A.8a}$$

$$\tilde{w} = W + \frac{D\lambda_4\big[\beta - (\lambda_4+1)(2\eta^2 + D\eta\lambda_4^2 - D\eta)\big]}{\beta\mu_4\left(D{\lambda_4}^2+\eta\right)}Z^2 - \frac{D}{D\lambda_4^2+\eta}UZ + \frac{cD}{D\lambda_4^2+\eta}WZ + \mathcal{O}(3), \tag{A.8b}$$

$$\tilde{z} = Z - \frac{\eta}{D\lambda_4^2+\eta}Z^2 + \mathcal{O}(3). \tag{A.8c}$$

We have the transformed boundary values

$$\tilde{P}^{\text{in}}_{\varepsilon 1} := \Big(\tilde{u}^{\text{in}}, r_1^{\text{in}}, \tilde{w}^{\text{in}}, \tilde{z}^{\text{in}}, \frac{\varepsilon}{A_1+\frac{\alpha}{\eta}}\Big) \quad \text{at } \tau = 0, \tag{A.9a}$$

$$\tilde{P}^{\text{out}}_{\varepsilon 1} := \Big(\tilde{u}^{\text{out}}, \varepsilon, \tilde{w}^{\text{out}}, \tilde{z}^{\text{out}}, 1\Big) \quad \text{at } \tau^* = \ln\frac{A_1+\frac{\alpha}{\eta}}{\varepsilon}, \tag{A.9b}$$

where $(\tilde{u}^{\text{in}}, \tilde{w}^{\text{in}}, \tilde{z}^{\text{in}})$ has the form

$$\begin{aligned}
\tilde{u}^{\text{in}} =& \Big(\frac{A_2+\frac{A_1}{\mu_3}+1-\frac{\alpha}{\eta}}{A_1+\frac{\alpha}{\eta}} - \frac{1}{\mu_4}\Big) - \frac{D\big[(\lambda_4+1)(2\eta^2 - Dc\eta\lambda_4) - \beta\big]}{\beta\mu_4\left(D{\lambda_4}^2+\eta\right)}\Big(\frac{\lambda_3 A_1}{A_1+\frac{\alpha}{\eta}} - \lambda_4\Big)^2 \\
& - \frac{D}{D\lambda_4^2+\eta}\Big(\frac{\lambda_1 A_2 + \frac{\lambda_3}{\mu_3}A_1}{A_1+\frac{\alpha}{\eta}} - \frac{\lambda_4}{\mu_4}\Big)\Big(\frac{\lambda_3 A_1}{A_1+\frac{\alpha}{\eta}} - \lambda_4\Big), \\
\tilde{w}^{\text{in}} =& \Big(\frac{\lambda_1 A_2 + \frac{\lambda_3}{\mu_3}A_1}{A_1+\frac{\alpha}{\eta}} - \frac{\lambda_4}{\mu_4}\Big) + \frac{D\lambda_4\big[\beta - (\lambda_4+1)(2\eta^2 + D\eta\lambda_4^2 - D\eta)\big]}{\beta\mu_4\left(D{\lambda_4}^2+\eta\right)}\Big(\frac{\lambda_3 A_1}{A_1+\frac{\alpha}{\eta}} - \lambda_4\Big)^2 \\
& + \frac{D}{D\lambda_4^2+\eta}\Bigg[- \Big(\frac{A_2+\frac{A_1}{\mu_3}+1-\frac{\alpha}{\eta}}{A_1+\frac{\alpha}{\eta}} - \frac{1}{\mu_4}\Big) + c\Big(\frac{\lambda_1 A_2 + \frac{\lambda_3}{\mu_3}A_1}{A_1+\frac{\alpha}{\eta}} - \frac{\lambda_4}{\mu_4}\Big)\Bigg]\Big(\frac{\lambda_3 A_1}{A_1+\frac{\alpha}{\eta}} - \lambda_4\Big), \\
\tilde{z}^{\text{in}} =& \Big(\frac{\lambda_3 A_1}{A_1+\frac{\alpha}{\eta}} - \lambda_4\Big) - \frac{\eta}{D\lambda_4^2+\eta}\Big(\frac{\lambda_3 A_1}{A_1+\frac{\alpha}{\eta}} - \lambda_4\Big)^2,
\end{aligned}$$

and $(\tilde{u}^{\text{out}}, \tilde{w}^{\text{out}}, \tilde{z}^{\text{out}})$ has the form

$$\begin{aligned}
\tilde{u}^{\text{out}} =& A_3 - \frac{1}{\mu_4} - \frac{D\big[(\lambda_4+1)(2\eta^2 - Dc\eta\lambda_4) - \beta\big]}{\beta\mu_4\left(D{\lambda_4}^2+\eta\right)}\Big(-\frac{c}{D} - \lambda_4\Big)^2 - \frac{D}{D\lambda_4^2+\eta}\Big(-cA_3 - \frac{\lambda_4}{\mu_4}\Big)\Big(-\frac{c}{D} - \lambda_4\Big), \\
\tilde{w}^{\text{out}} =& \Big(-cA_3 - \frac{\lambda_4}{\mu_4}\Big) + \frac{D\lambda_4\big[\beta - (\lambda_4+1)(2\eta^2 + D\eta\lambda_4^2 - D\eta)\big]}{\beta\mu_4\left(D{\lambda_4}^2+\eta\right)}\Big(-\frac{c}{D} - \lambda_4\Big)^2 \\
& + \frac{D}{D\lambda_4^2+\eta}\Bigg[- \Big(A_3 - \frac{1}{\mu_4}\Big) + c\Big(-cA_3 - \frac{\lambda_4}{\mu_4}\Big)\Bigg]\Big(-\frac{c}{D} - \lambda_4\Big), \\
\tilde{z}^{\text{out}} =& \Big(-\frac{c}{D} - \lambda_4\Big) - \frac{\eta}{D\lambda_4^2+\eta}\Big(-\frac{c}{D} - \lambda_4\Big)^2,
\end{aligned}$$

We can determine the related coefficients A_i, C_i $(i = 1, 2, 3)$ by patching the general solutions for $(\tilde{u}, \tilde{w}, \tilde{z})$ between the two sections $\widetilde{\Sigma}_1^{\text{in}}$ and $\widetilde{\Sigma}_1^{\text{out}}$ at the points of intersection $\tilde{P}^{\text{in}}_{\varepsilon 1}$ and $\tilde{P}^{\text{out}}_{\varepsilon 1}$, i.e., we solve the particular solution with specific boundary condition (A.9) in $(\tilde{u}, \tilde{w}, \tilde{z})$, which completes the construction of the orbit $\widetilde{\Gamma}_1$ in chart K_1; here, $\widetilde{\Gamma}_1$ denotes the approximation to the general solution of (A.8) by the second-order normal form transformation. We have the

patching equation as follows

$$\tilde{u}^{\text{in}} = -\lambda_2 C_1 - \lambda_1 C_2 + \frac{c(1-D)}{D\mu_3\mu_4} C_3 \tag{A.10a}$$

$$\tilde{w}^{\text{in}} = C_1 + C_2 + \frac{\eta - D}{D\mu_3\mu_4} C_3 \tag{A.10b}$$

$$\tilde{z}^{\text{in}} = C_3 \tag{A.10c}$$

$$\tilde{u}^{\text{out}} = -\lambda_2 C_1 \mathrm{e}^{\delta_1 \tau^*} - \lambda_1 C_2 \mathrm{e}^{\delta_2 \tau^*} + \frac{c(1-D)}{D\mu_3\mu_4} C_3 \mathrm{e}^{\delta_3 \tau^*} \tag{A.10d}$$

$$\tilde{w}^{\text{out}} = C_1 \mathrm{e}^{\delta_1 \tau^*} + C_2 \mathrm{e}^{\delta_2 \tau^*} + \frac{\eta - D}{D\mu_3\mu_4} C_3 \mathrm{e}^{\delta_3 \tau^*} \tag{A.10e}$$

$$\tilde{z}^{\text{out}} = C_3 \mathrm{e}^{\delta_3 \tau^*} \tag{A.10f}$$

From the above equations, we find that the coefficients A_i, C_i $(i = 1, 2, 3)$ depend on the speed c and cut-off threshold ε. After some work, we obtain two simplified equations denoted as $\widetilde{F}_i(A_1, A_2, c, \varepsilon) = 0, (i = 1, 2)$

$$\widetilde{F}_1 := \Big(\frac{\lambda_3 A_1}{A_1 + \frac{\alpha}{\eta}} - \lambda_4\Big) - \frac{\eta}{D\lambda_4^2 + \eta}\Big(\frac{\lambda_3 A_1}{A_1 + \frac{\alpha}{\eta}} - \lambda_4\Big)^2 - \Big(\lambda_3 - \frac{\eta\lambda_3^2}{D\lambda_4^2 + \eta}\Big)\Big(\frac{\varepsilon}{A_1 + \frac{\alpha}{\eta}}\Big)^{\delta_3}, \tag{A.11}$$

$$\begin{aligned}
\widetilde{F}_2 := {} & \left[\lambda_3^2\alpha_3 + \frac{(D\lambda_4^2 - D\lambda_3\lambda_4 + \eta)}{\mu_4(D\lambda_4^2 + \eta)}\right]\Big(c(D\lambda_4^2 + Dc\lambda_3 + \eta) + D\lambda_3\Big) \\
& + \left[\lambda_3^2\beta_3 + \frac{\lambda_4}{\mu_4} - \frac{D\lambda_3(1 - c\lambda_4)}{\mu_4(D\lambda_4^2 + \eta)}\right]\Big(D\lambda_4^2 + Dc\lambda_3 + \eta\Big) \\
& + \frac{(D\lambda_4^2 + Dc\lambda_3 + \eta)(1 - c\lambda_2) - D\lambda_2\lambda_3}{(\lambda_1 - \lambda_2)}\Big(\tilde{u}^{\text{in}} + \lambda_1\tilde{w}^{\text{in}} - \frac{D\lambda_2 + \eta\lambda_1 + c}{D\mu_3\mu_4}\tilde{z}^{\text{in}}\Big)\Big(\frac{\varepsilon}{A_1 + \frac{\alpha}{\eta}}\Big)^{-\delta_1} \\
& + \frac{(D\lambda_4^2 + Dc\lambda_3 + \eta)(1 - c\lambda_1) - D\lambda_1\lambda_3}{(\lambda_2 - \lambda_1)}\Big(\tilde{u}^{\text{in}} + \lambda_2\tilde{w}^{\text{in}} - \frac{D\lambda_1 + \eta\lambda_2 + c}{D\mu_3\mu_4}\tilde{z}^{\text{in}}\Big)\Big(\frac{\varepsilon}{A_1 + \frac{\alpha}{\eta}}\Big)^{-\delta_2} \\
& + \left[\frac{c\lambda_3(1-D)}{\mu_3\mu_4} + (D\lambda_4^2 + Dc\lambda_3 + \eta)\frac{c^2(1-D) + (\eta - D)}{D\mu_3\mu_4}\right]\tilde{z}^{\text{in}}\Big(\frac{\varepsilon}{A_1 + \frac{\alpha}{\eta}}\Big)^{-\delta_3}
\end{aligned} \tag{A.12}$$

Then, we can calculate the values of A_1 and A_2 by solving $\widetilde{F}_i = 0\,(i = 1, 2)$ numerically for given ε small, then substituting into the constraint of the c-a relation curve:

$$\tilde{a}_\varepsilon(c) = A_2 + \frac{A_1}{\mu_3} + 1 - \frac{\alpha}{\eta}. \tag{A.13}$$

Note that, we suppress the dependence on c and ε here for simplicity, i.e. $A_i = A_i(c, \varepsilon)$, $C_i = C_i(c, \varepsilon)$, and $\widetilde{F}_i = \widetilde{F}_i(A_1, A_2, c, \varepsilon)$. The proof of the existence of $\tilde{a}_\varepsilon(c)$ follows the same procedure as for $a_\varepsilon(c)$ in Section 2.4, which is equivalent to proving that we can get the unique solution from the two constraints $\widetilde{F}_i = 0\,(i = 1, 2)$ by the Implicit Function Theorem. We find analogous results as well, i.e., the persistence will be obtained by the Implicit Function Theorem.

A.2 Dynamics of the singular system

Recall the Equation (2.5):

$$u' = w, \tag{A.14a}$$

$$v' = z, \tag{A.14b}$$

$$w' = -cw + u + v - \theta(u - a), \tag{A.14c}$$

$$z' = -\frac{c}{D}z + \frac{\eta}{D}v - \frac{\alpha}{D}\theta(u - a). \tag{A.14d}$$

The steady states $Q^+ = (0,0,0,0)$ and $Q^- = (1-\frac{\alpha}{\eta}, \frac{\alpha}{\eta}, 0, 0)$ of Equation (A.14)are hyperbolic saddle points. Both have eigenvalues $\lambda_i\,(i = 1, ..., 4)$, with $\lambda_1 = \frac{1}{2}(-c + \sqrt{c^2+4})\,(+)$, $\lambda_2 = \frac{1}{2}(-c - \sqrt{c^2+4})\,(-)$, $\lambda_3 = \frac{1}{2D}(-c + \sqrt{c^2+4D\eta})\,(+)$ and $\lambda_4 = \frac{1}{2D}(-c - \sqrt{c^2+4D\eta})\,(-)$, here the eigenvalues λ_1 and λ_3 are positive, while λ_2 and λ_4 are negative. The corresponding eigenvectors $\mathbf{v}_1 = \big(1, 0, \lambda_1, 0\big)^T$, $\mathbf{v}_2 = \big(1, 0, \lambda_2, 0\big)^T$, $\mathbf{v}_3 = \big(1, \mu_3, \lambda_3, \mu_3\lambda_3\big)^T$ and $\mathbf{v}_4 = \big(1, \mu_4, \lambda_4, \mu_4\lambda_4\big)^T$, respectively, where $\mu_j = \lambda_j^2 + c\lambda_j - 1$, $(j = 3, 4)$.

We consider the travelling front solutions propagating from Q^- when $\xi \to -\infty$ to Q^+ when $\xi \to +\infty$. The general solutions for this problem in the regions can be written as follows:
In region I: $u \geqslant a$, for $\xi \leqslant \xi_0$

$$u_{g_1}(\xi) = A_2 e^{\lambda_1 \xi} + \frac{A_1}{\mu_3} e^{\lambda_3 \xi} + 1 - \alpha/\eta, \tag{A.15a}$$

$$v_{g_1}(\xi) = A_1 e^{\lambda_3 \xi} + \alpha/\eta. \tag{A.15b}$$

$$w_{g_1}(\xi) = \lambda_1 A_2 e^{\lambda_1 \xi} + \frac{\lambda_3}{\mu_3} A_1 e^{\lambda_3 \xi}, \tag{A.15c}$$

$$z_{g_1}(\xi) = \lambda_3 A_1 e^{\lambda_3 \xi} \tag{A.15d}$$

In region II: $u \leqslant a$, for $\xi \geqslant \xi_0$

$$u_{g_2}(\xi) = A_{22} e^{\lambda_2 \xi} + \frac{B_{24}}{\mu_4} e^{\lambda_4 \xi}, \tag{A.16a}$$

$$v_{g_2}(\xi) = B_{24} e^{\lambda_4 \xi}, \tag{A.16b}$$

$$w_{g_2}(\xi) = \lambda_2 A_{22} e^{\lambda_2 \xi} + \frac{\lambda_4}{\mu_4} B_{24} e^{\lambda_4 \xi}, \tag{A.16c}$$

$$z_{g_2}(\xi) = \lambda_4 B_{24} e^{\lambda_4 \xi}. \tag{A.16d}$$

Then we can solve for all coefficients A_{ij}, B_{ij} by patching the two regions together, using the conditions for continuity of functions. We obtain the front solutions explicitly, by choosing $\xi_0 = 0$ for sake of simplicity.

We have all the coefficients written as

$$B_{24} = \frac{\alpha/\eta}{1 - \frac{\lambda_4}{\lambda_3}}, \tag{A.17a}$$

$$A_1 = \frac{\alpha/\eta}{1 - \frac{\lambda_4}{\lambda_3}}, \tag{A.17b}$$

$$A_{22} = \frac{1}{\lambda_1 - \lambda_2}\Big[\lambda_1(1 - \frac{\alpha}{\eta}) + \frac{\alpha/\eta}{\lambda_3 - \lambda_4}(\frac{\lambda_4(\lambda_1 - \lambda_3)}{\mu_3} - \frac{\lambda_3(\lambda_1 - \lambda_4)}{\mu_4})\Big], \tag{A.17c}$$

$$A_2 = -1 + \frac{\alpha}{\eta}[1 + \frac{1}{\mu_3} + (\frac{1}{\mu_4} - \frac{1}{\mu_3})\frac{1}{1 - \frac{\lambda_4}{\lambda_3}}] + A_{22}, \tag{A.17d}$$

and the singular limit of the speed relation

$$a(c_0, 0) = (1 - \frac{\alpha}{\eta})\frac{\lambda_1}{\lambda_1 - \lambda_2} - \frac{\alpha}{\eta}\frac{1}{(\lambda_1 - \lambda_2)(\lambda_3 - \lambda_4)}\Big[\frac{\lambda_3}{\mu_4}(\lambda_2 - \lambda_4) - \frac{\lambda_4}{\mu_3}(\lambda_1 - \lambda_3)\Big] \tag{A.18}$$

Numerical simulation

We approximate numerically the c-a curves for the original sigmoidal system without cut-off , see Figure A.2, for $D = 1, 2, 5, 10$ with fixed $\eta = 0.12, \alpha = 0.08$.

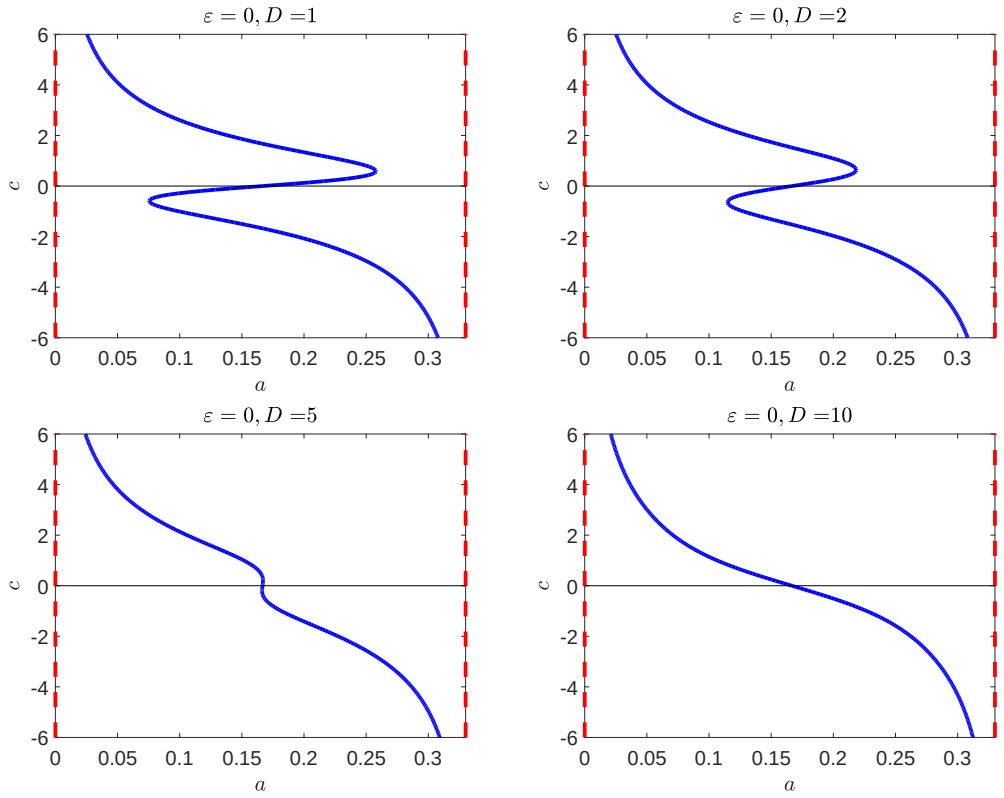

Figure A.2: The system without cut-off: Front speed c vs discontinuity position a relation, with $D = 1, 2, 5, 10$, fixed $\eta = 0.12, \alpha = 0.08$.

A.3 Geometric analysis of the u-component cut-off system

The dynamics of u-component cut-off system is best studied in an equivalent formulation of Equation (2.4) with $\phi = u$ that results from a blow-up transformation of the corresponding vector field near the origin in $(u, v, w, z, \varepsilon)$-space. To that end, we append the trivial equation $\varepsilon' = 0$ in (2.4);

$$u' = w, \tag{A.19a}$$
$$v' = z, \tag{A.19b}$$
$$w' = -cw - f(u, v)\theta(u - \varepsilon), \tag{A.19c}$$
$$z' = -\frac{c}{D}z - \frac{1}{D}g(u, v)\theta(u - \varepsilon), \tag{A.19d}$$
$$\varepsilon' = 0 \tag{A.19e}$$

The steady states of (A.19) are Q_ε^+ and Q_ε^-, where we keep the notations as they are same as those in v-component cut-off system.

Due to the change of cut-off component, the two coordinate charts K_1 and K_2 of the homogeneous blow-up transformation are obtained by $\bar{u} = 1$ and $\bar{\varepsilon} = 1$, respectively; yields

$$u = r_1,\ v = r_1 v_1,\ w = r_1 w_1,\ z = r_1 z_1,\ \text{and } \varepsilon = r_1 \varepsilon_1 \tag{A.20}$$

and

$$u = r_2 u_2,\ v = r_2 v_2,\ w = r_2 w_2,\ z = r_2 z_2,\ \text{and } \varepsilon = r_2, \tag{A.21}$$

respectively, for the coordinates in these charts. The change-of-coordinates transformation $\mathcal{K}_{12}$

between charts K_1 and K_2 is given by

$$\mathcal{K}_{12}:\ (r_1,v_1,w_1,z_1,\varepsilon_1)\mapsto\Big(r_2u_2,\frac{v_2}{u_2},\frac{w_2}{u_2},\frac{w_2}{u_2},\frac{z_2}{u_2},\frac{1}{u_2}\Big),\tag{A.22}$$

whereas its inverse $\mathcal{K}_{21}=\mathcal{K}_{12}^{-1}$ reads

$$\mathcal{K}_{21}:\ (u_2,v_2,w_2,z_2,r_2)\mapsto\Big(\frac{1}{\varepsilon_1},\frac{v_1}{\varepsilon_1},\frac{w_1}{\varepsilon_1},\frac{z_1}{\varepsilon_1},r_1\varepsilon_1\Big).\tag{A.23}$$

We define several sections for the flow of Equation (A.19) – or, rather, of the corresponding blown-up systems in charts K_1 and K_2:

$$\Sigma_1^{\text{in}}:=\big\{(a,v_1,w_1,z_1,\varepsilon_1)\,\big|\,v_1\in[v_*,v^*],\ w_1\in[w_*,w^*],\ z_1\in[z_*,z^*],\ \text{and}\ \varepsilon_1\in[0,1]\big\},\tag{A.24a}$$

$$\Sigma_1^{\text{out}}:=\big\{(r_1,v_1,w_1,z_1,1)\,\big|\,r_1\in[0,a],\ v_1\in[v_*,v^*],\ w_1\in[w_*,w^*],\ \text{and}\ z_1\in[z_*,z^*]\big\},\tag{A.24b}$$

$$\Sigma_2^{\text{in}}:=\big\{(1,v_2,w_2,z_2,r_2)\,\big|\,v_2\in[v_*,v^*],\ w_2\in[w_*,w^*],\ z_2\in[z_*,z^*],\ \text{and}\ r_2\in[0,\varepsilon_0]\big\}.\tag{A.24c}$$

Here, v_*, v^*, w_*, w^*, z_*, and z^* are suitably chosen constants; we remark that, by (A.23), the range for (v_2,w_2,z_2) may be chosen identical to that for (v_1,w_1,z_1), as $\varepsilon_1=1$ in $\Sigma_2^{\text{in}}=\mathcal{K}_{12}(\Sigma_1^{\text{out}})$. Moreover, the sections Σ_1^{in} and Σ_1^{out} clearly correspond to the respective boundaries between regions I and II and between regions II and III, when expressed in chart K_1; recall Section 2.1.

A.3.1 Dynamics in region I

In region I, where $a<u<1$, Equation (A.19) reduces to

$$u'=w,\tag{A.25a}$$

$$v'=z,\tag{A.25b}$$

$$w'=-cw+u+v-1,\tag{A.25c}$$

$$z'=-\frac{c}{D}z+\frac{\eta}{D}v-\frac{\alpha}{D},\tag{A.25d}$$

$$\varepsilon'=0\tag{A.25e}$$

as $\theta(u-\varepsilon)\equiv 1\equiv\theta(u-a)$ in that region. Clearly, the dynamics in region I corresponds to the dynamics in the "outer" region of (2.5). Hence, the geometric analysis in this region proceeds as in Section 2.2.1 as well.

Here, we show the expressions of the point P_ε as follows:

$$P_\varepsilon=\Big(A_2+\frac{A_1}{\mu_3}+1-\frac{\alpha}{\eta},A_1+\frac{\alpha}{\eta},\lambda_1A_2+\frac{\lambda_3}{\mu_3}A_1,\lambda_3A_1,\varepsilon\Big),\tag{A.26}$$

for ε fixed and small; for $\varepsilon=0$, $P_0=\big(A_2+\frac{A_1}{\mu_3}+1-\frac{\alpha}{\eta},A_1+\frac{\alpha}{\eta},\lambda_1A_2+\frac{\lambda_3}{\mu_3}A_1,\lambda_3A_1,0\big)$ in the section Σ^- , recall the constraint in (2.23)

$$a=A_2+\frac{A_1}{\mu_3}+1-\frac{\alpha}{\eta}.\tag{A.27}$$

where A_1 and A_2 are coefficients that are as yet undetermined.

A.3.2 Dynamics in region III

In region III, where $\theta(u-\varepsilon)\equiv 0$; hence, by the blow-up transformation in (A.21), Equation (A.19) reduces to

$$u_2' = w_2, \tag{A.28a}$$
$$v_2' = z_2, \tag{A.28b}$$
$$w_2' = -cw_2, \tag{A.28c}$$
$$z_2' = -\frac{c}{D}z_2, \tag{A.28d}$$
$$r_2' = 0 \tag{A.28e}$$

The steady states of (A.28) are the points on the (u_2, v_2, r_2)-sphere, however, only the points on the line $\ell_2^+ = \big\{(0,0,0,0,r_2)\,\big|\, r_2 \in [0,\varepsilon_0]\big\}$ are relevant here, which can correspond to ℓ^+ after transforming to the original (u,v,w,z,ε)-variables. We denote the points on ℓ_2^+ by $Q_{\varepsilon 2}^+$ for ε fixed. Equation (A.28) may be solved exactly: rewriting the above equations with u_2 as the independent variable and keeping in mind that $(v_2,w_2,z_2)(u_2)\big|_{u_2=0} = (0,0,0)$, we find the family of orbits $\Gamma_{\varepsilon 2}$, which correspond to the stable manifolds $\mathcal{W}_2^{\mathrm{s}}(Q_{\varepsilon 2}^+)$,

$$\Gamma_{\varepsilon 2} : \big(v_2,w_2,z_2\big)(u_2) = \Big(-\frac{D}{c}A_3 u_2^{\frac{1}{D}}, -cu_2, A_3 u_2^{\frac{1}{D}}\Big), \tag{A.29}$$

where $A_3 < 0$ is to be determined by matching the boundaries of the orbit in region II. The point of intersection of $\Gamma_{\varepsilon 2}$ with the section Σ_2^{in} in (A.24), which we denote by $P_{\varepsilon 2}^{\mathrm{in}}$ is determined by taking $u_2 = 1$ in Equation (A.29), whence

$$P_{\varepsilon 2}^{\mathrm{in}} : \Big(u_2^{\mathrm{in}}, v_2^{\mathrm{in}}, w_2^{\mathrm{in}}, z_2^{\mathrm{in}}, r_2^{\mathrm{in}}\Big) = (1, -\frac{D}{c}A_3, -c, A_3, \varepsilon). \tag{A.30}$$

where ε is small.

***Remark* A.1.** The family of orbits $\Gamma_{\varepsilon 2}$ is parametrised by $r_2(=\varepsilon)$, as c and A_3 are both r_2-dependent.

As for the singular orbit Γ_2, which corresponds to the stable eigendirection of $\mathcal{W}^{\mathrm{s}}(Q_0^+)$ in the original (u,v,w,z,ε)-variables, we obtain

$$\Gamma_2 : \ \big(v_2,w_2,z_2\big)(u_2) = \big(\mu_4 u_2, \lambda_4 u_2, \mu_4\lambda_4 u_2\big). \tag{A.31}$$

with $P_{02}^{\mathrm{in}} := \big(1,\mu_4,\lambda_4,\mu_4\lambda_4,0\big)$, by taking $u_2 = 1$.

***Remark* A.2.** The expression for Γ_2 is obtained from the weak-stable eigenvector $\mathbf{v}_4 = \big(1,\mu_4,\lambda_4,\mu_4\lambda_4\big)^T$ of Equation (A.14) at the origin, cf. Appendix A.2.

***Remark* A.3.** Here, λ_i $(i=1,\ldots,4)$ and μ_j $(j=3,4)$ are defined as in Lemma 2.1 in the analysis of the u-component cut-off system.

A.3.3 Dynamics in region II

The dynamics in region II is naturally described in chart K_1: substituting (A.20) into (A.19) and noting that $\theta(u-a)\equiv 0$, we find

$$r_1' = r_1 w_1, \tag{A.32a}$$
$$v_1' = -v_1 w_1 + z_1, \tag{A.32b}$$
$$w_1' = -cw_1 - w_1^2 + (1+v_1)\theta(1-\varepsilon_1), \tag{A.32c}$$
$$z_1' = -\frac{c}{D}z_1 + \frac{\eta}{D}v_1\theta(1-\varepsilon_1) - z_1 w_1, \tag{A.32d}$$
$$\varepsilon_1' = -\varepsilon_1 w_1. \tag{A.32e}$$

As we will only consider Equation (A.32) for $\varepsilon_1 \in [0,1]$, cf. the definition of the section Σ_1^{out}, we may take $\theta(1-\varepsilon_1)\equiv 1$ in the above equations. The steady states of (A.32) are located at

$P_1^{\pm} = (0, 0, \lambda_{1,2}, 0, 0)$ and at $\widetilde{P}_1^{\pm} = (0, \mu_{3,4}, \lambda_{3,4}, \mu_{3,4}\lambda_{3,4}, 0)$.

The following result is obtained via a straightforward linearisation argument:

Lemma A.1. *The steady states $P_1^{\pm}$ and $\widetilde{P}_1^{\pm}$ of Equation* (A.32) *are hyperbolic saddle points, with eigenvalues*

$$\begin{aligned}
&\lambda_2\,(-),\ \lambda_1-\lambda_2\ (+),\ \lambda_3-\lambda_2\ (+),\ \lambda_4-\lambda_2\ (+),\ \textit{and}\ -\lambda_2\ (+)\,\textit{for}\,P_1^-,\\
&\lambda_1\ (+),\ \lambda_2-\lambda_1\ (-),\ \lambda_3-\lambda_1\ (-),\ \lambda_4-\lambda_1\ (-),\ \textit{and}\ -\lambda_1\ (-)\,\textit{for}\,P_1^+,\\
&\lambda_4\,(-),\ \lambda_1-\lambda_4\ (+),\ \lambda_2-\lambda_4\ (-),\ \lambda_3-\lambda_4\ (+),\ \textit{and}\ -\lambda_4\ (+)\,\textit{for}\,\widetilde{P}_1^-,\\
&\lambda_3\ (+),\ \lambda_1-\lambda_3\ (+),\ \lambda_2-\lambda_3\ (-),\ \lambda_4-\lambda_3\ (-),\ \textit{and}\ -\lambda_3\ (-)\,\textit{for}\,\widetilde{P}_1^+.
\end{aligned}$$

The singular limit of $\varepsilon = 0$ in (A.19) yields two limiting systems of equations, which are obtained by setting $r_1 = 0$ and $\varepsilon_1 = 0$, respectively, in Equation (A.32):

$$\begin{aligned}
v_1' &= -v_1 w_1 + z_1,\\
w_1' &= -c_0 w_1 - w_1^2 + 1 + v_1,\\
z_1' &= -\frac{c_0}{D} z_1 + \frac{\eta}{D} v_1 - z_1 w_1,\\
\varepsilon_1' &= -\varepsilon_1 w_1
\end{aligned}$$

and

$$\begin{aligned}
r_1' &= r_1 w_1,\\
v_1' &= -v_1 w_1 + z_1,\\
w_1' &= -c_0 w_1 - w_1^2 + 1 + v_1,\\
z_1' &= -\frac{c_0}{D} z_1 + \frac{\eta}{D} v_1 - z_1 w_1;
\end{aligned}$$

here, $c_0 = c(\varepsilon)\big|_{\varepsilon=0}$.

In the invariant plane $\{\varepsilon_1 = 0\}$, we define the orbit Γ_1^-, which is passing through P_{01}^{in}, and is attracted to $\widetilde{P}_1^-$. We note here, that Γ_1^- corresponds to the 2-dimensional stable manifold $\mathcal{W}^{\text{s}}(Q_0^+)$ after transformation to chart K_1. To that end, we focus on orbits entering at P_0 in the section Σ^-, where the 2-dimensional unstable manifold $\mathcal{W}^{\text{u}}(Q_0^-)$ in region I ends. We have the following representation of P_{01}^{in}:

$$P_{01}^{\text{in}} := \big(r_1^{\text{in}}, v_1^{\text{in}}, w_1^{\text{in}}, z_1^{\text{in}}, 0\big) = \left(a, \frac{A_1 + \frac{\alpha}{\eta}}{a}, \frac{\lambda_1 A_2 + \frac{\lambda_3}{\mu_3} A_1}{a}, \frac{\lambda_3 A_1}{a}, 0\right) \tag{A.33}$$

where $A_1 < 0$ as in Proposition 2.1.

Similarly, in the invariant plane $\{r_1 = 0\}$, the orbit passing through $P_{01}^{\text{out}} = (0,\ \mu_4, \lambda_4,\ \lambda_4\mu_4,\ 1)$, which is labeled Γ_1^+, is attracted to $\widetilde{P}_1^-$ in backward "time", for $\xi \to -\infty$

$$\Gamma_1^+ := \big(v_1, w_1, z_1, \varepsilon_1\big)(\xi) = \Big(\mu_4, \lambda_4,\ \lambda_4\mu_4,\ \mathrm{e}^{-\lambda_4 \xi}\Big) \tag{A.34}$$

***Remark* A.4.** The points P_{01}^{in} and P_{01}^{out} correspond to the points $P_0 = \big(A_2 + \frac{A_1}{\mu_3} + 1 - \frac{\alpha}{\eta}, A_1 + \frac{\alpha}{\eta}, \lambda_1 A_2 + \frac{\lambda_3}{\mu_3} A_1, \lambda_3 A_1,\ 0\big)$ and $P_{02}^{\text{in}} = \big(1, \mu_4, \lambda_4, \lambda_4\mu_4, 0\big)$, under the transformation in (A.20) and $\mathcal{K}_{12}$ in (A.22), respectively.

Break in construction of Γ_1^-

Recall Section 2.2.3, in the u-component cut-off system, the value of u is always negative before approaching the origin, see panel (a) in Figure 2.6, which implies that that the current chart K_1 and K_2 are not proper for the u-component cut-off system. We need more charts, e.g. $\bar{u} = -1$. The local geometry in chart K_1 in $(u_1, w_1, \varepsilon_1)$-space is illustrated in panel (a) in Figure A.4, there Γ_1^- is repelling away in w_1-coordinate.

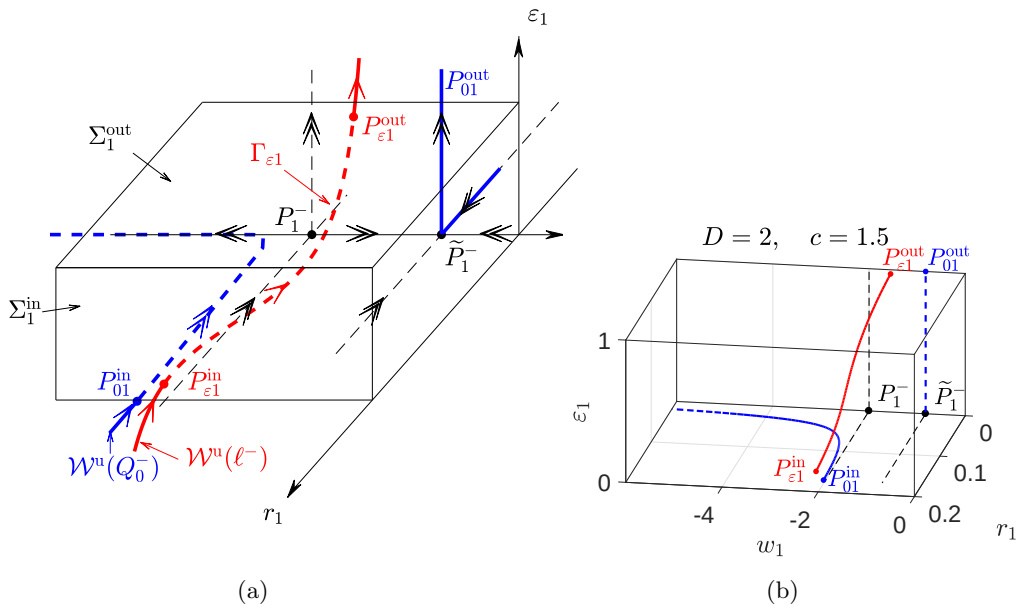

Figure A.3: The geometry of $(r_1, w_1, \varepsilon_1)$-space: the singular orbit (blue), the perturbed orbit (red); (a) Qualitative sketch. (b) Numerical simulation at $D = 2$, $c = 1.5$, $\varepsilon = 0.01$.

We present the simulations of orbits in chart K_1 for $c = 2, 4, 6, 8$, with $D = 2$ and $\varepsilon = 0.0001$; see Figure A.3. For the speed $c = 2$, the perturbed orbit $\Gamma_{\varepsilon 1}$ (red) repels away in the w_1-coordinate, in agreement with Γ_1^- (blue), while c increases, the perturbed orbit approaches Γ_1^- for $r_1 > 0$, which implies that the value of the original variable v at the cut-off remains in the neighbourhood of the origin. Hence, we can still apply the blow-up technique to obtain an approximation of the perturbed orbits in chart K_1 in region II, with suitably chosen speeds, e.g., for $c = 8$, $\Gamma_{\varepsilon 1}$ approaches Γ_1^- in $r_1 > 0$.

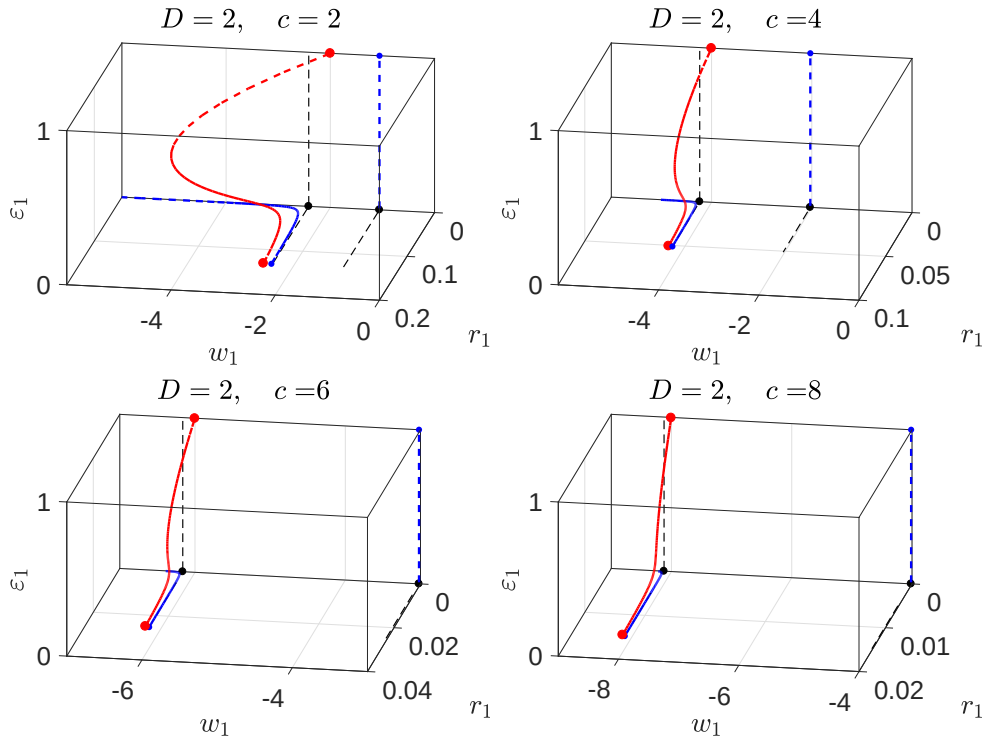

Figure A.4: The approximated geometry of $(r_1, w_1, \varepsilon_1)$-space, for $D = 2$ and $\varepsilon = 0.0001$.

A.3.4 Existence and asymptotics of the c-a relation

In this section, we motivate of the asymptotic heteroclinic orbit Γ for ε positive and sufficiently small. To that end, we combine the dynamics of the three regions obtained in the previous Sections.

In region I, the unstable manifold $\mathcal{W}^{\mathrm{u}}(Q_0^-)$ of the point Q_0^- will persist as the unstable manifold $\mathcal{W}^{\mathrm{u}}(Q_\varepsilon^-)$ of Q_ε^-. The manifold $\mathcal{W}^{\mathrm{u}}(\ell^-)$ of the line ℓ^- is then defined as a foliation in $\varepsilon \in [0, \varepsilon_0]$, with fibers $\mathcal{W}^{\mathrm{u}}(Q_\varepsilon^-)$.

Similarly, in region III, the orbit Γ_2 corresponds to the stable manifold $\mathcal{W}_2^{\mathrm{s}}(Q_0^+)$ of Q_0^+ will perturb smoothly for $r_2 > 0$ small and $u_2 \leqslant 1$, to the manifold $\mathcal{W}_2^{\mathrm{s}}(Q_{\varepsilon 2}^+)$ of $Q_{\varepsilon 2}^+$. And the stable manifold $\mathcal{W}^{\mathrm{s}}(\ell_2^+)$ of the line ℓ_2^+ is then given by $\bigcup_{\varepsilon\in[0,\varepsilon_0]} \mathcal{W}^{\mathrm{s}}(Q_{\varepsilon 2}^+)$. Next, we need to prove the existence of $\Gamma_{\varepsilon 1}$, which connects Γ^u and $\Gamma_{\varepsilon 2}$ in the region II, where we use the patching method at the corresponding boundaries. The argument will be carried out entirely in region II, i.e., in chart K_1. To that end, we firstly recall the definition of the two sections Σ_1^{in} and Σ_1^{out} for the flow of (A.32) defined in (A.24) and we label the corresponding patching points by $P_{\varepsilon 1}^{\mathrm{in}}$ and $P_{\varepsilon 1}^{\mathrm{out}}$, respectively. In particular, the section Σ_1^{in} and the point $P_{\varepsilon 1}^{\mathrm{in}}$ correspond to the section Σ^- and the point P_ε defined in Section A.3.1, respectively, after blown-up transformation to chart K_1. Similarly, the section Σ_1^{out} and the point $P_{\varepsilon 1}^{\mathrm{out}}$ correspond to the section Σ_2^{in} and the point $P_{\varepsilon 2}^{\mathrm{in}}$ of (A.30) in chart K_2 in Section A.3.2, respectively, under the change-of-coordinates $\mathcal{K}_{12}$. In other words, the section Σ_1^{in} defines the boundary between regions II and I, while Σ_1^{out} defines the boundary between regions II and III; in particular, the corresponding patching points are represented as

$$P_{\varepsilon 1}^{\mathrm{in}} := (r_1^{\mathrm{in}},\, v_1^{\mathrm{in}},\, w_1^{\mathrm{in}},\, z_1^{\mathrm{in}},\, \varepsilon_1^{\mathrm{in}}) = \left(a,\, \frac{A_1 + \frac{\alpha}{\eta}}{a},\, \frac{\lambda_1 A_2 + \frac{\lambda_3}{\mu_3} A_1}{a},\, \frac{\lambda_3 A_1}{a},\, \frac{\varepsilon}{a}\right), \tag{A.35a}$$

$$P_{\varepsilon 1}^{\mathrm{out}} := (r_1^{\mathrm{out}},\, v_1^{\mathrm{out}},\, w_1^{\mathrm{out}},\, z_1^{\mathrm{out}},\, \varepsilon_1^{\mathrm{out}}) = \big(\varepsilon,\, -\frac{D}{c} A_3,\, -c,\, A_3,\, 1\big), \tag{A.35b}$$

Next, we aim to approximate the transition map $\Pi_1 : \Sigma_1^{\mathrm{in}} \to \Sigma_1^{\mathrm{out}}$ that represents the corresponding portion of the persistent heteroclinic orbit lies in this region II.

A.3.4.1 Transition map Π_1

To approximate the transition map for the flow of Equation (A.32) between the two sections Σ_1^{in} and Σ_1^{out} defined in (A.24). We begin by dividing out a factor of $-w_1$ from (A.32), which corresponds to a transformation of the independent variable that leaves the corresponding phase portrait unchanged. (We note that $-w_1$ is positive and, hence, that the direction of the flow is unaltered, since we are restricting to a neighbourhood of P_1^- here.) Then, we shift P_1^- to the origin in K_1 by defining the new variable W via $w_1 = \frac{1}{2}(-c - \sqrt{c^2+4}) + W$. In sum, we hence obtain the transformed system of equations

$$r_1' = -r_1, \tag{A.36a}$$

$$v_1' = v_1 + \frac{z_1}{\frac{1}{2}(c + \sqrt{c^2+4}) - W}, \tag{A.36b}$$

$$W' = \frac{\sqrt{c^2+4} W + v_1 - W^2}{\frac{1}{2}(c + \sqrt{c^2+4}) - W}, \tag{A.36c}$$

$$z_1' = z_1 - \frac{\frac{c}{D} z_1 - \frac{\eta}{D} v_1}{\frac{1}{2}(c + \sqrt{c^2+4}) - W}, \tag{A.36d}$$

$$\varepsilon_1' = \varepsilon_1. \tag{A.36e}$$

where the prime now denotes differentiation with respect to the new independent time τ .

The principal equilibrium of Equation (A.36) is now located at the origin. A standard linearisation argument yields:

Lemma A.2. *The origin is a hyperbolic saddle point for* (A.36)*, with eigenvalues* -1*,* $\delta_1 = -\frac{\lambda_1}{\lambda_2} + 1\,(+)$*,* $\delta_2 = -\frac{\lambda_4}{\lambda_2} + 1\,(+)$*,* $\delta_3 = -\frac{\lambda_3}{\lambda_4} + 1\,(+)$ *and* 1*.*

We observe that resonances between the eigenvalues of the linearisation of (A.36) about the origin exist if and only if $D = 1$. However, as the (v_1, W, z_1)-subsystem in (A.36b) through (A.36d) is decoupled, i.e., independent of (r_1, ε_1), these resonances are not realised. Hence, Equation (A.36) may be linearised to any order in $(r_1, W, v_1, z_1, \varepsilon_1)$ via a sequence of near-identity transformations that only involve (v_1, W, z_1); in particular, it follows that the former will be defined on $(r_1, \varepsilon_1) \in [0, a] \times [0, 1]$, as no restriction has to be made on the two variables r_1 and ε_1. In fact, we can easily solve Equations (A.36a) and (A.36e) to find $r_1 = a\mathrm{e}^{-\tau}$ and $\varepsilon_1 = \frac{\varepsilon}{a}\mathrm{e}^{\tau}$, respectively; by patching the (r_1, ε_1)-coordinates of the boundaries, i.e., $r_1^{\mathrm{in}}(\tau_1) = a$, $r_1^{\mathrm{out}}(\tau_2) = \varepsilon$, $\varepsilon_1^{\mathrm{in}}(\tau_1) = \frac{\varepsilon}{a}$ and $\varepsilon_1^{\mathrm{out}}(\tau_2) = 1$; here, we choose $\tau_1 = 0$ for simplicity, then determine the corresponding value $\tau_2 = \tau^* = \ln \frac{a}{\varepsilon}$.

In a first step, we expand the common denominator in Equation (A.36) via

$$\frac{1}{\frac{1}{2}(c + \sqrt{c^2+4}) - W} = \frac{2}{c + \sqrt{c^2+4}}\Big[1 + \frac{2}{c + \sqrt{c^2+4}}W + \mathcal{O}(W^2)\Big],$$

keeping in mind that we assume $|W|$ to be small. Substituting into (A.36), we find that Equations (A.36b) through (A.36d) become

$$v_1' = v_1 + \frac{2}{c + \sqrt{c^2+4}}z_1 + \frac{4}{(c + \sqrt{c^2+4})^2}Wz_1 + \mathcal{O}(3), \tag{A.37a}$$

$$W' = \frac{2}{c + \sqrt{c^2+4}}v_1 + \frac{2\sqrt{c^2+4}}{c + \sqrt{c^2+4}}W + \frac{4}{\big(c + \sqrt{c^2+4}\big)^2}v_1W + \frac{8}{\big(c + \sqrt{c^2+4}\big)^3}W^2 + \mathcal{O}(3), \tag{A.37b}$$

$$z_1' = \frac{\eta}{D}\frac{2}{c + \sqrt{c^2+4}}v_1 + \Big(1 - \frac{2}{D}\frac{c}{c + \sqrt{c^2+4}}\Big)z_1 - \frac{4}{D}\frac{c}{\big(c + \sqrt{c^2+4}\big)^2}Wz_1 + \frac{\eta}{D}\frac{4}{\big(c + \sqrt{c^2+4}\big)^2}v_1W + \mathcal{O}(3), \tag{A.37c}$$

where $\mathcal{O}(3)$ denotes terms of order 3 and upwards in (v_1, W, z_1).

A.3.5 Formal linearisation

In this subsection, we consider a formal linearisation of Equation (A.36) which is obtained by neglecting terms of order 2 and upwards in (A.37):

$$\hat{v}_1' = \hat{v}_1 + \frac{2}{c + \sqrt{c^2+4}}\hat{z}_1, \tag{A.38a}$$

$$\widehat{W}' = \frac{2}{c + \sqrt{c^2+4}}\hat{v}_1 + \frac{2\sqrt{c^2+4}}{c + \sqrt{c^2+4}}\widehat{W}, \tag{A.38b}$$

$$\hat{z}_1' = \frac{\eta}{D}\frac{2}{c + \sqrt{c^2+4}}\hat{v}_1 + \Big(1 - \frac{2}{D}\frac{c}{c + \sqrt{c^2+4}}\Big)\hat{z}_1. \tag{A.38c}$$

The eigenvalues of Equation (A.46) at the origin are given by $\delta_i > 0$ $(i = 1, 2, 3)$, as defined in Lemma A.2, with corresponding eigenvectors $\mathbf{v}_1 = (0, 1, 0)^T$, $\mathbf{v}_2 = \big(-\frac{D\lambda_3}{\eta}, \frac{D\lambda_1\lambda_3}{\eta(\delta_1 - \delta_2)}, 1\big)^T$, and $\mathbf{v}_3 = \big(\frac{1}{\lambda_3}, -\frac{\lambda_1}{\lambda_3(\delta_1 - \delta_3)}, 1\big)^T$. Defining the change-of-variable matrix $\mathbf{P} = [\mathbf{v_1}|\mathbf{v_2}|\mathbf{v_3}]$, we write $\mathbf{w} = (\hat{v}_1, \widehat{W}, \hat{z}_1)^T = \mathbf{P}\mathbf{x}$, and $\mathbf{x} = (x_1, x_2, x_3)^T$; then, Equation (A.38) becomes $\mathbf{x}' = \mathrm{diag}(\delta_1, \delta_2, \delta_3)\mathbf{x}$, which has the following general solution for $\mathbf{x}$: $x_i = C_i\mathrm{e}^{\delta_i\tau}$, with undetermined constants C_i $(i = 1, 2, 3)$. It follows that the general solution for $\mathbf{w}$ can be written as

$$\hat{v}_1 = -\frac{D\lambda_3}{\eta}C_2\mathrm{e}^{\delta_2\tau} + \frac{1}{\lambda_3}C_3\mathrm{e}^{\delta_3\tau}, \tag{A.39a}$$

$$\widehat{W} = C_1\mathrm{e}^{\delta_1\tau} + \frac{D\lambda_1\lambda_3}{\eta(\delta_1 - \delta_2)}C_2\mathrm{e}^{\delta_2\tau} - \frac{\lambda_1}{\lambda_3(\delta_1 - \delta_3)}C_3\mathrm{e}^{\delta_3\tau}, \tag{A.39b}$$

$$\hat{z}_1 = C_2\mathrm{e}^{\delta_2\tau} + C_3\mathrm{e}^{\delta_3\tau}. \tag{A.39c}$$

Here, we can denote the approximation to the general solution of (A.36) by the formal linearisation as in (A.39) as $\widehat{\Gamma}_1$, noting that we have obtained the explicit solutions for $r_1 = a\mathrm{e}^{-\tau}$ and $\varepsilon_1 = \frac{\varepsilon}{a}\mathrm{e}^{\tau}$. We convert the corresponding boundaries in (A.35) into the new variables $(\hat{v}_1, \widehat{W}, \hat{z}_1)$ by formal linearisation, which yields

$$\widehat{P}^{\mathrm{in}}_{\varepsilon 1} := \big(a, \hat{v}_1^{\mathrm{in}}, \widehat{W}^{\mathrm{in}}, \hat{z}_1^{\mathrm{in}}, \frac{\varepsilon}{a}\big) = \Big(a, \frac{A_1 + \frac{\alpha}{\eta}}{a}, \frac{\lambda_1 A_2 + \frac{\lambda_3}{\mu_3} A_1}{a} - \lambda_2, \frac{\lambda_3 A_1}{a}, \frac{\varepsilon}{a}\Big) \text{ at } \tau = 0 \tag{A.40a}$$

$$\widehat{P}^{\mathrm{out}}_{\varepsilon 1} := \big(\varepsilon, \hat{v}_1^{\mathrm{out}}, \widehat{W}^{\mathrm{out}}, \hat{z}_1^{\mathrm{out}}, 1\big) = \Big(\varepsilon, -\frac{D}{c}A_3, -c - \lambda_2, A_3, 1\Big) \text{ at } \tau^* = \ln\frac{a}{\varepsilon}, \tag{A.40b}$$

A.3.5.1 Patching at boundaries

We can determine all coefficients A_i, C_i $(i = 1, 2, 3)$ by patching the general solutions between the two sections $\widehat{\Sigma}_1^{\mathrm{in}}$ and $\widehat{\Sigma}_1^{\mathrm{out}}$ at the points of intersection $\widehat{P}^{\mathrm{in}}_{\varepsilon 1}$ and $\widehat{P}^{\mathrm{out}}_{\varepsilon 1}$, i.e., we solve the particular solution with specific boundary condition (A.40) in $(\hat{v}_1, \widehat{W}, \hat{z}_1)$, which completes the construction of orbit $\widehat{\Gamma}_1$ in chart K_1. We obtain the explicit solutions for all the coefficients in dependence of (a, c, ε):

$$C_1 = \lambda_1\Big(\frac{\varepsilon}{a}\Big)^{\delta_1} + \frac{\lambda_1\alpha}{a\eta}\frac{D\lambda_3^2}{D\lambda_3^2+\eta}\Big(\frac{1}{\delta_1-\delta_2} + \frac{D\lambda_3^2}{\eta(\delta_1-\delta_3)}\Big)\Big(\frac{\varepsilon}{a}\Big)^{-\delta_2+\delta_1} \tag{A.41a}$$

$$C_2 = -\frac{\lambda_3\alpha}{a}\frac{1}{D\lambda_3^2+\eta} \tag{A.41b}$$

$$C_3 = \frac{\alpha}{a\eta}\frac{D^2\lambda_3^4}{(D\lambda_3^2+\eta)(D\lambda_3+c)}\Big(\frac{\varepsilon}{a}\Big)^{-\delta_2+\delta_3} \tag{A.41c}$$

$$A_1 = \frac{\alpha}{D\lambda_3^2+\eta}\Big(\frac{D^2\lambda_3^4}{\eta^2}\Big(\frac{\varepsilon}{a}\Big)^{\delta_3-\delta_2} - 1\Big) \tag{A.41d}$$

$$\begin{aligned} A_2 =& a\Big(\Big(\frac{\varepsilon}{a}\Big)^{\delta_1} - \frac{c}{\lambda_1} - 1\Big) + \frac{\alpha}{D\lambda_3^2+\eta}\Bigg[\frac{D\lambda_3^2}{\eta(\delta_1-\delta_2)}\Big(\Big(\frac{\varepsilon}{a}\Big)^{\delta_1-\delta_2} - 1\Big) \\ &+ \frac{D^2\lambda_3^4}{\eta^2(\delta_1-\delta_3)}\Big(\Big(\frac{\varepsilon}{a}\Big)^{\delta_1-\delta_2} - \Big(\frac{\varepsilon}{a}\Big)^{\delta_3-\delta_2}\Big) - \frac{\lambda_3}{\mu_3\lambda_1}\Big(\frac{D^2\lambda_3^4}{\eta^2}\Big(\frac{\varepsilon}{a}\Big)^{\delta_3-\delta_2} - 1\Big)\Bigg] \end{aligned} \tag{A.41e}$$

$$A_3 = \Big(-\frac{\lambda_3\alpha}{a}\frac{1}{D\lambda_3^2+\eta} + \frac{\alpha}{a\eta}\frac{D\lambda_3^4}{(D\lambda_3^2+\eta)(D\lambda_3+c)}\Big)\Big(\frac{\varepsilon}{a}\Big)^{-\delta_2} \tag{A.41f}$$

Recall the constraint in (A.27), after substituting the results of A_1 and A_2, we obtain the equation $F_\varepsilon(a, c, \varepsilon) = 0$, which is the desired c-a relation equation by formal linearisation patching; here, we suppress the dependence for simplicity.

$$\begin{aligned} F_\varepsilon :=& 1 - \frac{\alpha}{\eta} - a\Big(\frac{c}{\lambda_1} + 2\Big) + a\Big(\frac{\varepsilon}{a}\Big)^{\delta_1} - \frac{\alpha}{D\lambda_3^2+\eta}\Big(\frac{D\lambda_3^2}{\eta(\delta_1-\delta_2)} + \frac{\lambda_1-\lambda_3}{\mu_3\lambda_1}\Big) \\ &+ \frac{\alpha D\lambda_3^2}{\eta(D\lambda_3^2+\eta)}\Bigg[\frac{1}{\delta_1-\delta_2}\Big(\frac{\varepsilon}{a}\Big)^{\delta_1-\delta_2} + \frac{D\lambda_3^2}{\eta(\delta_1-\delta_3)}\Big(\Big(\frac{\varepsilon}{a}\Big)^{\delta_1-\delta_2} - \Big(\frac{\varepsilon}{a}\Big)^{\delta_3-\delta_2}\Big) + \frac{\lambda_1-\lambda_3}{\mu_3\lambda_1}\frac{D\lambda_3^2}{\eta}\Big(\frac{\varepsilon}{a}\Big)^{\delta_3-\delta_2}\Bigg] \end{aligned} \tag{A.42}$$

where $\delta_1, \delta_1-\delta_2, \delta_3-\delta_2 > 0$, and $a \in (\varepsilon, 1-\frac{\alpha}{\eta})$, which is necessary for the existence of a front connecting the two steady states as mentioned in Section 2.1.

A.3.5.2 Existence and uniqueness

In the singular limit of $\varepsilon = 0$ in (A.42), we obtain the corresponding singular orbit by $F_0 = 0$, which gives us an explicit expression for a as a function of c, that reads

$$a_0(c_0) = (1-\frac{\alpha}{\eta})\frac{\lambda_1}{\lambda_1-\lambda_2} - \frac{\alpha}{\eta}\frac{1}{(\lambda_1-\lambda_2)(\lambda_3-\lambda_4)}\Big[\frac{\lambda_3}{\mu_4}(\lambda_2-\lambda_4) - \frac{\lambda_4}{\mu_3}(\lambda_1-\lambda_3)\Big] \tag{A.43}$$

which corresponds to the existence of the singular orbit Γ, and can be verified the general patching method of Equation (A.19) without cut-off, for details see [74].

For ε positive and small, the existence of the function F_ε, we obtain $\frac{\partial F_\varepsilon}{\partial a}$,

$$\begin{aligned}\frac{\partial F_\varepsilon}{\partial a} =&(1-\delta_1)\Big(\frac{\varepsilon}{a}\Big)^{\delta_1} - \frac{c}{\lambda_1} - 2 + \frac{\alpha D\lambda_3^2}{\eta(D\lambda_3^2+\eta)}\frac{1}{a}\Bigg[- \Big(\frac{\varepsilon}{a}\Big)^{\delta_1-\delta_2} + \frac{D\lambda_3^2}{\eta}\Bigg(\frac{\delta_2-\delta_1}{\delta_1-\delta_3}\Big(\frac{\varepsilon}{a}\Big)^{\delta_1-\delta_2} - \frac{\delta_2-\delta_3}{\delta_1-\delta_3}\Big(\frac{\varepsilon}{a}\Big)^{\delta_3-\delta_2}\Bigg)\\ &+ \frac{\lambda_1-\lambda_3}{\mu_3\lambda_1}\frac{D\lambda_3^2}{\eta}(\delta_2-\delta_3)\Big(\frac{\varepsilon}{a}\Big)^{\delta_3-\delta_2}\Bigg]\end{aligned}$$

where we numerically find that $\frac{\partial F_\varepsilon}{\partial a}|_{(a^*,c^*,\varepsilon)} \neq 0$, where the values of (a^*, c^*, ε) satisfy the constraint $F_\varepsilon(a^*, c^*, \varepsilon) = 0$. According to the Implicit Function Theorem, there exists a unique function $a = a(c, \varepsilon)$ that satisfies $F_\varepsilon(a(c, \varepsilon), c, \varepsilon) = 0$.

Finally, we can approximate the position of the saddle-node bifurcation point on the curve $\{F_\varepsilon = 0\}$ by solving $\frac{da}{dc} = \frac{\frac{\partial F_\varepsilon}{\partial c}}{\frac{\partial F_\varepsilon}{\partial a}} = 0$. As $\frac{\partial F_\varepsilon}{\partial a}$ is nonzero, by the above, we only need to compute $\frac{\partial F_\varepsilon}{\partial c} = 0$, under the constraint that $F_\varepsilon = 0$.

$$\begin{aligned}\frac{\partial F_\varepsilon}{\partial c} =&a\Bigg[\delta_1'\Big(\frac{\varepsilon}{a}\Big)^{\delta_1}\ln\Big(\frac{\varepsilon}{a}\Big) - \frac{1}{\lambda_1} + \frac{c}{\lambda_1^2}\lambda_1'\Bigg] + \frac{\alpha(-\delta_2'(D\lambda_3^2+\eta) - 2D\lambda_3\lambda_3')}{(D\lambda_3^2+\eta)^2}\Bigg[\frac{D\lambda_3^2}{\eta(\delta_1-\delta_2)}\Bigg(\Big(\frac{\varepsilon}{a}\Big)^{\delta_1-\delta_2} - 1\Bigg)\\ &+ \frac{D^2\lambda_3^4}{\eta^2(\delta_1-\delta_3)}\Bigg(\Big(\frac{\varepsilon}{a}\Big)^{\delta_1-\delta_2} - \Big(\frac{\varepsilon}{a}\Big)^{\delta_3-\delta_2}\Bigg) + \frac{\lambda_1-\lambda_3}{\mu\lambda_1}\Bigg(\frac{D^2\lambda_3^4}{\eta^2}\Big(\frac{\varepsilon}{a}\Big)^{\delta_3-\delta_2} - 1\Bigg)\Bigg]\\ &+ \frac{\alpha}{D\lambda_3^2+\eta}\Bigg[\frac{2D\lambda_3\lambda_3'}{\eta(\delta_1-\delta_2)}\Bigg(\Big(\frac{\varepsilon}{a}\Big)^{\delta_1-\delta_2} - 1\Bigg) + \frac{4D^2\lambda_3^3\lambda_3'}{\eta^2(\delta_1-\delta_3)}\Bigg(\Big(\frac{\varepsilon}{a}\Big)^{\delta_1-\delta_2} - \Big(\frac{\varepsilon}{a}\Big)^{\delta_3-\delta_3}\Bigg)\\ &+ \frac{(\lambda_1'-\lambda_3')\mu_3\lambda_1 - (\lambda_1-\lambda_3)(\mu_3'\lambda_1+\mu_3\lambda_1')}{\mu_3^2\lambda_1^2}\Bigg(\frac{D^2\lambda_3^4}{\eta^2}\Big(\frac{\varepsilon}{a}\Big)^{\delta_3-\delta_2} - 1\Bigg)\\ &+ \frac{D\lambda_3^2}{\eta((\delta_1-\delta_2)^2)}\Bigg((\delta_1-\delta_2)(\delta_1'\Big(\frac{\varepsilon}{a}\Big)^{\delta_1} - \delta_2'\Big(\frac{\varepsilon}{a}\Big)^{\delta_2})\ln\Big(\frac{\varepsilon}{a}\Big) - (\Big(\frac{\varepsilon}{a}\Big)^{\delta_1} - \Big(\frac{\varepsilon}{a}\Big)^{\delta_2})(\delta_1'-\delta_2')\Bigg)\\ &+ \frac{D^2\lambda_3^4}{\eta^2(\delta_1-\delta_3)^2}\Bigg((\delta_1-\delta_3)(\delta_1'\Big(\frac{\varepsilon}{a}\Big)^{\delta_1} - \delta_3'\Big(\frac{\varepsilon}{a}\Big)^{\delta_3})\ln\Big(\frac{\varepsilon}{a}\Big) - (\Big(\frac{\varepsilon}{a}\Big)^{\delta_1} - \Big(\frac{\varepsilon}{a}\Big)^{\delta_3})(\delta_1'-\delta_3')\Bigg)\\ &+ \frac{\lambda_1-\lambda_3}{\mu_3\lambda_1}\Bigg(\frac{4D^2\lambda_3^3\lambda_3'}{\eta^2}\Big(\frac{\varepsilon}{a}\Big)^{\delta_3} + \frac{D^2\lambda_3^4}{\eta^2}\delta_3'\Big(\frac{\varepsilon}{a}\Big)^{\delta_3}\ln\Big(\frac{\varepsilon}{a}\Big) - \delta_2\Big(\frac{\varepsilon}{a}\Big)^{\delta_2}\ln\Big(\frac{\varepsilon}{a}\Big)\Bigg)\Bigg]\end{aligned}$$

where $'$ denotes the derivative to c. The above expression is too complicated to allow for an analytic solution; hence, we will evaluate it numerically in Section A.3.7 below.

A.3.5.3 Valid speed range

The dynamics of u-component cut-off system is best studied in an equivalent formulation of Equation (2.4) with $\phi = u$ that results from a blow-up transformation of the corresponding vector field near the origin in $(u, v, w, z, \varepsilon)$-space. The approach follows the same process as those we have derived for v-component cut-off system. Hence, we do not show the repeated analysis; for details see Appendix A.3. Note that, we also keep the symbols for basic notations for the sake of simplicity, e.g., we reuse A_i, C_i $(i = 1, 2, 3)$ denoting the corresponding coefficients in the analysis of u-component cut-off system.

As we have observed in Section 2.2.3, it requires an extra condition on applying the blow-up technique so that the value of v stays in a neighborhood of the origin. To that end, we define a valid range of speed consists of a maximum and a minimum speed.

The maximum speed c follows the same idea as we have given in v-component cut-off; see Section 2.4.2.3. Recall the definition of the region II, i.e., $u \in (\varepsilon, a)$ and $a \in [\varepsilon, 1 - \frac{\alpha}{\eta}]$, which is necessary for the existence of a front connecting the two steady states as mentioned in Section 2.1. we can approximate the maximum speed by substituting $\frac{a}{\varepsilon} \equiv 1$ in the c-a relation F_ε in

Equation A.42, which is an explicit formula obtained by formal linearisation patching, i.e., the region II is eliminated and the transition time $\tau = \tau^* = 0$, then we obtain an equation $F_{c1} = \varepsilon$, where

$$F_{c1} := \frac{\alpha c}{4\eta^2} \frac{(c - \sqrt{c^2+4})(c - \sqrt{c^2+4D\eta})(c - Dc + D\sqrt{c^2+4} - \sqrt{c^2+4D\eta})}{c(D-1)(c - \sqrt{c^2+4D\eta}) - 2D\eta + 2D^2} + \frac{1}{4}(1 - \frac{\alpha}{\eta})(c - \sqrt{c^2+4})^2 \tag{A.44}$$

where the value of c_{max} satisfies $F_{c1}|_{c=c_{max}} = \varepsilon$.

The minimum speed is defined to ensure the value of v stays at least in a neighborhood around the origin. Here, we define a "small" quantity σ, which is a constant or a function in dependent on ε; if the value of v at the cut-off threshold $u = \varepsilon$ satisfies the inequality: $v|_{u=\varepsilon} \leqslant \sigma$, then, we treat this point of $(u, v)|_{u=\varepsilon}$ as a neighborhood at the origin. Transferring this inequality into the equivalent blown-up space in chart K_1, i.e. $v = v_1 r_1$ with $u = r_1$, we obtain that $v_1^{\text{out}} r_1^{\text{out}} \leqslant \sigma$; note that, $v_1^{\text{out}} = -\frac{D}{c} A_3$ is defined in Σ_1^{out} of (A.40), and the solution of A_3 is given in (A.41). Hence, the desired formula of $v\,(= v_1^{\text{out}} r_1^{\text{out}})$ is labeled by $F_{c2} = \sigma$:

$$F_{c2} := -\frac{D\,\alpha}{c\sqrt{c^2 + 4\,D\,\eta}} \left(\frac{\left(c - \sqrt{c^2 + 4\,D\,\eta}\right)^4}{16\,D^3\,\eta^2} - 1 \right) \left(\frac{\varepsilon}{a}\right)^{\frac{c+\sqrt{c^2+4\,D\,\eta}}{D\,(c+\sqrt{c^2+4})}}, \tag{A.45}$$

where the values of c and a are obtained by the corresponding speed relation $F_\varepsilon = 0$ in (A.42).

The minimum speed c_{min} satisfied the above equation $F_{c2} = \sigma$; the speed in a range of $c \geqslant c_{min}$ will support the application of blow-up technique in u-component cut-off system. We note here, $\lambda_i\,(i = 1, ...4)$ are as defined in Lemma 2.1.

In all, the valid speed range for u-component cut-off system via the blow-up technique is represented by $(c_{min},\, c_{max})$, where $F_{c1}|_{c=c_{max}} = \varepsilon$ and $F_{c2}|_{c=c_{min}} = \sigma$ with $F_\varepsilon = 0$.

A.3.6 Second-order normal form

In the formal linearisation that resulted in Equation (A.36), we neglected terms of higher order in (v_1, W, z_1). Next, we perform a normal form transformation, which will allow us to eliminate all quadratic terms from Equation (A.37):

Proposition A.1. *Let*

$$\beta = (D-1)c\big(c + \sqrt{c^2+4}\big) + 2(D - \eta) \quad \textit{and} \quad \gamma = \sqrt{c^2+4}\big(c + \sqrt{c^2+4}\big);$$

then, the near-identity transformation

$$\begin{aligned}
v_1 &= \tilde{v}_1 + \frac{4D}{\beta\gamma}\tilde{z}^2 - \frac{2\big[D\sqrt{c^2+4} + c(D-2)\big]}{\beta\gamma}\tilde{v}_1\tilde{z}_1 + \frac{2}{\gamma}\widetilde{W}\tilde{z}_1,\\
W &= \widetilde{W} - \frac{2\big[D\sqrt{c^2+4} + c(D-2)\big]}{\beta\gamma}\tilde{v}_1^2 - \frac{c - \sqrt{c^2+4}}{\gamma}\widetilde{W}^2 + \frac{2\big[cD(c+\sqrt{c^2+4}) - 2(c^2-\eta)\big]}{\beta\gamma}\tilde{v}_1\widetilde{W}\\
&\quad + \frac{4D}{\beta\gamma}\tilde{v}_1\tilde{z}_1 - \frac{2D\big(c - \sqrt{c^2+4}\big)}{\beta\gamma}\widetilde{W}\tilde{z}_1,\\
z_1 &= \tilde{z}_1 - \frac{2\eta\big[D\sqrt{c^2+4} + c(D-2)\big]}{D\beta\gamma}\tilde{v}_1^2 - \frac{4c}{\beta\gamma}\tilde{z}_1^2 + \frac{2\eta}{D\gamma}\tilde{v}_1\widetilde{W} + \frac{2\big[cD(c+\sqrt{c^2+4}) - 2(c^2+D\eta)\big]}{D\beta\gamma}\tilde{v}_1\tilde{z}_1\\
&\quad - \frac{2c}{D\gamma}\widetilde{W}\tilde{z}_1
\end{aligned}$$

transforms Equation (A.37) *into*

$$\tilde{v}_1' = \tilde{v}_1 + \frac{2}{c+\sqrt{c^2+4}}\tilde{z}_1 + \mathcal{O}(3), \tag{A.46a}$$

$$\widetilde{W}' = \frac{2}{c+\sqrt{c^2+4}}\tilde{v}_1 + \frac{2\sqrt{c^2+4}}{c+\sqrt{c^2+4}}\widetilde{W} + \mathcal{O}(3), \tag{A.46b}$$

$$\tilde{z}_1' = \frac{\eta}{D}\frac{2}{c+\sqrt{c^2+4}}\tilde{v}_1 + \Big(1 - \frac{2}{D}\frac{c}{c+\sqrt{c^2+4}}\Big)\tilde{z}_1 + \mathcal{O}(3). \tag{A.46c}$$

Proof. We make the Ansatz analogous as those in Section 2.4.4 of v-component cut-off system, details are omitted here. □

The obtained second-order normal form transformation allows us to eliminate the quadratic terms, which improves the accuracy of the approximation in Equation (A.37); in particular, the results obtained by the new system (A.46) will also be improved. To that end, the derivation follows the same process as the formal linearisation pathing in Section A.3.5. Firstly, we invert the transformation as following

$$\begin{aligned}
\tilde{v}_1 &= v_1 - \frac{4D}{\beta\gamma}z_1^2 + \frac{2\big[D\sqrt{c^2+4}+c(D-2)\big]}{\beta\gamma}v_1z_1 - \frac{2}{\gamma}Wz_1 + \mathcal{O}(3),\\
\widetilde{W} &= W + \frac{2\big[D\sqrt{c^2+4}+c(D-2)\big]}{\beta\gamma}v_1^2 + \frac{c-\sqrt{c^2+4}}{\gamma}W^2 - \frac{2\big[cD(c+\sqrt{c^2+4})-2(c^2-\eta)\big]}{\beta\gamma}v_1W\\
&\quad - \frac{4D}{\beta\gamma}v_1z_1 + \frac{2D\big(c-\sqrt{c^2+4}\big)}{\beta\gamma}Wz_1 + \mathcal{O}(3),\\
\tilde{z}_1 &= z_1 + \frac{2\eta\big[D\sqrt{c^2+4}+c(D-2)\big]}{D\beta\gamma}v_1^2 + \frac{4c}{\beta\gamma}z_1^2 - \frac{2\eta}{D\gamma}v_1\ W - \frac{2\big[cD(c+\sqrt{c^2+4})-2(c^2+D\eta)\big]}{D\beta\gamma}v_1z_1\\
&\quad + \frac{2c}{D\gamma}Wz_1 + \mathcal{O}(3)
\end{aligned}$$

Then, we transform the boundary conditions at $P_{\varepsilon 1}^{\text{in}}$ and $P_{\varepsilon 1}^{\text{out}}$ of (A.35) in section Σ_1^{in} and Σ_1^{out} into $\widetilde{P}_{\varepsilon 1}^{\text{in}}$ and $\widetilde{P}_{\varepsilon 1}^{\text{out}}$ in section $\widetilde{\Sigma}_1^{\text{in}}$ and $\widetilde{\Sigma}_1^{\text{out}}$ for our second-order normal form patching:

$$\widetilde{P}_{\varepsilon 1}^{\text{in}} := \big(a, \tilde{v}_1^{\text{in}}, \widetilde{W}^{\text{in}}, \tilde{z}_1^{\text{in}}, \frac{\varepsilon}{a}\big) \text{ at } \tau = 0 \tag{A.47a}$$

$$\widetilde{P}_{\varepsilon 1}^{\text{out}} := \big(\varepsilon, \tilde{v}_1^{\text{out}}, \widetilde{W}^{\text{out}}, \tilde{z}_1^{\text{out}}, 1\big) \text{ at } \tau^* = \ln\frac{a}{\varepsilon}, \tag{A.47b}$$

where the transformed boundaries in $(\tilde{v}_1, \widetilde{W}, \tilde{z}_1)$-variables after eliminating higher order terms are detailed in Appendix A.3.9.

We can determine the related new coefficients A_i, C_i $(i = 1, 2, 3)$ in the general solution of Equation (2.59) with the $\mathcal{O}(3)$-terms omitted, by patching at the boundaries between two sections $\widetilde{\Sigma}_1^{\text{in}}$ and $\widetilde{\Sigma}_1^{\text{out}}$ at the points of intersection $\widetilde{P}_{\varepsilon 1}^{\text{in}}$ and $\widetilde{P}_{\varepsilon 1}^{\text{out}}$, i.e., we solve the particular solution with specific boundary condition (A.47) in $(\tilde{u}, \tilde{w}, \tilde{z})$, which completes the construction of the orbit $\widetilde{\Gamma}_1$ in chart K_1; here, $\widetilde{\Gamma}_1$ denotes the approximation to the general solution of (2.59) by the second-order normal form patching; as for details on the patching process, see Appendix A.3.9; there, we then obtain two equations $\widetilde{F}_{\varepsilon_i} = 0\,(i = 1, 2)$ in dependence on (a, A_1, c, ε). The results of the c-a relation by the second-order normal form patching is labeled by $\widetilde{F}_\varepsilon$.

We prove the existence by following the same procedure for $a_\varepsilon(c)$ in Section 2.4, which is equivalent to proving that we can get the unique solution from the two constraints $\widetilde{F}_{\varepsilon_i} = 0\,(i = 1, 2)$ by applying the Implicit Function Theorem. We find similar results as well, i.e., the persistence of $\widetilde{F}_\varepsilon$ for $\varepsilon > 0$ small will be obtained by the Implicit Function Theorem.

A.3.7 Numerical simulation

In this section, we present the numerical simulations of the obtained speed relation F_ε and $\widetilde{F}_\varepsilon$ defined in (A.42) and (A.59), respectively, by formal linearisation and the second-order normal

form in Sections A.3.5 and A.3.6, respectively. We also display the c-a relation obtained by the general patching, labeled G_ε, are obtained by matching the general solution at the patching points: connecting regions I and II, and regions II and III, respectively, for the sake of the continuity of the general solution in each region in the original ODE system; for details we refer to Appendix A.3.8.

A.3.7.1 Simulation of F_ε

We first compute the result of F_ε obtained by formal linearisation in Section A.3.5, in a range of values for the cut-off threshold ε in Figure A.5, where $\varepsilon = 0.1$, 0.05, 0.001 and $\varepsilon = 0$ for the values of $D = 1, 2, 5$ and $D = 10$. In the limit of $\varepsilon = 0$ (solid black), the upper branches of the curves show that the speed c grows as a decreases and may reach infinity when $a \to 0$; in particular, for $D = 1$, 2 and $D = 5$, one saddle-node bifurcation occurs in agreement with the study of bifurcation scenarios in Section 2.4.3, which admit the existence of a neutrally stable front at the bifurcation [57]. Moreover, we find the curves would go across the horizontal line axis to negative values of the speed c, which should be considered in a symmetric situation; here, we only consider $c > 0$.

For D fixed, e.g., $D = 1$, the valid range of the speed c becomes wider as $\varepsilon \to 0$, i.e., the value of c_{max} increases by decreasing ε, the same phenomenon occurs for $D = 2$, 5, 10, in agreement with the definition of c_{max} in Equation (A.44) in Section A.3.5.3. The fit of the perturbed curves to the singular curve improves as ε decreases; in particular, for ε sufficiently small, e.g. $\varepsilon = 0.001$ (dotted magenta), the perturbed curves persist to the corresponding singular one, while for $\varepsilon = 0.1$ (dash-dotted blue) and $\varepsilon = 0.05$ (dashed red) with D large, e.g. $D = 5$ or $D = 10$, in a range of the speed, e.g. $c \in (0, 1)$, the bad performance suggests that our blow-up patching fails in that speed range. Recall the valid speed range of (c_{min}, c_{max}) in Section A.3.5.3, here, we approximate the values of c_{min} and c_{max} by setting $\sigma = \varepsilon$ for easy computation; the corresponding valid speed range see Table A.1.

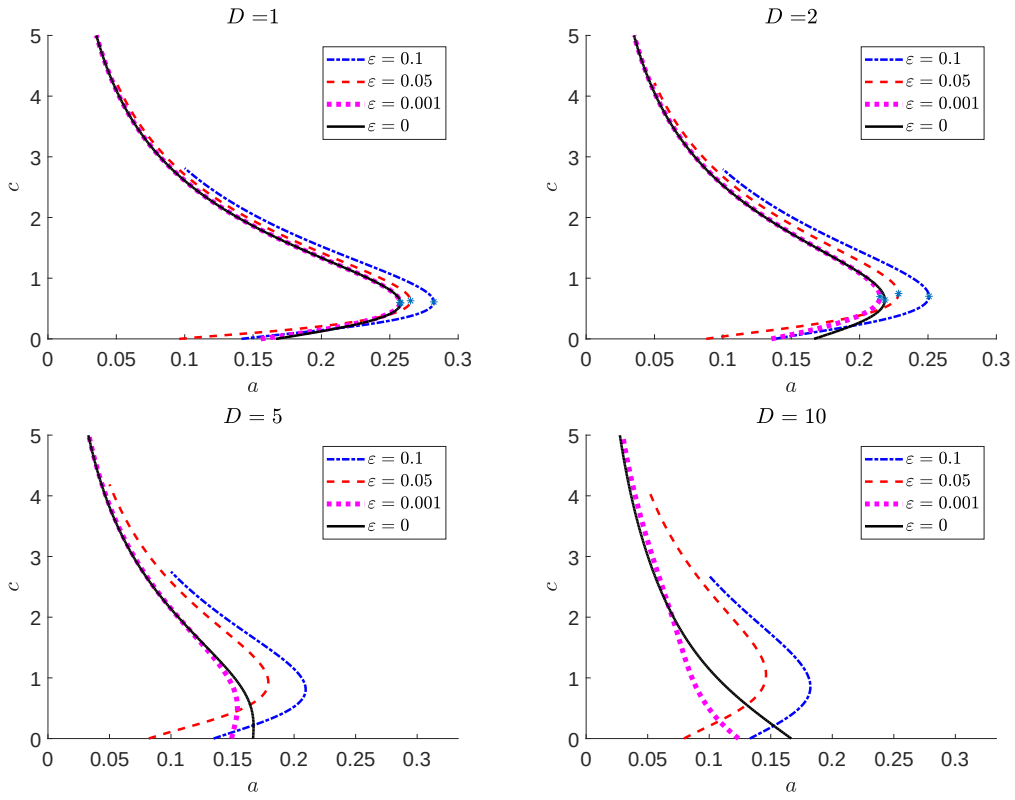

Figure A.5: Speed relation obtained by formal linearisation patching F_ε, for $D = 1, 2, 5, 10$, with $\varepsilon = 0.1, 0.05, 0.001$ and $\varepsilon = 0$, for fixed $\eta = 0.12$, $\alpha = 0.08$.

.

Table A.1: Approximated valid speed range (c_{min}, c_{max}), for $D = 1, 2, 5$ and $D = 10$ with $\varepsilon = 0.01,\ 0.05,\ 0.01$, and $\sigma = \varepsilon$, for fixed $\eta = 0.12$, $\alpha = 0.08$

ε	0.1	0.05	0.01
$D = 1$	(0.5050, 2.8136)	(0.6302, 4.2291)	(0.8766, 9.8919)
$D = 2$	(0.8677, 2.8005)	(1.1870, 4.2191)	(2.1936, 9.8878)
$D = 5$	(1.6132, 2.7507)	(2.4080, 4.1885)	(5.5943, 9.8755)
$D = 10$	(2.4176, 2.6570)	(3.6717, 4.1349)	(8.7047, 9.8548)

We approximately compute the values at bifurcation points via solving equations $F_\varepsilon = 0$ and $\partial F_\varepsilon / \partial c = 0$, for $\varepsilon = 0.1,\ 0.05$ and $\varepsilon = 0.001$; see Table A.2. For $D = 1, 2$ and $D = 5$, we find that the perturbed bifurcation approaches the corresponding singular one as $\varepsilon \to 0$; note that, no bifurcation exists for $D = 10$.

Table A.2: Approximated bifurcation points (a_b, c_b) obtained by formal linearisation patching F_ε, for $D = 1, 2, 5$ with $\varepsilon = 0.1,\ 0.05,\ 0.001$ and $\varepsilon = 0$, for fixed $\eta = 0.12$, $\alpha = 0.08$

ε	0.1	0.05	0.001	0
$D = 1$	$(0.2822, 0.6094)$	$(0.2651, 0.6276)$	$(0.2574, 0.5985)$	$(0.2579, 0.5915)$
$D = 2$	$(0.2507, 0.7014)$	$(0.2289, 0.7464)$	$(0.2149, 0.6949)$	(0.2185,0.6407)
$D = 5$	$(0.2094, 0.8101)$	$(0.1791, 0.9267)$	$(0.2149, 0.6949)$	(0.1430,0.9212)

A.3.7.2 Comparison of F_ε and G_ε

In this section, we compare the results of F_ε and G_ε, which are obtained by formal linearisation patching and general patching with $D = 1, 2, 5, 10$ and $\varepsilon = 0.01,\ 0.05,\ 0.001$; see Figure A.6. The solid red curves correspond to the results of F_ε by formal linearisation patching; the dash-dotted blue curves describe the results of G_ε by general patching; while the thin black curves represent the corresponding singular solutions. The small rectangular area along the curves is zoomed-in to the bottom left axes.

We find that the formal linearisation patching results F_ε match the general patching solution G_ε well above the bifurcation point, where the error between them is $\mathcal{O}(\varepsilon^2)$, i.e. both methods perform well for stable fronts, while for $\varepsilon = 0.1$ (dash-dotted blue) and $\varepsilon = 0.05$ (dashed red) with D large, e.g. $D = 5$ or $D = 10$, in a range of the speed, e.g. $c \in (0, 1)$, the bad performance suggests the valid speed range of $\big(c_{min}, c_{max}\big)$ in Section A.3.5.3, approximated values of c_{min} and c_{max} by setting $\sigma = \varepsilon$, see Table A.1. The bad performance of general patching G_ε may due to the computation limitation.

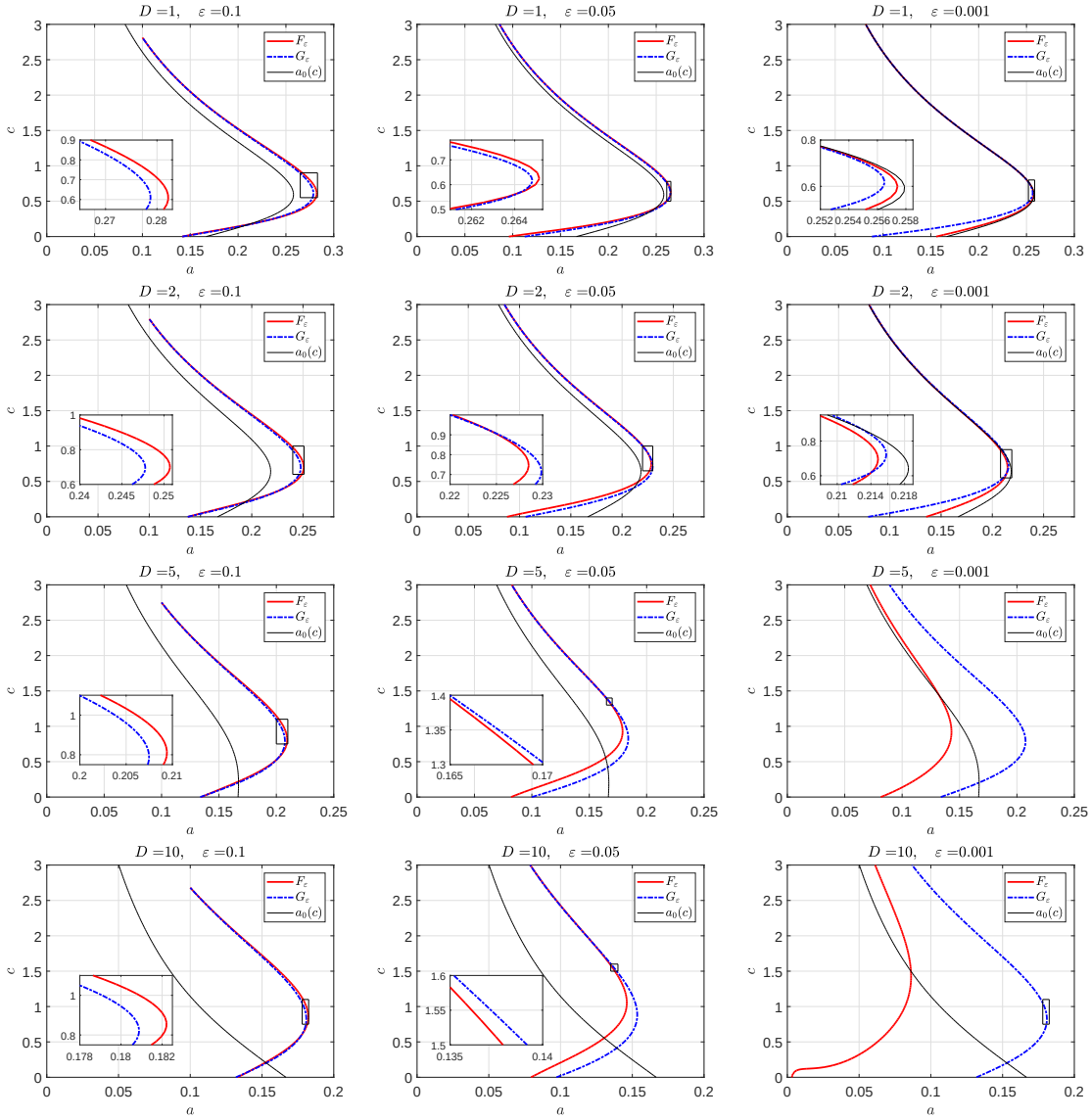

Figure A.6: Speed relation obtained by formal linearisation patching F_ε, general patching G_ε and the singular limit $a_0(c)$, for $D = 1, 2, 5, 10$ with $\varepsilon = 0.01,\ 0.05,\ 0.001$, for fixed $\eta = 0.12, \alpha = 0.08$; here, the small rectangular area is zoomed-in to the bottom left axes.

A.3.7.3 Simulation of $\widetilde{F}_\varepsilon$

We approximate the solutions of the equations $\widetilde{F}_{\varepsilon_i} = 0\,(i = 1, 2)$ in (A.59), which are obtained by the second order normal form transformation patching. Then compare the results with those obtained by formal linearisation patching and the general patching as well; see Figure A.7. We find that the second order normal form patching provides a better fit to the general patching than the formal linearisation for $\varepsilon = 0.1$ and $\varepsilon = 0.05$, as the maximum error is much smaller around the bifurcation, which seems to be $\mathcal{O}(\varepsilon^3)$. When ε is decreasing, the second-order normal form patching is time-consuming that the formal linearisation patching would provide a qualitative approximation to the results of general patching. Moreover, there might be some computation limitation around the bifurcation node and below, which are omitted here.

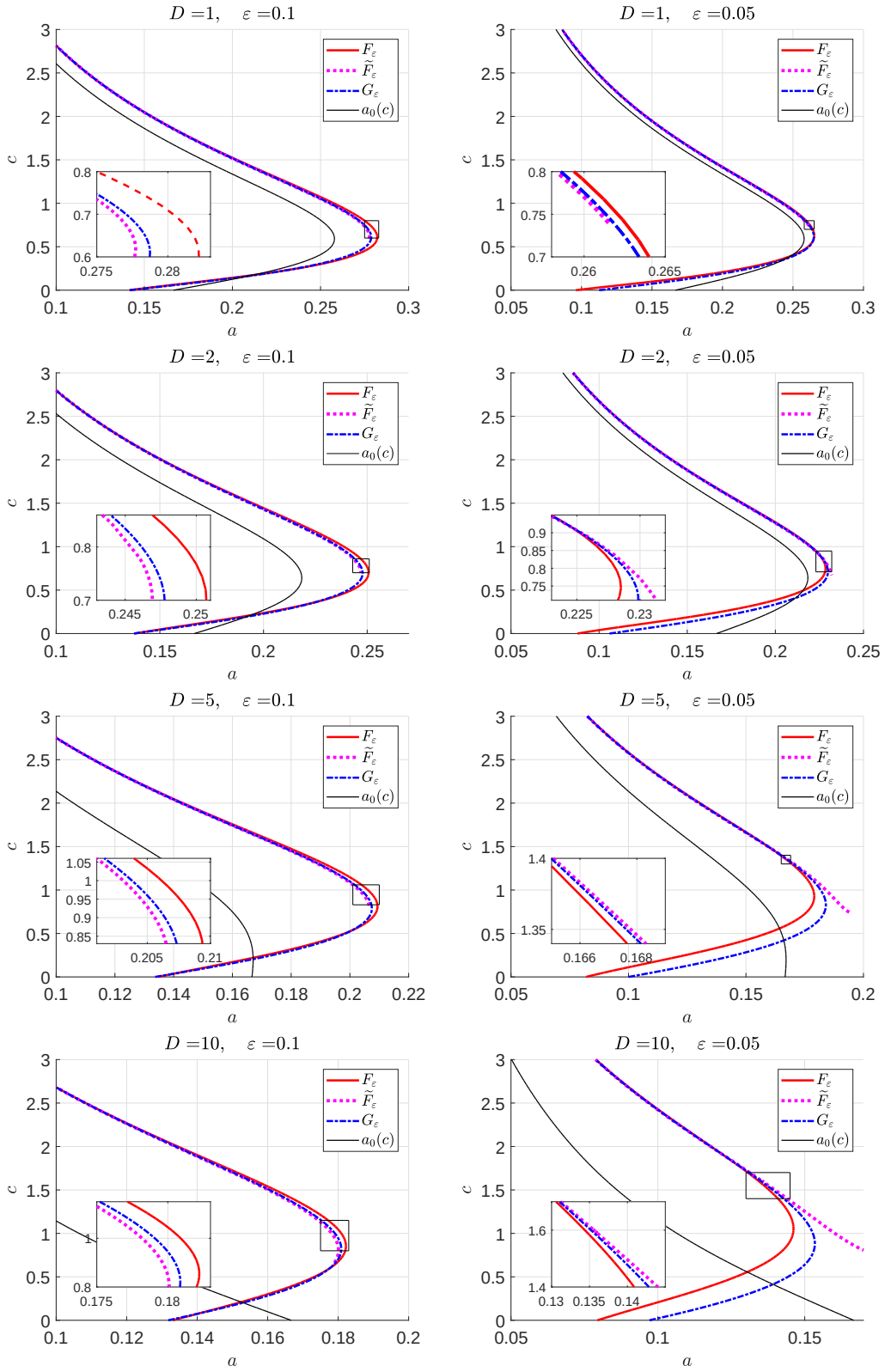

Figure A.7: Speed relation obtained by formal linearisation patching F_ε (solid red), second-order normal form $\widetilde{F}_\varepsilon$ (dotted magenta), general patching G_ε (dash-dotted blue) and the singular limit $a_0(c)$ (solid black), for $D = 1, 2, 5, 10$ with $\varepsilon = 0.1, 0.05$, for fixed $\eta = 0.12, \alpha = 0.08$; here, the small rectangular area is zoomed-in to the bottom left axes.

A.3.7.4 The effect of the cut-off

From the numerical simulation of the results among the three methods: the formal linearisarion patching method, the second-order normal form transformation patching method and the general patching method for Equation (A.19), we observe that the cutoff prevents u-variable reacting in the negative region for $\varepsilon > 0$ small, so that the front profiles are shifted to the positive region in (u, v)-variables. Moreover, as in the singular limit case by the general patching method, the speed may grow to infinity as a tends to 0, the cutoff also prevents unlimited speed, where the maximum value of speed decreases as the cutoff threshold ε increases at fixed discontinuity position a, i.e. speed range gets smaller as ε increases.

A.3.8 General patching

We consider the travelling front solutions propagating from Q^- when $\xi \to -\infty$ to Q^+ when $\xi \to +\infty$. The general solutions for this problem in the regions can be written as follows:
In region I: $u \geqslant a$ and $v \geqslant \varepsilon$, for $\xi \leqslant \xi_0$

$$u_{g_1}(\xi) = A_2 e^{\lambda_1 \xi} + \frac{A_1}{\mu_3} e^{\lambda_3 \xi} + 1 - \alpha/\eta, \tag{A.48a}$$

$$v_{g_1}(\xi) = A_1 e^{\lambda_3 \xi} + \alpha/\eta. \tag{A.48b}$$

$$w_{g_1}(\xi) = \lambda_1 A_2 e^{\lambda_1 \xi} + \frac{\lambda_3}{\mu_3} A_1 e^{\lambda_3 \xi}, \tag{A.48c}$$

$$z_{g_1}(\xi) = \lambda_3 A_1 e^{\lambda_3 \xi} \tag{A.48d}$$

In region II: $\varepsilon \leqslant u \leqslant a$, for $\xi_0 \leqslant \xi \leqslant \xi^*$

$$u_{g_2}(\xi) = A_{21} e^{\lambda_1 \xi} + A_{22} e^{\lambda_2 \xi} + \frac{B_{23}}{\mu_3} e^{\lambda_3 \xi} + \frac{B_{24}}{\mu_4} e^{\lambda_4 \xi}, \tag{A.49a}$$

$$v_{g_2}(\xi) = B_{23} e^{\lambda_3 \xi} + B_{24} e^{\lambda_4 \xi}, \tag{A.49b}$$

$$w_{g_2}(\xi) = \lambda_1 A_{21} e^{\lambda_1 \xi} + \lambda_2 A_{22} e^{\lambda_2 \xi} + \frac{\lambda_3}{\mu_3} B_{23} e^{\lambda_3 \xi} + \frac{\lambda_4}{\mu_4} B_{24} e^{\lambda_4 \xi}, \tag{A.49c}$$

$$z_{g_2}(\xi) = \lambda_3 B_{23} e^{\lambda_3 \xi} + \lambda_4 B_{24} e^{\lambda_4 \xi}. \tag{A.49d}$$

In region III: $u \leqslant \varepsilon$, for $\xi \geqslant \xi^*$

$$u_{g_3}(\xi) = A_0 e^{-c\xi}, \tag{A.50a}$$

$$v_{g_3}(\xi) = B_0 e^{-\frac{c}{D}\xi}, \tag{A.50b}$$

$$w_{g_3}(\xi) = -c A_0 e^{-c\xi}, \tag{A.50c}$$

$$z_{g_3}(\xi) = -\frac{c}{D} B_0 e^{-\frac{c}{D}\xi} \tag{A.50d}$$

where $\lambda_{1,2} = \frac{-c \pm \sqrt{c^2+4}}{2}, \lambda_{3,4} = \frac{-c \pm \sqrt{c^2+4D\eta}}{2D}$, and $\mu_j = \lambda_j^2 + c\lambda_j - 1 \, (j = 3, 4)$.

Then we can solve for all coefficients A_{ij}, B_{ij} by patching the three regions together, using the conditions for continuity of functions, with two more constraints $u_{g_2}(\xi_0) = a$, $u_{g_2}(\xi^*) = \epsilon$.We obtain the front solutions explicitly, by choosing $\xi_0 = 0$ for simplicity.

All the coefficients are the same as in (A.5), while two constraints obtained at the patching points are $u_{g_2}(\xi_0) = a$, $u_{g_2}(\xi^*) = \varepsilon$, written as

$$G_{\varepsilon_1}(a, \xi^*, c, \varepsilon) := A_{21} + A_{22} - \frac{1}{\mu_3}\frac{\lambda_3}{\lambda_4} e^{(\lambda_4 - \lambda_3)\xi^*} \frac{\alpha/\eta}{1 - \frac{\lambda_4}{\lambda_3}} + \frac{1}{\mu_4} \frac{\alpha/\eta}{1 - \frac{\lambda_4}{\lambda_3}} - a = 0, \tag{A.51a}$$

$$G_{\varepsilon_2}(a, \xi^*, c, \varepsilon) := \big(\frac{\lambda_1}{\lambda_2} - 1\big) A_{22} \mathrm{e}^{\lambda_2 \xi^*} + \Big(\frac{\lambda_3 - \lambda_1}{\mu_3}\frac{\lambda_3}{\lambda_4} + \frac{\lambda_1 - \lambda_4}{\mu_4}\Big) \frac{\alpha/\eta}{1 - \frac{\lambda_4}{\lambda_3}} \frac{\mathrm{e}^{\lambda_4 \xi^*}}{\lambda_2} + \varepsilon = 0. \tag{A.51b}$$

Existence and uniqueness

In the singular limit defined as $\varepsilon = 0$ and $\xi^* \to \infty$ in Equation (A.51), we can obtain an explicit expression of $a(c_0, 0)$,

$$a(c_0,0) = (1-\frac{\alpha}{\eta})\frac{\lambda_1}{\lambda_1-\lambda_2} - \frac{\alpha}{\eta}\frac{1}{(\lambda_1-\lambda_2)(\lambda_3-\lambda_4)}\Big[\frac{\lambda_3}{\mu_4}(\lambda_2-\lambda_4) - \frac{\lambda_4}{\mu_3}(\lambda_1-\lambda_3)\Big] \tag{A.52}$$

which is also the result of the general patching method for singular system, for details see Appendix A.2 or [74]. In particular, the denominators $(\lambda_1 - \lambda_2)$, $(\lambda_3 - \lambda_3)$, μ_3 and μ_4 are well-defined; the existence of $a_0(c_0)$ has been proved in Section 2.4 as well.

To that end, we prove that there exists a unique solution from the two constraints $G_{\varepsilon_i}(c_0, 0) = 0\,(i = 1, 2)$ in (A.51) by applying the Implicit Function Theorem. We consider the Jacobian matrix with respect to a and ξ^* at $(c, \varepsilon) = (c, \varepsilon)$,

$$J = \begin{bmatrix} \frac{\partial G_{\varepsilon_1}}{\partial a} & \frac{\partial G_{\varepsilon_1}}{\partial \xi^*} \\ \frac{\partial G_{\varepsilon_2}}{\partial a} & \frac{\partial G_{\varepsilon_2}}{\partial \xi^*} \end{bmatrix} = \begin{bmatrix} -1 & \frac{\partial G_{\varepsilon_1}}{\partial \xi^*} \\ 0 & \frac{\partial G_{\varepsilon_2}}{\partial \xi^*} \end{bmatrix}, \text{ and } Det(J)\big|_{(a^*,\xi^*,c^*,\varepsilon)} = -\frac{\partial G_{\varepsilon_2}}{\partial \xi^*}$$

We compute the determinant of J for each solution $(a^*, \xi^*, c^*, \varepsilon)$, which satisfy $G_{\varepsilon_i} = 0\,(i = 1, 2)$ and find that J tends to a small nonzero limit for c large for $\varepsilon = 0.0001$. Then, we can say there exist a solution for these two equation (A.51), and there also exist a unique solution for G_ε by the Implicit Function Theorem, i.e., the persistence of G_ε for ε positive and small by the Implicit Function Theorem.

Numerical simulation

For the bifurcation result, we solve the two constraints (A.51) numerically and obtain the relation between speed c and discontinuity position a for the u-variable cut-off sigmoidal system, plotted with $D = 1, 2, 5, 10$ with $\varepsilon = 0.1, 0.05, 0.001$, see Figure A.8.

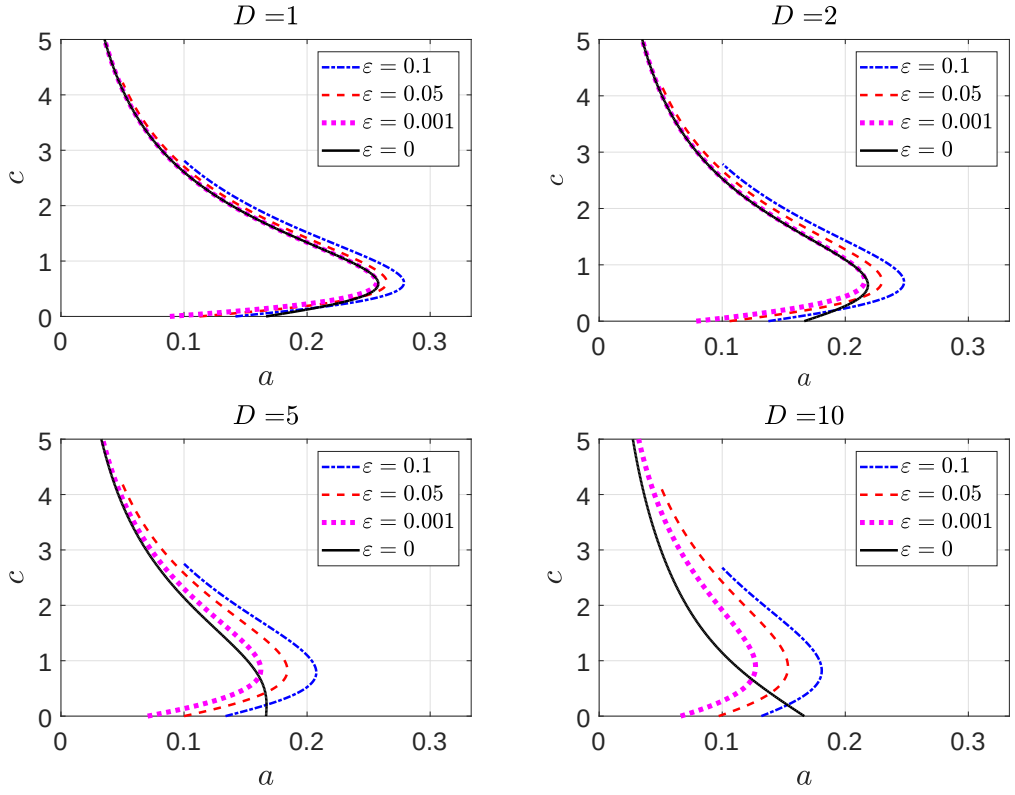

Figure A.8: Speed relation obtained by general patching G_ε, for $D = 1, 2, 5, 10$, with $\varepsilon = 0.1, 0.05, 0.001$ and $\varepsilon = 0$, for fixed $\eta = 0.12$, $\alpha = 0.08$.

A.3.9 Derivation of second-order normal form patching

Recall the transformed the boundaries $\widetilde{\Sigma}_1^{\text{in}}$ and $\widetilde{\Sigma}_1^{\text{out}}$ for our second-order normal form patching in (A.47), where $(\tilde{v}_1^{\text{in}}, \widetilde{W}^{\text{in}}, \tilde{z}_1^{\text{in}})$ has the form

$$\tilde{v}_1^{\text{in}} = v_1^{\text{in}} - \frac{4D}{\beta\gamma}(v_1^{\text{in}})^2 + \frac{2v_1^{\text{in}} z_1^{\text{in}}}{\beta\gamma}\Big[D\sqrt{c^2+4} + c(D-2)\Big] - \frac{2}{\gamma}\big(w_1^{\text{in}} - \lambda_2\big) z_1^{\text{in}}, \tag{A.53a}$$

$$\begin{aligned}\widetilde{W}^{\text{in}} = {} & w_1^{\text{in}} - \lambda_2 + \frac{2(v_1^{\text{in}})^2}{\beta\gamma}\Big[D\sqrt{c^2+4} + c(D-2)\Big] + \frac{c-\sqrt{c^2+4}}{\gamma}\big(w_1^{\text{in}} - \lambda_2\big)^2 \\ & - \frac{2\Big[cD(c+\sqrt{c^2+4}) - 2(c^2-\eta)\Big]}{\beta\gamma} v_1^{\text{in}}\big(w_1^{\text{in}} - \lambda_2\big) - \frac{4D}{\beta\gamma} v_1^{\text{in}} z_1^{\text{in}} \\ & + \frac{2D}{\beta\gamma}\big(c - \sqrt{c^2+4}\big)\big(w_1^{\text{in}} - \lambda_2\big) z_1^{\text{in}},\end{aligned} \tag{A.53b}$$

$$\begin{aligned}\tilde{z}_1^{\text{in}} = {} & z_1^{\text{in}} + \frac{2\eta(v_1^{\text{in}})^2}{D\beta\gamma}\Big[D\sqrt{c^2+4} + c(D-2)\Big] + \frac{4c}{\beta\gamma}(z_1^{\text{in}})^2 - \frac{2\eta}{D\gamma} v_1^{\text{in}}\big(w_1^{\text{in}} - \lambda_2\big) \\ & - \frac{2v_1^{\text{in}} z_1^{\text{in}}}{D\beta\gamma}\Big[cD(c+\sqrt{c^2+4}) - 2(c^2+D\eta)\Big] + \frac{2c}{D\gamma}\big(w_1^{\text{in}} - \lambda_2\big) z_1^{\text{in}}\end{aligned} \tag{A.53c}$$

and $(\tilde{v}_1^{\text{out}}, \widetilde{W}^{\text{out}}, \tilde{z}_1^{\text{out}})$ has the form

$$\tilde{v}_1^{\text{out}} = \Big[-\frac{D}{c} + \frac{c-\sqrt{c^2+4}}{\gamma}\Big] A_3 - \frac{2D^2}{\beta\gamma c}\big(c + \sqrt{c^2+4}\big) A_3^2 \tag{A.54a}$$

$$\begin{aligned}\widetilde{W}^{\text{out}} = {} & \Big[\frac{-c+\sqrt{c^2+4}}{2} + \frac{(c-\sqrt{c^2+4})^3}{4\gamma}\Big] - \frac{2D}{\beta\gamma c}\Big[2c(D+1) + \eta(c-\sqrt{c^2+4})\Big] A_3 \\ & + \frac{2D^3}{\beta\gamma c^2\sqrt{c^2+4}} A_3^2,\end{aligned} \tag{A.54b}$$

$$\begin{aligned}\tilde{z}_1^{\text{out}} = {} & \Big[1 + \frac{(-c+\sqrt{c^2+4})}{\gamma}\big(\frac{\eta}{c} + \frac{c}{D}\big)\Big] A_3 \\ & + \frac{2}{\beta\gamma c}\Big[D\eta(-c+\sqrt{c^2+4}) + c^2 D\eta(c+\sqrt{c^2+4}) + c(D-2)\Big] A_3^2\end{aligned} \tag{A.54c}$$

We then determine the coefficients $C_i, A_i (i = 1, 2, 3)$ by matching the boundaries in (A.47), which yields

$$\tilde{v}_1^{\text{out}} = -\frac{D\lambda_3}{\eta} C_2 \mathrm{e}^{\delta_2 \tau^*} + \frac{D\lambda_1\lambda_3}{\eta(\delta_1 - \delta_2)} C_3 \mathrm{e}^{\delta_3 \tau^*}, \tag{A.55a}$$

$$\widetilde{W}^{\text{out}} = C_1 \mathrm{e}^{\delta_1 \tau^*} + \frac{1}{\lambda_3} C_2 \mathrm{e}^{\delta_2 \tau^*} - \frac{\lambda_1}{\lambda_3(\delta_1 - \delta_3)} C_3 \mathrm{e}^{\delta_3 \tau^*} \tag{A.55b}$$

$$\tilde{z}_1^{\text{out}} = C_2 \mathrm{e}^{\delta_2 \tau^*} + C_3 \mathrm{e}^{\delta_3 \tau^*} \tag{A.55c}$$

$$\tilde{v}_1^{\text{in}} = -\frac{D\lambda_3}{\eta} C_2 + \frac{D\lambda_1\lambda_3}{\eta(\delta_1 - \delta_2)} C_3 \tag{A.55d}$$

$$\widetilde{W}^{\text{in}} = C_1 + \frac{1}{\lambda_3} C_2 - \frac{\lambda_1}{\lambda_3(\delta_1 - \delta_3)} C_3 \tag{A.55e}$$

$$\tilde{z}_1^{\text{in}} = C_2 + C_3 \tag{A.55f}$$

We obtain the explicit expressions of coefficients as following,

$$C_1 = \left(\widetilde{W}^{\text{out}} + \frac{\eta(\delta_1-\delta_2)\tilde{v}_1^{\text{out}} - D\lambda_1\lambda_3\tilde{z}_1^{\text{out}}}{D\lambda_3^2(\lambda_1+\delta_1-\delta_2)} + \frac{\lambda_1(\delta_1-\delta_2)(\eta\tilde{v}_1^{\text{out}} + D\lambda_3\tilde{z}_1^{\text{out}})}{D\lambda_3^2(\delta_1-\delta_3)(\lambda_1+\delta_1-\delta_2)}\right)\left(\frac{\varepsilon}{a}\right)^{\delta_1} \tag{A.56a}$$

$$C_2 = -\frac{\eta(\delta_1-\delta_2)\tilde{v}_1^{\text{out}} - D\lambda_1\lambda_3\tilde{z}_1^{\text{out}}}{D\lambda_3(\lambda_1+\delta_1-\delta_2)}\left(\frac{\varepsilon}{a}\right)^{\delta_2} \tag{A.56b}$$

$$C_3 = \frac{(\delta_1-\delta_2)(\eta\tilde{v}_1^{\text{out}} + D\lambda_3\tilde{z}_1^{\text{out}})}{D\lambda_3(\lambda_1+\delta_1-\delta_2)}\left(\frac{\varepsilon}{a}\right)^{\delta_3} \tag{A.56c}$$

$$A_2 = -\frac{A_1}{\mu} + a - 1 + \frac{\alpha}{\eta} \tag{A.56d}$$

where $\tilde{v}_1^{\text{out}}, \widetilde{W}^{\text{out}}, \tilde{z}_1^{\text{out}}$ are terms of order 2 in A_3. Then, Equation (A.55) reduce to

$$\tilde{v}_1^{\text{in}} = \frac{\eta(\delta_1-\delta_2)\tilde{v}_1^{\text{out}} - D\lambda_1\lambda_3\tilde{z}_1^{\text{out}}}{\eta(\lambda_1+\delta_1-\delta_2)}\left(\frac{\varepsilon}{a}\right)^{\delta_2} + \frac{\lambda_1(\eta\tilde{v}_1^{\text{out}} + D\lambda_3\tilde{z}_1^{\text{out}})}{\eta(\lambda_1+\delta_1-\delta_2)}\left(\frac{\varepsilon}{a}\right)^{\delta_3} \tag{A.57a}$$

$$\begin{aligned}\widetilde{W}^{\text{in}} =& \widetilde{W}^{\text{out}}\left(\frac{\varepsilon}{a}\right)^{\delta_1} + \frac{\eta(\delta_1-\delta_2)\tilde{v}_1^{\text{out}} - D\lambda_1\lambda_3\tilde{z}_1^{\text{out}}}{D\lambda_3^2(\lambda_1+\delta_1-\delta_2)}\Big[\left(\frac{\varepsilon}{a}\right)^{\delta_1} - \left(\frac{\varepsilon}{a}\right)^{\delta_2}\Big] \\ &+ \frac{\lambda_1(\delta_1-\delta_2)(\eta\tilde{v}_1^{\text{out}} + D\lambda_3\tilde{z}_1^{\text{out}})}{D\lambda_3^2(\delta_1-\delta_3)(\lambda_1+\delta_1-\delta_2)}\Big[\left(\frac{\varepsilon}{a}\right)^{\delta_1} - \left(\frac{\varepsilon}{a}\right)^{\delta_3}\Big]\end{aligned} \tag{A.57b}$$

$$\tilde{z}_1^{\text{in}} = -\frac{\eta(\delta_1-\delta_2)\tilde{v}_1^{\text{out}} - D\lambda_1\lambda_3\tilde{z}_1^{\text{out}}}{D\lambda_3(\lambda_1+\delta_1-\delta_2)}\left(\frac{\varepsilon}{a}\right)^{\delta_2} + \frac{(\delta_1-\delta_2)(\eta\tilde{v}_1^{\text{out}} + D\lambda_3\tilde{z}_1^{\text{out}})}{D\lambda_3(\lambda_1+\delta_1-\delta_2)}\left(\frac{\varepsilon}{a}\right)^{\delta_3} \tag{A.57c}$$

where $\tilde{v}_1^{\text{in}}, \widetilde{W}^{\text{in}}, \tilde{z}_1^{\text{in}}$ are terms of order 2 in A_1. We rewrite the right-hand side of Equation (A.57) in the powers of A_3, label the coefficients by $L_{ij}(a, c, \varepsilon)\,(i = 1, 2, 3,\ j = 1, 2)$

$$\tilde{v}_1^{\text{in}} = L_{12}\,A_3^2 + L_{11}\,A_3 \tag{A.58a}$$

$$\widetilde{W}^{\text{in}} = L_{22}\,A_3^2 + L_{21}\,A_3 + L_{20} \tag{A.58b}$$

$$\tilde{z}_1^{\text{in}} = L_{32}\,A_3^2 + L_{31}\,A_3 \tag{A.58c}$$

As $A_3 < 0$, we solve equation (A.58a), which implies $A_3 = \frac{1}{2L_{12}}\Big(-L_{11} + \sqrt{L_{11}^2 + 4L_{12}\tilde{v}_1^{\text{in}}}\Big)$. Then, we obtain two constraints, denoted by $\widetilde{F}_{\varepsilon_i} = 0\,(i = 1, 2)$,

$$\widetilde{F}_{\varepsilon_1} := \widetilde{W}^{\text{in}} - \frac{L_{22}}{4L_{12}^2}\Big(L_{11} - \sqrt{L_{11}^2 + 4L_{12}\tilde{v}_1^{\text{in}}}\Big)^2 + \frac{L_{21}}{2L_{12}}\Big(L_{11} - \sqrt{L_{11}^2 + 4L_{12}\tilde{v}_1^{\text{in}}}\Big) - L_{20} \tag{A.59a}$$

$$\widetilde{F}_{\varepsilon_2} := \tilde{z}_1^{\text{in}} - \frac{L_{32}}{4L_{12}^2}\Big(L_{11} - \sqrt{L_{11}^2 + 4L_{12}\tilde{v}_1^{\text{in}}}\Big)^2 + \frac{L_{31}}{2L_{12}}\Big(L_{11} - \sqrt{L_{11}^2 + 4L_{12}\tilde{v}_1^{\text{in}}}\Big) \tag{A.59b}$$

***Remark* A.5.** Here, $C_i = C_i(a, A_3, c, \varepsilon)\,(i = 1, 2, 3)$, the values of $\big(\tilde{v}_1^{\text{in}}, \widetilde{W}^{\text{in}}, \tilde{z}_1^{\text{in}}\big)$, $A_j\,(j = 2, 3)$ and $\widetilde{F}_{\varepsilon_i}\,(i = 1, 2)$ are in dependence of (a, A_1, c, ε).

***Remark* A.6.** To solve equation (A.58a), we should obtain two roots of A_3, $\frac{1}{2L_{12}}\Big(-L_{11} + \sqrt{L_{11}^2 + 4L_{12}\tilde{v}_1^{\text{in}}}\Big)$ and $\frac{1}{2L_{12}}\Big(-L_{11} - \sqrt{L_{11}^2 + 4L_{12}\tilde{v}_1^{\text{in}}}\Big)$ according to numerical simulation that $L_{11,12}$ are negative, since $\tilde{v}_1^{\text{in}}$ is positive, we find that the formal root is more reasonable.

Existence and uniqueness

The existence of a unique solution for Equation $\widetilde{F}_{\varepsilon_i} = 0\,(i = 1, 2)$ in (A.59), follows the same procedure as in previous proofs by the Implicit Function Theorem. Now the determinant of the Jacobian matrix of (A.59) becomes $Det(J)\big|_{a^*, A_1^*, c^*, \varepsilon} = \left|\frac{\partial\widetilde{F}_{\varepsilon_1}}{\partial a}\frac{\partial\widetilde{F}_{\varepsilon_2}}{\partial A_1} - \frac{\partial\widetilde{F}_{\varepsilon_2}}{\partial a}\frac{\partial\widetilde{F}_{\varepsilon_1}}{\partial A_1}\right|$. We numerically compute the values of $Det(J)$ and find that Δ are nonzero at least for $\varepsilon = 0.0001$, which implies the persistence of $\widetilde{F}_\varepsilon$ for ε positive and small by the Implicit Function Theorem.